DEVELOPMENT OF A TIME DOMAIN REFLECTOMETRY SENSOR FOR CONE PENETRATION TESTING

A Thesis
Submitted to the College of Graduate Studies and Research
In Partial Fulfillment of the Requirements
for the
Degree of Master of Science
in the
Department of Civil and Geological Engineering
University of Saskatchewan
Saskatoon

By
Michael Jason Amos

PERMISSION TO USE

The author has agreed that the library, University of Saskatchewan, may make this thesis freely available for inspection. Moreover, the author has agreed that permission for extensive copying of this thesis for scholarly purposes may be granted by the professors who supervised the thesis work recorded herein or, in their absence, by the Head of the Department or the Dean of the College in which the thesis work was done. It is understood that due recognition will be given to the author of the thesis and to the University of Saskatchewan in any of the use of the material in this thesis. Copying or publication or any other use of the thesis for financial gain without approval by the University of Saskatchewan and the author's written permission is prohibited.

Requests for permission to copy or to make any other use of material in this thesis in whole or in part should be addressed to:

Head of Department of Civil and Geological Engineering
University of Saskatchewan
Engineering Building
57 Campus Drive
Saskatoon, Saskatchewan
Canada, S7N 5A9

ABSTRACT

An essential component for evaluating the performance of a mine site after its closure includes the tracking of water movement through mine waste such as tailings and overburden. A critical element of this evaluation is the measurement of the volume of water stored in the closure landform. The objective of this project was to design a time domain reflectometry (TDR) device that could be used to measure the volumetric water content of a soil profile to depths of 10 to 20 m. Upon completion of this project, the device will be integrated onto ConeTec's cone penetration testing (CPT) shaft for initially monitoring Syncrude Canada Limited's northeastern Alberta oil sands mine site.

The objective of this project will be achieved through at least two phases of research and development; this thesis concentrates on the first phase. In this phase, research focused on prototype development through laboratory testing to determine appropriate TDR probe geometries and configurations that could be integrated onto a CPT shaft. Considerations also had to be made for protecting the integrity of the probe during field use and mitigating the effects of highly electrically conductive soils common in reclaimed mine sites.

A number of different prototype designs were initially investigated in this research, leading to the development of a refined prototype for advanced testing. Testing for the project was carried out first in solutions of known dielectric constants and salinities, and then proceeded to soils with a range of known water contents and salinities.

Good quality electrical connections were found to be crucial for generating waveforms that were easy to interpret; bad connections resulted in poor results in a number of cases. Decreased probe sensitivity was observed in response to increased rod embedment within the probe variants. A far greater decrease in sensitivity was seen in the results of the fully sheathed rods, although the sheathing was effective for extending the range of the probe in electrically conductive testing conditions. Despite poor results that were seen in some of the tests, overall the results were promising. In particular, results from the push-test showed that the probe was able to monitor changes in water content with depth.

ACKNOWLEDGEMENTS

Completing a thesis and the research behind it is, of course, not an easy endeavour. There are many people who help out along the way in order to bring it to completion. My hope is to thank all of the people who helped me complete my thesis without leaving anyone out.

Firstly I want to thank my supervisor, Dr. Lee Barbour, for his guidance and patience throughout the process, especially when the forest got lost in the trees. My co-supervisor, Dr. Bing Si also deserves much thanks for his input and expertise on the project. I would like to thank my committee members Dr. Ian Fleming and Dr. Andrew Ireson, my External Examiner, Dr. Jane Elliott, as well as Dr. Gordon Sparks who served as the Chair before his retirement, and Dr. Amin Elshorbagy who was the Chair for my defence. Special thanks go out to Dr. Wei Hu for his statistics help, Dr. Ron Cooley and Annalisa Kolbeck for help with thesis edits, as well as Dr. Jeff Dobchuk, Dr. Eric Salt, Dr. Scott Noble, Dr. Jim Merriam, Dr. Sam Butler and Trevor Zintel for helping me figure out how TDR works. Thanks also to Dr. Chris Hawkes and Dr. Jim Kells for their unexpected, but much appreciated, advice on the process of writing and defending my thesis.

A great deal of thanks is also due to the Civil Engineering laboratory technicians: Dale Pavier, Brennan Pokoyoway, Adam Hammerlindl, Helen Yin and Doug Fisher. Their help with the various aspects of my research was very much appreciated, and their friendships have been a great source of enjoyment for me over my time here. Erin Schmeling is also to be thanked for her help with laser diffraction testing. Thanks, too, to the people at Engineering Shops who built and modified my final probes and testing equipment, and loaned to me various tools, supplies and expertise in my hours of need.

Many thanks are due to my fellow grad students, who helped out when I needed an extra hand (sometimes literally), and generally were there for discussion and conversation. In particular I would like to thank the following people in Geo-Environmental Engineering and Soil Science: Thomas Baer, Joel Steeves, Erik Ketilson, Sean Deen, Matt Buchynski, Mingbin Huang, Kathryn Dompierre, James Tipman, Alana DeBusschere, Trent Pernitsky, Henry Chau, Mark Sigouin,

Eric Neil and Min Li. Thanks also to my adoptive family in Structural Engineering, particularly Roanne Kelln, Denise Sanchez and Ouafi Saha. Dyan Pratt also deserves a tremendous amount of thanks – without her help and insight for widget-making, as well as her machining ability, this project would not have been completed. Thank you very much!

Most importantly, I want to thank all of my family. My curiosity of the natural world, which got me into this whole thing in the first place, is a huge part of who I am thanks to the influence of my parents, grandparents, cousins, aunts and uncles...even my great-grandparents, although I never met them. This curiosity brings pleasure to so much of engineering for me, but more importantly my life in general – I hope we can be as successful at passing this along to our kids. The support of my parents and my family has been instrumental in this whole process. Thanks to our kids, Brayden, Logan and Bryony, for putting up with me being in school for so much of their lives (when will you get a real job, Dad?). Huge thanks to Dana for working night shifts and picking up my slack to put me through yet *another* degree. Three is enough. Really. Hope you enjoy your (semi-?) retirement! Love you!

I must also thank the others that helped us out, as a family, along the way. In particular, Curtis and Rachelle Kelln have been a tremendous support to all of us, offering advice and friendship through the whole thing as people who have been there before.

Last but definitely not least, I want to thank the good Lord for getting both myself and our family through this whole thing together. Heaven knows there have been days where this did not seem possible!

Financial help for this project has generously been provided by ConeTec Investigations Ltd., NSERC Syncrude-IRC, the Saskatchewan Innovation and Opportunity Scholarship, the Department of Civil and Geological Engineering, Mr. George Carter, the family of the late Mr. Clarence R. Forsberg, Dr. J.D. Mollard, as well as the Canadian Institute of Mining, Metallurgy and Petroleum's Saskatoon Chapter and Maintenance, Engineering and Reliability Society. I truly am thankful for this funding.

TABLE OF CONTENTS

LIST OF TABLES

LIST OF FIGURES

1 INTRODUCTION

Tracking the movement of water through mine site waste such as tailings and overburden is an essential component in the evaluation of the performance of these sites following mine closure. A critical element of this monitoring is the measurement of the volume of water stored within the closure landform.

This research project involves the design and testing of a time domain reflectometry (TDR) device for measuring the volumetric soil water content of a soil profile over depths of 10 to 20 m. This device will ultimately be integrated onto an insertion probe that will allow the measurement of water content with depth, providing the opportunity to create a water content profile over that depth. Adding soil resistivity and isotope well logging tools to this probe will also allow the source of the water to be characterized (e.g. process-affected water or recently infiltrated meteoric water).

Repeatedly conducting these measurements across the site with time will detect changes in the distribution of stored water volume, and allow for estimations of the rates of flushing and percolation of the cover soil. Water volumes can change with time in response to the initially dynamic nature of the mine waste. For example, unsaturated overburden can undergo ‘wetting up’ or ‘draining down’ following placement, and the porosity of the saturated tailings can change as the tailings consolidate. Volumes of water associated with different sources of water can also be determined and related to estimates of net percolation in unsaturated mine waste. This can be done if a unique change in the chemical or isotopic nature of the recharging water can be differentiated from that of the initial waste (Hilderman 2011, Baer 2014). In more general terms, these measurements could also be used to gather information on the presence of the water table,

whether perched or not, the porosity of the soil in saturated zones, and an estimate of the field capacity within unsaturated zones. All of this data can be used to gauge the performance of the landscape, and to validate and improve the models for its groundwater flow.

Development of this device is being done in concert with ConeTec, currently the largest site characterization contractor in the Canadian oil sands mining industry, for initial use in Syncrude Canada Limited's oil sands mine site in northeastern Alberta, Canada. The particular insertion probe on which the TDR device will be integrated will be ConeTec's cone penetration testing (CPT) probe.

While TDR was chosen for this project, it is not the only method by which to measure volumetric water content. The most accurate method is to take an undisturbed soil sample from the field and measure its gravimetric water content and dry density in the laboratory; however, this process is time-consuming and destructive. In situ methods for directly determining water content also exist, but they too have their drawbacks. Depending on the method, these drawbacks can include site-specific calibrations of the sensors, installation of access tubes, and work with radioactive sources. All of these drawbacks can be problematic in terms of time efficiency or on-site logistics. TDR, however, obtains measurements quickly and does not emit radiation. In general terms, TDR does not require calibration, although in some instances initial calibration is required. One drawback to TDR, however, is its susceptibility to signal degradation in highly electrically conductive soils, as could be encountered in mine tailings. This can cause issues with interpretability of the TDR signal, but through efforts to mitigate this effect, TDR was considered appropriate for the project (Noborio 2001, Jones et al. 2002, Mojid et al. 2003, Strangeways 2003, Casanova et al. 2012b).

The overall purpose of this project is to develop a TDR probe device that can be routinely used on ConeTec's CPT platform. The primary objective of this combination TDR-CPT probe will be to obtain water content profiles at various locations across Syncrude's reclaimed sites including sand and fine tailings as well as overburden dumps. This project will be accomplished through at least two phases of development and testing, of which this thesis describes the work from the first phase.

This first phase has consisted of initial prototype development through laboratory testing for the prototypes. Objectives for this phase were as follows:

1) Determine an appropriate configuration for the TDR probe that could potentially be adapted to a CPT shaft (e.g. having the same diameter and being of reasonable length) through various stages of laboratory testing;
2) Identify a method for sheathing the probe to mitigate the effect of electrically conductive soils, with considerations for protecting the integrity of the probe as it is pushed into the ground; and,
3) Determine a suitable method for manually analyzing the TDR signal waveform data.

Testing for evaluating and refining the prototypes took place in solutions with known properties, compacted tailings sand with different water and salinity contents, fine fluidized tailings, and a push-test in a sand column.

Recommendations for further prototype development have also been made for the next phase of the project. In addition to the continued refinement of the prototype, further testing in laboratory settings and both controlled and full-scale field conditions will be required. Identification of a data cable that can both provide a high quality signal and be integrated with ConeTec's relatively slim CPT cable bundle will also be necessary.

2 LITERATURE REVIEW

2.1 Introduction

A review of literature associated with water content measurement methods, the physics of TDR, the use of TDR for determining soil water content in both conventional and highly electrically conductive conditions, as well as the development of combination TDR and CPT devices was completed. A number of key papers that helped guide the project in terms of prototype design, testing, and data interpretation are identified. Details of these papers are presented below.

2.2 Volumetric Water Content Measurement

As discussed in Chapter 1, the most accurate method for measuring volumetric soil water content is by determining an undisturbed soil sample's dry density and gravimetric water content. Since this is time-consuming, expensive and destructive, a number of in situ methods have been developed for determining the volumetric water content directly, although these methods have their own drawbacks as well. Two commonly used electrically-based methods include frequency domain (FD) and capacitance probes. These methods, however, require calibrations in different soils that are tested. FD sensors are also susceptible to poor results from testing in highly electrically conductive conditions. Neutron probes are another commonly used method, but they use a radiation source, require installation of access tubes and also need site-specific calibrations. The installation of the access tubes, in addition to the time-consuming nature of the readings, can be inefficient for some applications. TDR, however, obtains measurements quickly and does not emit radiation. In general terms, conventional TDR probes also do not require site-specific calibration. While TDR is susceptible to signal degradation in highly electrically conductive soils, overall it is still a desirable method for in situ volumetric water content measurement

(Hilhorst and Dirksen 1994, Shinn et al. 1998, Noborio 2001, Jones et al. 2002, Mojid et al. 2003, Strangeways 2003, Hignett and Evett 2008, Casanova et al. 2012b).

It should be noted that, under ideal conditions, the accuracy of directly determining the volumetric soil water content using the gravimetric method described above is ±0.003 m^3/m^3, while TDR is accurate to within ±0.02 m^3/m^3. This gravimetric method is used to calibrate and compare all the other methods of volumetric water content determination (Ferré and Topp 2002a, Hignett and Evett 2008).

2.3 Fundamental TDR Papers

TDR was initially developed for use in the utility industry to find faults in buried cables, and is also closely related in principle to radar (Cassel et al. 1994, Evett 2000a, Noborio 2001, Jones et al. 2002, Strangeways 2003). Work by Fellner-Feldegg (1969) showed that it was possible to determine the dielectric constants for different materials using TDR. Hoekstra and Delaney (1974) and Davis and Chudobiak (1975) then applied these findings to soils, showing that dielectric constant changed with volumetric water content. This led to the seminal work by Topp et al. (1980) which related volumetric water content to the dielectric constant of a soil, producing what is known as Topp's equation,

$$\theta_v = -5.3 \times 10^{-2} + 2.92 \times 10^{-2}\varepsilon_b - 5.5 \times 10^{-4}\varepsilon_b^2 + 4.3 \times 10^{-6}\varepsilon_b^3 \qquad [2\text{-}1]$$

where θ_v is the volumetric soil water content, and ε_b is the bulk dielectric constant of the soil obtained from TDR readings. Generally speaking, the dielectric constant for soil is bounded by the dielectric constants of its principal components: air, mineral soil grains and water. The values for these components are 1, 3 to 5, and 80 to 81, respectively (Jones et al. 2002, Moret et al. 2006, Wohlfarth 2013). Because the dielectric constant for water is much greater than air and soil grains, a strong relationship between soil water content and dielectric constant can be made. In Topp et al.'s (1980) research it was found that the dielectric constant of soil at a given water content was nearly independent of soil texture, density, salinity and temperature. The error of measurement for Topp et al.'s (1980) work was within 1.3% of the actual soil water content.

Topp et al. (1980) developed their equation primarily through research in mineral agricultural soils. While it worked well in those soils, a number of cases have been documented where the equation did not perform as satisfactorily in other soils (e.g. Kelly et al. 1995, Schaap et al. 1996, Jones et al. 2002, Sorta et al. 2013). In particular, Sorta et al. (2013) applied the Topp equation to oil sands tailings and found that it underestimated the water content quite substantially in wet tailings. In order to more accurately calculate the water content of tailings above approximately 0.45 m^3/m^3, Sorta et al. (2013) generated their own equation in the following form:

$$\theta_v = -3.08 \times 10^{-5}\varepsilon_b^3 - 7.40 \times 10^{-3}\varepsilon_b^2 + 2.05\varepsilon_b - 3.04 \qquad [2\text{-}2]$$

It should be noted that the resulting value from this equation provides the volumetric water content in percent; to express the value in decimal form, which is the chosen form for this thesis, the value should be divided by 100.

2.4 TDR Theory

A TDR unit is an electronic instrument made up of three components:

- A pulse generator which generates electrical signal pulses with an extremely fast signal rise time. This rise time may be as low as 17.5 ps, although it is typically 200 ps. The Mohr CT100HF TDR unit used in this project has a rise time of 60 ps;
- A sampler, or receiver, which receives the high frequency reflected signals from the cable and converts them into lower frequency outputs; and,
- An oscilloscope that displays the received signals (Fellner-Feldegg 1969, Davis and Chudobiak 1975, Kelly et al. 1995, O'Connor and Dowding 1999, Evett 2000a, Strangeways 2003, Mohr 2012).

The electrical signal pulse generated by the TDR unit travels to and from the TDR probe along a coaxial cable that is typically 50 Ω in impedance (Strangeways 2003). The inner conductor of the cable carries the signal from the unit to the probe (the "live" conductor), while the outer conductor (the ground conductor) carries the signal returning from the probe. The outer

conductor shields the cable so that the generated electric and magnetic fields are isolated and contained within the cable (Mojid et al. 1998).

After being generated by the TDR unit, the electrical signal pulse travels along the cable until it encounters a change in impedance in the cable. This change could be a change in the nature of the cable, such as wire damage, a connection, or a change in the material carrying the signal. In the case of soil testing, this change is associated with the portion of the system where the rods of the TDR probe at the end of the cable are in contact with the soil (or other testing medium). When any of these changes are encountered, a fraction of the signal is reflected back along the cable to the TDR unit, where a change in the voltage of the reflected signal is detected, as shown in Figure 2.1. This change in voltage is compared to the initial voltage sent out by the unit through the calculation of a reflection coefficient, ρ (rho), that is displayed on the y-axis of the oscilloscope. The elapsed time (or distance, depending on the model of TDR being used) for the return of the reflection to the unit is displayed on the x-axis of the oscilloscope, and is used to determine the dielectric constant. The dielectric constant is ultimately what the TDR measures (Fellner-Feldegg 1969, Andrews 1994, O'Connor and Dowding 1999, Jones et al. 2002).

When the signal travels into the probe in the soil, the resulting reflection differs based on the dielectric constant of the soil or other testing medium. As a result, even though the length of the probe contacting the soil remains constant, an *apparent length* of the probe contacting the soil is displayed by the TDR. This apparent length will vary as a function of the travel time of the signal moving from the live rod to the ground rod(s) through the soil: the higher the dielectric constant of the soil (i.e. the higher the soil's water content) the slower the signal moves through the soil. It is from this apparent length that the dielectric constant of the soil can be calculated (Jones et al. 2002, Robinson et al. 2003).

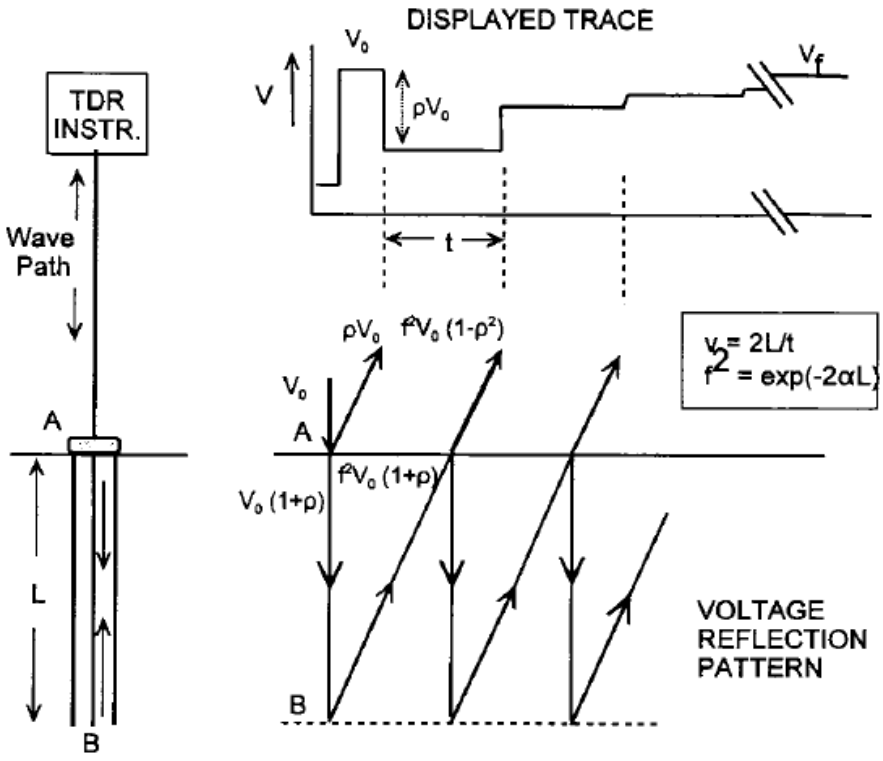

Figure 2.1 – Schematic of a TDR system with individual rods of length L inserted in the soil (left), with the various reflections of the signal shown (bottom right), and the corresponding idealized TDR waveform oscilloscope display (upper right). The 't' in the waveform display indicates the apparent probe length, defined with an initial peak and a subsequent trough in the waveform (Topp et al. 2000).

Jones et al. (2002) present an equation to calculate the dielectric constant from the TDR waveform,

$$\varepsilon_b = \left(\frac{x_2 - x_1}{V_p\, L}\right)^2 \qquad [2\text{-}3]$$

where $(x_2 - x_1)$ is the apparent length of the probe, V_p is the propagation velocity of the signal relative to the speed of light, expressed as a ratio, and L is the true length of the individual rods. If the individual rods are different in length, L is their average length (Heimovaara 1993). The apparent length of the probe is shown, ideally, as 't' in the upper right of Figure 2.1.

Measurements by TDR are a weighted average of the various dielectric constants that are encountered along the length of the probe within its sensing volume (Mojid et al. 1998). Since the water content of the soil may change over the length of a probe, the chosen probe length can have an impact on the resolution of its water content measurement. In this project, the desired resolution for the probe should be considered in the latter stages of design.

It should be noted that the dielectric constant can be more precisely determined through the use of a dielectric mixing model, of which a number of models have been proposed (e.g. Dobson et al. 1985, Roth et al. 1990, Whalley 1993, Heimovaara et al. 1994, Schwartz et al. 2009). Generally speaking, in the dielectric mixing model, dielectric constants of each of the different soil components (and presumably other materials within the sensing volume) are weighted according to their respective volumetric fractions within the sensed volume. Depending on the particular model, a number of different factors may be applied to the weighted components, but each component term is summed to determine the overall dielectric constant of the sensed soil volume. In order to apply this model, each component's dielectric constant and respective volumetric fraction, as well as the overall sensing volume of the probe, need to be known.

2.5 Complications with TDR

There are two main complications that can arise when using TDR for soil water content determination: excessive cable length and energy losses. Both of these complications will be explored in this section.

2.5.1 Excessive Cable Length

A long cable attenuates the TDR's signal by acting as a filter, decreasing the amplitude and definition of the waveform progressively as the cable length increases. Eventually, a point will be reached where the initial peak of the waveform disappears altogether, and the descending limb of the initial peak intersects with the ascending limb of the trough (Heimovaara 1993, Evett 2000a). This makes interpretation of the waveform difficult, if not impossible, depending on the lack of definition in the waveform. A general guideline for the maximum length of cable of

approximately 25 m has been proposed, although longer cable lengths have been successfully used (Herkelrath et al. 1991, Heimovaara 1993, Cassel et al. 1994).

In the field testing phase of this project, it will be ideal to use the TDR to depths of approximately 20 m, with more cable required to reach the TDR unit itself. This makes for a total cable length near the maximum used in the literature.

2.5.2 Energy Losses

In addition to issues with cable length, complications also exist with energy loss. While in general terms TDR measures dielectric constant, more precisely it is actually the bulk dielectric constant that is measured: a complex expression that includes both real and imaginary components. The real component describes the volumetric water content, while the imaginary component represents losses resulting from conductive or relaxation losses. In most cases both of these types of losses are negligible and the underlying assumption holds; however, in lossy conditions this translates into an overestimate of water content (Mojid et al. 1998, 2003, O'Connor and Dowding 1999, Topp et al. 2000, Robinson et al. 2003, Bittelli et al. 2008).

Conductive losses occur as a result of the live rod, which carries the signal's current, being in direct contact with conductive materials (e.g. clay or saline soils) that dissipate the signal's energy (Mojid et al. 1998, Topp et al. 2000, Nichol et al. 2002, Robinson et al. 2003, Bittelli et al. 2008). This effect becomes increasingly pronounced with increasing electrical conductivity, to the point that at approximately 2 dS/m the waveform is sufficiently attenuated that no reflection of the signal from the end of the probe is detected. The waveform appears as a short circuit, and interpretation of the waveform is all but impossible (Mojid et al. 1998, Strangeways 2003, McIsaac 2010). This is of particular concern to this project, as the electrical conductivity of mine waste such as tailings can easily exceed 2 dS/m (Lefebvre 1997, Nichol et al. 2002). The progressive attenuation of waveforms in response to increasing levels of electrical conductivity is shown in Figure 2.2.

Relaxation losses, however, result from molecular responses to the TDR signal. When the signal pulse enters the soil through the probe, polar molecules, like water, align themselves to the field. This stores energy which is released when the signal pulse stops and the molecules return to their random orientations. At certain frequencies the polar molecules are unable to keep up to the continual "on again, off again" alternating application of the electric field in the soil, losing energy as heat. Other constituents such as salts or alcohols can further affect these losses. Generally, losses from relaxation are more important at high frequencies, while conductive losses are more important at low frequencies. Conductive losses are typically greater than relaxation losses (Stogryn 1971, Klein and Swift 1977, Jackson and O'Neill 1987, Mojid et al. 1998, 2003, Topp et al. 2000, Robinson et al. 2003, Gadani et al. 2012).

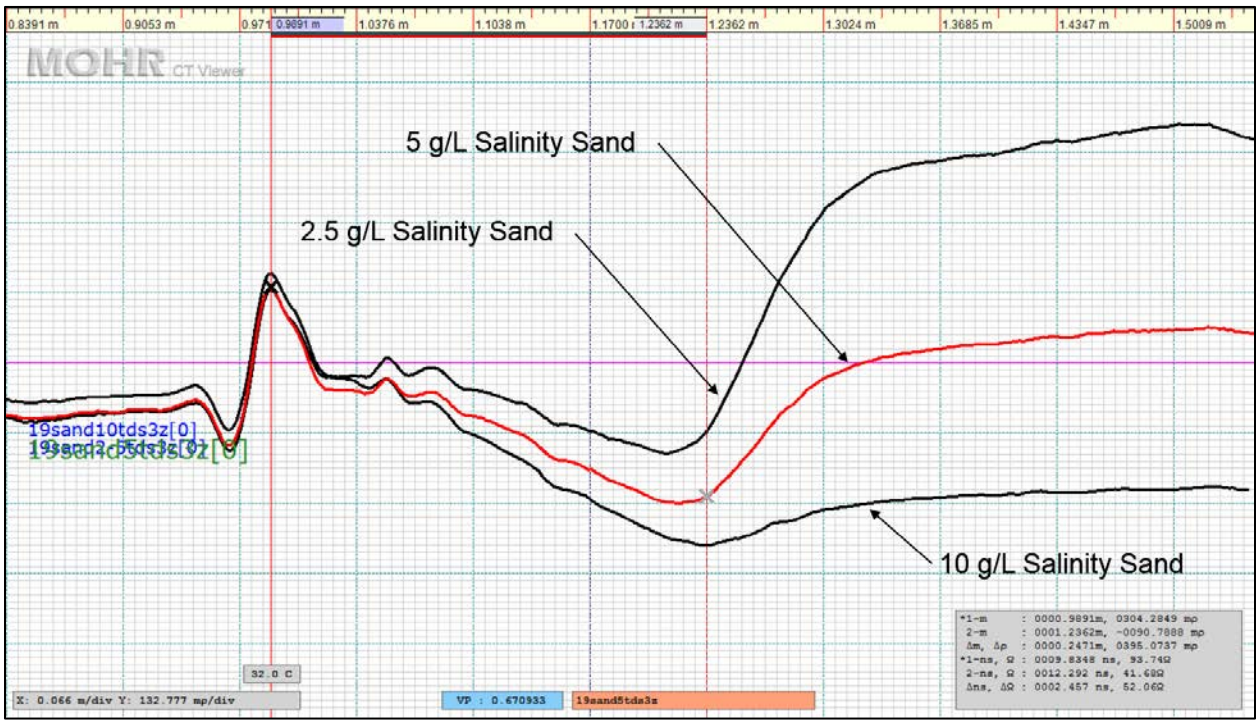

Figure 2.2 – TDR waveforms for low, moderate and high electrically conductive soils as shown by increasing salinity. It should be noted than in a sufficiently highly conductive soil there would be no reflection from the end of the probe (i.e. no trough).

Correcting the results to account for the effects of losses would seem to be a logical approach to obtain an accurate water content. This has been attempted (e.g. Topp et al. 2000, Bittelli et al.

2008), but it is not an easy task. The TDR signal contains a wide bandwidth of frequencies ranging approximately from 20 kHz to 1.5 GHz, and each of these frequencies has its own level of susceptibility to energy loss. As alluded to above, this susceptibility can be compounded by additional constituents in the testing medium, such as salts and alcohols. If any of these frequencies experience energy loss their return to the TDR unit will be delayed, with the degree of delay being a function of the amount of energy loss. As the TDR waveform is essentially the integral of the arrivals of each reflected frequency, delays in the return of different frequencies will result in a less well-defined (i.e. less sharp) end-of-probe reflection in the waveform. The difficulty in the task of correcting for these losses involves choosing only one effective frequency to adjust from the entire bandwidth of frequencies that makes up the TDR signal. This is further complicated by the fact that this effective frequency changes based on the soil conditions being tested. Additionally, the impact of changing water content on the effect of conductivity is not fully understood. No attempt was made to correct for the effect of losses in this project, but if the complexities could be simplified it would clearly improve the functionality of TDR (Stogryn 1971, Klein and Swift 1977, Ledieu et al. 1986, Jackson and O'Neill 1987, Topp et al. 2000, Nichol et al. 2002, Robinson et al. 2003, Bittelli et al. 2008, Gadani et al. 2012).

2.6 Sheathing

The effects of excessive electrical conductivity on the TDR signal can be mitigated by applying an insulating coating to the TDR probe; examples of this are well documented in the literature (e.g. Kelly et al. 1995, Ferré et al. 1996, Mojid et al. 1998, Nichol et al. 2002, Fujiyasu et al. 2004, McIsaac 2010, Chen et al. 2014). Coating, or sheathing, TDR rods eliminates the direct contact of the probe with the surrounding soil, thereby minimizing the conductive losses (Mojid et al. 1998, Nichol et al. 2002). Sheathing only the current-conducting live rod, however, produces the greatest effect, thereby allowing the maximum extension of the probe's range in highly electrically conductive soils (Mojid et al. 1998). As a result, sheathing of only the live rod was done for this project. Even though the metal of the sheathed live rod is not in direct contact with the soil, the transverse electromagnetic wave energy still extends outside of the coating since it is not shielded (Mojid et al. 1998, Nichol et al. 2002, Collier 2013). This allows

the field to form in the soil or other testing material, and the signal to return to the TDR unit through the ground conductor rod(s).

Sheathing has been shown to be very effective in extending the range of TDR measurement in electrically conductive testing media. Nichol et al. (2002), for instance, successfully obtained an analyzable waveform for a saline solution with an electrical conductivity of 70 dS/m through the use of a sheathed probe. This level of conductivity is quite high, and no higher levels are anticipated in the field testing phase of this project.

Using sheathing materials unfortunately comes with two drawbacks. The main drawback with a sheathed probe is its difference in sensitivity from unsheathed probes. In soils that are not highly electrically conductive a sheathed probe will underestimate the measured dielectric constant, and therefore also the soil water content (Ferré et al. 1996, Mojid et al. 1998, Nichol et al. 2002). Moreover, Ferré et al. (1996) and Mojid et al. (1998) both found that the degree of underestimation increased with increasing water content. However, in highly electrically conductive conditions the sheathed probe was found to overestimate the dielectric constant (Mojid et al. 1998), suggesting a "cross-over" in probe response at some point. This requires some degree of calibration in order to properly interpret the data. The other drawback with sheathed probes is a decrease in sensing volume. This, along with the decrease in probe sensitivity, can be mitigated to some degree by using thinner sheath coatings (Ferré et al. 1996, 1998, Fujiyasu et al. 2004). Decreases in sensitivity can also be reduced in less electrically conductive conditions by leaving some of the rod exposed. As the conductivity increases, however, more of the rod needs to be sheathed in order to prevent the conductive losses from becoming too great (McIsaac 2010).

A number of sheathing materials have been investigated in the literature for mitigating the effects of highly electrically conductive testing media. These include Teflon® heat shrink tubing (Kelly et al. 1995), polyolefin heat shrink tubing (Nichol et al. 2002, McIsaac 2010), adhesive insulators (Mojid et al. 1998), polyvinyl chloride (Ferré et al. 1996), Delrin® (Chen et al. 2014), a coating mixture of epoxy resin, graphite powder and $BaTiO_3$ (Moret-Fernández et al. 2009), enamel paints, and an epoxy-ceramic nanocomposite (Fujiyasu et al. 2004). Commercially-available

sheathed rods also exist (Lefebvre 1997, Fujiyasu et al. 2004, McIsaac 2010). Standard commercially-available insulated stranded copper wire was also successfully used for TDR rods, although not specifically for electrically conductive media (Cataldo et al. 2014).

It should be noted that the effects of decreased probe sensitivity associated with increased sheathing thickness can be diminished by the use of sheathing materials with higher dielectric constants (i.e. 30 to 40, approximately the same value of a saturated soil) (Fujiyasu et al. 2004). One such material is Fujiyasu et al.'s (2004) epoxy-ceramic nanocomposite, which had a dielectric constant of 35. This is compared to conventional insulating materials which have much lower, and roughly equal, dielectric constants (i.e. between 2 and 5) (Ferré et al. 1998, Nichol et al. 2002, Fujiyasu et al. 2004). Despite the benefit associated with the nanocomposite, the cost for such an exotic material is assumed to be prohibitive. As a result, only conventional insulating materials were considered in this project.

2.7 TDR Probe Configurations

A summary of conventional TDR probe configurations as well as past designs combining TDR probes with insertion shafts is presented in this section. Given the deliverables for this project, this is clearly important in terms of the probe design process.

2.7.1 Conventional Probe Configurations

A number of conventional TDR probe configurations have been evaluated in previous studies. Initial testing performed by Topp et al. (1980) used a coaxial sample holder for the soil, with a central conductor and a conducting exterior wall (Figure 2.3). This is analogous to the coaxial cable connecting the TDR unit with the probe. The geometry of the holder takes full advantage of the electric field generated by the TDR signal and gives high quality measurements (Topp et al. 1980, Lin et al. 2006). Unfortunately, this configuration is not practical in a field context (Topp et al. 1980, Zegelin et al. 1989). Two parallel rods inserted in the soil were initially used for field testing (Davis and Chudobiak 1975, Topp et al. 1980, Topp and Davis 1981, Zegelin et al. 1989); however, there were some issues with regards to ease of analysis and susceptibility to signal degradation in electrically conductive soils (Zegelin et al. 1989). As a result, Zegelin et al.

(1989) suggested using more than two rods to more closely emulate a coaxial sample holder, and to increase the accuracy of the volumetric soil water content measurement. In general, the greater the number of rods, the more closely the probe imitates the coaxial cell, and the more accurate the data. However, more rods also mean increased soil disturbance and effort involved in inserting the probes manually (Zegelin et al. 1989). Zegelin et al. (1989) recommend using a three-rod probe for field use.

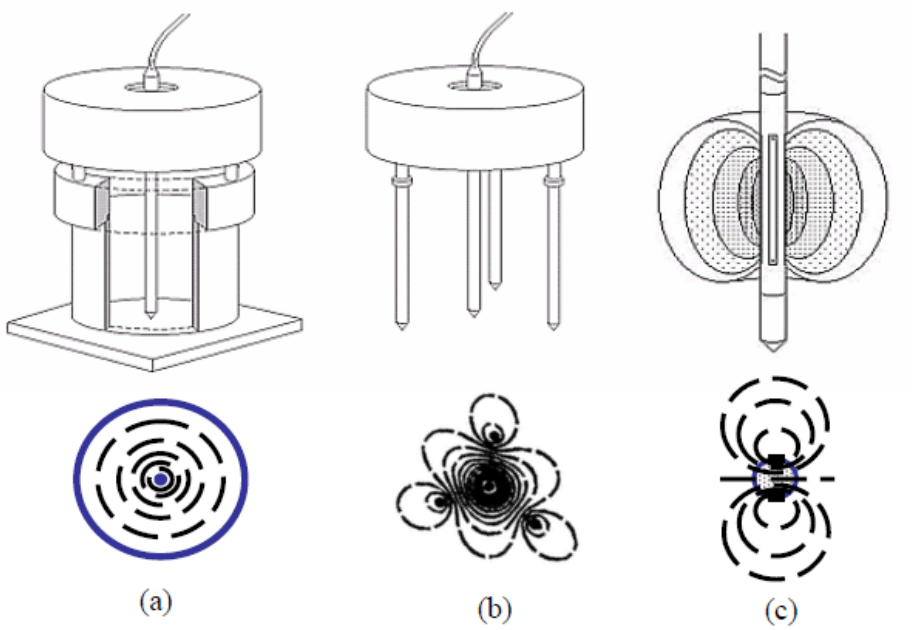

Figure 2.3 – Electrical fields generated by different TDR probe designs: (a) coaxial sample holder; (b) four-rod TDR probe; and, (c) conductors placed on a shaft (Lin et al. 2006).

Using more than two rods increases the quality of the measurement in terms of the waveforms that are generated (Zegelin et al. 1989); however, for the same overall rod spacing (i.e. outside rod to outside rod), it also results in a decrease in the sample volume, as seen in Figure 2.3 (Knight et al. 1994). Increasing the rod spacing gives a larger, more representative value of the soil water content, but it also reduces the resolution of the waveform (Knight et al. 1994, O'Connor and Dowding 1999). This leads to decreased measurement accuracy, which could further be exacerbated with highly electrically conductive soils, and clearly highlights the trade-

off between representative sample volume and accuracy. It should be noted that the sampling area is roughly cylindrical or elliptically cylindrical in shape, with no sensitivity past the "top" or "bottom" ends of the rods (O'Connor and Dowding 1999, Ferré and Topp 2002b, Mojid et al. 2003).

Probe length also plays a role in the quality of the data collected. Probes that are too short will generate a waveform that is lacking in detail, with the waveform features potentially blending together. Conversely, probes that are too long will begin to attenuate the signal. Long probes are also more susceptible to the effect of highly electrically conductive soils (O'Connor and Dowding 1999, Ferré and Topp 2002b). Ferré and Topp (2002b) recommend a minimum probe length of 0.1 m, referring to larger errors that start to occur with probe lengths of less than 0.075 m. They also suggest a maximum probe length of 0.2 m in clayey, electrically conductive soils. There are a number of exceptions to this, however, as probe lengths of less than 0.075 m have been described in the literature (e.g. Mojid et al. 2003, Chen et al. 2014, Yoon et al. 2014). In order for these short probes to be successful, however, the travel time through the probe needs to be longer than the TDR pulse rise time (Nissen et al. 1998, Mojid et al. 2003). This can be achieved through either a "faster" TDR pulse rise time, which is costly, or by use in situations that increase the TDR signal's travel time, for example wetter conditions (Nissen et al. 1998). Longer probes have also been used, as Nichol et al. (2002) successfully used sheathed probe lengths of 0.28 m in highly electrically conductive soils.

Another design guideline is that of a rod separation to diameter ratio. As a rule of thumb, a ratio of less than 10 is recommended in order to avoid the development of a "skin effect" (Knight 1992, Ferré et al. 1998, Ferré and Topp 2002b). This is described by Knight (1992) as being an overly strong concentration of the energy around the individual rods, leading to a high weighting of the conditions immediately surrounding the rods. This would not be an issue if the water content was homogenous. However, compaction from probe insertion, with an associated local change in water content, or the presence of large air gaps could have a considerable effect on a measurement in these situations (Knight 1992, Knight et al. 1994, Ferré and Topp 2002b, Robinson et al. 2003). Ferré (1997) noted, however, that air gaps that surround less than

approximately 30° of the rod circumference are unlikely to be problematic. In general, though, air gaps are more serious with smaller diameter, shorter rods (Kelly et al. 1995).

2.7.2 TDR Insertion Probe Configurations

Inserting conventional probes into the soil works well for a number of different applications, but not for measuring soil water content conditions with depth. Integrating rods onto an insertion shaft, however, is one method that can be used for this purpose. A number of designs for this purpose have been developed, including the following:

- Coiled rods, wrapping the TDR rods around the insertion shaft (Nissen et al. 1998, Topp et al. 2001, 2003, 2006, Vaz and Hopmans 2001, Persson and Wraith 2002, Vaz 2003, Kosugi et al. 2009, Yamakawa et al. 2010);
- Vertical conductor strips or rods attached to the side of the shaft (Lefebvre 1997, Strangeways 2003, Lin et al. 2006); and,
- Rings oriented perpendicular to the axis of the probe (Lefebvre 1997, O'Connor and Dowding 1999, Miyamoto and Chikushi 2006, Persson and Dahlin 2010).

Another method for measuring water content with depth, and a similar design to the vertical conductor rods, was also tested by Maheshwarla et al. (1995), Redman and DeRyck (Ferré et al. 1998) and (Casanova et al. 2012a). These designs attached vertical rods to the outside of a plastic access tube in soil.

The rods for each of the probe designs were typically attached to some sort of insulating material on the insertion shaft (or tube), and similar designs were considered for testing in this project. While no reference has been found in the literature for specifically sheathing TDR probes on an insertion shaft, the idea of using the shaft's insulator to extend the effective testing range of the TDR in saline soils was investigated.

Assuming that attaching the rods to the insulator could be analogous to sheathing, partially embedding the rods in the insulator may prove useful for extending the TDR's range into saline soils. As previously discussed, partial embedment could be beneficial since sheathing the entire probe is not necessary for moderately conductive soils, and appears to lessen the drop in

sensitivity typically seen in fully sheathed probes (McIsaac 2010). Fully embedding a rod in the insulator may also be similar enough to a conventional sheathed probe to further extend the TDR's range into the most conductive soils, thereby increasing its utility.

Given the deliverables of this project, the resiliency of typical sheathing materials is questionable since the probe will be subjected to considerable abrasion and contact with sharp rocks in the ground. Any damage to the sheathing layer resulting in decreased sheathing thickness or even exposure of the rod could substantially decrease the performance of the probe (Ferré et al. 1998, Fujiyasu et al. 2004). The implications of this type of damage should be considered and tested for in later stages of the project.

The probes designed by Maheshwarla et al. (1995), Redman and DeRyck (Ferré et al. 1998) and Casanova et al. (2012a) all used partially embedded rods. Research on these probes suggests that as with conventional probes, increased rod separation increases the sample volume of the probe (Ferré et al. 1998, Casanova et al. 2012a). Interestingly, despite the case with conventional probes, sample volume appears to be somewhat insensitive to differences in rod diameter (Ferré et al. 1998). Increased rod separation, however, also increases its susceptibility to the effects of electrically conductive soils (Casanova et al. 2012a). It is assumed that these effects would also be associated with fully embedded rods. Studies of sheathed conventional probes also found that relative to unsheathed probes the sample volume decreased more for two-rod probes than it did for three-rod probes (Ferré et al. 1998). The same effect is assumed to apply to insertion probes.

Other considerations for probe design include probe construction materials. Robinson et al. (2003) state that for insulators on the shaft with higher dielectric constants, more signal energy is stored in the material and less penetrates the surrounding material of interest (i.e. the soil). However, since the dielectric constants for the insulating materials considered in this project are so close, as discussed in Section 2.6, the choice of insulators for probe construction is unlikely to generate much of a difference in response. Additionally, the presence of a steel core in the shaft has been found to decrease the sensitivity and accuracy of the probe (Persson and Dahlin 2010). Given the rigours of insertion, it is hard to avoid all of the disadvantages associated with the different materials, as each of the materials play a role in the construction of a successful probe. As a result, some of these effects must be accepted.

Overall, a determination of which effects are more or less desirable in terms of the design of the probe will need to be considered in light of the expected site conditions and desired probe performance. Indeed, it will not be possible to construct a TDR probe that can successfully be adapted to a CPT insertion shaft for field use in saline soils that performs as well as a conventional unsheathed TDR probe in ideal laboratory testing conditions.

2.8 TDR Waveform Analyses

Determining the TDR probe's apparent length from a waveform should, in theory, be easy. However, properties of the TDR probes, soil, and soil water can affect the waveform dramatically (Evett 2000a). To have a level of repeatability and standardization it is necessary to utilize a specific algorithm for the analysis. A number of different algorithms have been suggested (Topp et al. 1980, Heimovaara 1993, Evett 2000a). Topp et al. (1980) and Heimovaara (1993) both specify graphical algorithms that rely on manually placing tangent lines on the waveform. While graphical methods are suitable, they can prove to be ineffective under certain testing conditions (Evett 2000a), as well as being generally tedious and time-consuming when many waveforms are being analyzed. Computer programs have been developed to automate this process, and in some cases also perform more complicated data transformations, such as derivatives, which allow for more robust and accurate analysis (Evett 2000a). Two such computer programs that are readily available include TACQ and WinTDR (Wraith and Or 1999, Evett 2000b). Unfortunately, the TDR unit available for this project did not interface with these programs, so only manual waveform interpretations could be used. Specifics on the algorithm used for waveform interpretation are provided in following sections of this thesis.

It should be noted that waveform interpretation can also theoretically be improved by adding shorting diodes to the probe to help determine the beginning and end of the probe (Hook et al. 1992). Physical modifications such as this were not considered in this phase of the project, but may be worth considering in subsequent stages of the project.

3 MATERIALS AND METHODS

3.1 Introduction

This chapter describes the prototype designs, the prepared ethanol, saline and soil samples, and the testing methods all used in this phase of the project. Tests were done in this phase both with prototype and conventional probes in a number of different media to compare results. Where available, results from the different probes were also compared with those in the literature.

Testing of a number of different preliminary prototype probes was done primarily in ethanol and saline solutions with known properties, with some testing also being done in soils with various water contents. The results from this testing led to the selection of one prototype design for refinement and advanced testing. Variations of this refined prototype were tested initially in the ethanol and saline solutions, and then in a range of prepared soil mixtures including sand, saline sand, and Fluid Fine Tailings (FFT). Testing culminated with insertion of a preferred prototype into a constructed soil profile to simulate field use of the completed probe.

3.2 Prototype Design

As discussed in Section 2.7.2, three general types of rod configurations have been used in insertion type TDR probes: coiled rods; vertical rods; and horizontal rings. Given the fact that long rods with close spacing would not be advantageous for this project, the coiled rod design was neglected; however, the other two designs were considered to be viable. Using various rod materials and configurations, a preliminary investigation was carried out to build an understanding of how the different horizontal ring and vertical rod prototype designs might function. Delrin® cylinders were used for the most part, although one design involved using a steel pipe as the ground for the TDR probe as opposed to a standard rod that was used on other

prototypes. The horizontal "rings" for the Delrin® cylinder prototypes were constructed by bending a wire in a circle, leaving a gap between the start and end of the "ring". These rings were slightly longer than the vertical rods. A length of rebar was also included in the centre of the Delrin® cylinder in the latter stages of the preliminary prototype testing. This was done to determine whether a shaft used for structural purposes would have a notable impact on the response of the probe.

The preliminary testing indicated that both vertical rods and horizontal rings were feasible; however, it was felt that the horizontal rings would be more susceptible to damage during insertion (e.g. catching on rocks). Vertical rods would be less likely to be damaged in this manner due to their position parallel to the direction of insertion. As a result, vertical rods were the chosen configuration for this probe.

Conventional TDR field probes typically consist of either two or three rods that are pushed into the soil. There are advantages and disadvantages associated with both of these designs, as discussed previously. However, neither of these probe types had a substantial advantage over the other. As a result, the prototype probes were designed with the capability to test both two- and three-rod geometries.

It was found that sheathing one of the rods with an insulator limited conductive losses and consequently increased its ability to measure water content in saline soils. It appeared from the literature that the type of insulator used to sheath the rod was not critical, as long as it had insulating properties. Delrin®, an acetyl resin (DuPont), was selected for the probe given the requirements for strength, resistance to frictional wear, electrical insulation, and ease of machining and fabrication.

3.2.1 Rod Spacing and Geometry

Given that the diameter of the probe was constrained to be similar to that of a conventional CPT tip and rod, the only choice in design was in the spacing of the rods around the probe's circumference. As a result, four different rods were attached to each probe to provide a level of

flexibility in testing different rod spacings, as well as allowing for two- and three-rod geometries, and sheathing, to be evaluated. These rods were spaced at 90° intervals around the perimeter of the probe, with one of the rods inserted within the Delrin®. This inserted rod served as the sheathed rod for the probe. The Delrin® prototypes were all machined to be the same nominal diameter as the CPT cone tip.

Having the ability to select rods that were diametrically opposed allowed for sensing as large of an area as possible. This would obtain the most representative water content and minimize the effect of any localized change in water content associated with probe insertion.

3.2.2 Sheathing Effects of Partial Embedment

Three different variants of the refined prototype were constructed with varying amounts of embedment for the unsheathed rods. Two of the prototypes, D1 and D2, had channels machined in the Delrin® into which the rods were epoxied, as shown in Figure 3.1. The D1 prototype had the deepest embedment, with the outside of the rods sitting flush with the outside of the Delrin® cylinder. The D2 prototype was machined to allow half of the rod to sit outside the Delrin®. Rods on the third prototype, D3, were epoxied directly to the outside of the Delrin® cylinder. No channels were machined into the Delrin®. Efforts were made in this case to minimize the amount of epoxy applied in order to keep it from effectively sheathing the rods. Spacing between opposite unsheathed rods was approximately 39, 44 and 49 mm, on centre, for the D1, D2 and D3 probes, respectively. Spacing between the sheathed rod and the opposite unsheathed rod was approximately 38, 40 and 42 mm, respectively.

The rationale for investigating the depths of rod embedment was to determine whether it was possible to extend the range of an unsheathed TDR probe in saline soils by partial embedment as opposed to complete sheathing. If so, the probe may still be effective in saline soils but retain a greater amount of sensitivity than a fully sheathed rod. The various depths of embedment were also used to provide some insight as to how to address the trade-off between increased sensitivity (e.g. less embedment) and robustness (e.g. more embedment) of the sensor.

It should be noted that the suggested ratio for rod separation to diameter discussed in Section 2.7.1 was not met with the D3 probe design, although it was very close. Since the value was so close, and it was a design guideline rather than a requirement, not meeting the guideline did not cause a tremendous amount of concern. However, the differences in impact of the prototype probe components over a conventional probe on the development of a skin effect was not known. Despite this unknown, it is felt that sensing the maximum area for the given diameter of the probe was the best way to proceed with testing.

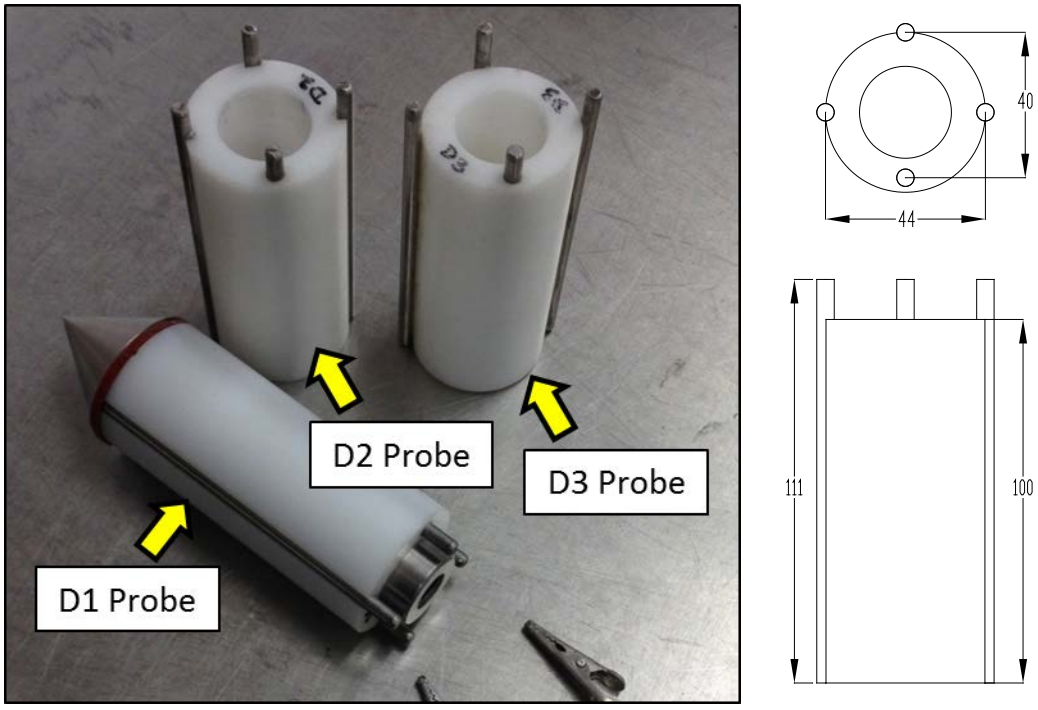

Figure 3.1 – Delrin® probe prototypes: D1 probe, flush rods; D2 probe, partly exposed rods; and D3 probe, fully exposed rods (left). Rod length and diameter: 111 mm, and 4.8 mm, respectively; Delrin® probe length, outside and inside diameters: 100 mm, 44.0 mm, and 25.3 mm, respectively. Cross-section and front view of D2 probe with partial dimensions shown on right. Dimensions in mm.

3.2.3 Additional Components to the TDR Probe

There were a number of other components added to the TDR probe during testing not directly associated with the TDR probe itself. These additional components were included in the testing

to more fully represent the actual probe configuration during field insertion. The additional components included the following, as shown in Figure 3.2:

- a CPT cone tip;
- a stainless steel shaft insert that was inserted inside the Delrin® cylinder, ultimately connecting to the cone tip and carrying the probe insertion force;
- a rubber washer placed between the cone tip and the Delrin® cylinder; and,
- a probe-stabilizing rod.

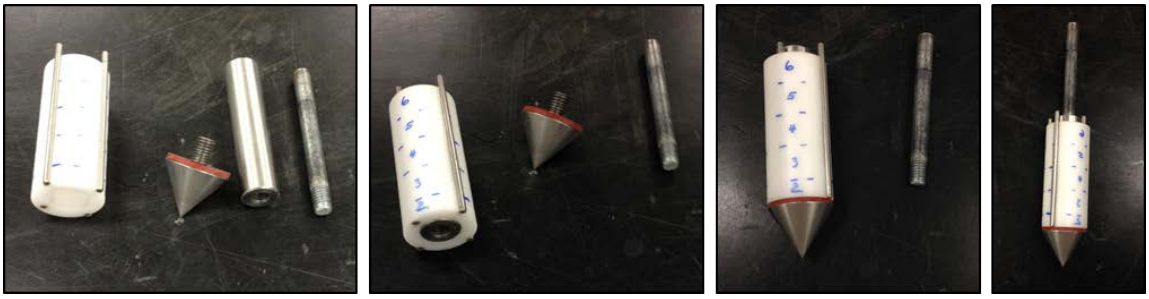

Figure 3.2 – Assembly of probe components. Components, as shown in leftmost picture, from left to right: Delrin® cylinder (D2 shown); CPT cone tip with rubber washer; shaft insert; and, probe-stabilizing rod.

The shaft insert was a stainless steel cylinder, 25.3 mm in diameter and 110 mm in length machined to fit tightly within the annulus of the Delrin® cylinder. Holes were drilled into either end of the insert and tapped to accommodate a 12.7 mm diameter bolt. A standard stainless steel CPT cone tip, with an attached 12.7 mm diameter shank, was inserted in one end of the insert, while a bolt or threaded rod was inserted in the other end for support. The angle of the cone tip was 60° from the plane perpendicular to the axis of the probe assembly. A 3 mm thick rubber washer was placed between the cone tip and the rods as an insulator to prevent the probe from "grounding out". The washer was cut to be slightly smaller than the diameter of the cone tip.

3.2.4 Conventional TDR Probes

Conventional two- and three-rod TDR probes, including sheathed variants, were used for comparison purposes against the Delrin® prototype probes. For the sheathed probe testing the unsheathed rod was connected to the grounded conductor. The two-rod probe consisted of two 4.8 mm diameter stainless steel rods that were 111 mm long. When the connecting steel clips were attached, these rods were capable of being inserted 100 mm into the soil (the same as the rods in the Delrin® prototype probe). A picture of the conventional two-rod probe is shown in Figure 3.3.

Figure 3.3 – Conventional two-rod probe. Sheathed rod on left, unsheathed on right.

The three-rod probe also consisted of 4.8 mm diameter stainless steel rods. The length of these rods was 110 mm. These rods were threaded on one end and screwed into the probe head. The centre rods were slightly misaligned during fabrication which led to those rods sitting slightly off-square to the probe head after being screwed in. As a consequence, the centre rod was only screwed in far enough to ensure stability while also keeping the distance between the rods as

similar as possible. In each case, the rods were screwed in to the point that at least 100 mm of the rod could be inserted into the soil. Figure 3.4 presents the conventional three-rod probe.

Figure 3.4 – Conventional three-rod probe. Sheathed variation shown (central rod sheathed).

The sheathing used for the two- and three-rod probes was polyolefin heat-shrink tubing. In order to apply this heat-shrink tubing, a length of tubing slightly longer than the rod was cut, allowing for possible longitudinal shrinkage during the heating process. The rod was then inserted less than 10 mm into the chuck of a drill press. Once the chuck was tightened, the length of heat-shrink tubing was passed on to the exposed length of the rod. The height of the drill press was adjusted to have the bottom of the tubing resting against a piece of wood, and the top of the tubing at the bottom of the chuck. Using a convertible power control unit connected to the power supply of the drill press, the drill press was turned on, and the power control adjusted so as keep the drill rotating sufficiently slowly. A heat gun was then used to shrink the tubing,

being careful to apply even heat along the length of the rod as it was turned by the drill. Once the tubing had been shrunk, it was trimmed to be flush with the bottom of the rod, and sufficiently down from the top to allow for electrical connection. Sheathing thickness for the two-rod probe was approximately 0.8 mm, and approximately 0.4 mm for the three-rod probe.

3.2.5 Cabling

An RG58A/U coaxial cable was used for connecting the TDR unit to the various probes. For the Delrin® prototypes and the two-rod probe a 5 m long cable was used. A male BNC connector was attached to one end of the cable for connecting to a female BNC-male SMA adapter on the TDR unit, while steel clips were connected on the other end for attaching to the rods. On the clip end of the cable the outer and inner conductors had been separated from each other approximately 0.17 m from the end, and sheathed with heat-shrink tubing. This was done to allow the steel clips to be attached to the cable, as well as to give sufficient flexibility for inserting the rods into soil.

In the case of the three-rod probe, a 1 m long coaxial cable was used. Male BNC connectors were attached to both ends of the cable for connecting to the TDR unit and probe head, while a female BNC connector was screwed to the probe head itself to receive the male connector. A short wire was soldered to the central conductor of the female connector to establish an electrical connection with the central rod.

A long (46 m), thin coaxial cable (RG174/U) which satisfies ConeTec's cabling requirements was also evaluated. Their preferred cable length is 45 m, and a standard RG58A/U cable would be too thick to fit in their standard cable bundle. Testing was abandoned after it was determined that the attenuation from the cable length was too great to obtain any data. While the cable could have been cut to a more typical length, it was decided to conduct all of the testing for this phase of the project with the standard RG58A/U cable instead. It is likely that the RG174/U cable would work for testing, although investigations would have to be made into the quality of the resulting TDR waveforms.

A Mohr CT100HF TDR unit was used for all of the testing in this project. The signal propogation velocity (V_p), a ratio of the signal velocity to the speed of light, can be adjusted on the TDR unit. This adjustment is used in cable testing to determine the distance to a fault in a particular cable. Since different cables have different properties, the V_p needs to be set appropriately to accurately find this distance. The V_p for the RG58A/U cable was manually set for this project by first measuring the length of the 5 m cable. After taking this measurement, the cable was connected to the TDR unit and the V_p adjusted until the "length" of the cable on the TDR waveform was the same as that of the cable measurement. This V_p was found to be 0.670933. After the V_p was determined, it was discovered that the fine adjustment of the V_p had not actually been properly completed. Had this not been the case, the "length" of the cable indicated on the unit would have been more accurate.

It is important to note that the V_p setting is not critical for the measurements being carried out in this study since Equation [2-3] accounts for any chosen V_p. For simplicity, the value could have been set to a standard value of "1" instead, although since some data had already been gathered, it was chosen to continue using the original V_p value for consistency.

3.3 Testing Materials

3.3.1 Laboratory Testing Overview

The prototype designs were evaluated in two stages of testing: reference solution testing and testing in sand and other prepared soils. The reference solutions included solutions with known dielectric constants (ethanol solutions), and known salinities (saline solutions), while the soils (tailings sand, fluidized fine tailings and Beaver Creek sand) had varying water contents and salinities. These various materials and the methods used to prepare and characterize them are described in this section.

3.3.2 Reference Solutions

Testing in reference solutions has the benefit of ensuring complete immersion without air gaps around the probes. These conditions should yield ideal results. Two types of reference solutions

were used in the first part of testing: ethanol-water mixtures and saline-water solutions. All solutions were mixed and stored in sealed 1 L glass mason jars that were approximately 140 mm tall, and 80 mm in inside diameter.

The choice to use ethanol-water mixtures for testing was based on the fact that ethanol and water each have unique dielectric constants that are quite different in magnitude from each other. As a result, a wide range of dielectric constant values can be created by changing their respective proportions in the mixtures, making for simple comparison of the TDR data to the theoretical values. Six mixtures were tested, including the following:

- De-ionized water (dielectric constant of 81.0);
- 20 percent ethanol, 80 percent de-ionized water (dielectric constant of 67.3);
- 40 percent ethanol, 60 percent de-ionized water (dielectric constant of 56.3);
- 60 percent ethanol, 40 percent de-ionized water (dielectric constant of 41.6);
- 80 percent ethanol, 20 percent de-ionized water (dielectric constant of 29.6); and,
- Pure ethanol (dielectric constant of 19.0) (all dielectric constant values based on Miyamoto and Chikushi (2006)).

Each of these solutions were mixed by mass; for example, a 20% ethanol solution would have 20% of its mass as ethanol and 80% as de-ionized water. The solutions were made inside a fume hood, with a container jar placed on an electronic balance. A pre-determined amount of de-ionized water was first added to the container. Ethanol was then added using a squeeze bottle until the total solution mass matched the pre-determined target mass for the solution. The solution was then transferred to the mason jar and covered immediately to prevent evaporation.

Saline solutions at six different concentrations were also tested (Table 3.1). The primary purpose of testing in the saline solutions was to evaluate the maximum level of salinity for which the prototype probes were able to return an interpretable signal. These solutions were made by adding the required mass of sodium chloride to a 1 L volumetric flask, then adding de-ionized

water to bring the solution level up to the 1 L mark on the flask. The solutions were thoroughly mixed and transferred to the mason jars.

Table 3.1 – Electrical conductivity of saline solutions.

Saline Solution Concentration (g/L)	Electrical Conductivity (dS/m)	Temperature (°C)
5	9.13	24.3
10	17.4	24.7
15	26.2	24.6
20	33.4	24.9
25	41.2	24.8
30	48.6	24.7

For the purpose of complete testing, the prototypes were also tested in air, which has a dielectric constant of 1 (Jones et al. 2002, Moret et al. 2006).

3.3.3 Oil Sands Tailings Sand

The primary soil used in testing was a tailings sand collected from a dry beach on the South West Sand Storage tailings dyke at Syncrude Canada's Mildred Lake mine site. This deposit is formed by hydraulic deposition with process water, whose concentrations of dissolved solids typically range between 2.50 and 3.50 g/L (W. Zubot, personal communication 2014). The deposit is flushed over time by recharging meteoric water. Tailings sand was used in testing since these soils represent a significant portion of the reclaimed soil at Syncrude's site, and as a result would be commonly encountered in the field. Testing was done in tailings sand with both non-elevated and elevated salinities. In the case of the non-elevated salinity sand, testing was done at a number of different water contents, while the elevated salinity sand was tested at the same water content but with varying levels of salinity. Each of these tests involved packing the sand around the prototype probes.

3.3.3.1 Non-elevated Salinity Tailings Sand

All of the sand used for testing was air-dried and then mixed thoroughly in a drum pulverizer run without the ball bearings prior to being stored in three 20 L buckets. Air-drying was undertaken by spreading the sand over a sheet of plastic no thicker than approximately 60 mm. The sand was allowed to dry over a few days, intermittently mixing it by hand, until no wet pockets of sand remained.

The sand was prepared at a number of target gravimetric water contents: air-dried, 7%, 14%, and 19%. Testing at higher water contents was avoided in order to prevent near-saturated conditions in which the sand exhibits undesirable slurry-like properties. Preparing the sand at each of the target water contents involved adding an appropriate amount of air-dried sand to a 20 L bucket on an electronic scale followed by the necessary amount of water to arrive at the desired gravimetric water content.

Thorough mixing of the sand and water was done using a clean plastic scoop, after which time the bucket's tight-fitting lid was put on. In order to ensure uniform water content throughout the sand, the mixture was allowed to sit overnight to equilibrate. Following the equilibration period, the sand was mixed again, and a 60 g to 100 g sample removed to confirm the actual gravimetric water content. This sample was placed in a clean tare container of known mass, weighed and placed in the oven at 105°C for 24 hours to dry. After drying, the mass of the container was again recorded, and the actual gravimetric water content calculated.

In all cases, the actual gravimetric water content was somewhat lower than the target gravimetric water content. This may have been due to absorption of the water into the walls of the plastic buckets, or water evaporating through the bucket's lid. The actual gravimetric water content was the value used for testing.

It should be noted that air-dried rather than oven-dried sand was used throughout testing since logistically it was far easier to air dry this amount of sand than to oven dry it. Any reduction in water content gained by oven drying was seen as negligible.

Characterizing the Tailings Sand

The particle size distribution (PSD) and the leachable salt content of the sand was measured in the laboratory. The PSD curve for the sand (Figure 3.5) was obtained by dry sieving more than 300 g of dry sand through 9.5 mm, 4.75 mm and 2.00 mm sieves. The stack of sieves was shaken for 10 minutes. A representative sample of the sand passing the 2.00 mm sieve (e.g. approximately 3 g) was run through a Malvern Mastersizer 2000 laser diffraction particle size analyzer following procedure recommendations set out by Sperazza et al. (2004) with some minor modifications. These modifications included a laser obscuration of 10 to 15% as opposed to 15 to 20%, a dispersion pump speed of 2000 rotations per minute (rpm) as opposed to 2200 rpm (although still within the recommended range of speeds), an ultrasonic tip displacement of 3 μm as opposed to 10 μm, and a sample analysis time of 20 seconds as opposed to 12 seconds. The sample was analyzed three times, with the reported results being the average of these three analyses. This analysis characterized the sand as being a poorly graded sand using the Unified Soil Classification System (USCS).

The leachable salt content was determined using a saturated extract test on a representative sample based on a slightly modified method from Bower and Wilcox (1965). A sample of the sand was oven dried (105°C for at least 24 hours) and then 15.77 g of the sand was added to a clean 50 mL test tube followed by 31.54 g of de-ionized water (a 2:1 ratio of water to sand by mass). Bower and Wilcox (1965) used only 1:1 or 5:1 ratios and they also recommend against oven-drying beforehand, a point that was recognized after the fact. Four test tubes were filled in this manner. The test tubes were capped and shaken vigorously by hand to mix the slurry. This process was repeated a number of times over the course of a few days, allowing the slurry to have a sufficient amount of contact time. This differed from Bower and Wilcox (1965), who suggested four separate shakings of the slurry at 30 minute intervals. No sodium hexametaphosphate solution was added as part of this test either. Following this period, the test tubes were put in a centrifuge and centrifuged at 5000 rpm for 15 minutes at 21°C in order to separate the supernatant from the sand. Centrifuging of the sample was not discussed in Bower and Wilcox (1965). The supernatant was then removed from the test tubes with a pipette and placed in a clean, covered glass jar. A Hach electrical conductivity meter was then used to determine the electrical conductivity of the supernatant.

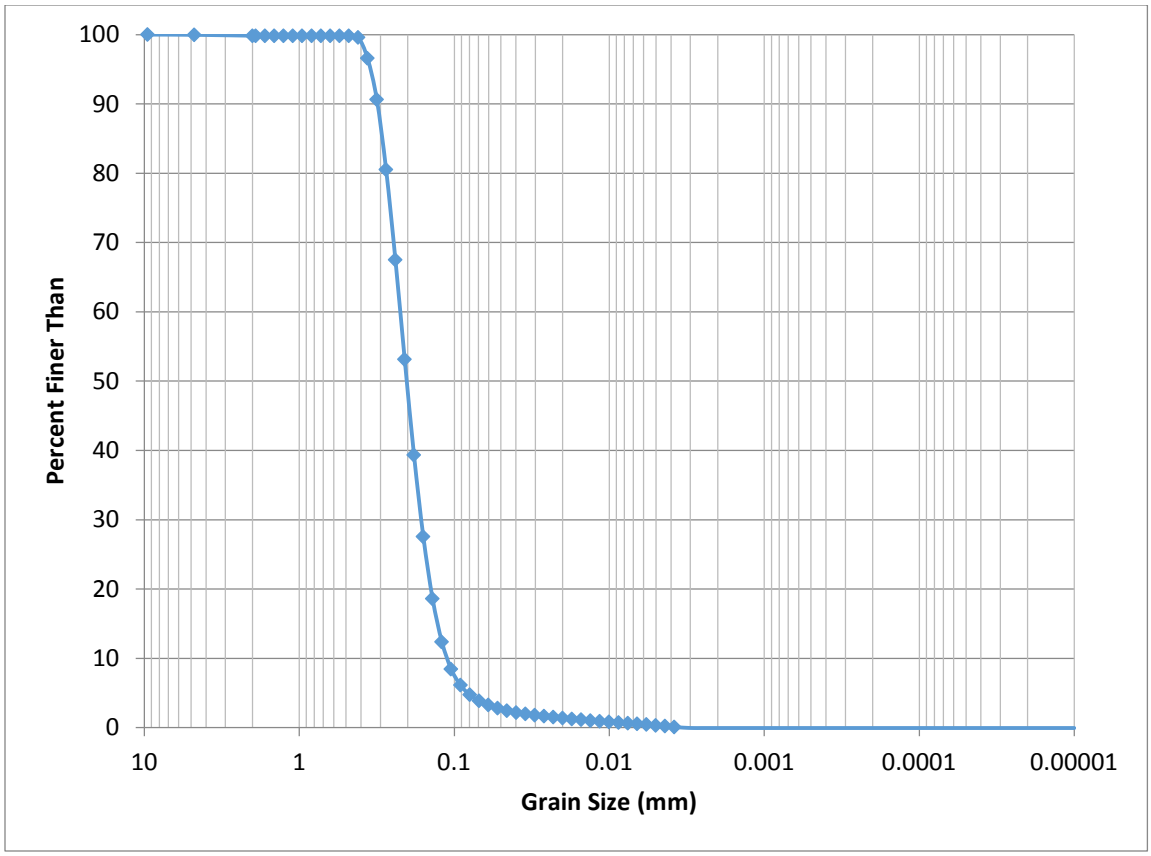

Figure 3.5 – Particle size distribution curve for Syncrude oil sands tailings sand.

In order to determine the TDS, the supernatant was first passed through the glass-fibre filter disk of a vacuum flask filtration apparatus, followed by the use of de-ionized water to wash down the sides of the filter funnel. Pipettes were used to measure the volume of supernatant transferred to the filtration apparatus. As there was too much filtrate to fit in one crucible, the filtrate was transferred to two cleaned, dried and weighed crucibles. The crucibles were put into the oven at 178°C, which was within the range suggested by American Public Health Association et al. (2005). After the water had evaporated, the crucibles were moved to a desiccator. The mass of each crucible was measured at least three times with an electronic balance after they were placed in the desiccator to ensure their masses had stabilized. The last mass was taken at least 24 hours after the evaporation process began. Each of the masses was obtained from an electronic balance that had a readability of 0.0001 g.

The amount of total dissolved solids (TDS) in this sample was calculated using the following formula:

$$TDS = \left(\frac{mass_{initial} - mass_{final}}{sample\ volume}\right) \quad [3\text{-}1]$$

where $mass_{initial}$ is the sum of the intial masses of the crucibles with the filtrate, $mass_{final}$ is the sum of the stabilized masses of the crucibles after drying, and the sample volume is the volume of supernatant initially transferred into the filtration apparatus. During the period of desiccation, there were some instances where the crucibles' masses would increase slightly over consecutive measurements rather than remaining constant. Assuming this to be the result of fluctuations in the balance, the final mass used in Equation [3-1] was the sum of the average measurements for each of the two crucibles. No decrease in mass was observed in any of the consecutive measurements. It should also be noted that the oven's temperature was seen to fluctuate on some occasions outside of the recommended tolerance. The duration of these fluctuations was unknown.

The TDS of the solution was found to be 0.11 g/L, while the electrical conductivity was 0.14 dS/m.

3.3.3.2 Elevated Salinity Tailings Sand

The sand with elevated salinity was prepared from air dried samples of non-saline sand. Target elevated salinities for the sand of 2.5, 5.0 and 10.0 g/L, in terms of TDS, were chosen for the testing. A maximum salinity of 10 g/L was chosen based on the fact that the sheathed refined prototype probes would "short out" in the salt solutions around this salinity. The other two salinities were chosen because they were one half and one quarter of the maximum salinity. A target gravimetric water content of 19% was chosen, as it was slightly easier to compact the sand at higher water contents. Using the previously determined value for the tailings sand's in situ TDS, additional amounts of salt were added to the water to obtain these target levels of salinity. It was assumed that the TDS was comprised completely of salt.

The respective salt solutions were made using a 50 g/L stock solution which was prepared in a volumetric cylinder with de-ionized water and table salt. For each solution, an appropriate amount of stock solution was mixed with de-ionized water in order to arrive at the necessary volume and concentration of solution to add to the dry sand. It was assumed that the density of the salt solution was equivalent to that of water.

Adding and mixing the salt solution with the sand was done in the same manner as the non-saline sand mixtures. Samples of the wetted sand were also collected after equilibration to confirm the actual gravimetric water content. In all but one case, as with the non-saline sand mixtures, the sand was dried in the oven. In the exceptional case, the 2.5 g/L sand mixture, confirmation of the gravimetric water content was done by drying the sample in the microwave oven as time was critical. The procedure from ASTM D4643-08 (American Society for Testing and Materials 2008), which describes this method, was followed for this testing. It should be noted that the samples for the other mixtures were kept in the oven for greater than 24 hours before recording their dried mass. This was done in order to account for any reduction in drying rate associated with elevated salt solutions (Ho 1985).

3.3.4 Fluidized Fine Tailings

Limited testing was also undertaken on a sample of fluidized fine tailings (FFT) provided by Syncrude. FFT is a waste product from the process of extracting bitumen from the oil sands and a substantial portion of the waste produced at an oil sands mine. FFT is a thickened mixture of clay and silt particles in water, with traces of bitumen and naphtha also being present (Syncrude Canada Ltd. 2012). The water content of the FFT sample was very high (e.g. up to 190% gravimetric water content), allowing the probe to be evaluated in both an elevated electrical conductivity and a high water content testing medium. The fluidity of the FFT also allowed the probe to be inserted directly into the medium, similar to how it would be inserted in the field.

Testing was done on the FFT at five different water contents. Three of the water content tests used sub-samples taken from different levels of the 20 L bucket containing the original sample. This could be done as settlement had occurred in the bucket over the period of a few months.

However, despite the fact that the gravimetric water content of these sub-samples ranged between 190 and 132%, the actual difference in volumetric water content was minimal. As a result, two of the sub-samples were dried to obtain a greater spread in the water contents. Drying took place partly in a fume hood to accelerate drying. One of the sub-samples was tested after eight days of drying, while the last (i.e. driest) test was conducted after one month of drying. In order to have enough depth of FFT to fully submerge the TDR probes, the last sub-sample actually was a mixture of the original two sub-samples due to the volume loss from drying. All of the sub-samples were placed in 4 L buckets for testing and drying, and all sub-samples were stirred thoroughly prior to testing.

Electrical conductivity measurements of the wettest and driest sub-samples were performed using a Hach electrical conductivity meter. The conductivity of these sub-samples were 2.07 and 2.35 dS/m, respectively.

3.3.5 Push-Test Sand

Beaver Creek sand was used for a simple test at the end of the testing program to assess the performance of the probe if it was pushed into a typical soil profile rather than having soil packed around it. Performing a test in this manner was important since the finished probe will be used in this way in the field. This testing was done at the end of program, and as such there was not enough "clean" (i.e. non-elevated salinity) tailings sand to be used for the test. As a result, readily available Beaver Creek sand was used instead. Electrical conductivity and TDS tests were conducted on this sand using the saturated extract test described above.

Beaver Creek sand is a calcareous fine to medium sand that is characterized according to the USCS as a poorly sorted sand. It originated as a natural aeolian deposit, and was obtained southeast of Saskatoon, Saskatchewan. It has been used in numerous research studies including those of Wilson (1990), Bruch (1993), Wilson et al. (1994) and Huang et al. (2013). Electrical conductivity of the solution from the saturated extract test was found to be 0.11 dS/m, and the TDS was 0.10 g/L. The fact that the Beaver Creek sand was very similar to the tailings sand in terms of electrical conductivity and TDS was somewhat surprising since the tailings sand would

be exposed to the highly saline process water. However, since the tailings sand was collected from a dry beach the salts from the sand would have been flushed out through the infiltration of rain and snowmelt. This would have resulted in the observed tailings sand values being lower than expected.

Three lifts of sand were used in the testing: two at gravimetric water contents of 17% and one at 7%. The sand-water mixtures were mixed in the same fashion as the tailings sand mixtures, although due to the volume of water necessary for this test, tap water was used rather than distilled water. No efforts were made to verify the gravimetric water contents of the sand after mixing due to the time-sensitive nature of the push-test.

3.4 Prototype Testing

Testing began with a number of preliminary prototypes in reference solutions, followed by refining the vertical rod prototype for advanced testing. This advanced testing for all three variations (D1, D2 and D3) began in reference solutions, followed by testing in compacted tailings sand of both natural in-situ and elevated salinity. Prototype evaluation for this phase of testing concluded with tests of the D2 probe in FFT slurries and a push-test into Beaver Creek sand. All testing was done at room temperature in the laboratory. This section describes how the tests were set up and conducted, and how the testing conditions were confirmed.

3.4.1 Reference Solution Testing

As previously discussed, testing was done with both prototype probes and conventional probes; conventional probes were used to confirm the results from the prototypes. Sheathed variants of the probes were tested in both the ethanol and saline solutions, while unsheathed variants were only successfully tested in the ethanol solutions.

3.4.1.1 Insertion of Probes in Reference Solutions

Prior to testing, each jar of solution was shaken to ensure the uniformity of the solution. The respective prototype probe was then inserted into the reference solution until the top of the probe body was flush with the top of the solution. Insertion of the preliminary probes involved holding

on to the wires of the cable as the measurement was done. Testing with the refined prototypes, however, involved screwing a 12.7 mm diameter 71 mm long bolt part way into the shaft insert and holding onto the bolt while the measurement was done. Nitrile gloves were used in both cases for personal protection and to prevent skin contact on the probe's electrical connections, which could influence the results. During the refined prototype testing the cone tip was not installed so that the probe could be easily submerged in the jar. Testing of the conventional probes was done in a similar way, although for the two-rod probes a piece of cardboard was taped to the split wires on the cable just above the clips to control the spacing. The conventional three-rod probes were inserted until the plastic portion of the probe head was just in contact with the top of the solutions.

Testing in air was simply done by holding each of the respective probes in the air.

The inside diameter of the mason jars used in the solution testing was approximately 80 mm, which would not fully contain the electrical field generated by the probes according to theory set out by Knight et al. (1994). However, given that these were reference solutions (fluids) rather than soils, and the test was primarily related to performance relative to the standard probes, it was felt that truncating the field would not be critical.

3.4.1.2 Probe Connections

In the case of the preliminary prototype probes, the steel clips on the end of the coaxial cable were attached to leads connected to the desired rods. For the refined vertical rod prototypes, connections for the two-rod configurations were typically made with the steel clips installed vertically on the end of the rods, as shown in Figure 3.6. Connections for the unsheathed two-rod configuration were made between the two opposing unsheathed rods, while for the sheathed configuration the opposing sheathed and unsheathed rods were connected. In the case of the sheathed probe configuration, the grounded conductor (outer conductor) of the coaxial cable was connected to the unsheathed rod, while the "live" conductor (inner conductor) was connected to the sheathed rod. In addition to the reference solutions, this method of electrically connecting the refined prototype probes was typical for the tailings sand as well as the FFT.

Figure 3.6 – Typical two-rod connection on Delrin® prototype.

Connections for the three-rod configurations of the refined prototypes involved the use of a "jumper" cable which was placed on the two opposing unsheathed rods, as shown in Figure 3.7. This jumper cable was then connected to the ground conductor, while the live conductor was connected to either the remaining unsheathed or sheathed rod. This was also the typical connection methodology for the tailings sand and FFT testing.

3.4.2 Controlled Compaction Testing of Tailings Sand

All three refined prototype probes (D1, D2 and D3) were tested in tailings sand at various water contents and salinities. This section describes the setup of the testing as well as the methodology of the testing itself, and how the testing conditions were confirmed.

Figure 3.7 – Typical three-rod connection on Delrin® prototype with "jumper cable" shown.

3.4.2.1 Testing Equipment and Set Up

In order to properly evaluate the response of the prototype probes to the various water contents and salinities it was necessary to create a column of sand with a uniform volumetric water content. This was done by compacting the sand-water mixtures around the probe in a cylinder. The sand was placed and compacted in 6 lifts to ensure a relatively uniform soil profile. Compaction was undertaken using a hydraulic press (Instron 600DX) to push a compaction plate down into the cylinder. A description of the entire compaction assembly used in this process is done through a series of pictures. The compaction apparatus as a whole is presented in Figure 3.8 and shows the components of the hydraulic press, the compaction plate, and the cylinder.

The first step in setting up the assembly was to mount the compaction plate to the crosshead. This was accomplished through the use of a threaded receiver, which accepts a 12.7 mm bolt. The threaded receiver was secured in the crosshead by means of an Allen screw, shown in Figure 3.9. After the receiver was secured, the compaction plate assembly was then attached to the receiver with the bolt and a number of washers, as shown in Figure 3.10. The compaction plate as shown in the figure was set up to compact a cylinder with a Delrin® prototype probe in place, as shown by the open probe access hole. Insertion of conventional probes, however, would be done after compaction, so an access hole in the middle of the plate was not required for packing of those cylinders. Consequently, the access hole in the middle of the plate was closed by adding

an additional plate which filled the hole with a wooden plug. The closed hole is shown in Figure 3.11.

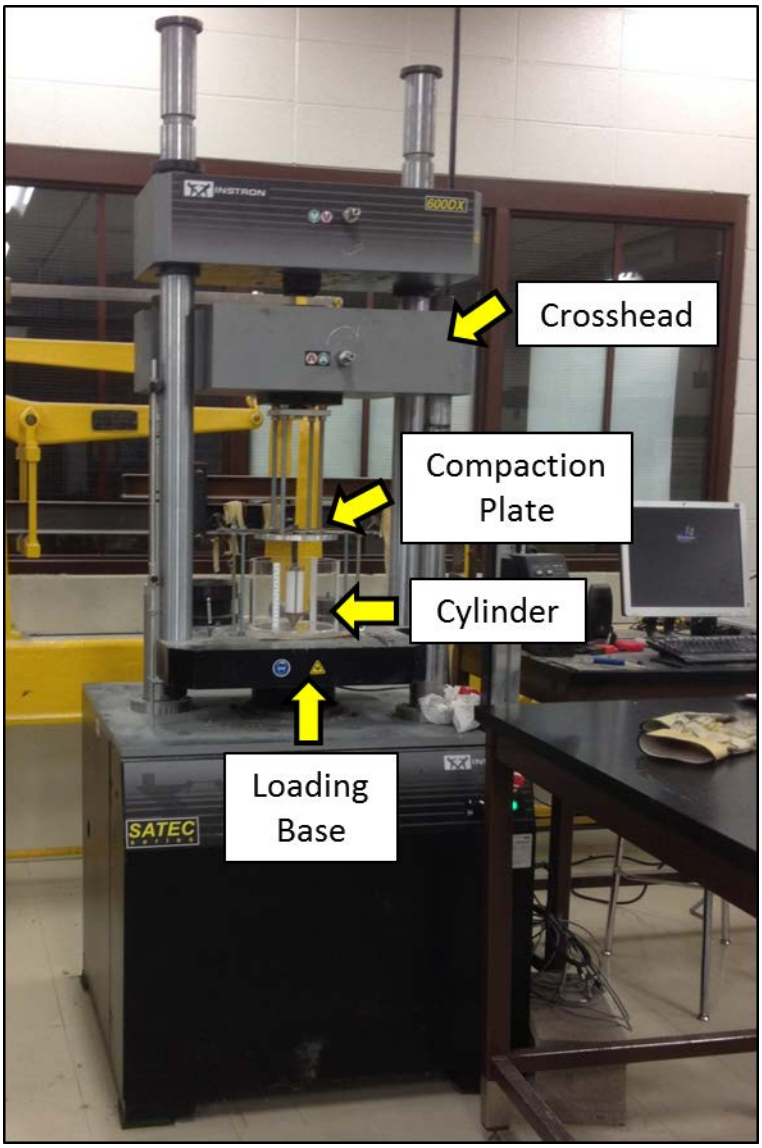

Figure 3.8 – Compaction apparatus.

Figure 3.9 – Threaded receiver secured in place with Allen screw.

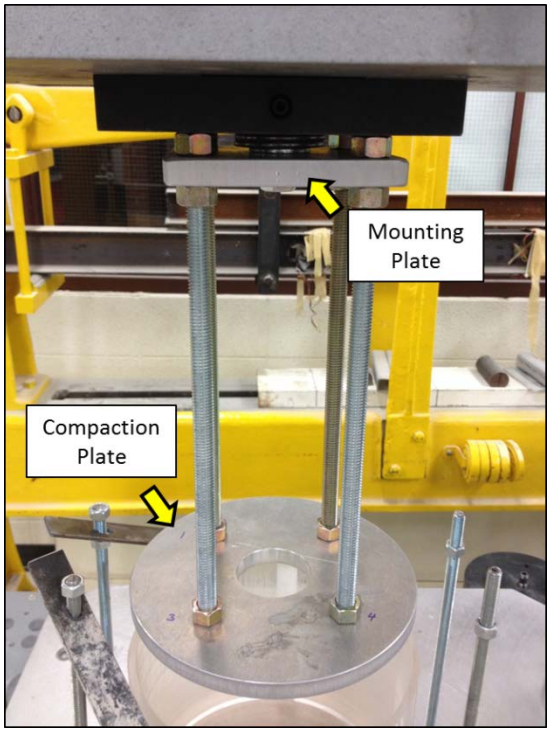

Figure 3.10 – Compaction plate assembly mounted to crosshead.

Figure 3.11 – Bottom of compaction plate with wooden plug to close access hole for conventional probe testing.

The aluminum compaction plate was 202.2 mm in diameter and 12.7 mm thick. Four threaded holes were tapped in the compaction plate. These holes were spaced around the large 53.8 mm diameter hole that accommodated the Delrin® probe. The additional plate which was used to close the probe access hole consisted of a 6 mm thick steel plate, with a 12.7 mm thick, 53.5 mm diameter plywood disc epoxied to the plate which closed the hole. Four 310 mm long, 12.7 mm diameter threaded rods were threaded into the tapped holes in the compaction plate. They were screwed into the plate until they were flush with its bottom. A 123 mm-square, 13.3 mm thick aluminum mounting plate was attached to the other end of the threaded rods through 12.7 mm diameter holes drilled in the plate. These holes corresponded with the location of the holes in the compaction plate. Nuts were used to secure the threaded rods on both sides of the mounting plate, and on the top of the compaction plate. A central hole in the mounting plate was also drilled, through which the 12.7 mm bolt passed to mount the assembly to the crosshead.

A very tight fit existed between the compaction plate and the cylinder. In order to minimize the chance of the compaction plate binding in the cylinder during compression, and possibly breaking it, the plates were set as close to parallel as possible. This involved placing a level across the mounting plate and the compaction plate in the two axes of the plates. Adjustments

were made by adjusting the nuts on the mounting plate, or the threaded rod insertion depth on the compaction plate.

Following the mounting of the compaction plate assembly, the cylinder was placed on the loading base. In the case of the Delrin® probe prototype testing, a probe-securing frame was also installed in threaded holes tapped in the loading base to secure the probe in a vertical position. The frame was made from two pieces of steel strapping approximately 25 mm wide, 380 mm long, and 3 mm thick. As a whole, the frame was secured through slotted holes in the strapping to the loading base with four 9.5 mm diameter threaded rods. Holes were also drilled in the middle of each piece of strapping where the two pieces intersected. Through these holes the probe-stabilizing rod, a 12.7 mm diameter smooth rod, could be passed. The probe assembly was then screwed onto the stabilizing rod, and the probe was thus secured horizontally, as shown in Figure 3.12. The use of slotted holes, loose nut tightening and a smooth rod helped to maintain freedom of movement in the system, which prevented binding in the cylinder.

The cylinder into which the sand was placed and compacted was made of acrylic. An acrylic plate 12 mm thick was attached to the bottom of a 202.2 mm inside-diameter acrylic tube with 6.5 mm thick walls. A small hole was drilled in the middle of the base of the cylinder in which the probe's cone tip could sit. This kept the cone tip stationary during compaction.

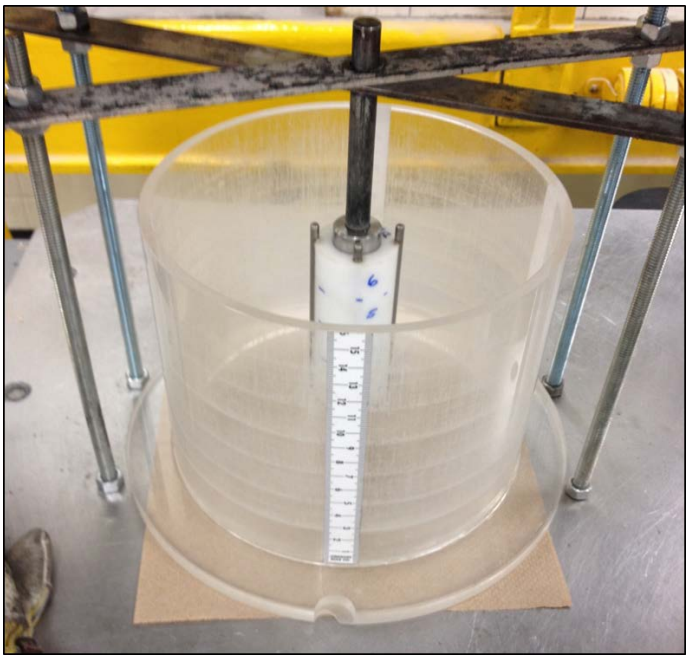

Figure 3.12 – Delrin® prototype probe inserted in probe-stabilizing frame.

3.4.2.2 Preparation of Testing Medium

The initial target dry density used for the testing was 1.60 g/cm^3; however, it was found that this was difficult to achieve for the air-dried sand. As a result, the target dry density was adjusted at the start of the 7% gravimetric water content sand testing to be 1.40 g/cm^3. This dry density was used for the remainder of the sand testing.

All six lifts were divided up evenly in thickness according to the increments of the measuring tape adhered to the outside of the cylinder. The top of the Delrin® prototype probe sat at the 13.3 cm mark of the cylinder's measuring tape, so the top of the lifts were set to the following points on the cylinder: 2.2 cm, 4.4 cm, 6.6 cm, 8.8 cm, 11.0 cm and 13.3 cm.

The mass of sand added in each lift was determined from the target bulk density and a depth-volume relationship developed for the cylinder. The particular bulk density for a given water content was calculated using the actual gravimetric water content determined after initial mixing of the sand and water. The same bulk density value was used for all testing at a given water content. Evaporation from the sand during the course of testing was assumed to be negligible.

For placing a lift of sand, an appropriate amount of sand mixture was added to a bowl on an electronic balance and transferred to the cylinder. The sand was distributed around the interior of the cylinder, with a disposable plastic fork used to level the top of the sand. In an effort to control the uniformity of the wet sand lift's density, the fork was then "poked" into the sand to break up any clumps. The compaction plate was then lowered onto the sand in order to compact the lift to its appropriate thickness. A comprehensive description of the compaction procedure is provided in Appendix A.

Since the water content was assumed to be constant for all the sand in a given test, controlling evaporative losses during the testing process was critical. The 20 L buckets that were used to store the sand mixtures had tight-fitting lids which were kept closed as much as possible. When sand was transferred to the bowl on the electronic balance, a cover was placed over it to limit evaporation when masses were not being recorded. During the packing of the lifts, the compaction plate limited the exposure of the sand to the drier room air. A ventilation duct that was in the vicinity of the apparatus was also taped shut to reduce air movement in the area.

When compaction was not actively taking place, a snug, flexible cap was placed over the cylinder. However, if there was a longer period between lift placement, a tighter-fitting, hard cap was placed over the cylinder. In cases where there was an even longer period between lift placement, for instance overnight, the hard cap would be duct taped to the cylinder. Containers of water would also be placed on the top of the sand to maintain a very high relative humidity inside the cylinder, thereby limiting evaporation.

3.4.2.3 Test Description

Prototype Probe Testing and Re-Insertion

The prototype probes were placed in the cylinder prior to sand compaction; however, re-packing the cylinder for each individual prototype at a given water content was found to be very time consuming. Consequently, an alternative method was employed in which the first probe used was removed and replaced with a second probe with re-compaction. In this re-insertion procedure, the cylinder was originally packed with the D1 prototype probe in place. Then, the

D1 probe was removed with the D2 probe inserted in its place, followed by the D3 probe. All probes were inserted in the same orientation. Progressing through increasing amounts of rod exposure in the same orientation allowed the expansion of the rod channels left in the sand from the previous probe. This minimized the formation of air gaps and also produced better test results. After the D3 probe was removed, the D1 probe was re-inserted to confirm the initial test results. However, the D1 probe was rotated approximately 45° about the insertion shaft so full contact with the sand could be achieved. In the case of the saline sand testing, only the D2 probe was tested, and it was re-inserted twice to confirm the results. On the second re-insertion, the probe was rotated 45°. It was necessary to ensure that the cylinder was not damaged by excessive force on re-insertion of the probes.

Re-insertion of the probes was achieved using a drill chuck held in place by friction in the hole of the crosshead which held the compaction plate assembly's threaded receiver. This is shown in Figure 3.13. Once inserted, the drill chuck was aligned to be as plumb as possible. The jaws of the drill chuck would then be closed around the probe-stabilizing rod for removing and re-inserting the respective probes. The compaction plate assembly and the probe-securing frame were removed for this procedure; however, where rod clearance allowed, the compaction plate assembly would be re-attached following re-insertion of a given probe. This was done to re-compact any sand that may have been loosened during probe removal. If clearance around the probe was not adequate, as was often the case for the D3 probe, any disturbed sand would be pushed gently back into place by fingertips or a small capped PVC pipe. Care was taken to not increase the density of the packed sand. In some cases a small amount of extra sand was gently placed around the top of the probe to close any air gaps that had formed and similarly packed into place.

A more comprehensive description of the procedure used to remove and re-insert the probes is provided in Appendix B.

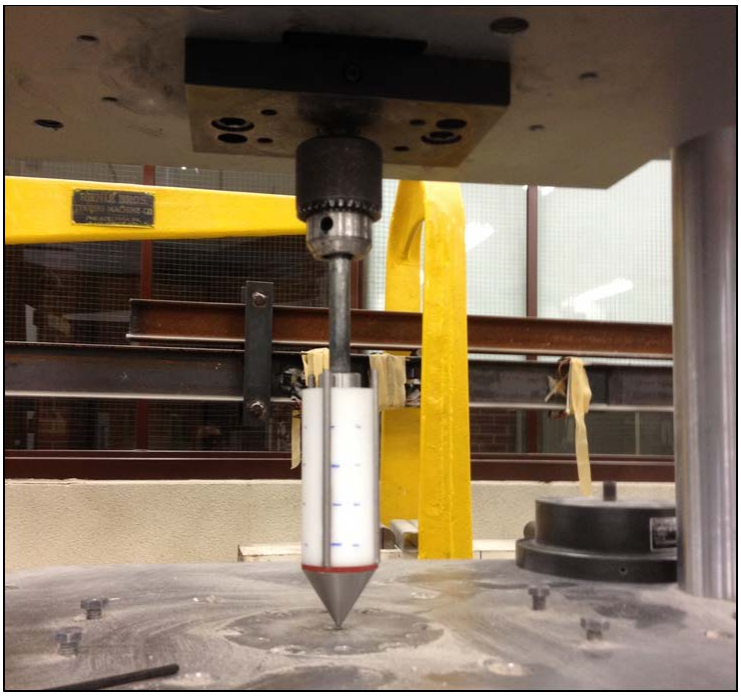

Figure 3.13 – Drill chuck holding Delrin® probe for extraction and re-insertion procedure.

Conventional Probe Testing

Testing of conventional probes in the various sand mixtures was done following compaction of the sand in the cylinder. For the sake of efficiency, each of the conventional probe configurations were tested in the same packed cylinder. Choosing the rod insertion points required consideration of electrical field distribution in order to avoid interference from either the cylinder walls or air gaps left from the insertion of other probes. Knight et al. (1994) suggests 95% of the electrical field's full cylinder of influence as being a reasonable approximation to the full field. As a result, the probes' insertion locations were chosen based on having at least an uninterrupted 95% cylinder of influence. The insertion pattern for the various probes is shown in Figure 3.14.

Since the two-rod probe has a larger cylinder of influence than the three-rod probe, the two-rod probe was inserted first to avoid air gaps generated by the three-rod probes. The unsheathed rods were inserted by pushing them vertically into the sand in a slow, smooth fashion to a depth of

100 mm. Following testing, one of the rods was slowly and smoothly extracted, and a sheathed rod similarly re-inserted in its place to complete the sheathed probe testing.

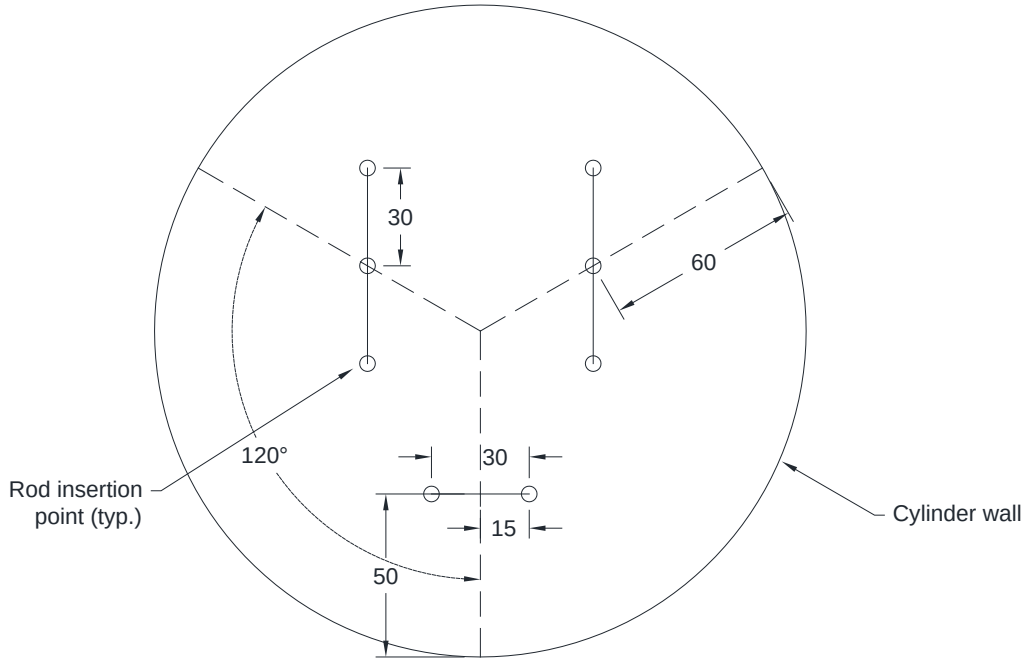

Figure 3.14 – Conventional probe insertion diagram. All dimensions in mm.

Insertion of the two variants of the three-rod Zegelin-type probes (i.e. sheathed and unsheathed) were done 120° from each other and the two-rod insertion site. The axes of the three-rod probes were parallel to each other and perpendicular to the two-rod probe rod axis in order to avoid interference from air gaps or the cylinder wall. Separate insertions for the sheathed and unsheathed probes were done, with the central rod switched from the unsheathed to the sheathed rods from one insertion to the next. As previously discussed, the threads for the central rods were cut slightly off-square, and as a result the central rods were slightly out of plane with the outside rods. Efforts were made, however, to make this difference in planarity as small as possible.

Inserting the three-rod probes had to be carefully done, as unlike the two-rod probe, all the rods are simultaneously inserted. The probe was pushed gently and steadily vertically into the sand until the probe head contacted the top of the sand. Care was taken to avoid introducing air gaps during insertion by avoiding changes in insertion direction and minimizing non-planarity of the rods.

Determining the insertion length of the three-rod probes was done by measuring the length of the rods from the probe head's plastic insert to the tip of the rods. This insert, which the central rod was connected through, sat slightly further out from the rest of the probe body. As such, it would be the point at which the probe would stop when it was inserted in the sand. In general the insertion length was uniform for each rod, but if not an average length was used for Equation [2-3].

Probe Connection Configurations

In later stages of the saline sand testing, horizontal connection configurations, as opposed to vertical ones, were attempted on the prototype and two-rod probes. This was done to determine if the increased connector contact area available from the horizontal orientation of the steel clips would affect the results. Later stages of testing also investigated the effect of rod spacing using adjacent, as opposed to opposite, rods in the two-rod probe configurations. This was explored for the fact that there may have been a difference in the electric field generated between closer rods than those further away from each other. A picture showing the horizontal connector orientation and the close rod spacing is shown in Figure 3.15.

Figure 3.15 – Closely-spaced two-rod horizontally-oriented connection on Delrin® prototype.

Concerns were also raised late in testing about the difference in cable length created by the jumper cable, since the jumper cable effectively increased the length of one side of the connection. To investigate this, a "secondary" jumper cable was introduced. This cable was comprised of a conductor and a single alligator clip combination similar to the original "primary" cable, but half the length. Testing with the secondary jumper cable was only done in a re-testing of the ethanol reference solutions given the stage of the project when the concerns were raised. The two jumper cables are shown in Figure 3.16. Care had to be taken during testing to ensure the jumper cables did not ground out on the 12.7 mm bolt or the shaft insert.

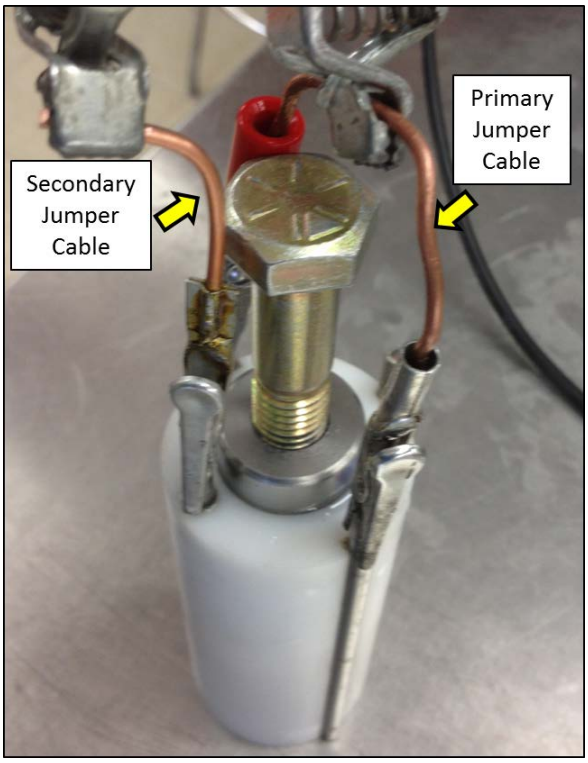

Figure 3.16 – Three-rod connection on Delrin® prototype using "primary" and "secondary" jumper cables.

Water Content Verification Testing

Following TDR testing, samples of the sand were collected using a flat-bottomed scoop and used to determine the gravimetric water content of the lifts. The scoop was kept close to level during the removal of the sand in order to track which lift the sand had come from. Samples were originally obtained for Lifts 2, 4 and 6; however, this was changed later to include Lifts 2 through 6 in order to obtain a more representative sampling of the water contents. Lift 1 was not sampled as it was below the TDR rods. The procedure for determining the gravimetric water content of the sand was the same as was done following the initial mixing of the sand and water. In the case of the saline sand, however, the mass of the samples was recorded multiple times to ensure it had stabilized after a period of drying of more than 24 hours.

Some variability in the repeated electronic balance readings occurred during the saline sand testing. Despite sheltering the scale from the effects of air currents in the room, the recorded

masses of the same samples varied up to 0.10 g. This apparent change in mass was not due to further drying of the sand. Changing balances was considered at that point; however, this was dismissed as introducing more uncertainty was not desired. While this uncertainty was concerning, the maximum effect these variations would have on the calculated gravimetric water content would be an increase or decrease of approximately 0.1%. This was seen to be negligible in terms of the results, and so the final reading was used for calculations.

3.4.3 FFT Testing

Testing in the FFT took place using the D2 prototype probe and a conventional three-rod Zegelin-type probe with unsheathed and sheathed rods. As with testing in the previous media, the conventional three-rod probes were inserted until the plastic portion of the probe head was just in contact with the top of the FFT. Nitrile gloves were also worn for protective reasons and to prevent skin contact on the probe's electrical connections, which could influence the results. Due to the nature of testing in slurries, only vertically-oriented connections on the prototype probe were employed for this testing. A picture of the FFT insertion method is shown in Figure 3.17.

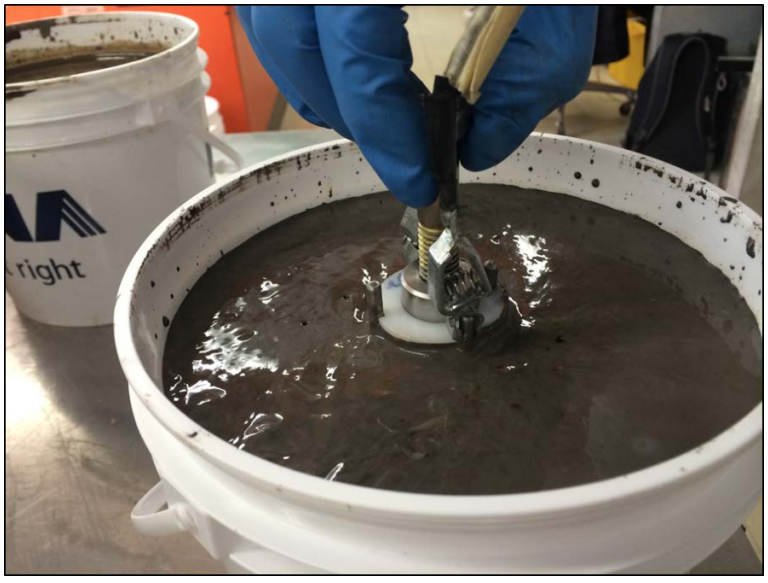

Figure 3.17 – Insertion of Delrin® prototype probe into FFT. Note nitrile glove holding bolt to prevent electrical interference in the reading.

Given the nature of FFT, determination of volumetric water content was challenging since it was not packed at a specific bulk density. As a result, a simplistic method was adopted that involved assuming densities of the solid and liquid phases of the FFT together with their respective proportions. Since the volumetric water content is essentially the proportion of the volume of water to the total volume of soil, the equation used was in the form:

$$\theta = \frac{\left(\frac{m_l}{\rho_l}\right)}{\left[\left(\frac{m_l}{\rho_l}\right) + \left(\frac{m_s}{\rho_s}\right)\right]} \qquad [3\text{-}2]$$

where m_l is the mass of liquid and m_s is the mass of solids, as obtained from gravimetric water content testing. Densities were assumed to be 1.00 g/cm^3 for the liquid phase, ρ_l, with a further assumption that the amount of residual hydrocarbons was negligible, and 2.65 g/cm^3 for the solid phase, ρ_s (Li et al. 2014). The FFT was assumed to be saturated, with only two phases present.

3.4.4 Push-Testing in Beaver Creek Sand

The final stage of testing involved pushing a modified D2 probe into a profile of Beaver Creek sand placed at various water contents. The setup and methodology for the test, as well as the details of the probe modifications and the confirmation of testing conditions are described in this section.

3.4.4.1 Testing Equipment and Setup

Conducting a push-test was done to determine probe sensitivity to variations in water content with depth, essentially mimicking field use of the finished device. In this test, a plastic garbage container approximately 0.4 m in diameter and 0.6 m in height was filled in three lifts with Beaver Creek sand. The bottom lift was approximately 0.16 m thick, the middle lift approximately 0.17 m thick, while the top lift was approximately 0.15 m thick. Sand for the bottom and top lifts was mixed to gravimetric water contents of 17%, while sand for the middle lift was mixed to a gravimetric water content of 7%. As discussed previously, no effort was made to either verify the gravimetric water content or control the density of the lifts; this was

done in order to avoid evaporative losses. However, an approximate determination of the lift depth (volume), and consequently bulk density, was achieved through roughly smoothing and levelling the top of each lift. The volume of each lift was calculated from a height-volume relationship developed for the container.

In order to minimize evaporative losses when lifts were not actively being placed, the garbage container was covered with a tarp (Figure 3.18), and a cup of water placed on the top of the lift. As seen in the figure, a different hydraulic press was used for this round of testing as it had greater clearance and a longer stroke length, making it more suitable for a push-test.

Figure 3.18 – Hydraulic press and tarp-covered plastic garbage container used for push-test.

3.4.4.2 Test Description

Push-Test Probe Insertion

In order to insert the probe into the sand, a receiver was attached to the crosshead that fit over the end of the 12.7 mm diameter smooth probe-stabilizing rod used in the compacted sand tests. The connection between the receiver and the probe-stabilizing rod was a relatively loose slip fit one.

The probe-stabilizing rod was in turn screwed into a coupler nut which was attached to a section of 12.7 mm diameter threaded rod. This threaded rod was screwed into the probe's shaft insert, and insertion of the probe could begin. As the probe was inserted, additional intermediate sections of threaded rod were connected together as necessary with other coupler nuts. Having a slip fit connection between the receiver and the smooth rod allowed easy additions of the threaded rod sections and reduced problems with binding if the probe was to go off plumb during insertion. Sections of threaded rod were used instead of one long one as the press' stroke length was too short to accomplish the entire push at once. Furthermore, even if the stroke was long enough, there were concerns that a single rod could buckle under the forces experienced during insertion. A picture of the probe being inserted is shown in Figure 3.19.

Only one push-test was done, and it was done using the unsheathed two-rod configuration of the D2 probe. Like the FFT test, the D2 probe was seen to hold the most potential for a feasible design, and configuring the electrical connections was easiest with the two-rod probe. No conventional rods were used in this testing. The TDR measurements, and subsequent gravimetric verification sampling, was conducted just below the surface of the top lift, and approximately in the middle of the bottom and middle lifts. TDR measurements that were not verified were also conducted over the interfaces of the top and middle, and middle and bottom, lifts.

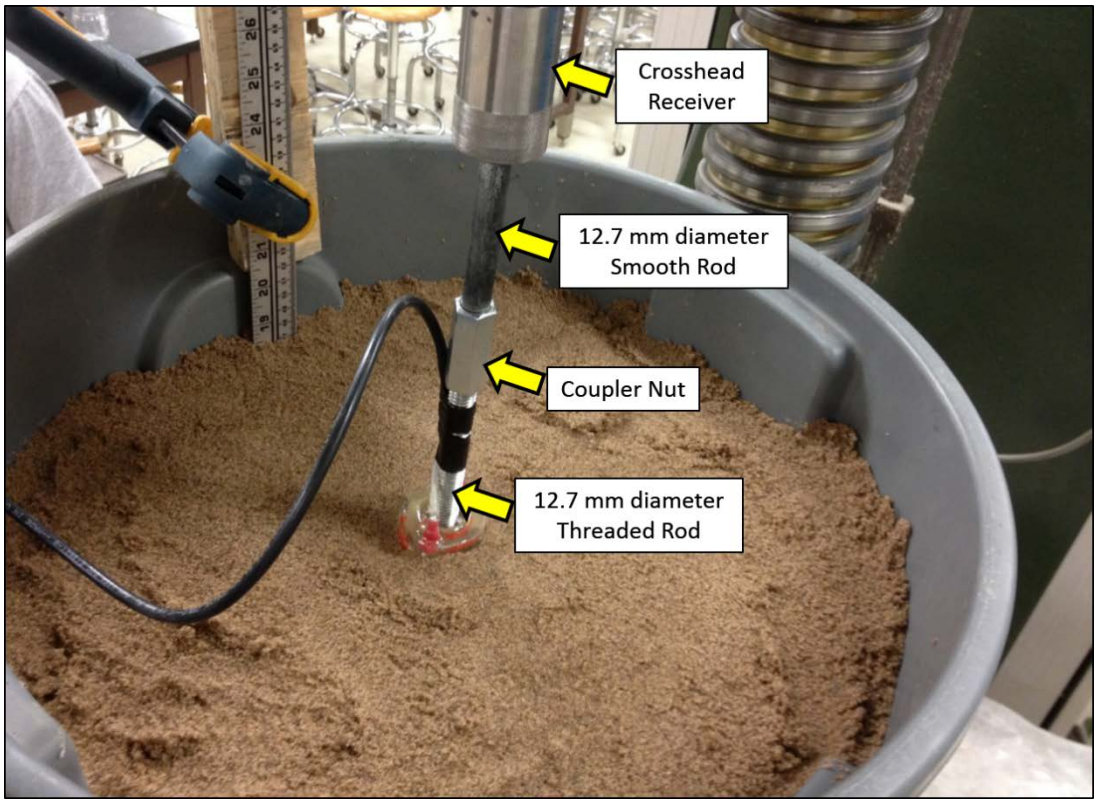

Figure 3.19 – Push-test in progress.

Probe Connection for Push-Test

Completing the push-test required a change in the rod configuration to prevent the connectors from being sheared off during insertion. Given the permanent nature of the probe modifications and the fact that only one push would be completed, changes were made solely to the two-rod unsheathed probe configuration of the D2 prototype. The original opposed, unsheathed rods were removed and replaced with slightly longer rods (i.e. 120 mm) of the same diameter that were bent at the top of the Delrin® cylinder. This bend allowed the connectors to be inset from the probe's exterior. The method of connection was also changed from steel clips to a female 22-18 AWG sleeve-type crimp fitting that was inserted on top of the rod. The coaxial conductors were then soldered to the top end of the fittings. An epoxy ring secured the fittings in place on top of the Delrin® cylinder. A picture of the modified probe is shown in Figure 3.20.

Figure 3.20 – D2 probe modified for push-test with epoxy ring and sleeve-style crimp fittings.

Verification of Testing Conditions

The volumetric water content of the sand was calculated from measured gravimetric water contents and dry densities on samples collected using thin walled tubes pushed into the sand. These samples were collected at the same depth and vicinity of the TDR measurements. Standard gravimetric water content samples (i.e. samples taken with a scoop) were also taken at numerous points in the cylinder. The volumetric water content at these points was approximated using the density of each lift.

Two different types of thin walled tubes were used: small tubes cut from a section of copper pipe, and a larger metal tube which had a beveled end. The small copper tubes were approximately 14.4 mm in inside diameter, and ranged in length from approximately 50 to 55 mm, depending on the tube. The larger metal tube was approximately 122.5 mm long, and 38.1 mm in inside diameter.

The smaller tubes were used to take samples from more specific areas, capturing differences in water content along the length of the probe. The larger tube, however, was used to sample across the entire length of the prototype probe which could capture an average water content.

Care was taken to preserve the integrity of the sample during both insertion and extraction of the tubes; however, this became difficult as the water content increased. Using a mallet to quickly drive the tube into the soil minimized the binding of the wetter sand to the interior of the tubes upon insertion; however, in some cases the binding was unavoidable. In these cases, the tube would have to be driven deeper than the surrounding sand in order to completely fill it, potentially increasing the sand's density inside the tube. Increasing water content also made the extraction of the tubes challenging, as the sample would tend to slip out. In the wettest sand it was necessary to first insert the tube, then carefully dig under the end of the tube by hand to hold the sand in place during extraction. In all cases, a finger was used to brush off the sand that protruded from the end of the tubes. However, in some cases, especially for the larger tube, the action of brushing the sand off also filled in any minor depressions that were left in the sand at the ends of the tubes. While a number of these procedures could lead to erroneous results, they were seen to be the best way to quickly obtain reasonable quality data. Any delays at the time of sample extraction could lead to further drying of the sand, thereby decreasing the quality of the data.

Following sample extraction, the samples were weighed as soon as possible and placed in the oven to dry using the same procedure as had been followed in previous tests. After the process of drying was completed the respective volumetric and gravimetric water contents could be calculated.

Despite attempts to thoroughly mix the sand initially, a pocket of dry sand was encountered during general drying of the sand from the top lift after the test. This sand was not encountered during the deconstruction of the column immediately following the testing, so its location and extent were unknown. A slow leak was also observed in the garbage container both during the test to calibrate its volume with the measuring tape and metre stick and during the push-test. The

amount of water which leaked out was considered to be negligible in terms of significantly affecting the test results.

3.5 Data Analysis Method

Waveforms were saved for each TDR measurement that was carried out, and downloaded for computer analysis using Mohr Associates' CT Viewer program, version 1.2.2.0. Downloaded files were then imported to the software's database, at which point any number of waveforms could be displayed on-screen for analysis.

As previously discussed, there are two critical points to be obtained from each waveform in order to determine the medium's dielectric constant, and consequently its volumetric water content. The x_1 point corresponds to the first peak of the waveform, the point where the signal first encounters the soil along the probe. The x_2 point corresponds to the mid-point of the transition from the local minimum to the ascending limb of the waveform. This is the reflection generated by the signal reaching the end of the probe.

Determining the position of x_1 entailed placing one of the two cursors in CT Viewer at the peak of the waveform. The x_2 point was defined by the intersection of a horizontal line passing along the lowest point in the wave form and a line tangent to the ascending limb of the waveform. The tangent line for the ascending limb was located using a straight edge laid on top of the monitor screen and positioning it along the ascending limb of the waveform. A horizontal gridline was used for the horizontal tangent line. The second cursor would then be placed at the intersection of these two tangent lines. The signal path positions associated with the two cursors would then be input to a Microsoft Excel spreadsheet along with the V_p and rod length values. From these values, the respective dielectric constants were calculated using Or et al's equation (Equation [2-3]), while the volumetric water content was calculated using Topp et al's equation. Sorta et al's equation was also used to calculate the volumetric water content for the FFT results. A diagram depicting the general methodology for determining x_1 and x_2 is shown in Figure 3.21.

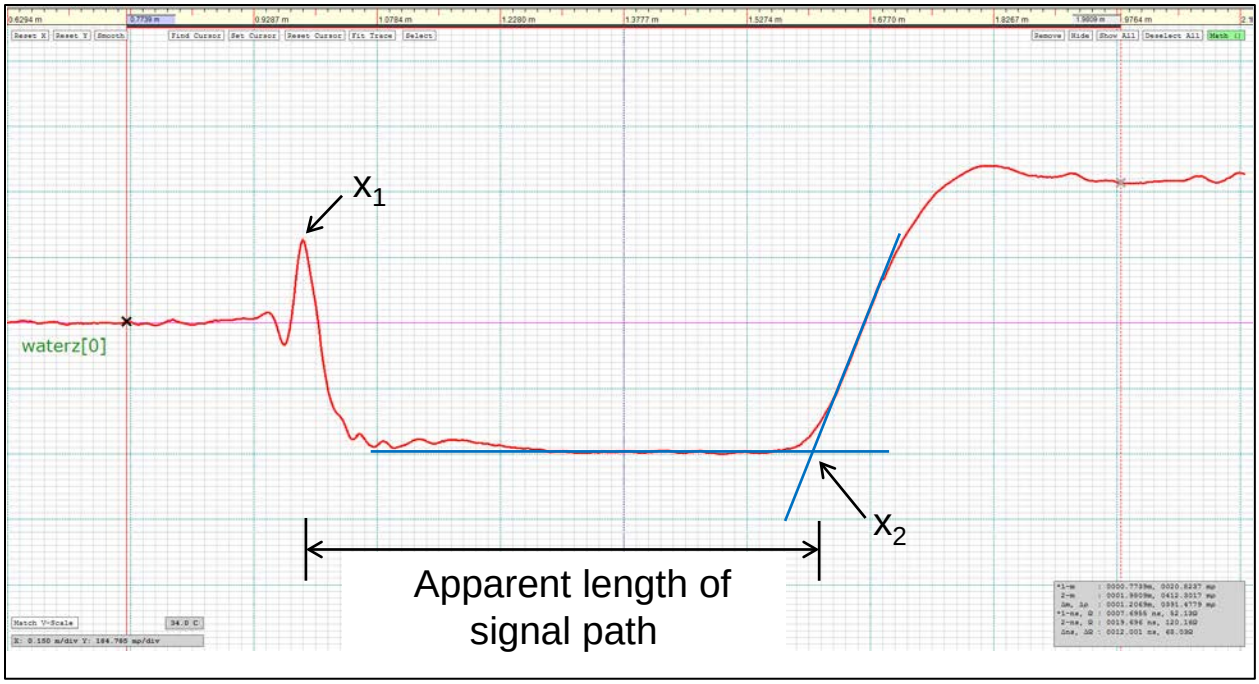

Figure 3.21 – Basic waveform interpretation points.

While this methodology appears straightforward, in many cases the waveforms were not easy to interpret. Selection of x_1 and x_2 was made difficult by waveforms that were not well-defined, leading to ambiguity in the determination of the two points. It was found that the best way to analyze waveforms was to consider an aggregate of waveforms from a particular probe configuration under similar testing conditions, e.g. plotting all of the waveforms at once which were generated from the three-rod unsheathed D2 probe configuration for each water content from the non-elevated salinity sand tests. An example of such an aggregate waveform is shown in Figure 3.22. As can be seen, there is generally a common location for x_1 and a clear progression of the x_2 points as the water content in the soil increases. However, it is also clear that determining the exact x_1 point to use for each individual waveform could be difficult. This was perhaps the most challenging part of the data analysis process.

In general, deciding on the x_1 location was the most difficult, although the x_2 location could also be challenging to determine. Typically, the general location of an individual x_1 point would be established based on where the majority of the x_1 points occurred on the aggregate plot. This

information would then be compared with the individual waveform, and a decision on the exact location to use was made. It was necessary to consult the individual waveform rather than choosing a single x_1 point to apply to all the waveforms, as issues such as slight differences in the cable connections could affect the actual location of x_1. Challenges with choosing the location of x_2 typically centered around uncertainty with selecting an appropriate local minimum or tangent line to the ascending limb. These locations were typically determined on a case-by-case basis, with the aggregate waveform being one possible tool to use. Overall, recalling the general theory in terms of where the two points would be selected on an ideal waveform was helpful for maintaining perspective. A further discussion on the specifics of waveform interpretation for this particular project is saved for the next chapter.

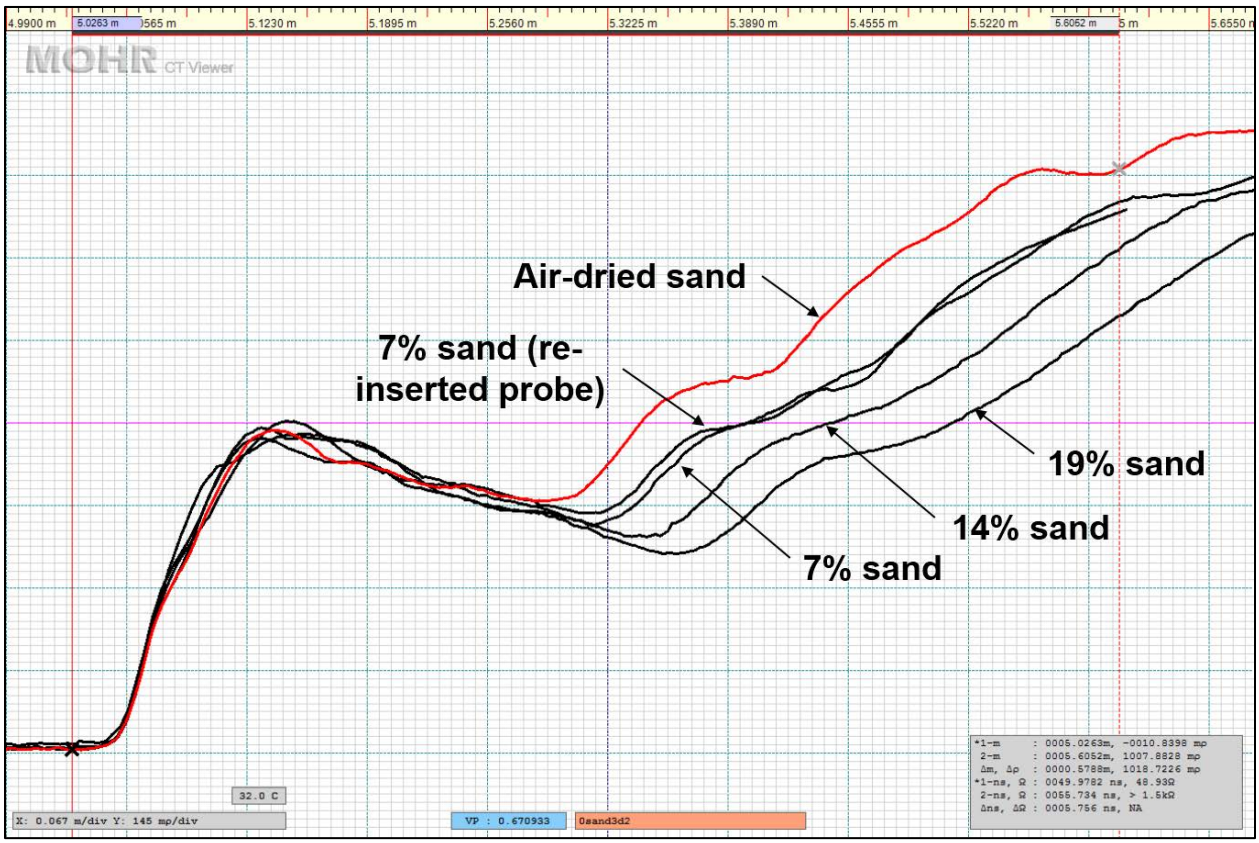

Figure 3.22 – Aggregate waveform plot of three-rod unsheathed D2 probe testing in non-elevated salinity tailings sand.

It should be noted that both Topp et al's and Sorta et al's equations are only truly valid for conventional unsheathed probe results. The presence of the conventional probe sheathing or the Delrin® would affect the observed dielectric constant, and as a result would not return the true volumetric water content for the tests. While this is understood, these equations were used in absence of a more suitable alternative.

4 RESULTS AND ANALYSIS

4.1 Introduction

This chapter contains a discussion of laboratory test results including basic soil properties and the findings from the various stages of prototype testing. Specific to the refined Delrin® prototype testing, the discussion will also address the challenges associated with waveform analysis. The ultimate goal of this chapter, and this portion of the project, is to determine the best probe configuration to proceed forward with to the next phase of the project. This recommendation, along with correction equations for the most promising probe configurations will be provided at the end of the chapter.

The testing program began with an evaluation of the preliminary prototypes, which led to refinements of the prototype design. More rigorous testing of the refined Delrin® prototypes was then completed to evaluate a range of field conditions such as non-elevated and elevated salinity soils, slurries, and insertion into unsaturated soil. Conventional probes were used in most rounds of testing for confirmation of the prototype probe results. It was expected that the conventional probes would have superior results to the prototype probes.

4.2 Waveform Interpretation Specifics

A general description of waveform interpretation was provided in Section 3.5. As discussed, one of the challenges in interpretation is deciding on the true locations of x_2, and especially x_1. This leads to ambiguity in the analysis. To help diminish this ambiguity, more specific details on the analysis methodology used for this phase of the project are presented here.

Interpretability of the waveforms becomes more challenging once the configuration of the conventional probe is changed, particularly when the rods are embedded in other materials (e.g. Delrin®), as in the case of this project. Differences in electrical connections and testing media, as well as the presence of air gaps can also cause changes and inconsistencies in the waveforms. Despite these issues, "good" waveforms can still be generated with the prototype probes used in this project. An example of a "good" aggregate waveform from a refined Delrin® prototype probe tested in ethanol solutions is shown in Figure 4.1. In this example, the selection of x_1 and x_2 for each waveform is clear. There is also a common x_1 peak for the various waveforms making up the aggregate, and a distinct progression to the x_2 locations as the dielectric constant increases. The good quality of this waveform shows the benefit of testing in fluids.

The x_1 points in Figure 4.1 are defined by the local maximum after the initial rise in the waveform. The x_2 points are defined by the transition of the curve following the local minimum, as discussed in Section 3.5. For the air waveform, the x_2 point is defined by the initial transition of the curve from its horizontal run immediately following the drop from x_1. It should be noted that the transition point for testing done in air may not have a horizontal leg immediately preceding it; however, there generally still is an obvious waveform transition. A horizontal line should be placed just before this transition, with a tangent line placed on the ascending limb. The intersection of these lines indicates the location of the x_2 point.

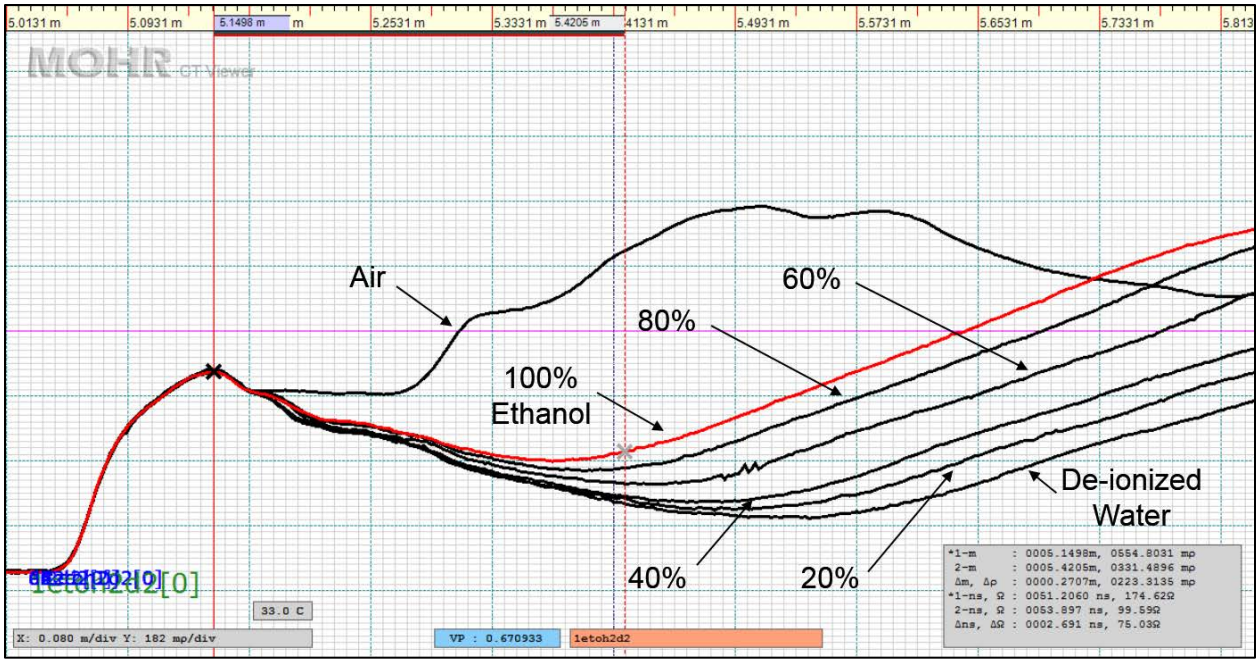

Figure 4.1 – Example of a "good" aggregate waveform showing a common and obvious x_1 peak, and clear x_2 points defined by the "troughs" and ascending limbs as well. Points for x_1 and x_2 are indicated for the 100% ethanol waveform with x's. "80%" in the figure corresponds to an 80% ethanol, 20% de-ionized water (by mass) mixture; similar interpretation for other labels. (Data from the unsheathed two-rod D2 probe in reference solution testing shown. Vertical scales matched for all waveforms.)

An example of a "poor" aggregate waveform, on the other hand, generated from one of the refined Delrin® probes is shown in Figure 4.2. In this example there are double peaks for most waveforms following the initial rise, with a number of their locations not corresponding with the others. This made the decision of which x_1 point to use difficult. A number of reasons could be named for the poor waveforms, but the most likely are air gaps from probe re-insertion and electrical connection issues with the jumper cables. In cases such as this where a number of different selections for x1 and x2 could be made, an attempt was made to keep the methodology as consistent as possible. This was not easy to do when inconsistencies between the individual waveforms existed.

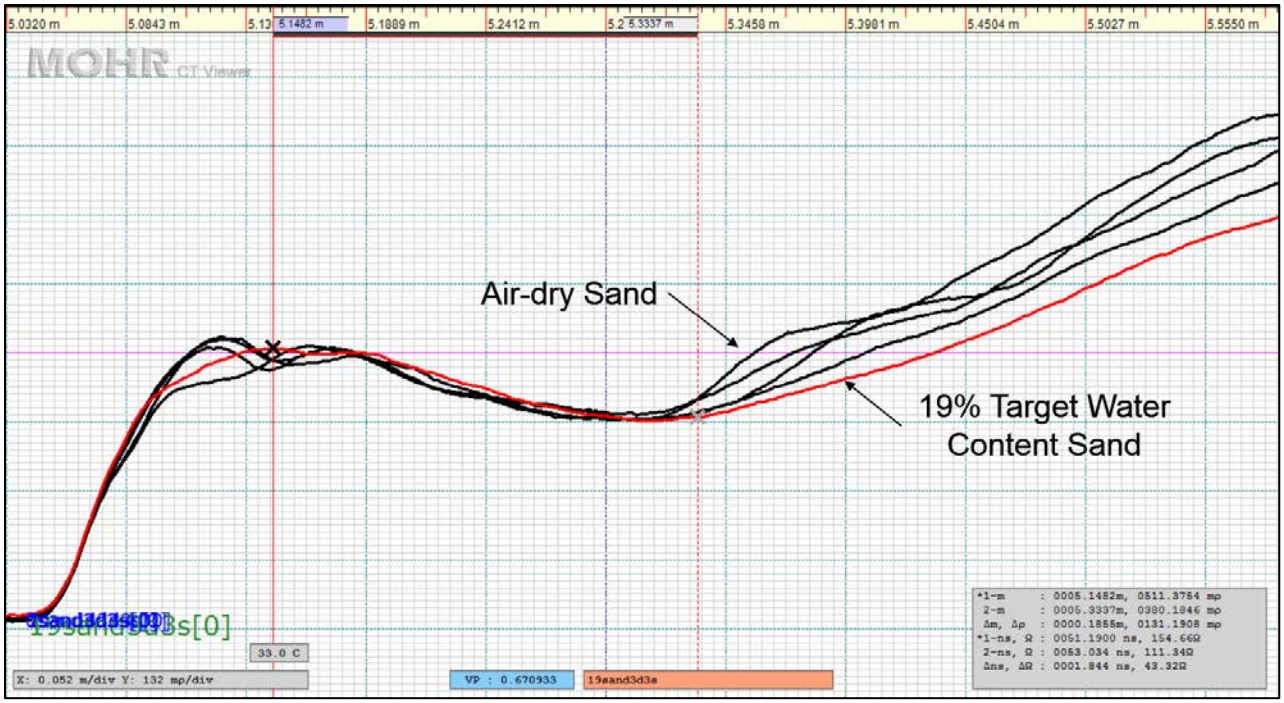

Figure 4.2 – Example of a "poor" aggregate waveform showing double initial peaks, of which some are not common, making the decision of choosing x_1 difficult. Deciding on the location of x_2 was not as challenging, however. Points for x_1 and x_2 are indicated for the 19% target gravimetric water content waveform with x's. Labelling of all individual waveforms neglected for clarity. (Data from the sheathed three-rod D3 probe in non-elevated salinity sand shown. Vertical scales matched for all waveforms.)

Generally speaking, in cases of atypical peaks (e.g. plateaus or double peaks, including peaks of different amplitude) the selection of x_1 could be based on one of the following guidelines:

- If all of the waveforms in an aggregate share a reasonably common x_1 point, and one does not, yet has a similar shape to the others, the equivalent x_1 point based on the waveform's shape for the non-conforming waveform should be chosen.
- In the case of two major peaks with similar amplitudes (particularly prevalent in the three-rod probes), the second should be used for x_1; however, if the amplitudes are substantially different the highest peak should be used.
- If there is a short plateau (i.e. approximately the same "length" as a regular peak, but without the explicit peak), the middle of the plateau should be chosen.

- If the plateau is long (i.e. a long, generally flat distance between the main ascending and descending limbs of the peak), the transition point between the plateau and the descending limb should be used.

While the majority of the issues of interpretability were related to deciding on the location for x_1, issues could also be encountered for x_2. The following criteria were considered when choosing the location for x_2:

- In the case of two clear and substantial local minima in a waveform, compare with other waveforms in the aggregate, choosing the point that is similar to the others.
- When there are minor "bumps" in the ascending limb following the trough, use the main slope for the tangent line, ignoring the bumps.
- If there is more than one main slope in the ascending limb prior to the inflection point, choose the one that will place x_2 closest to the middle of the transition curve between the minimum and the ascending limb. This is in accordance with the general theory on waveform interpretation.

There are cases, however, where these selection criteria do not help to determine the points of interest, and a number of them are presented as examples in the aggregate waveforms found in this chapter. In these cases, the choice of potential points of interest can be evaluated with results that could be expected based on other similar tests (e.g. tests at similar water contents), assuming there are other potential points to choose from. This is not an ideal method, and should only be used as a last resort. Clearly, this tactic could not be used in the field where the conditions were not known. Further, there are some instances where the guidelines do not help to narrow down the choice to just one single point of interest. In these cases, the decision of which point to use should be applied as consistently as possible to other waveforms in the aggregate to minimize the subjectivity of the interpretation. Though not entirely helpful to the reader, experience is a very important aspect in analyzing waveforms.

The underlying assumption to the application of all of these guidelines is that the waveform in question generally "fits in" with the rest of the waveforms in the aggregate plot in terms of shape. If the waveform differs substantially there could be another influencing factor such as the probe shorting out in the testing medium, or one of the electrical connections inadvertently shorting or grounding out. In these cases the results are likely to be outliers.

Overall, much improvement could be made to the results if the location of x_1 in particular was more obviously known. The easiest probe modification to achieve this end would be improved electrical connections, e.g. soldered (such as was used in the push-test) or friction fit slip-on connections as opposed to steel clips. Shorting diodes at the top of the probe may also be helpful for physically indicating x_1, as documented in the literature.

4.3 Evaluation of Waveforms

A number of general features were used to evaluate the quality of the waveforms generated in the testing. For fluid testing, it was observed that the distance to the x_2 points increased with increasing dielectric constant. Ideally, the spacing between waveforms should shift with the relative difference in dielectric constant between fluids. This was a simple way to quickly evaluate the fit of the data. Inconsistency in the location of x_1 points in soil testing did not allow easy comparison of the waveform progression, so it was not generally considered as a criterion in those evaluations.

Quality and interpretability were other criteria used in the evaluation of the waveforms. A good quality waveform is defined as being free of noise (i.e. no jagged portions in the waveform either over a short or long distance) and "bumps", or departures from the general trend of the line. The interpretability of the waveform was essentially evaluated by how much the interpretation of the waveform deviated from the methodology set out in Section 3.5. "Good interpretability" would not deviate from the methodology, whereas poor interpretability would require applying numerous judgments, as discussed above, to the interpretation of the waveforms.

One factor that could artificially influence the quality and interpretability of a waveform was the scale of the waveform on the computer screen during interpretation. If the waveform was "zoomed in" too far, substantial amounts of noise could be seen on the waveform. As a result, efforts were made to maintain a suitable scale during interpretation. Capturing too broad of a portion of the waveform during testing could also decrease the resolution of the zone of interest of the waveform. This could not be adjusted after the fact, but attempts were made to avoid this from happening during testing.

Separate evaluations were also made on the sensitivity and quality of data of the individual probes in estimating volumetric water content. The sensitivity of the probe to changes in water content was evaluated based on the slope of the line of measured water content data points plotted against the corresponding actual water content. A high level of sensitivity would result in a steeper slope, indicating that the probe could more easily differentiate between similar dielectric constants or water contents. Scatter and goodness of fit was measured using the R^2 value for the trendlines.

Another method for evaluating the performance of the prototype probes would be to compare the measured dielectric constant with the actual dielectric constant. The actual dielectric constant could be determined by using a dielectric mixing model; however, since the sensing volume for the various prototype probes was unknown, such a model could not be developed for this phase of the project.

Overall, this phase of the project dealt with determining whether a reasonable relationship existed between the probe-measured and actual volumetric water contents. No calibration of the probes was done, and as a result a rigorous evaluation of the probes' accuracy and estimation error could not be done.

4.4 Preliminary Prototype Testing

Test screening of the preliminary prototypes was done using reference solutions as described in Section 3.4, as well as some testing in soils of different water contents. While results from the

reference solution testing were of use, those from the soil testing generally were not. This was due in part to lack of control in probe construction, soil preparation and testing methodology. Regardless of the overall quality of the results, however, the goal of this testing was to observe the relative response of the probes to the different testing media. Based on this testing, a prototype design was selected for further refinement and controlled testing.

Three general preliminary prototypes were investigated: a ring mounted on a short section of steel pipe; rings mounted horizontally on a Delrin® cylinder; and, vertical rods mounted on a Delrin® cylinder. The first round of testing involved the use of the steel pipe prototype together with two-rod and two-ring Delrin® cylinder prototypes in the air and ethanol reference solutions. Testing was also done in saline solutions for the sheathed probe variants of the Delrin® prototypes.

Overall, the steel pipe prototype was the least promising. While it did produce the standard elements seen in a waveform (i.e. initial peak and following trough), and a general progression in the waveforms in response to various solutions, the overall quality of the waveforms was not good. It was not considered for further testing.

Results from the testing on both the Delrin® prototypes showed a reasonable progression of waveforms. The ring probe began to show indications of shorting out in the 10 g/L saline solution while the rod prototype did not short out in any of the saline solutions. The quality of the waveforms varied, but overall was mediocre.

4.4.1 Second Round of Preliminary Testing

Improvements and additions to the ring and rod style Delrin® prototypes were made for the second round of preliminary testing, as described in Section 3.2. Testing also included inserting a piece of rebar in the interior of the cylinder.

These probes again demonstrated progressive shifts in the waveforms with changing dielectric constant. There were minimal differences in the waveform response from the insertion of the

rebar. The ring prototype began to show signs of shorting out in the 15 g/L saline solutions, while, like the two-rod prototype, the sheathed three-rod probe did not short out in any of the solutions. Again, the quality of the waveforms varied, but overall was not exceptional.

One interesting observation in both the sheathed two- and three-rod tests was that there were very minor changes in the location of x_2 (the reflection from the end of the probe) from the de-ionized water waveform through to the most saline solution. This suggests minimal conductive losses in the saline solutions, as an increasing shift in the trough position with increasing electrical conductivity would typically be expected. The shift in the trough position would then lead to an overestimation of the solution's dielectric constant.

4.4.2 General Commentary on Preliminary Testing

After completion of the preliminary testing it was apparent that either the rod or ring style of probe could be successfully implemented onto the CPT shaft in terms of generating suitable results. The reduced potential for damage to the vertical rods combined with the fact that they did not short out in the saline solutions led to the decision to move forward to advanced testing with vertical rod prototypes. It is hypothesized, however, that the rings may have shorted out at lower salinities because the length of the "rings" was greater than the length of the rods. Assuming this to be the case, it is possible that shorter rings might have a greater range in saline conditions.

Evidence of the fact that the rebar did not negatively impact the response of the probes was encouraging for the use of a shaft insert to transfer the pushing force in the refined prototypes.

4.5 Refined Prototype Reference Solution Testing

Following the construction of the refined Delrin® prototypes, testing again took place with the reference solutions to determine the response for each configuration of the three probe variants: D1, D2 and D3. Results from this testing were in part used to help determine which probe would be suitable to proceed with in the next phase of research. For comparison purposes, testing of

sheathed and unsheathed conventional two- and three-rod probes was also done. Interpreted waveform results are found in Appendix C.

4.5.1 Air and Ethanol Solutions

A summary of the results from testing of the different probe configurations in air and ethanol solutions follows. The response of each probe in relation to each other and the conventional probes is compared. Results are also included for the secondary jumper cable testing.

4.5.1.1 Two-Rod Unsheathed Probe Configurations

In general, the two-rod unsheathed probe configurations provided waveforms that had good progression in response to changing dielectric constants of the various solutions. Most aggregate waveforms had some amount of noise in at least one waveform, but their overall quality was good. Interpretation of the waveforms was also generally straight-forward, although there was a minor lack of definition in the reflection at the end of the probes in the waveforms. Determination of the x_1 points was clear, and an essentially common x_1 point between the various waveforms was present (Figure 4.1).

A plot showing the dielectric constants for the air and ethanol solutions measured by each of the probes is shown in Figure 4.3, and is compared with the corresponding theoretical dielectric constants. A table summarizing the trendline parameters is also provided in Table 4.1. As can be seen, the sensitivity of the probes increases with decreasing amounts of rod embedment (i.e. from D1 to D3). As the dielectric constant of the testing medium decreases, however, the measured dielectric constants for each of the probes begin to converge near the data point for pure ethanol. This trend goes from underestimating to overestimating in the case of air, with the interpreted dielectric constant for air increasing with increasing amounts of rod embedment. The conventional probe overestimated the dielectric constants for all of the data points, but was nearly parallel with the entire theoretical data trendline. In all cases the data points for each of the probes fit quite closely to their respective trendlines, given the high R^2 values.

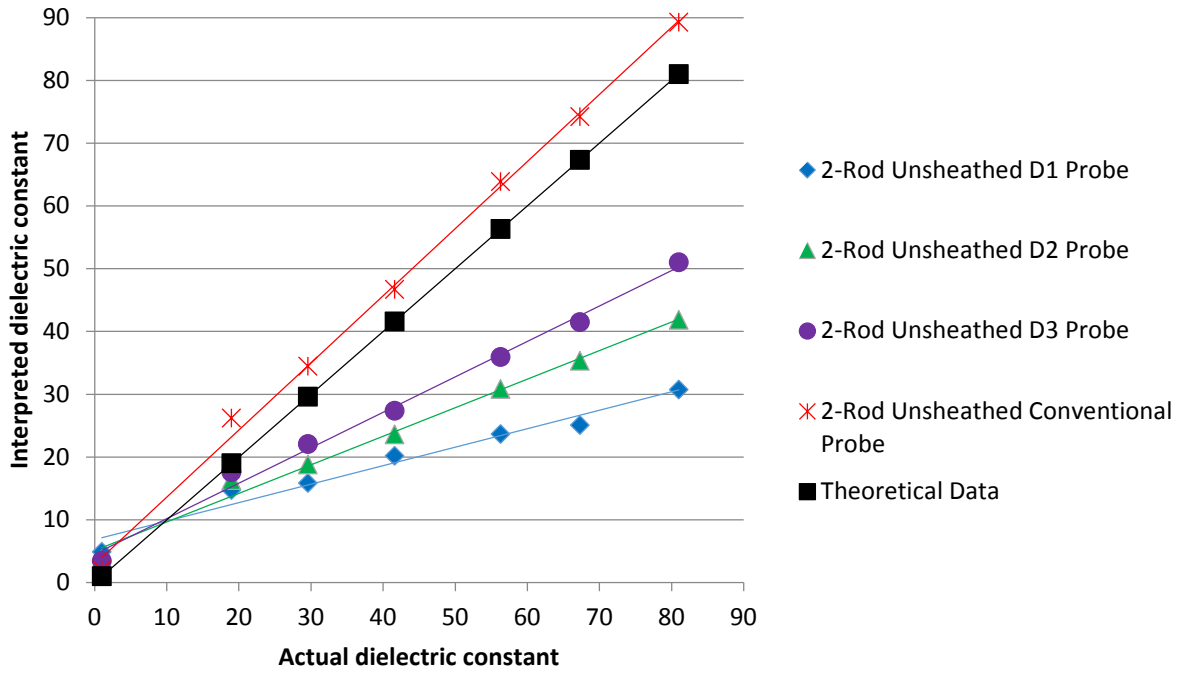

Figure 4.3 – Interpreted dielectric constants from air and ethanol reference solution testing using two-rod unsheathed Delrin® prototype and conventional probes.

Table 4.1 – Trendline parameters for two-rod unsheathed Delrin® prototype and conventional probes from air and ethanol reference solution testing.

Probe	Slope	Y-intercept	R^2
D1	0.295	6.85	0.967
D2	0.455	5.10	0.990
D3	0.565	4.54	0.993
Conventional	1.069	2.92	0.997

4.5.1.2 Two-Rod Sheathed Probe Configurations

The waveforms for the sheathed two-rod probe configurations showed only slight differences from the unsheathed ones. The progression of the waveforms was good, but there were also instances of noise in the waveforms and bumps in some of the ascending limbs. Additionally, there appeared to be more "low-level" noise in terms of the waveforms being less smooth overall. Interpretability of the waveforms was very similar to those of the unsheathed probes, being generally straight-forward but having a lack of definition in the reflection at the end of the probe. While there were some instances of flatter peaks, in each instance there was enough definition to confidently pick the maximum point of the peak for the location of x_1.

A typical aggregate waveform for the sheathed two-rod probes is shown in Figure 4.4. As with the two-rod unsheathed probes, the x_1 location was quite similar for each waveform.

Dielectric constants measured by each of the probes in the different air and ethanol solutions along with the theoretical values are plotted in Figure 4.5. A summary of the respective trendline parameters is also given in Table 4.2. Each of the probes had very similar levels of low sensitivity, with no substantial difference with probe type. As with the unsheathed probes, increasing rod exposure generally resulted in less underestimation of the dielectric constants for ethanol solutions, although to a much lesser extent. There was not a lot of difference in the degree of overestimation of the dielectric constant of air between the different prototype probes. The interpreted dielectric constants for each probe also came close to convergence in the vicinity of pure ethanol. The fit for each of the trendlines was substantially worse than the unsheathed data, as evidenced by the lower R^2 values. Had the data been plotted only for the ethanol solutions, however, the fit would have been better as there was a substantial change in response between the air and pure ethanol data points. It would appear that a logarithmic relationship may be more applicable than a linear relationship for the conventional probe; however, the logarithmic trendline did not result in a better fit.

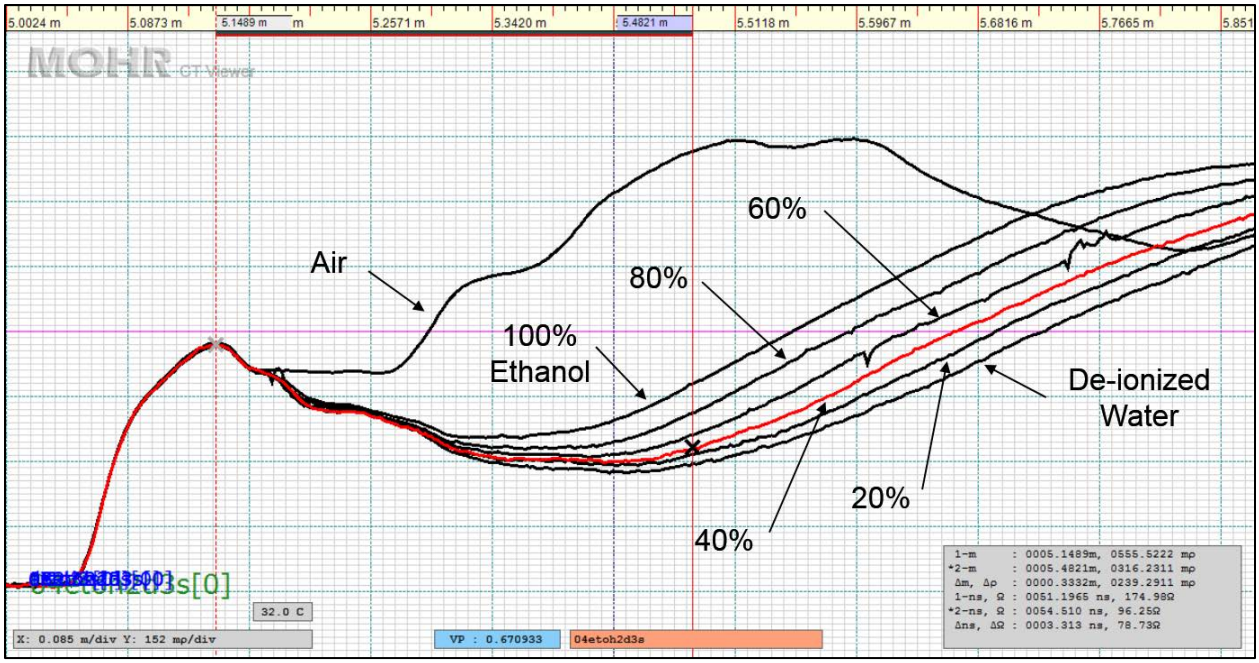

Figure 4.4 – Typical two-rod sheathed Delrin® prototype probe aggregate waveform for air and ethanol solutions (D3 probe data shown). Cursors show the locations of x_1 and x_2 for the 40% ethanol solution (red waveform). "80%" in the figure corresponds to an 80% ethanol, 20% de-ionized water (by mass) solution; similar interpretation for other labels. Vertical scales matched for all waveforms.

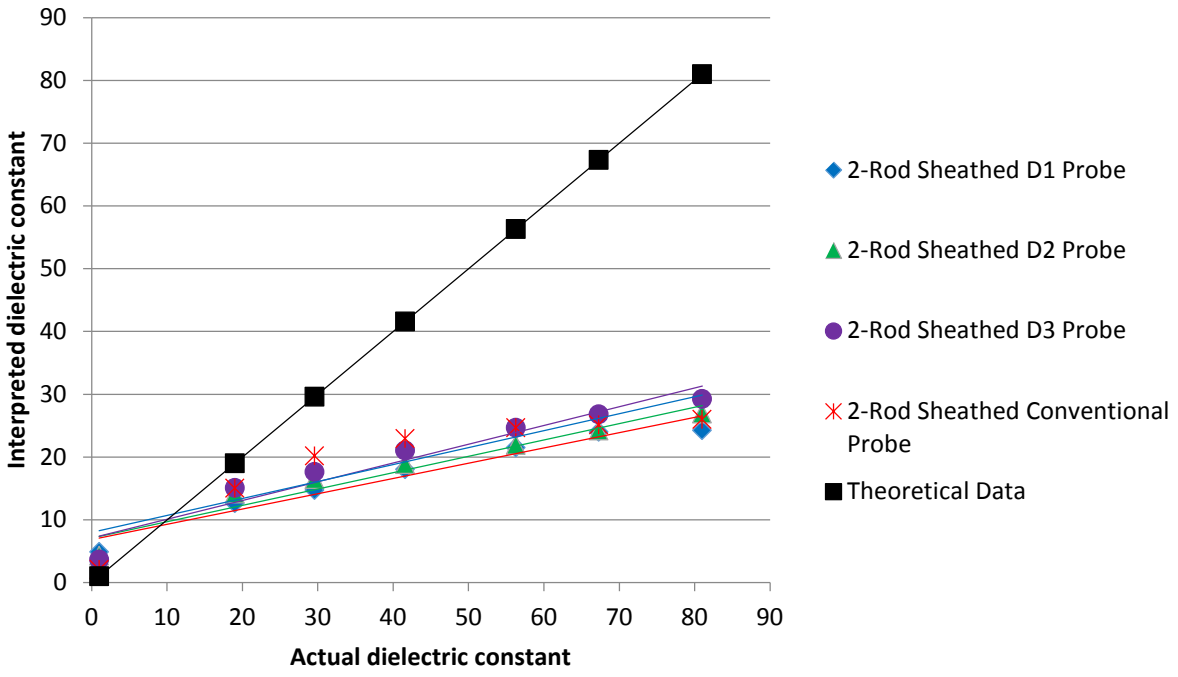

Figure 4.5 – Interpreted dielectric constants from air and ethanol reference solution testing using two-rod sheathed Delrin® prototype and conventional probes.

Table 4.2 – Trendline parameters for two-rod sheathed Delrin® prototype and conventional probes from air and ethanol reference solution testing.

Probe	Slope	Y-intercept	R^2
D1	0.243	6.86	0.951
D2	0.261	7.11	0.943
D3	0.299	7.09	0.935
Conventional	0.270	8.03	0.791

4.5.1.3 Three-Rod Unsheathed Probe Configurations

Overall, the three-rod unsheathed probe configurations provided waveforms that had good progression, although there were some instances where the spacing between waveforms was minimal. Similar amounts of noise to the two-rod probes, both localized and general low-level, were seen in the waveforms for these probes. Interpretation of the waveforms was slightly more difficult than it was for the two-rod probes as there were more bumps in the ascending limbs. Definition of the reflection at the end of the probe was again lacking to a small degree. On the whole, however, the waveforms were still generally unambiguous to interpret, and the x_1 points were quite consistent across the different waveforms (Figure 4.6).

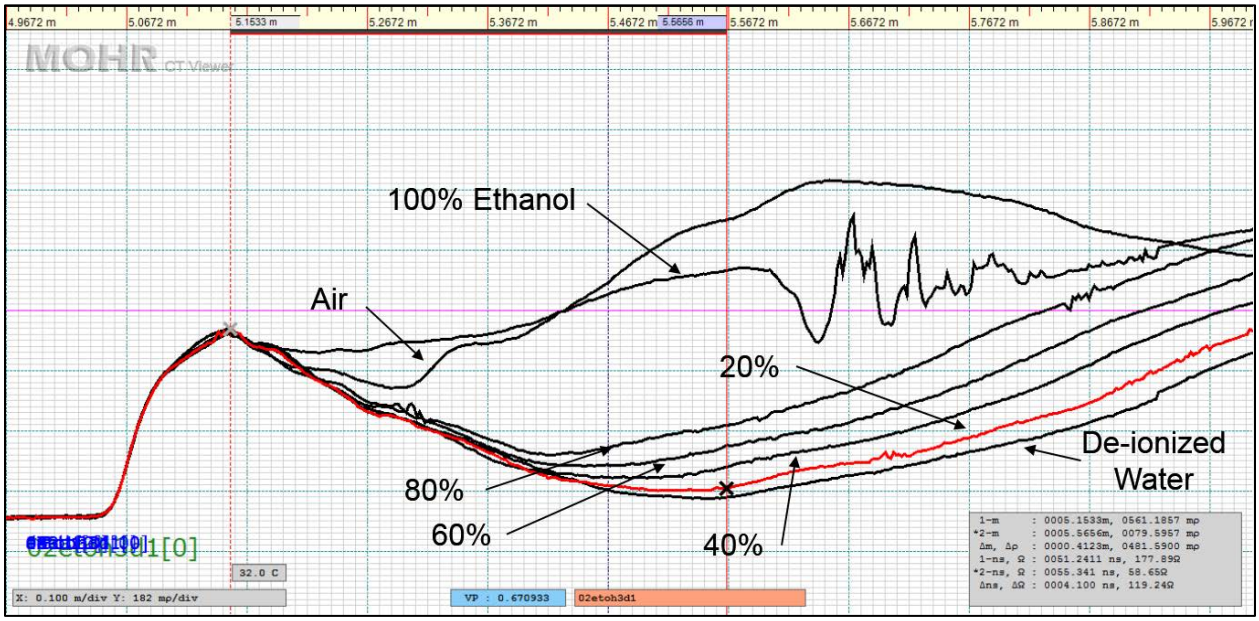

Figure 4.6 – Three-rod unsheathed Delrin® prototype probe aggregate waveform for air and ethanol solutions (D1 probe data shown). Note low degree of some aspects of waveform quality, particularly with noise and bumps, as well as some unequal spacing. Cursors show the locations of x_1 and x_2 for the 20% ethanol solution (red waveform). "80%" in the figure corresponds to an 80% ethanol, 20% de-ionized water (by mass) solution; similar interpretation for other labels. Vertical scales matched for all waveforms.

Figure 4.7 plots the dielectric constants calculated from the testing for each of the probes along with their theoretical values, while parameters of the respective trendlines are presented in Table

4.3. The degree of dielectric constant underestimation and overestimation for each probe is less than was seen in the two-rod probes, with higher levels of sensitivity as well. Similar to the two-rod probes, increasing rod exposure yields less underestimation and overestimation of ethanol solutions and air dielectric constants, respectively. This is with the exception of the D3 probe, however, as it overestimated the dielectric constant of air more than the D2 did. Values for the probes again converge near the value of pure ethanol, although the D3 probe begins overestimating the dielectric constant between the 80% ethanol solution and pure ethanol data points. Generally, more scatter was evident in this ethanol solution data than had been seen in the two-rod data, but the R^2 values were still high. In the case of the D3 probe data, though, the R^2 value appears to be artificially high since there are a number of outliers from the trendline. This is likely due to a balancing of errors. Fit for the conventional probe data to the theoretical data was very good, as was its accuracy.

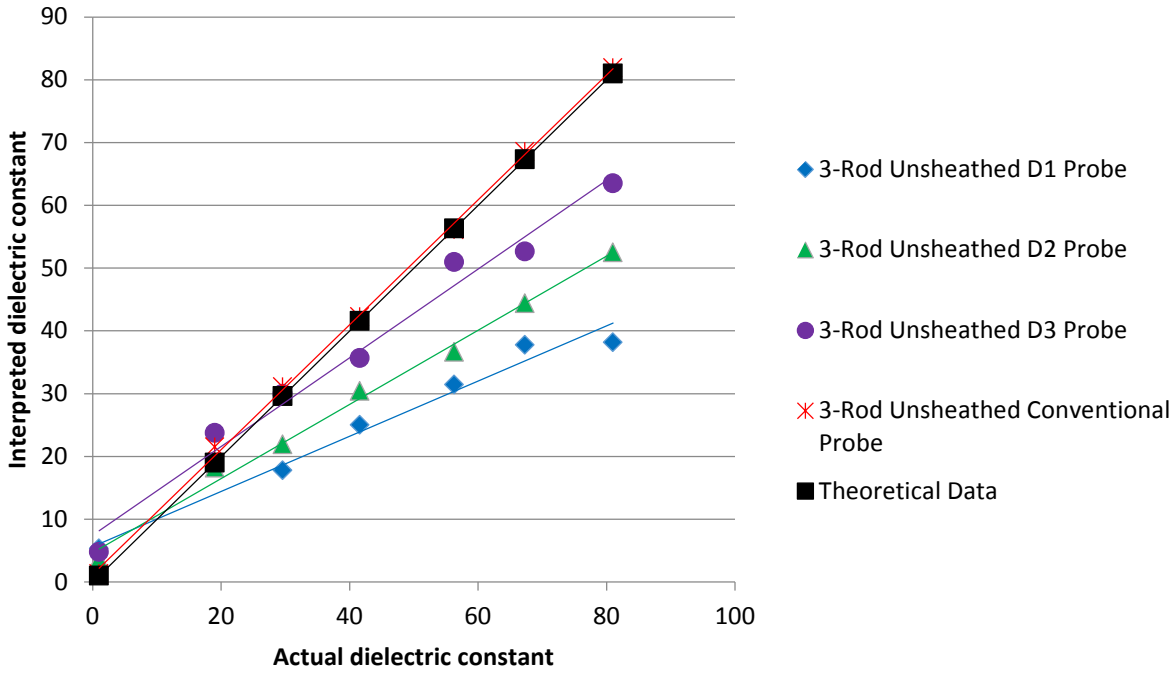

Figure 4.7 – Measured dielectric constants from air and ethanol reference solution testing using three-rod unsheathed Delrin® prototype and conventional probes.

Table 4.3 – Trendline parameters for three-rod unsheathed Delrin® prototype and conventional probes from air and ethanol reference solution testing.

Probe	Slope	Y-intercept	R^2
D1	0.439	5.65	0.976
D2	0.591	4.69	0.993
D3	0.707	7.47	0.982
Conventional	0.994	1.22	0.999

4.5.1.4 Three-Rod Sheathed Probe Configurations

Differences in the waveforms for the sheathed three-rod probes as compared with the unsheathed three-rod probes were more substantial than with the two-rod probes. The most obvious difference was in the progression of the waveforms. In each of the aggregate waveforms, the de-ionized water waveform, and the 20% ethanol solution in the case of the D3 probe, was substantially removed from the others. There were also instances of minimal separation between the waveforms for a number of the ethanol solutions, which was particularly pronounced in the D2 and D3 probe data. Noise in the probes' waveforms was not overly substantial except for some instances with the D1 probe. Waveform interpretability was complicated by the presence of bumps in the waveforms and secondary troughs, as well as some lack of definition in the reflection from the end of the probe (Figure 4.8). Despite these issues, interpretation was reasonably straight-forward, although less so than for the other probe configurations.

Measured dielectric constants for the different probes are plotted in Figure 4.9, with the trendline parameters presented in Table 4.4. A lack of sensitivity was exhibited by all the probes, although this was particularly evident in many of the D2 and D3 probe data points. In general these two probes underestimated the ethanol solution dielectric constants quite considerably compared with the D1 probe. Overestimation of the dielectric constant of air between the probes was very similar, although D1 was slightly higher than D3, while D2 was the least overestimated. The characteristics of the three-rod sheathed D1 probe were very similar to those

of the same two-rod configuration, with decreased sensitivity from the unsheathed variants and similar levels of underestimation. The probe also converged near the theoretical dielectric constant of pure ethanol, as did the conventional probe. A substantial drop in the measured values between pure ethanol and air also existed, as had been seen in the sheathed two-rod probes. Overall, the fit of the data for all of the probes was poor, especially for the D2 and D3 probes, mainly due to poor waveform progression. Similar to the two-rod sheathed testing, the conventional probe data appears to be better represented by a logarithmic relationship rather than a linear one, and the R^2 value was higher. However, given that the general relationship of the theoretical data is linear this relationship was not investigated further.

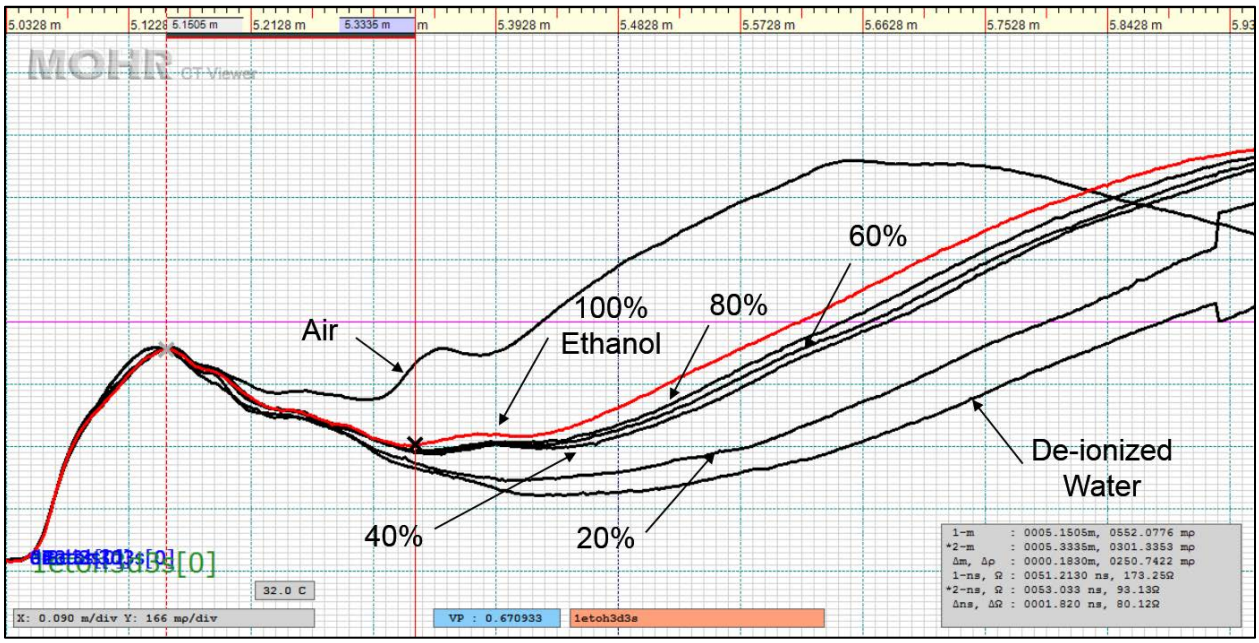

Figure 4.8 – Three-rod sheathed Delrin® prototype probe aggregate waveform for air and ethanol solutions (D3 probe data shown). Note low degree of some aspects of waveform quality, in particular secondary troughs as well as unequal spacing. Cursors show the locations of x_1 and x_2 for pure ethanol (red waveform). "80%" in the figure corresponds to an 80% ethanol, 20% de-ionized water (by mass) solution; similar interpretation for other labels. Vertical scales matched for all waveforms.

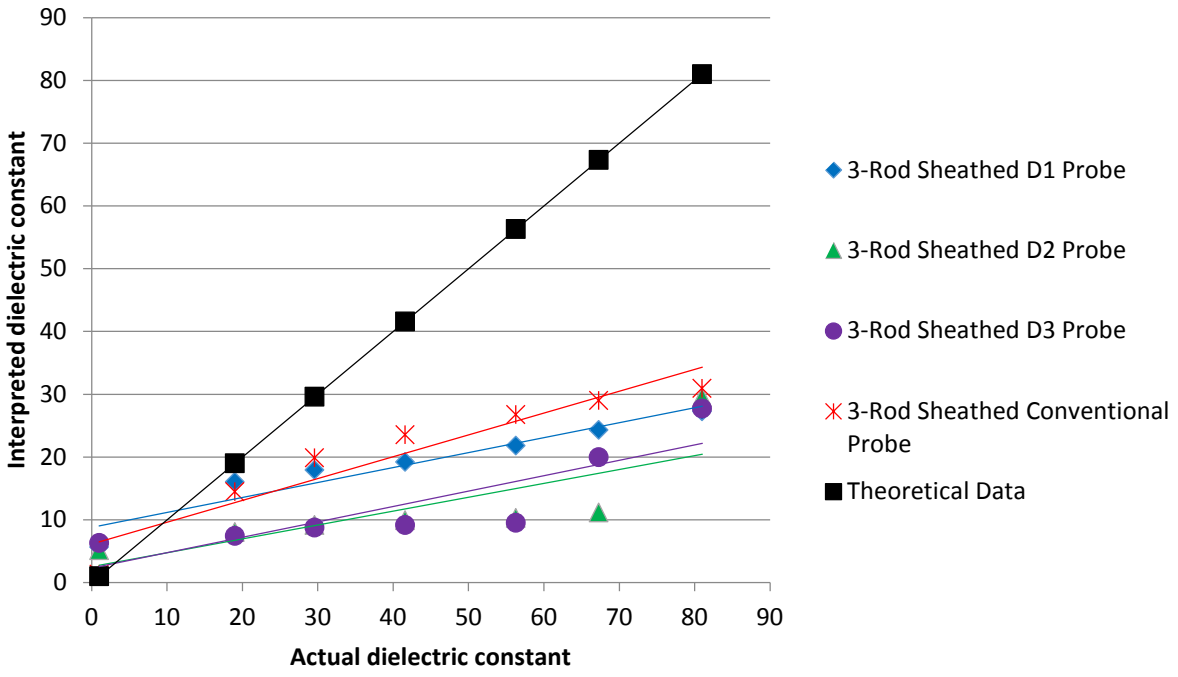

Figure 4.9 – Measured dielectric constants from air and ethanol reference solution testing using three-rod sheathed Delrin® prototype and conventional probes.

Table 4.4 – Trendline parameters for three-rod sheathed Delrin® prototype and conventional probes from air and ethanol reference solution testing.

Probe	Slope	Y-intercept	R^2
D1	0.238	8.81	0.916
D2	0.221	2.56	0.600
D3	0.245	2.34	0.736
Conventional	0.348	6.15	0.901

4.5.1.5 Secondary Jumper Cable Testing

Testing was also undertaken to see whether a jumper cable to connect the two ground rods of the refined Delrin® sheathed and unsheathed three-rod probe configurations would affect the probe performance by adding a non-symmetric element to the signal path. This was investigated by adding a secondary jumper cable to the "live" rod of the probe in order to make a symmetric signal path on both sides of the cable. This testing was done much later in the research program, and only the D2 probe was tested. Ethanol reference solutions were solely used in order to benefit from the advantages of testing in liquids and across a wide range of dielectric constants. Testing was done both with and without the secondary jumper cable. The conventional unsheathed three-rod probe was also tested to determine whether any change in solution properties had occurred since the initial testing a number of months prior.

The biggest difference in the waveforms with the secondary jumper cable was the addition of a second peak, which was evident in both the sheathed and unsheathed testing. On an individual level, the unsheathed probe configuration with the secondary jumper cable had less uniform spacing in the waveforms compared with both the original (i.e. initial reference solution testing) and re-tested non-secondary jumper cable data. There was also less noise, but more bumps than the non-secondary jumper cable data. Interpretability was generally good, although the reflection from the end of the probe was poorly defined in some instances. Progression of the waveforms in the sheathed configuration was generally inconsistent between the original and re-tested non-secondary jumper cable waveforms and the secondary jumper ones. There were minimal amounts of noise, but more bumps in the secondary jumper waveforms both before and after the end of probe reflection. The bumps following the reflection made the interpretation of the x_2 points more challenging. Interpretation of the x_1 points were straight-forward, however. An image of the sheathed waveform with secondary jumper cables is shown in Figure 4.10.

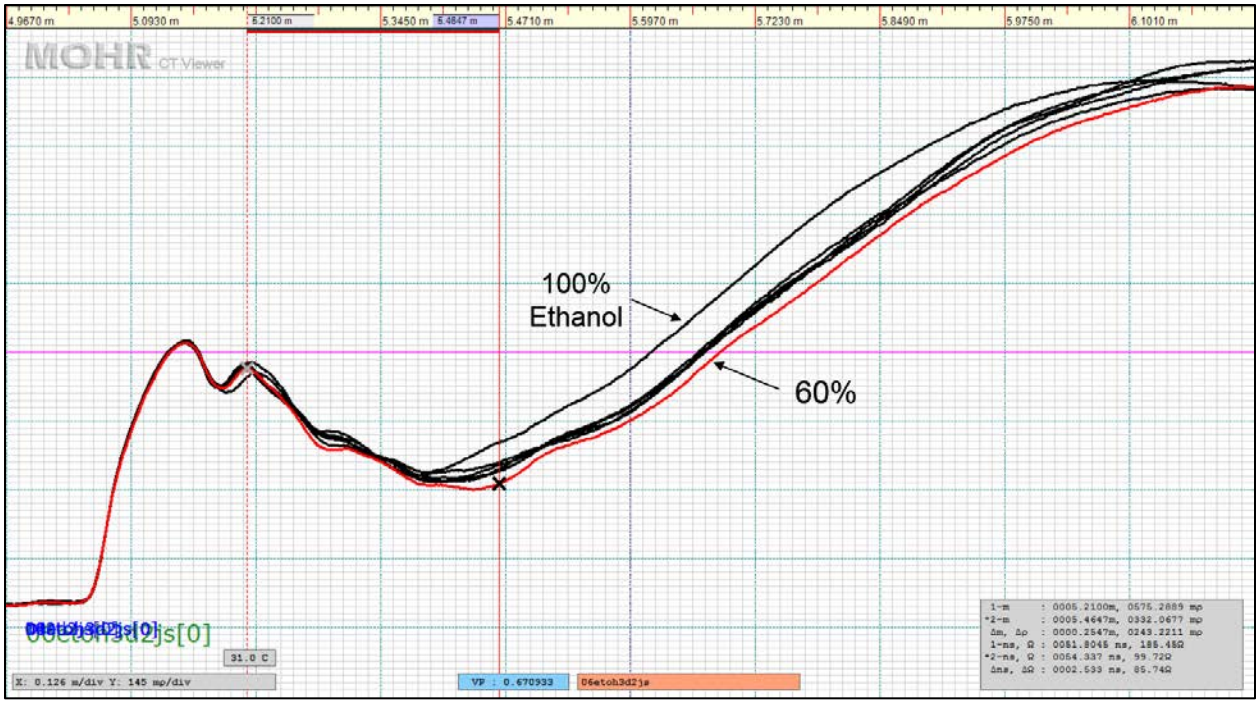

Figure 4.10 – Three-rod sheathed D2 Delrin® prototype probe aggregate waveform with secondary jumper cable for water and ethanol solutions. Note bumps after the end of probe reflection and unequal waveform spacing. "60%" in the figure corresponds to a 60% ethanol, 40% de-ionized water (by mass) solution. Cursors show the locations of x_1 and x_2 for the 60% ethanol and 40% water solution (red waveform). Vertical scales matched for all waveforms.

Dielectric constants calculated from the results of this testing are plotted in Figure 4.11 and Figure 4.12, for the unsheathed and sheathed variants, respectively. In both of the plots there appears to be a slight increase in the value of the interpreted dielectric constants for the re-tested data over the initial data. However, the unsheathed conventional probe testing does not indicate this change. This suggests the change is related to the prototype probes rather than a physical change in the solutions. By inspection, the fit of the secondary jumper cable data for both the unsheathed and sheathed data is much lower in quality compared to that of the non-secondary jumper data. As a result, an attempt to do a detailed comparison of the data was not done. There seems to be a slight underestimate of the dielectric constant from the secondary jumper data, although it is not consistent. It is suspected that the addition of extra cabling and connections has degraded the signal, and a conclusion on whether differential cable length makes a difference on the three-rod results cannot be reached.

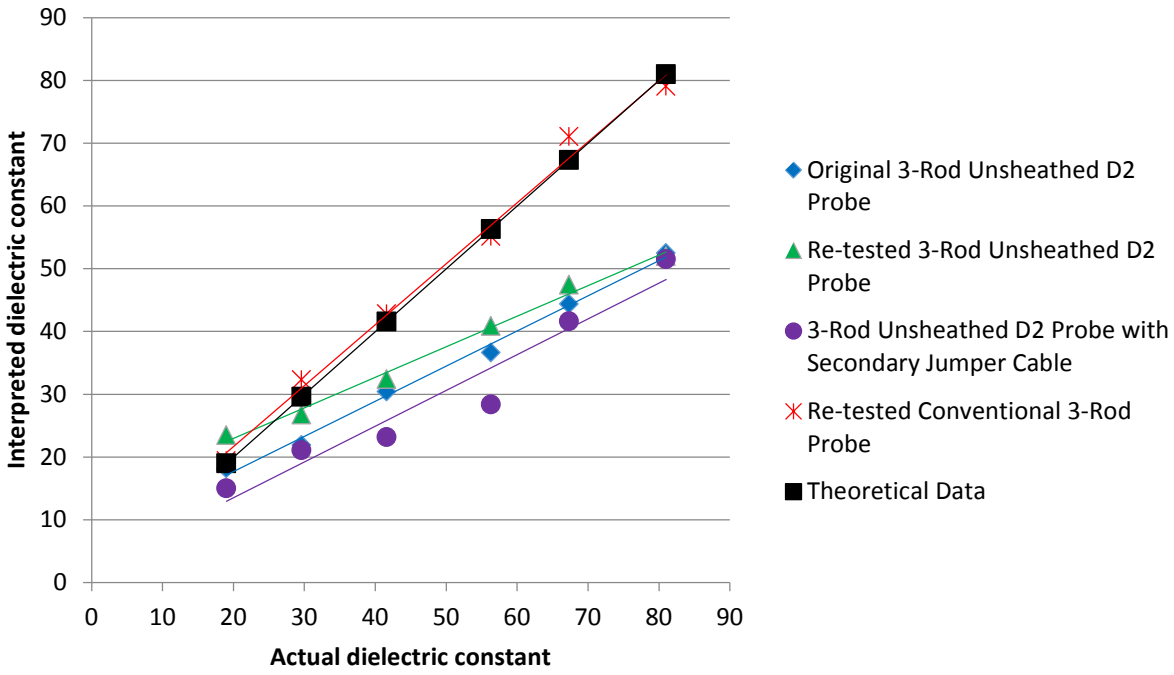

Figure 4.11 – Measured dielectric constants from ethanol reference solution testing with secondary jumper cables using the three-rod unsheathed D2 prototype.

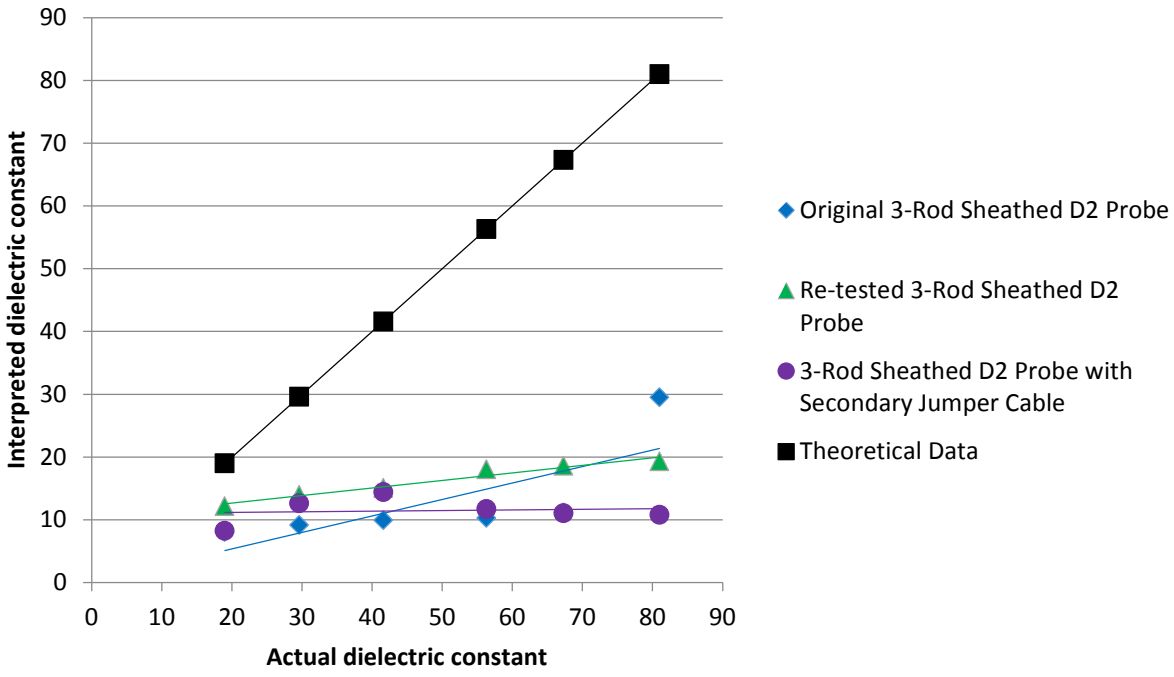

Figure 4.12 – Measured dielectric constants from ethanol reference solution testing with secondary jumper cables using the three-rod sheathed D2 prototype.

4.5.2 Saline Solutions

The refined prototype probes were also tested in saline solutions to observe their response to increasingly conductive conditions. Only sheathed probes were tested, as all unsheathed probes shorted out in the lowest concentration solution tested, 5 g/L.

In most cases the measured dielectric constants were initially very similar to that of de-ionized water in the 5 g/L saline solution, but increased quickly at higher salinities for every case but the two-rod D2 probe and the conventional three-rod probe. Definition of the trough and ascending limb of the waveform was poor in most cases, making the interpretation of the exact points of x_2 difficult. This lack of definition became worse as concentration, and therefore electrical conductivity, of the solution increased, eventually resulting in the lack of a discernible trough. At this point the waveform was said to have shorted out. Definition was comparatively better for both conventional probes, and in the case of the two-rod conventional probe there was enough definition in each of the waveforms to determine the location of x_2 up to the 30 g/L solution,

albeit very approximately. The three-rod conventional probe shorted out after the 15 g/L solution despite the fact that it was not strongly affected by electrical conductivity until that point. General low-level noise was also seen in many waveforms, further complicating the interpretability of x_2. The location of x_1 was quite constant for most of the probes, however, making for straight-forward interpretability of those points. Results from the testing are presented graphically in Figure 4.13 and Figure 4.14. The aggregate waveform of the two-rod D2 probe is shown in Figure 4.15.

Of the prototype probes, the two-rod D2 probe provided interpretable waveforms up to 20 g/L, while most others shorted out between 10 and 15 g/L. In general, the three-rod probes provided more "realistic" values (i.e. similar to de-ionized water) up to 10 g/L, whereas the two-rod probes started to increase after 5 g/L. There was also a weak pattern that suggested slightly less susceptibility to the effects of electrical conductivity for increased rod embedment, with the pattern being more obvious in the three-rod probes.

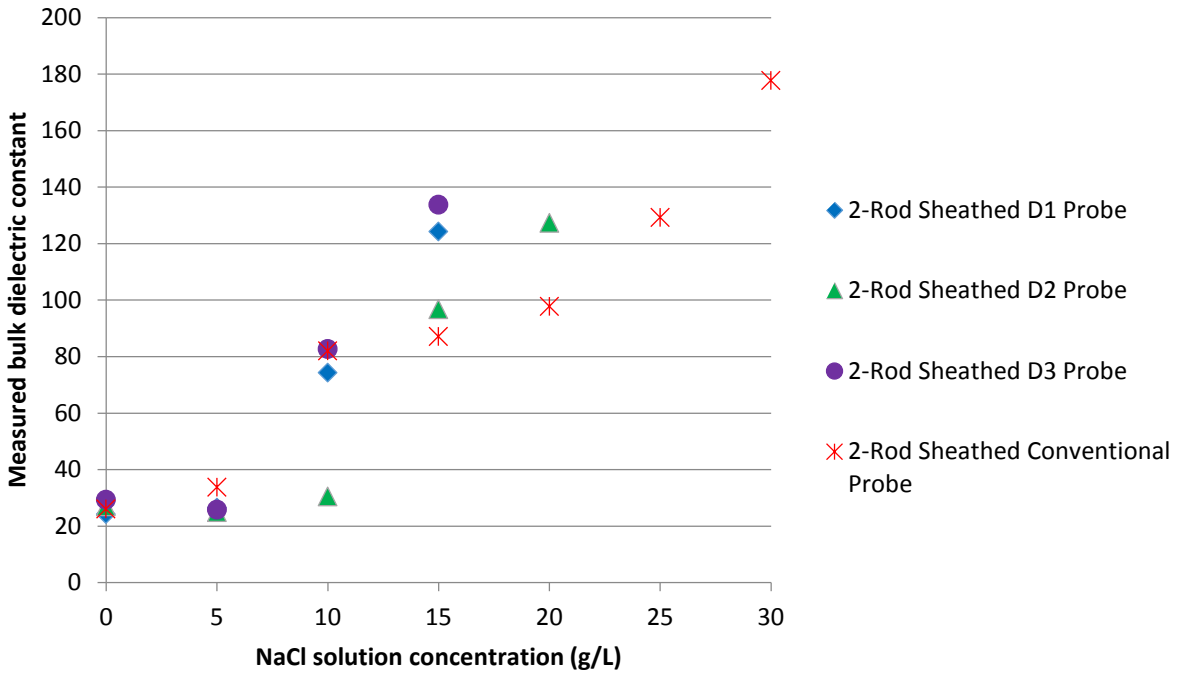

Figure 4.13 – Measured dielectric constants of saline solution testing using two-rod sheathed Delrin® prototype and conventional probes.

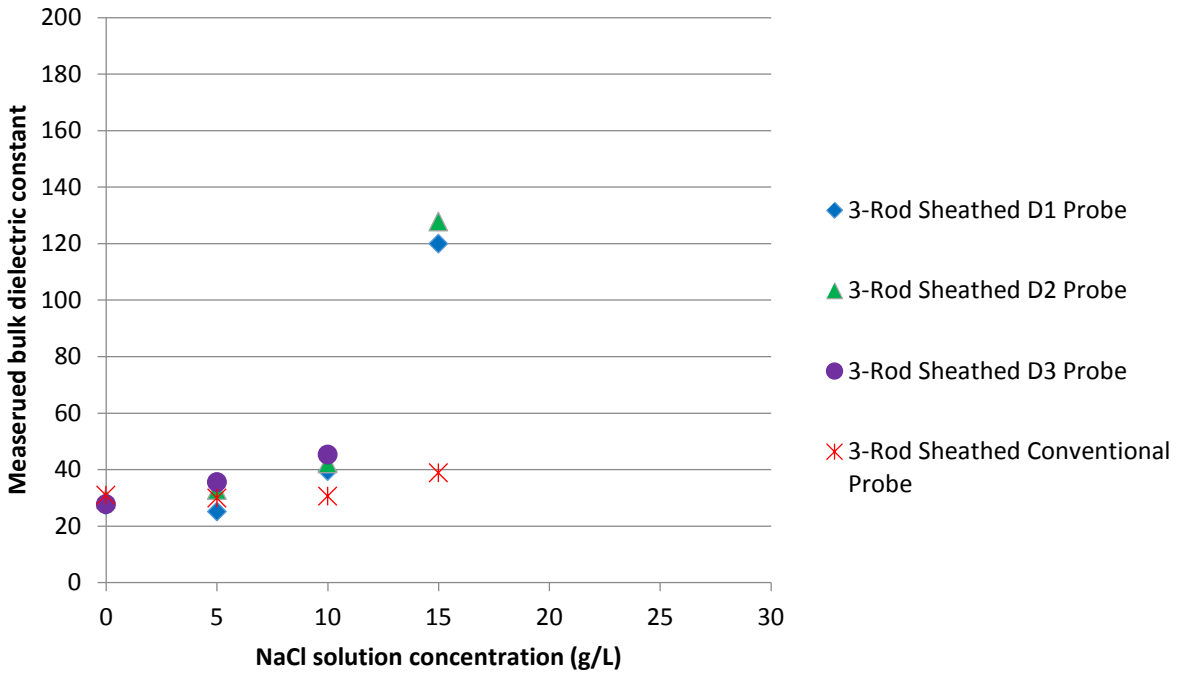

Figure 4.14 – Measured dielectric constants of saline solution testing using three-rod sheathed Delrin® prototype and conventional probes.

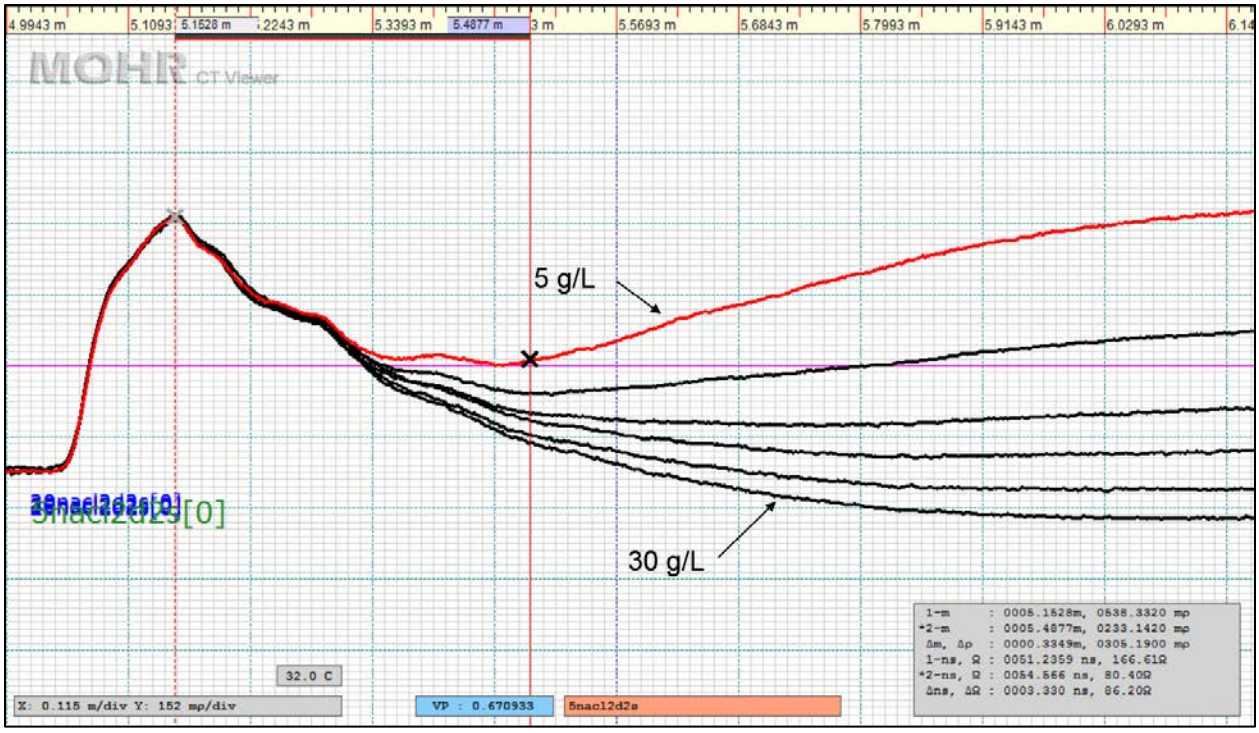

Figure 4.15 – Two-rod sheathed Delrin® prototype probe aggregate waveform for saline solution testing. Waveforms progress from the 5 g/L solution on the top through to the 30 g/L on the bottom. Note lack of definition in trough and ascending limb, with absence of discernable trough in the 25 and 30 g/L solutions. (D2 probe data shown. Vertical scales matched for all waveforms.)

4.5.3 General Commentary on Reference Solution Testing

Testing with the air and ethanol reference solutions provided good results for comparison purposes. In general, there was a substantial difference between unsheathed and sheathed probes in terms of sensitivity for both the two- and three-rod probes, with sheathed probes being much less sensitive to changing dielectric constants. The sheathed probes also saw a substantial change in response between the air and pure ethanol data points, with the interpreted air data points falling off the linear trendlines. This could be of concern since the dielectric constant of ethanol is equivalent to a volumetric water content of 0.33 m^3/m^3 using the Topp equation, which is quite a wet soil.

A common trend of increased probe sensitivity to the ethanol solutions with decreasing rod embedment was also evident. While overestimated, lower dielectric constants (i.e. more

accurate) were also measured for air with decreasing rod embedment in some instances as well. These trends are reasonable, as the rods are being more directly exposed to the testing medium itself, and less influenced by the Delrin® and other probe materials.

Overall, the two-rod unsheathed probes had less scatter than the unsheathed three-rod probes. Of all the probes, the sheathed three-rod probes gave the worst data, which was largely due to poor waveform progression. The specific reason for this poor data is unknown, but multiple electrical connections and decreased sensitivity from the sheathing likely played a role. The issue of degrading results from numerous electrical connections was also seen in the secondary jumper cable testing, with no conclusive results from the testing due to the excessive data scatter. Interpretability of the waveforms for all probes, however, was largely straight-forward.

Saline solution testing showed that the Delrin® probes shorted out far more prematurely than anticipated, given the favourable results seen in the preliminary vertical probe testing both in terms of good definition and similar x_2 points. These more favourable results suggest less impact from conductive losses, and may be a result of shorter rod lengths in the preliminary probes. While there was some evidence to suggest that increased rod embedment decreased the effect of electrical conductivity, the evidence was quite weak. In general, there was not a lot of difference between the response of the two- and three-rod prototype probes. The better response from the conventional two-rod probe over the three-rod probe was unexpected, however, as the literature suggests otherwise (e.g. Zegelin et al. 1989).

Of all the probes, the two-rod unsheathed configurations seem to provide the best data. Less rod embedment translated to a more sensitive probe, but in terms of fit, the D2 was typically best or second best. The two-rod probe configurations appeared to provide the best data in highly electrically conductive media, although the results were not exceptional, and not much different from those of the three-rod.

4.6 Compacted Non-Elevated Salinity Tailings Sand Testing

Once testing had been done to characterize the general response of the refined prototypes, testing began on tailings sand at various water contents. This testing would allow the evaluation of the probes in soil prior to deciding which probe to use in the following stages of this project. Conventional two- and three-rod probes were also tested for comparison purposes. The following sections describe the response for each of the prototype probe configurations.

Interpreted results for the individual probes are provided in Appendix C, while water content results for the various cylinder packings are given in Appendix D.

4.6.1 Two-Rod Unsheathed Probe Configurations

The obvious progression and common x_1 points evident in the reference solution testing were not as characteristic of the prototype waveforms from sand testing. This was particularly evident in the D1 aggregate waveform, shown in Figure 4.16. The quality of the individual waveforms was generally good, with no bumps or noise that had a substantial effect on interpretability. Interpretability was, however, more difficult with the sand waveforms than with the reference solutions. Generally the reflection from the end of the probe was relatively well defined for the unsheathed two-rod probes, but in some cases the D1 and D2 probes had what appeared to be two reflections. Issues with double peaks, peaks that moved relative to others and peaks that were poorly defined also contributed to the difficulties in interpreting the waveforms.

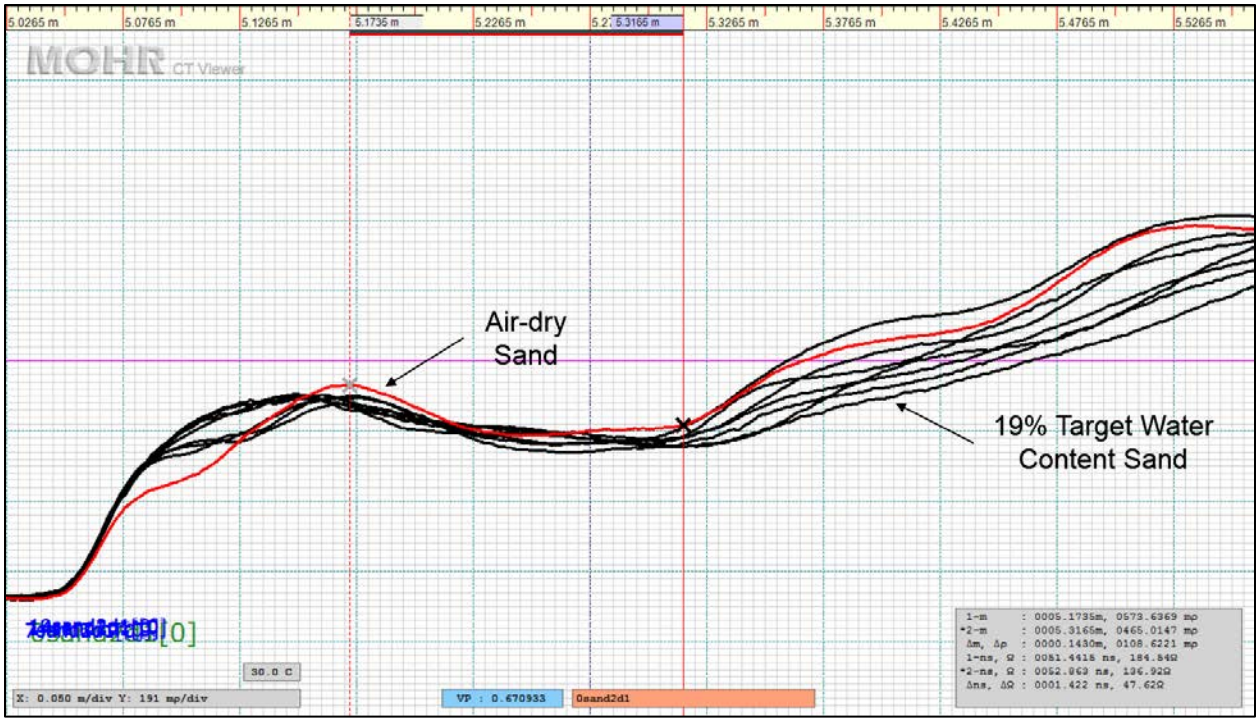

Figure 4.16 – Two-rod unsheathed Delrin® prototype probe aggregate waveform for compacted non-elevated salinity sand testing. Waveforms generally progress from air-dry (red waveform – x_1 and x_2 points indicated) to 19% target gravimetric water content. Note inconsistent x_1 locations and lack of strong progression of waveforms. (D1 probe data shown. Vertical scales matched for all waveforms.)

A plot showing the measured volumetric water content for each test as compared with the calculated water content using the Topp equation is presented in Figure 4.17. Trendline parameters for the plot are also summarized in Table 4.5. Some similar trends to the reference solution testing are seen, including the decrease in sensitivity with increasing rod embedment (i.e. from D1 to D3). There is also a trend towards overestimating the dielectric constant, and therefore the water content, at lower water contents. The conventional probe continued to overestimate the water content, while the prototype probes had a trend towards underestimating. All probes provided very similar results for the air-dry sand. The fit for the data was very good for the conventional probe, while the D2 probe had the best fit of the prototypes, and D1 the worst. Without the air-dry sand data point, however, the D1 probe would have had better fit.

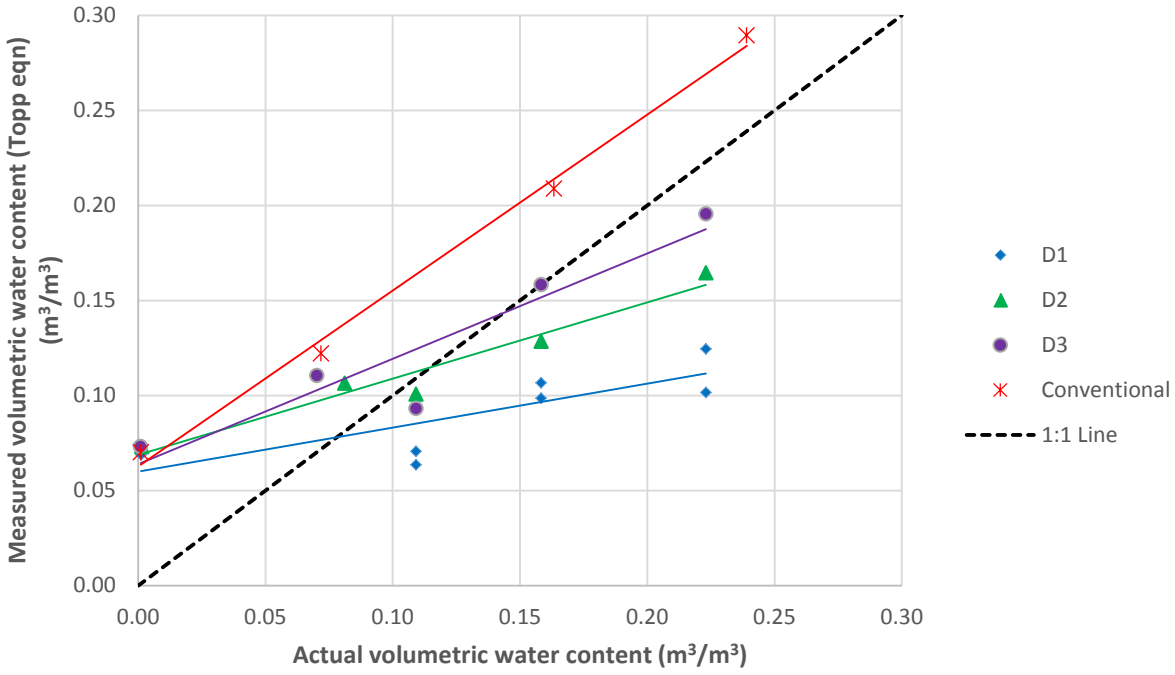

Figure 4.17 – Measured volumetric water content from compacted non-elevated salinity tailings sand testing at various water contents using two-rod unsheathed Delrin® prototype and conventional probes.

Table 4.5 – Trendline parameters for two-rod unsheathed Delrin® prototype and conventional probe testing in compacted non-elevated salinity tailings sand testing at various water contents.

Probe	Slope	Y-intercept	R^2
D1	0.231	0.060	0.598
D2	0.401	0.069	0.950
D3	0.554	0.064	0.877
Conventional	0.926	0.063	0.995

4.6.2 Two-Rod Sheathed Probe Configurations

Noise was evident to some degree in each of the prototype probe aggregate waveforms, as shown in Figure 4.18, along with bumps in some of the D3 waveforms, but neither to any level of great significance. Interpretation of the waveforms was somewhat difficult for some of the x_1 determinations, as there were "plateaus" and other poorly defined peaks along with generally inconsistent locations for the x_1 points. Determination of the x_2 points was not as difficult for the most part as the reflection from the end of the probes were reasonably well defined. There were instances, however, of atypical reflections for the D1 probe.

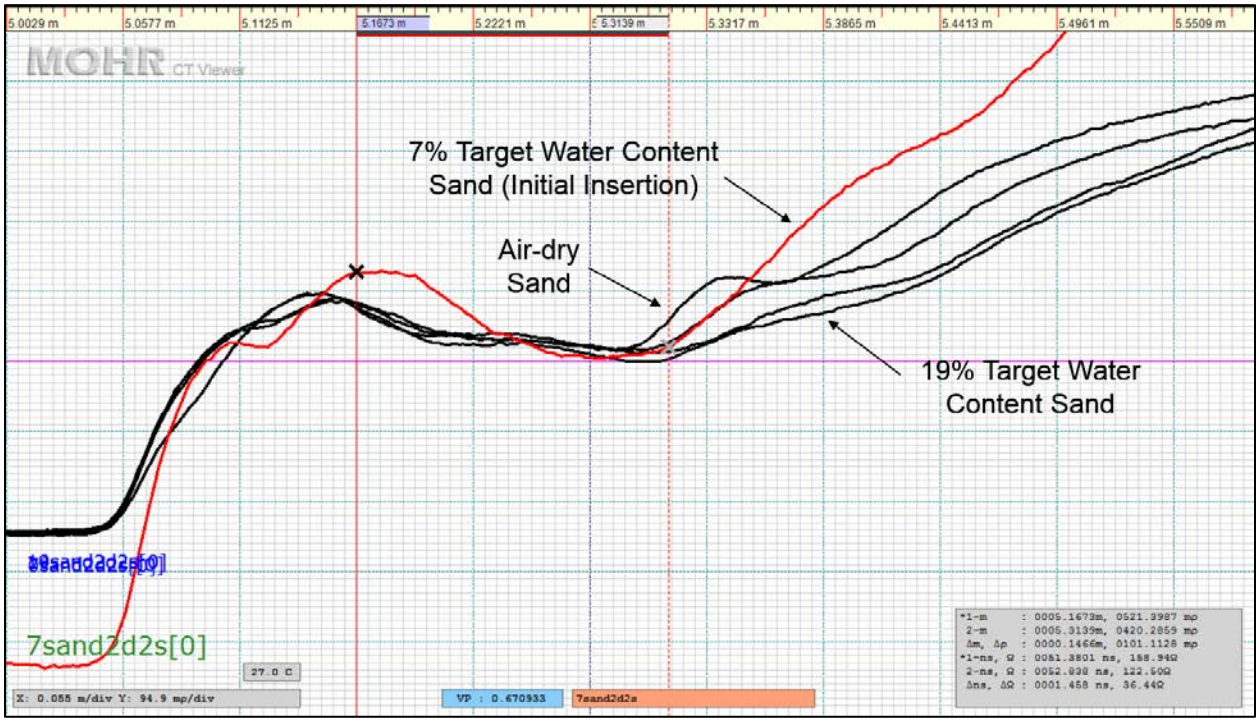

Figure 4.18 – Two-rod sheathed Delrin® prototype probe aggregate waveform for compacted non-elevated salinity sand testing. Waveforms generally progress from air-dry to 19% target gravimetric water content (D2 probe data shown). Note "plateau" peak with some noise for the x_1 location of the initial insertion 7% gravimetric water content sand waveform (red waveform – scale exaggerated for illustrative purposes, but vertical scales matched for all other waveforms). Locations for both x_1 and x_2 points are indicated by the cursors.

Measured volumetric water contents for each probe compared with the actual water contents are shown in Figure 4.19, with parameters from the trendlines summarized in Table 4.6. As with the unsheathed probe results, there are similarities to the reference solution testing, the most obvious being the lack of sensitivity and common response in each of the prototype probes. Interestingly, the conventional probe is substantially more sensitive in this testing, overestimating all but the wettest of the tested sands. The prototype probes show an overestimation of water content in sands lower than approximately 0.08 m^3/m^3. Measured values for the air-dry sand are very similar for each of these probes. Fit for this data is not good, with the exception of the conventional probe. As in previous plots, the fit for the D1 trendline would be better if there were no air-dry sand data points.

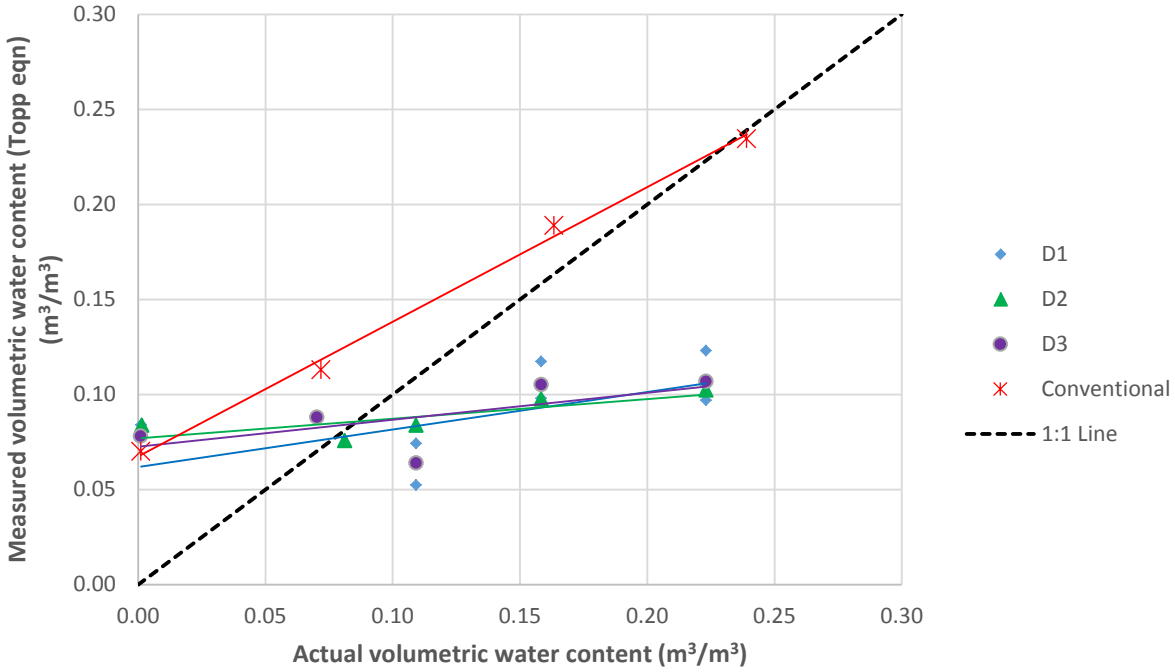

Figure 4.19 – Measured volumetric water content from compacted non-elevated salinity tailings sand testing at various water contents using two-rod sheathed Delrin® prototype and conventional probes.

Table 4.6 – Trendline parameters for two-rod sheathed Delrin® prototype and conventional probe testing in compacted non-elevated salinity tailings sand testing at various water contents.

Probe	Slope	Y-intercept	R^2
D1	0.198	0.062	0.330
D2	0.104	0.077	0.621
D3	0.142	0.073	0.434
Conventional	0.709	0.067	0.996

4.6.3 Three-Rod Unsheathed Probe Configurations

Some degree of progression in the waveforms was seen in this portion of testing (Figure 4.20). The quality of the three-rod unsheathed waveforms was generally good, with some minor instances of noise and bumps. Interpretability of the waveforms was also good, although there were some minor difficulties in determining the location of the x_1 points due to plateaus or double peaks. Determination of the x_2 points was straight-forward. The waveforms from the conventional probe were of good quality and very easy to interpret, and the x_1 points coincided well, suggesting the benefits of fixed connections. It should be noted that the 14% target gravimetric water content sand waveform was not completely captured making the determination of x_2 somewhat approximate for the conventional probe.

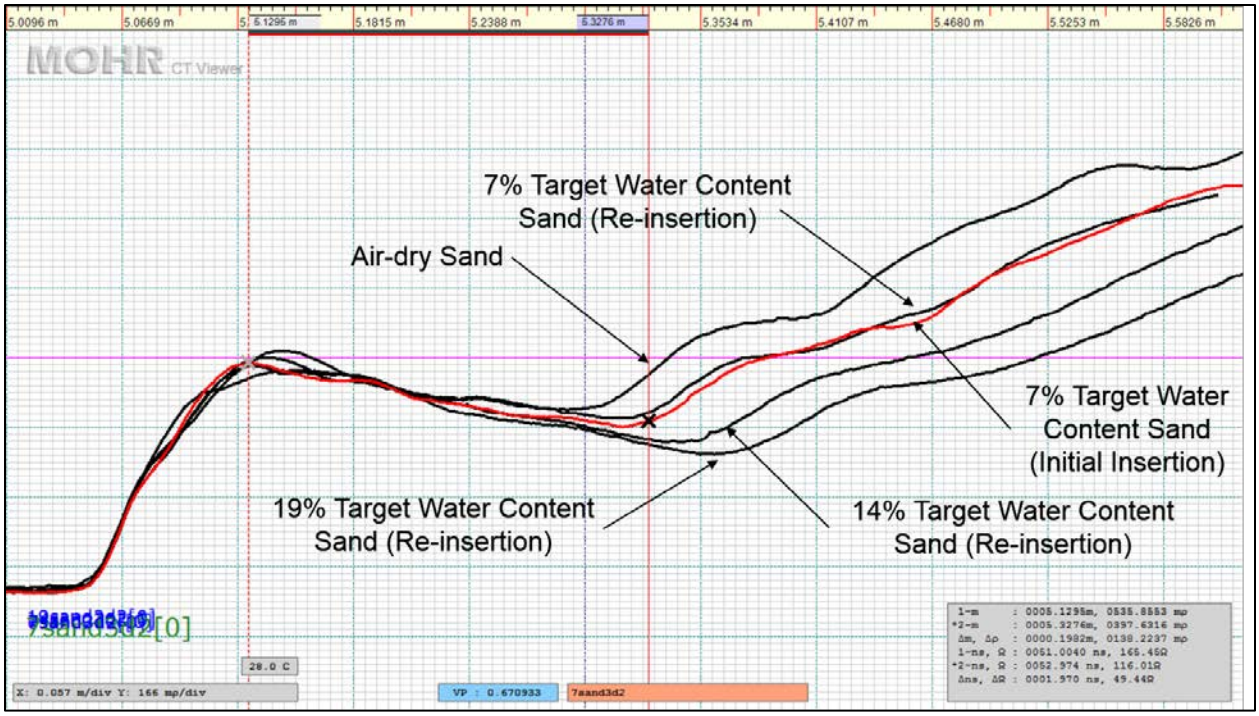

Figure 4.20 – Three-rod unsheathed Delrin® prototype probe aggregate waveform for compacted non-elevated salinity sand testing. Note minor "double peak" for the x_1 location of the initial insertion 7% target gravimetric water content sand waveform. Locations for both x_1 and x_2 points are indicated by the cursors. (D2 probe data shown. Vertical scales matched for all waveforms.)

Despite the good characteristics of the waveforms, however, the fit of the plots comparing the measured and actual volumetric water contents was poor, as can be seen in Figure 4.21. The D3 probe had the best fit of the prototype probes, but there were still a number of outliers. Variability in the results of the D1 probe was again quite substantial, with a large change in response from the 7% target gravimetric water content to that of the air-dry sand. The sensitivity of the probes increased with decreasing rod embedment, while overestimation of water content was seen in all but the D1 probe's response to the wetter sands. The measured value of air-dry sand was very similar with the D2 and D3 probes. Water contents calculated from the conventional probe results plotted very close to the 1:1 line. A summary of the trendline parameters are presented in Table 4.7.

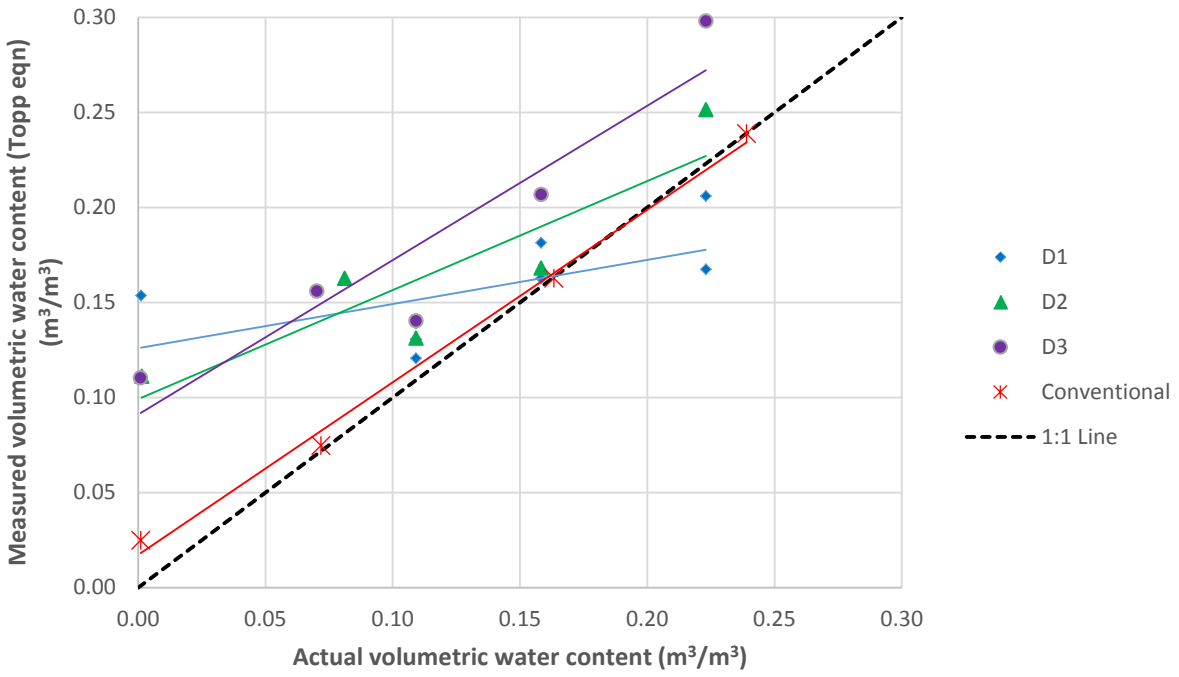

Figure 4.21 – Measured volumetric water content from compacted non-elevated salinity tailings sand testing at various water contents using three-rod unsheathed Delrin® prototype and conventional probes.

Table 4.7 – Trendline parameters for three-rod unsheathed Delrin® prototype and conventional probe testing in compacted non-elevated salinity tailings sand testing at various water contents.

Probe	Slope	Y-intercept	R^2
D1	0.232	0.126	0.357
D2	0.574	0.099	0.790
D3	0.812	0.091	0.871
Conventional	0.908	0.017	0.995

4.6.4 Three-Rod Sheathed Probe Configurations

The quality of the waveforms collected from this testing was good, with minimal amounts of noise present. Interpretability of the waveforms, however, was difficult for the D1 and D3 probes. This was because of issues in determining the x_1 locations from dual or poorly defined peaks and inconsistent x_1 locations in general, as discussed in Section 4.2. The data provided by the D2 probe was relatively straight-forward to interpret. Determining the x_2 points was generally straight-forward for each of the prototype probes, although some of the reflections at the end of the probe were lacking in definition. The conventional probe waveforms were generally good, but as with the unsheathed probe, the waveform for the 14% target gravimetric water content sand was not completely captured, resulting in an approximate reading for the x_2 location. The waveform for the air-dry sand was also unusual, making it difficult to determine the x_1 and x_2 positions, and also giving a nonsensical result.

The fit for the data from these particular probes was quite poor, as shown in Figure 4.22 and Table 4.8. While there appears to be more sensitivity for the D1 and D2 probes than with the two-rod sheathed probes, the scatter of the plots is quite substantial suggesting poorer data. While poor, the results from the D1 and D2 probes are useful to some degree, although those from the D3 probe are not given the negative slope to the trendline. Volumetric water contents are underestimated by these two probes above approximately 0.11 m^3/m^3, and measured water contents for the air-dry sand is similar for both probes. There is not a large difference in response between the air-dry sand and the 7% target gravimetric water content sand. Ignoring the erroneous air-dry data point, the fit for the conventional probe would have been substantially better. Apart from this, the sensitivity of the conventional probe was quite good.

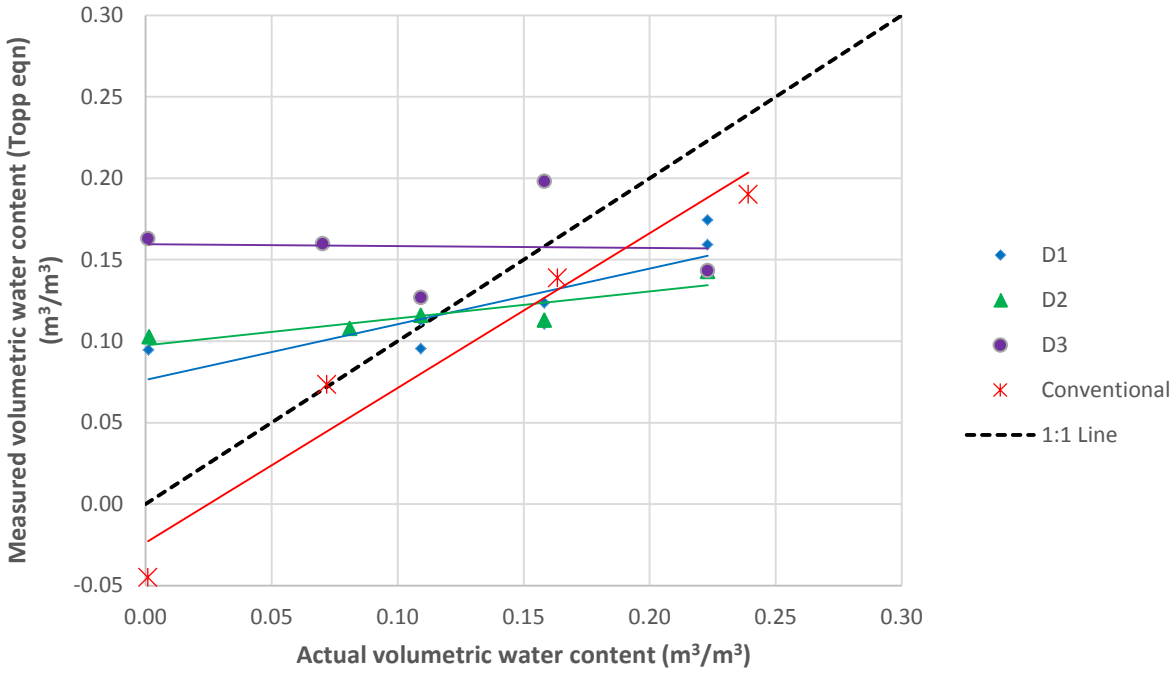

Figure 4.22 – Measured volumetric water content from compacted non-elevated salinity tailings sand testing at various water contents using three-rod sheathed Delrin® prototype and conventional probes.

Table 4.8 – Trendline parameters for three-rod sheathed Delrin® prototype and conventional probe testing in compacted non-elevated salinity tailings sand testing at various water contents.

Probe	Slope	Y-intercept	R^2
D1	0.341	0.076	0.725
D2	0.165	0.097	0.775
D3	-0.011	0.159	0.001
Conventional	0.950	-0.024	0.949

4.6.5 General Commentary on Compacted Non-Elevated Salinity Tailings Sand Testing

The amount of scatter was generally higher for the non-elevated salinity tailings sand testing than the reference solutions, making it harder to draw strong conclusions from the data. There were, however, a number of obvious trends that existed despite the scatter. One of these was the marked difference that continued to exist between the sheathed and unsheathed probes in terms of sensitivity, with the unsheathed probes being more sensitive. Trends of increasing sensitivity with decreasing rod embedment also continued to be seen in these results, but not to the same extent as with the reference solutions. Determining whether a similar trend existed for air-dry sand was difficult as there were some instances of large amounts of scatter in the data points.

In many cases the prototype probes had a different response to the air-dry sand than to the wetter sand. If a trendline was to be drawn for the wetter data points (i.e. target gravimetric water contents of 7% and greater), the measured volumetric water contents for the air-dry sand would typically fall above the trendline. A change in probe response was also noted by Miyamoto and Chikushi (2006) for dry soils, with the measured dielectric constant for their very dry sand being greater for their prototype probe than the conventional three-rod probe. They suggested this to be due to the presence of plastic (acrylic) used in the construction of the probe. Aside from the difference in Delrin® prototype probe response for the air-dry sand, it would appear that there was no substantial change in response among the wetter data points. This was promising as the change in response between pure ethanol and air seen in the reference solution testing had caused some concern that this may not have been the case.

One interesting difference between this testing and the reference solution testing was the increased sensitivity of the conventional sheathed probes. The reason for this difference is unknown.

Clearly from the discussion here, scatter has been a major barrier to the collection of good data, and minimizing it would improve the evaluation of the probes. Improvements that could be made to the testing methodology to decrease scatter include eliminating air gaps around the probe during re-insertion and improving the electrical connections. While the electrical

connections could be easily improved, eliminating air gaps could be more difficult as air gaps were still present despite strong efforts to avoid them. Fortunately, this problem would likely be less of an issue in probe insertions in the field.

Other sources of scatter could be caused from errors in recording the probe insertion depth in re-insertion tests (i.e. how much of the probe's rods were above the soil surface), and changes in the soil water content. Issues existed with the re-inserted length of the probe not being recorded in the 7% and some of the 14% target gravimetric water content testing. Full insertion was assumed, but the true depth was unknown. Should any of these probes not have been completely inserted the measured dielectric constant, and therefore the calculated volumetric water content, would have been higher.

Errors in the actual volumetric water content determination also existed, and originated from the collection of gravimetric water content samples used in their calculation. The samples were collected during deconstruction of the cylinder following testing, and as such the sand would have dried out over the period of testing. This was particularly the case in the re-insertion tests where the sand was exposed to the air for longer periods of time than in the cylinders where no re-insertion was done. Tests done immediately after the initial packing would therefore have actually occurred at higher water contents, thus skewing the results. A trend suggesting this had occurred was seen in many of the measured water contents for the D1 probe (Appendix D), with progressively lower water contents measured for successive probe insertions in the same packed sand. For example, the measured volumetric water contents for the three-rod unsheathed D1 probe went from 0.139 to 0.131 to 0.121 m^3/m^3 in the 7% target gravimetric water content sand, and from 0.206 to 0.167 m^3/m^3 in the 19% target gravimetric water content sand over successive insertions.

Another observed phenomenon which would add error to the water content determination was water that moved down through the sand during testing. In most cases the water content was greater with depth when sampled at the end of testing, with increasing differences with depth in the wetter sand. For example, the gravimetric water content for the D2 probe in the 7% target gravimetric water content sand was 5.6% in the lift at the top of the probe (Lift 6), and 5.8% at

the bottom of the probe (Lift 2). In the 19% target gravimetric water content sand for the prototype probes the gravimetric water content was 14.9% in Lift 6 and 18.7% in Lift 2. Presumably the water content in the bottom lift (Lift 1) was even greater, potentially leading to an underestimate in the measured water content since the TDR measures the average water content only along the length of the probe. No sensing is achieved beyond the end of the probe, so excess water that had drained into Lift 1 would not be accounted for in the reading. Assuming that more water would drain into Lift 1 as the testing progressed, the volumetric water content measured by the probes would appear to drop with progressive TDR readings.

Overall, the D2 probe appeared to be the best in terms of fit, and its interpretability was also relatively good. While it did not have the highest levels of sensitivity, its levels were typically still reasonable. As a result, the D2 probe was chosen as the probe to move forward with to the following rounds of testing. A case could have been made for using the D3 probe instead of the D2, as it exhibited better sensitivity on the whole from the testing program. Realistically, however, using a probe in the field with non-embedded rods would have a much higher likelihood of having its rods torn off during insertion, as discussed previously.

4.7 Compacted Elevated Salinity Tailings Sand Testing

The D2 probe was tested further to evaluate its response to increasing levels of salinity in the tailings sand at a constant water content. This testing would help to determine the limitations of the probe to increasing salinity and electrical conductivity. Additional testing was also done to examine the effects of connection orientation and, for the two-rod probe configurations, rod spacing. As with the previous tests, conventional two- and three-rod probes were also tested for comparison.

Results interpreted from the individual probes are presented in Appendix C, and water content results from the packed cylinders are given in Appendix D.

4.7.1 Two-Rod Unsheathed Probe Configurations

Waveforms for the elevated salinity tailings sand testing were generally noisier than the equivalent non-elevated salinity ones, with increased noise in the higher salinity soils. However, the general increase in noise was partly due to the fact that when the waveform was captured on the TDR unit during testing, a much larger portion of the waveform was captured than necessary. As a result, "zooming in" on the section of interest made for a noisier waveform as the available resolution for that portion of the waveform was reduced, as discussed in Section 4.3. Noise was not an issue for interpretability in the 2.5 and 5 g/L salinity sand, but did have an effect on the interpretation of the 10 g/L salinity sand waveform. An excessively high dielectric constant was also measured in one of the 10 g/L re-insertions. This measurement was assumed to be the result of the probe grounding out on the steel shaft insert as opposed to shorting out in the soil, since more typical measurements were also found at this salinity.

Bumps were seen in each of the aggregate waveforms to some degree, but were more exaggerated in the 5 and 10 g/L salinity sand waveforms for the closely spaced rod testing. This was especially the case after the end of probe reflection, which complicated the interpretability of the x_2 points slightly. It appeared that there was some relation between poor definition in the trough and horizontal rod connections in the 10 g/L salinity sand. Likewise, a relationship seemed to exist between double peaks or plateaus for the vertical rod connections, making the determination of the x_1 points somewhat ambiguous. A sample aggregate waveform is shown in Figure 4.23.

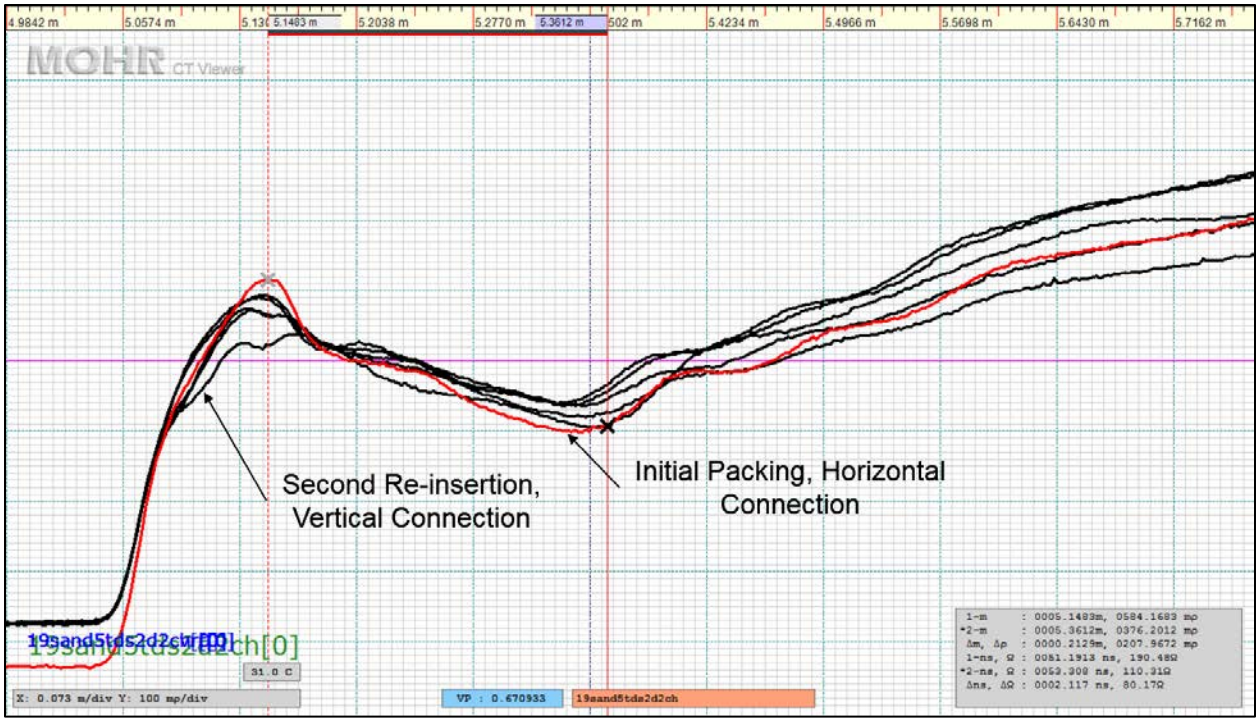

Figure 4.23 – Two-rod unsheathed closely-spaced D2 prototype probe aggregate waveform from compacted 5 g/L elevated salinity sand testing. Note double peak for labelled vertically connected configuration, and bumps following end of probe reflection in horizontally connected configuration. Locations for both x_1 and x_2 points indicated by cursors for horizontally connected configuration. Labelling of all individual waveforms neglected for clarity. Vertical scales matched for all waveforms, except for red waveform whose scale is exaggerated for emphasis.

4.7.2 Two-Rod Sheathed Probe Configurations

Noise in the two-rod sheathed probe testing was not as obvious as that in the unsheathed testing, and did not have any impact on the interpretability of the waveforms. Bumps were again present, but did not cause any issues with interpretability. Double peaks were also noted, and seemed to be more prevalent for vertically oriented connections. This, combined with instances of inconsistent peak locations, made some of the interpretation of x_1 locations challenging. There were a few cases of poorly defined troughs as well, but they did not affect the interpretability of the waveforms. In general, the interpretability of these waveforms was straight-forward. One instance of what is assumed to be a probe grounding out on the steel shaft insert is shown in the aggregate waveform in Figure 4.24.

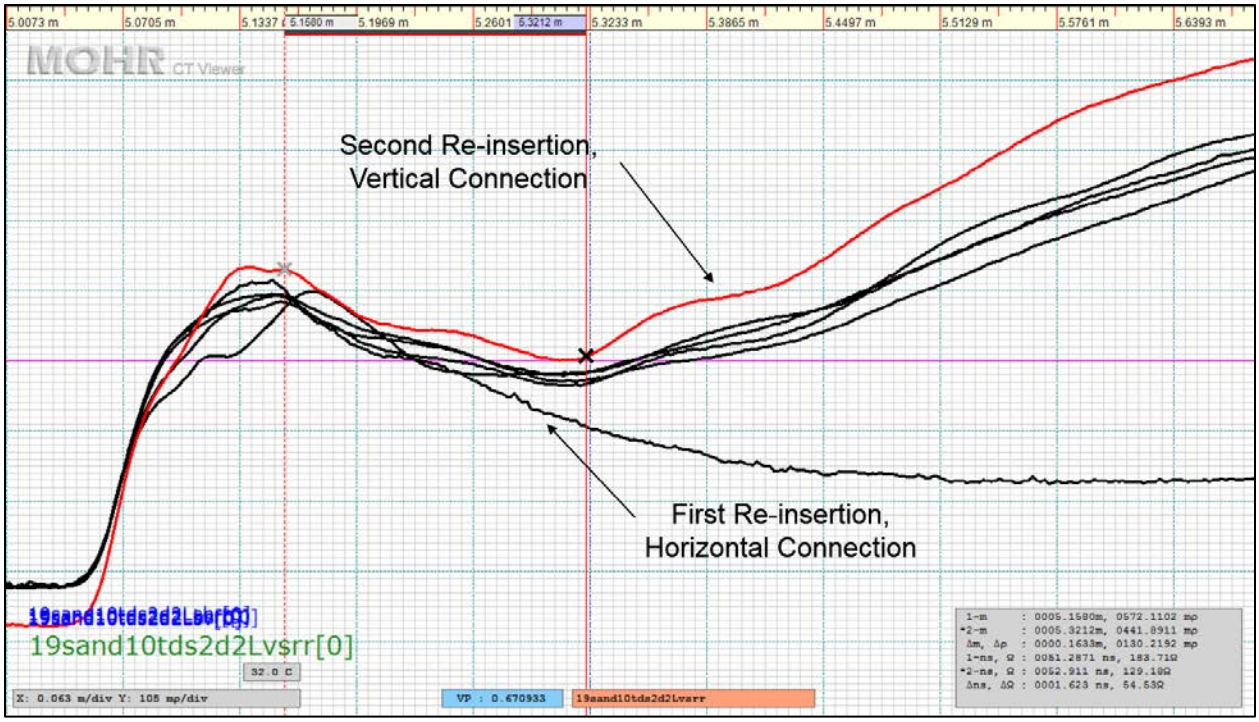

Figure 4.24 – Two-rod sheathed long-spaced D2 prototype probe aggregate waveform from compacted 10 g/L elevated salinity sand testing. Note subtle double peak for labelled vertically connected configuration. Waveform for what is assumed to be a grounded out probe shown for labelled horizontally connected configuration. Locations for both x_1 and x_2 points indicated by cursors for vertically connected configuration. Labelling of all individual waveforms neglected for clarity. Vertical scales matched for all waveforms, except for red waveform whose scale is exaggerated for emphasis.

4.7.3 Three-Rod Unsheathed Probe Configurations

Noise was more evident in the three-rod unsheathed probe testing than in the two-rod unsheathed probe testing, especially in the 5 and 10 g/L salinity sand testing. In the latter case, there was sufficient noise to affect interpretability. Noise in the 2.5 g/L salinity sand was negligible. The noisiest waveforms in the 10 g/L salinity sand appeared to be associated with the horizontally orientated connections, and excessively high dielectric constants were measured in two of these instances. As with the unsheathed two-rod results, these two measurements were assumed to be the result of the probe grounding out on the steel shaft insert.

Bumps were also found to be present, although they did not pose a challenge for most of the interpretation. There were instances, however, in the 10 g/L salinity sand testing where poorly defined troughs and double troughs made interpretation difficult (Figure 4.25). Double peaks were again noted in a number of the waveforms, with most of them occurring with the vertically oriented connections. This complicated the interpretation of the actual x_1 locations. No double peaks were noted in the 10 g/L salinity sand testing, interestingly.

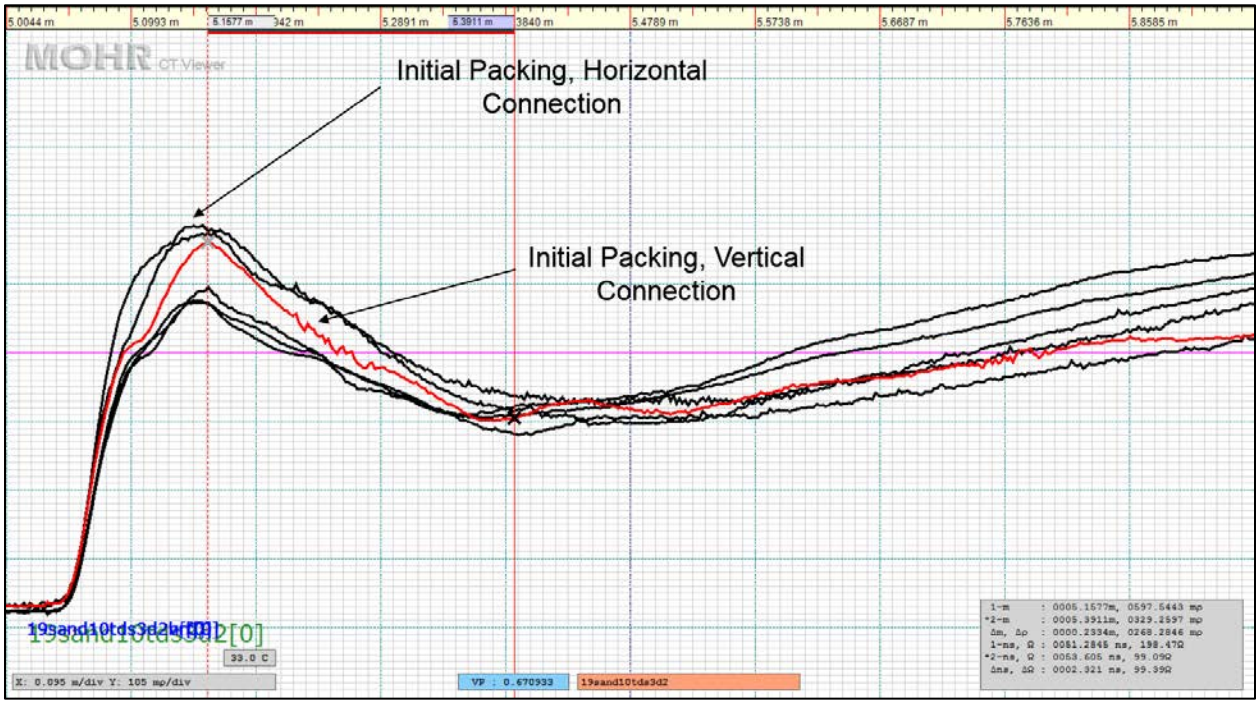

Figure 4.25 – Three-rod unsheathed D2 prototype probe aggregate waveform from compacted 10 g/L elevated salinity sand testing. Note double trough and noisiness for labelled vertically connected configuration, and general noisiness for labelled horizontally oriented connection. No double peaks were seen in the testing at this salinity. Locations for both x_1 and x_2 points indicated by cursors for vertically connected configuration. Labelling of all individual waveforms neglected for clarity. Vertical scales matched for all waveforms.

4.7.4 Three-Rod Sheathed Probe Configurations

Similar to the sheathed two-rod testing, the amount of noise evident in the waveforms was less than with their unsheathed counterparts; however, in this case there was less noise than with the two-rod testing. Few bumps were seen in the waveforms, but in some instances they occurred

after the trough, making the determination of the x_2 position more challenging. Issues with double and plateau peaks or peaks that were inconsistent in location were experienced for a number of the waveforms, causing ambiguity in the determination of the x_1 positions. Once again, these occurrences appeared to be linked more strongly to vertically oriented connections. An example of the waveforms from this testing is presented in Figure 4.26.

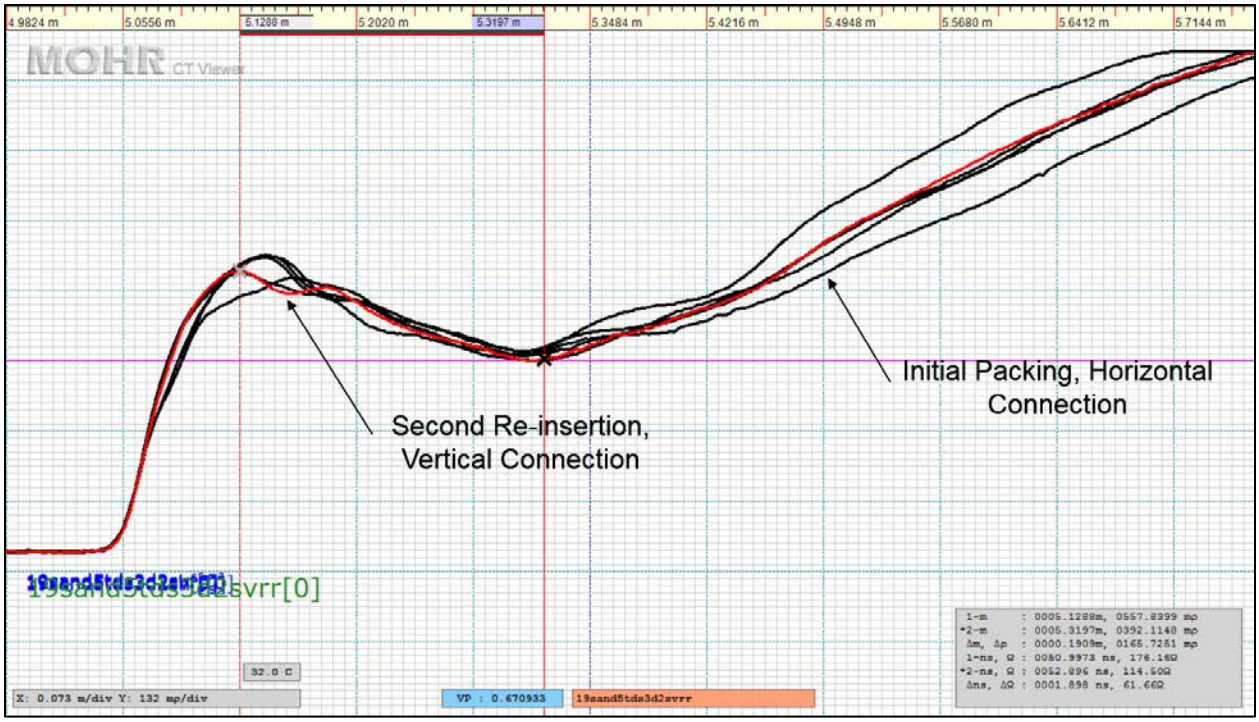

Figure 4.26 – Three-rod sheathed D2 prototype probe aggregate waveform from compacted 5 g/L elevated salinity sand testing. Note double peak for labelled vertically connected configuration, and bump after the trough for labelled horizontally oriented connection. Locations for both x_1 and x_2 points indicated by cursors for vertically connected configuration. Labelling of all individual waveforms neglected for clarity. Vertical scales matched for all waveforms.

4.7.5 Conventional Probe Configurations

Substantial differences existed between the two-rod and three-rod conventional probe waveforms, with the three-rod waveforms being much higher quality. The three-rod probe waveforms were much better defined with less noise and bumps. In both the unsheathed probe variants, and to a lesser extent in the three-rod sheathed probe, the influence of increasing

salinity was evident. The waveforms "degraded" as the salinity increased, to the point of the unsheathed two-rod probe shorting out in the 10 g/L salinity sand. Double peaks, although more subtle than were seen in a lot of the prototype probe testing, were found in a number of the two-rod probe waveforms. This did not affect interpretability of the waveforms substantially, but seemed to be more prevalent with the vertically connected steel clips. Aggregate waveforms from the two-rod unsheathed probe and the three-rod sheathed probe are shown in Figure 4.27 and Figure 4.28, respectively.

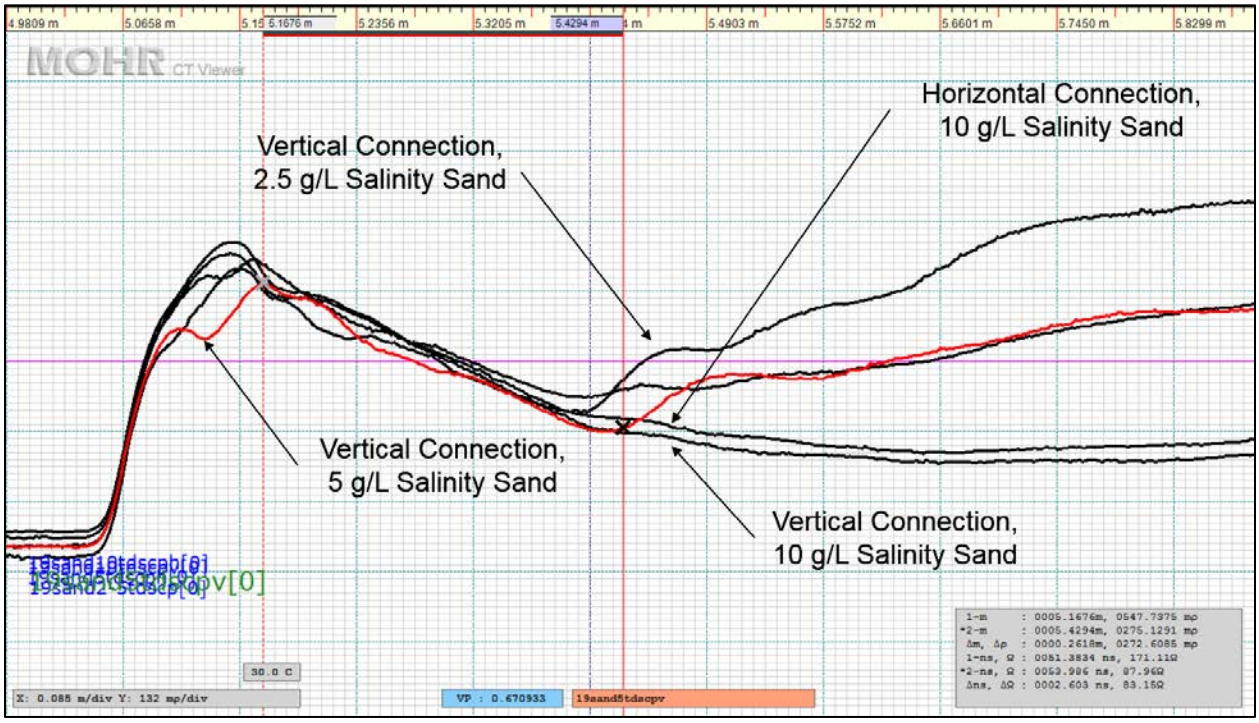

Figure 4.27 – Conventional unsheathed two-rod probe aggregate waveform from elevated salinity sand testing. Note shorted out waveforms from the 10 g/L salinity sand testing. Locations for both x_1 and x_2 points indicated by cursors in vertically connected 5 g/L salinity sand (red waveform). Labelling of all individual waveforms neglected for clarity. Vertical scales matched for all waveforms.

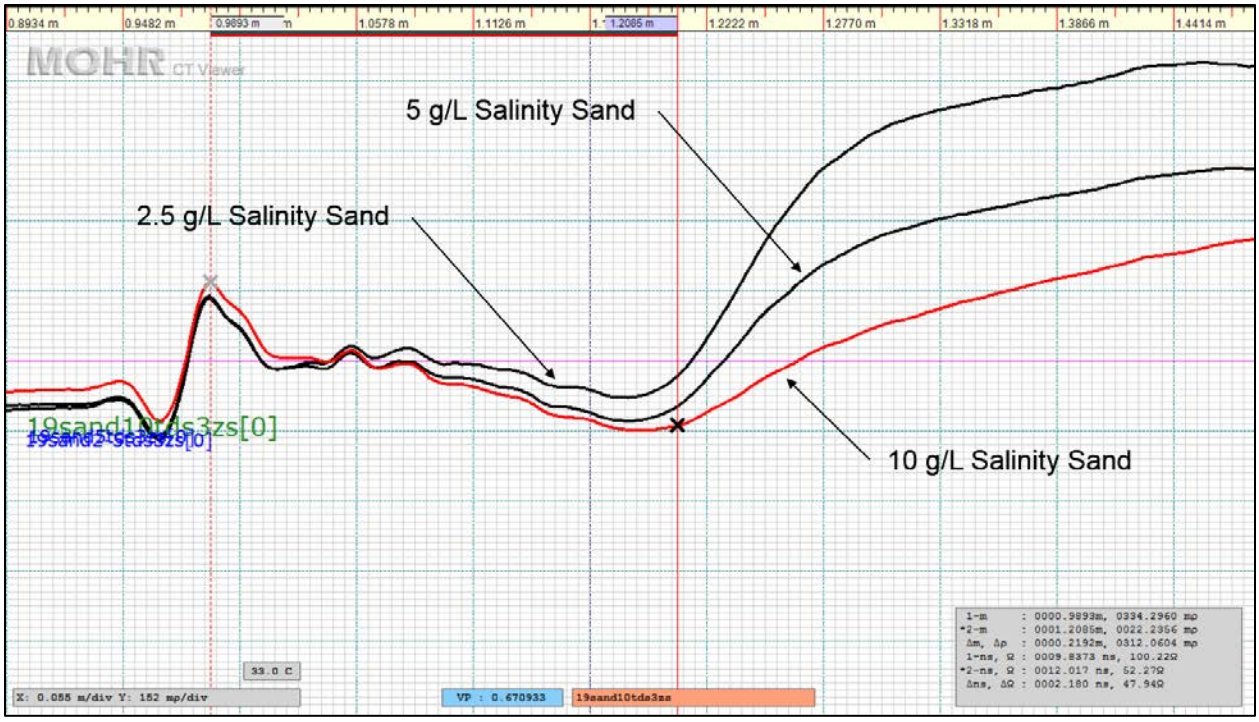

Figure 4.28 – Conventional sheathed three-rod probe aggregate waveform from elevated salinity sand testing. Note decrease in waveform amplitude with increased salinity. Locations for both x_1 and x_2 points indicated by cursors in 10 g/L salinity sand (red waveform). Vertical scales matched for all waveforms.

4.7.6 General Commentary on Compacted Elevated Salinity Tailings Sand Testing

Since all of the testing for this round was done at a constant water content, comparisons between different "treatments", e.g. horizontal or vertical connections, were more difficult to make. As a result, statistical analyses of the data were done to determine which treatments were significant in terms of the results. The statistical program IBM SPSS Statistics, Version 22 (IBM 2013), was used for the analysis of variance (ANOVA) on the means of the different treatments. Multiple comparisons of the observed means were done using the least significant difference (LSD) test. An α level of significance of 0.05 was used for all testing. Results that were attributed to the probe either grounding or shorting out were considered to be outliers, given their excessively high measured volumetric water contents. These results were not considered in the analysis. The actual volumetric water contents for the tests, 0.221, 0.215 and 0.214 m^3/m^3, and 0.227, 0.233 and 0.234 m^3/m^3, for prototype and conventional probe testing at increasing salinities, respectively, were assumed to be identical for the purposes of this analysis since they

are within the range of measurement error for TDR (±0.02 m^3/m^3). A summary of the outputs from SPSS are found in Appendix E.

Salinity was found overall to be statistically significant in the two-rod testing, but not in the three-rod testing. Whether this was actually the case for the two-rod testing, however, was questionable since the mean of the measured water contents for the 5 g/L salinity sand test was significantly different from the 2.5 and 10 g/L tests, but the 2.5 and 10 g/L results were not significantly different from each other. This is shown in Figure 4.29. It would appear that the trend of these results was not linked to increasing salinity. Furthermore, since the difference of the means of the measured water contents are within 0.02 m^3/m^3 of each other, it is reasonable to assume that this spread in results would be within the measurement error range. Nonetheless, in order to more fully investigate this, testing in a broader range of soil salinities would be required.

Response of the conventional three-rod probes showed effects of increasing electrical conductivity degrading the signal (i.e. decreasing the slope following the end of probe reflection; see Figure 4.28), although throughout the elevated salinity testing they did not short out. The conventional two-rod unsheathed probe did short out in the 10 g/L salinity sand testing, confirming the results of Zegelin et al. (1989) that a conventional two-rod probe performs more poorly than a three-rod probe in saline soils. While there were a few instances of excessively high dielectric constants measured in the 10 g/L salinity sand with the unsheathed prototype probes, most of the measurements were typical. This suggests that there may be some increase in the range of the prototypes into elevated salinity soils as a result of the partial rod embedment.

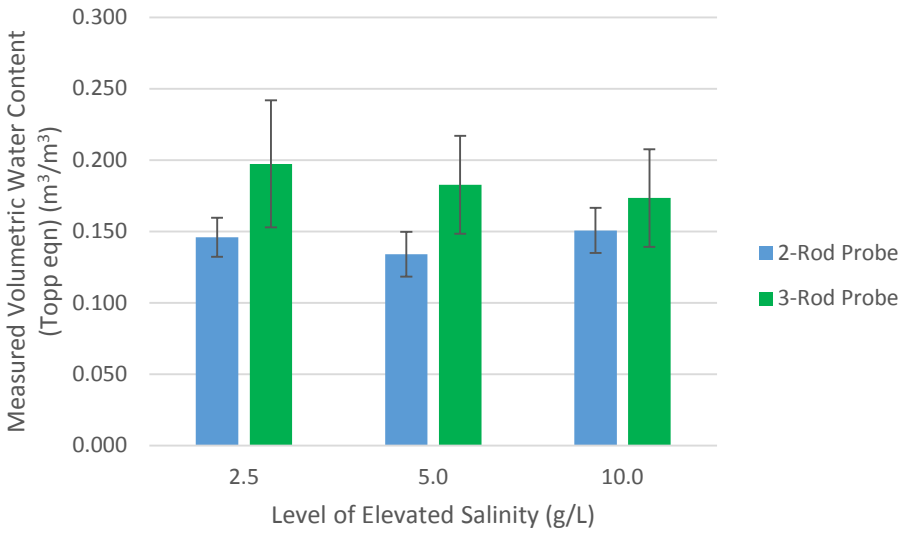

Figure 4.29 – Comparison of the effect of elevated salinity in tailings sand on the mean volumetric water content values measured by two- and three-rod Delrin® prototype probes. Error bars indicate the 95% confidence intervals. Average actual water content for prototype probe tests: 0.217 m^3/m^3.

Changing the rod spacing in the two-rod prototype probes was not found to produce significantly different results in the measured volumetric water contents. It is expected, though, that there may be a difference at even higher salinities where the larger fields generated by far-spaced rods would be subject to a proportionally higher amount of salt. This increased salinity would likely start to degrade the signal. The fact that the spacing did not generate significantly different results also suggests that the establishment of a skin effect was not an issue in the far-spaced probe configuration.

Qualitatively, there appeared to be better peak quality (i.e. less double peaks) in the waveforms when connections were made to the rods horizontally rather than vertically. A difference in the results was also found to be significant in the two-rod testing, with the horizontal connections generating a higher mean in the measured water contents, as shown in Figure 4.30. This potentially translates to more accurate results. Horizontal connections may have been significant in the three-rod testing as well, had the steel clips on the jumper cable been different. The ones that were used lacked the greater surface area of the “sleeves” in the clips at the end of the

coaxial cable. Regardless of whether the differences were significant, however, it can be said that improving the quality of the electrical connections would be beneficial from the perspective of improving waveform interpretation. Possible improvements to accuracy, as seen by Casanova et al. (2012a), would be another clear benefit.

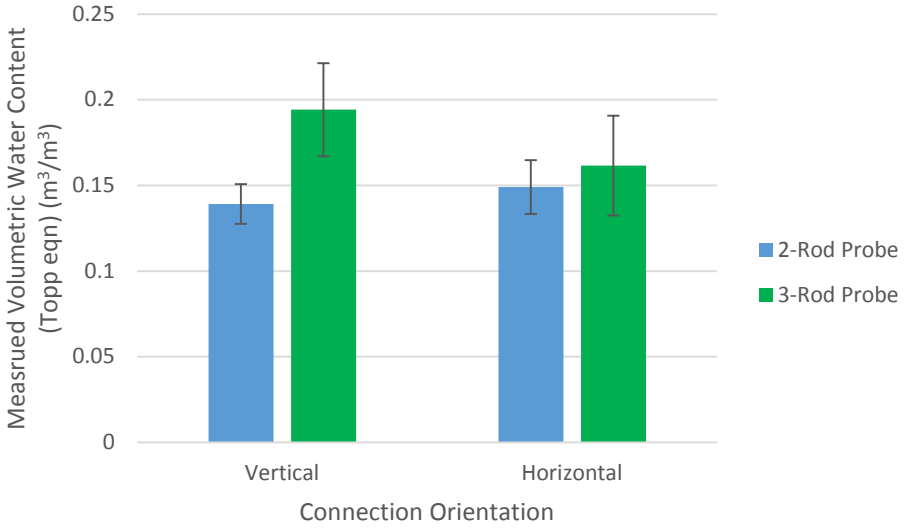

Figure 4.30 – Comparison of the effect of electrical connection orientation on the mean volumetric water content values measured by two- and three-rod Delrin® prototype probes. Error bars indicate the 95% confidence intervals. Average actual water content for prototype probe tests: 0.217 m^3/m^3.

Not surprisingly, sheathed probes produced quite significantly different results from unsheathed ones. Conventional probes also produced significantly different results than the Delrin® prototype probes, with the measured values for the water content being greater for the conventional probes. No significant difference was found between the two- and three-rod data for the combined conventional and prototype probe data. However, there was a significant difference between the results of the two- and three-rod prototype probes, with the three-rod probes generating greater measured values for the water content. It should be noted that because only one insertion was done for the conventional probe testing, comparisons between the number of rods and probe type (i.e. conventional and prototype probes) were based solely on the initial packing.

The effect of probe re-insertion on the measured value of the water content was significant for the two-rod probe, but not for either the three-rod probe or the combined results of both the two- and three-rod prototype probes. In the case of the two-rod probe, the mean value for the first insertion was lower than the second (i.e. first re-insertion), but higher than the third, as shown in Figure 4.31. As with the effect of salinity, it is unclear whether this was a true effect or not, since it would intuitively be expected that the water content would drop with increasing re-insertions. Considering again the difference in the means of the measured water contents, the values are all well within the measurement error range of 0.02 m^3/m^3.

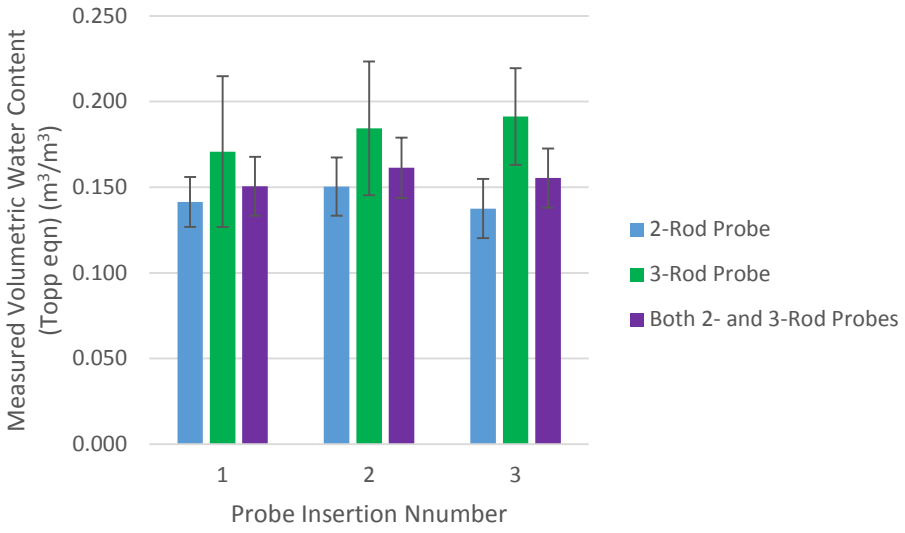

Figure 4.31 – Comparison of the effect of probe re-insertion on the mean volumetric water content values measured by two- and three-rod Delrin® prototype probes. Error bars indicate the 95% confidence intervals. Average actual water content for prototype probe tests: 0.217 m^3/m^3.

Two-way ANOVA testing was performed on the results of the various treatments as well. Of the tests which showed statistical significance, only the relationship between sheathing and salinity was physically meaningful. As previously discussed, while the effect of sheathing was definitely significant, the effect of salinity was questionable. Regardless of the actual results seen in the testing, it would be reasonable that in general use, as the salinity of the soil increased, the probe's response would be increasingly different depending on whether it was sheathed or unsheathed.

The results of the conventional two- and three-rod sheathed probes were not compared to determine whether sheathing thickness would be influential. Given the large differences in the nature of the two probe types, however, it would likely not be statistically relevant to investigate this. It is assumed, though, that similar to the effects of increasing sensitivity with decreased probe embedment in the unsheathed prototype probes, a thinner sheathing layer would increase the sensitivity of the probes in general, as suggested by Ferré et al. (1996) and Fujiyasu (et al. 2004). While a thinner sheathing layer would possibly have benefits for the prototype probes, it would also be more susceptible to damage from rocks or friction in the soil. This could possibly compromise the performance of the probe. A consideration of these factors would be necessary in conducting further development of the probe.

It should be noted that similar to the non-elevated salinity sand testing, the water contents that were calculated gravimetrically at the end of each test increased towards the bottom of the column. Despite this increase, however, there was no clear trend in the water content measured by the probe decreasing with successive re-insertions for this testing. The reason for this is unknown, but the lack of trend suggests that the results for the elevated salinity sand testing have a higher level of variance than the non-elevated results did, obscuring the trend. Overall, the most substantial influence on performance, and therefore the quality, appeared to be due to the orientation of the connection with the probe. Spacing was not found to be significant, although this could change with higher levels of salinity. In terms of prototype probe response, there did appear to be some indication of the effective range of the probe being extended in elevated salinity soils.

Increasing salinity degraded the quality in the waveforms of the different prototype probe configurations, although more so for the unsheathed configurations than the sheathed. For the two different types of configurations the two-rod unsheathed probe and the three-rod sheathed probe produced the best waveforms.

4.8 FFT Testing

The D2 probe was also evaluated using FFT samples to observe its response to high water contents and elevated salinity. Rod spacing and connection orientation typical of the non-elevated salinity tailings sand testing was used for the Delrin® probe configurations. Three-rod conventional probes were also used for comparison testing. The results from this testing follow.

4.8.1 Waveform Observations

The responses of all the probe configurations tested will be discussed in this section.

As with the tailings sand testing, common x_1 points were again not generally characteristic of the waveforms from the prototype testing in FFT. However, the variability in x_1 location seen in the unsheathed probes was lower than that seen in the sand testing. Despite the increased levels of salinity in the FFT, excess noise and bumps were not strongly obvious in the unsheathed probe configurations, although definition in the end of probe reflections was lacking, as seen in Figure 4.32. This was most likely due to the high salinities in the FFT causing the probes to verge on shorting out. Noise was not that substantial in the sheathed probe configurations either, although there were considerably more bumps, with multiple troughs also being noted. This caused challenges with determining the respective x_2 locations. There were also many instances of double or inconsistent peaks (Figure 4.33) which complicated the determination of the x_1 points as well. Apart from the poor definition in the unsheathed end of probe reflections, interpretation of those waveforms was straight-forward.

The interpreted waveform results from the individual probes are provided in Appendix C.

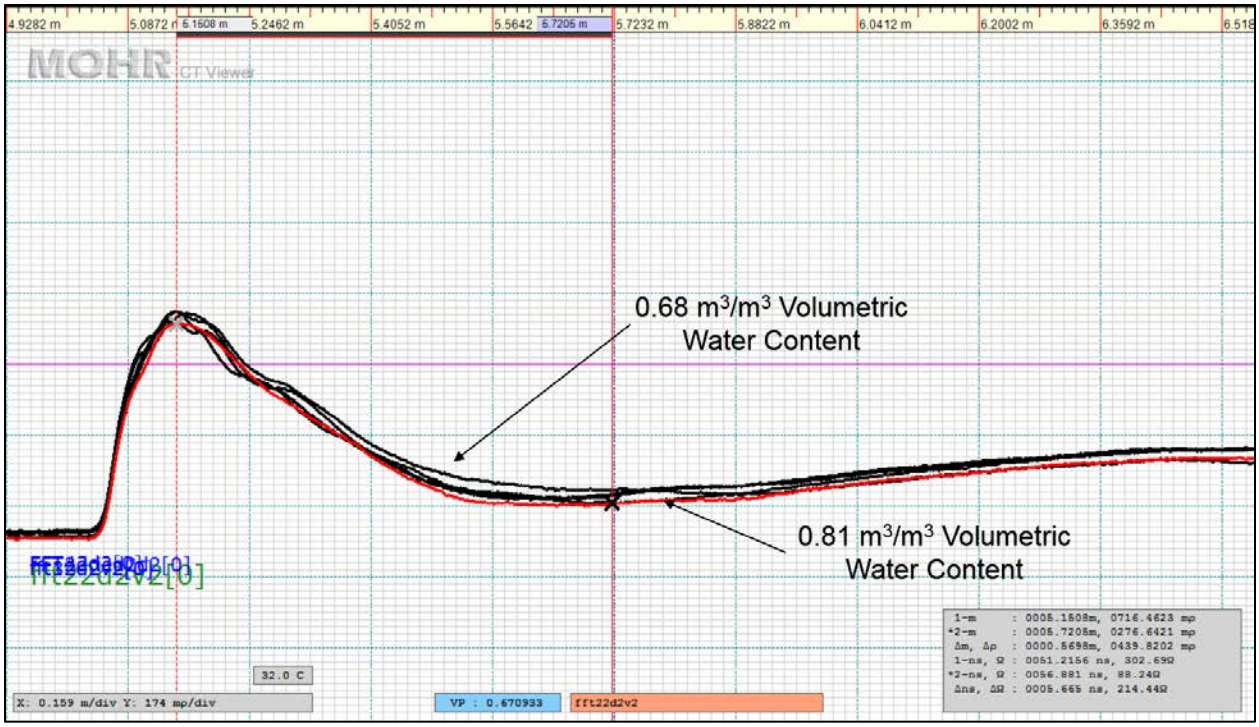

Figure 4.32 – Two-rod unsheathed Delrin® D2 prototype probe aggregate waveform for FFT testing. Note relatively consistent x_1 locations but poor definition in the end of probe reflections. Locations for both x_1 and x_2 points of the 0.81 m^3/m^3 volumetric water content FFT indicated by cursors (red waveform). Labelling of all individual waveforms neglected for clarity. Vertical scales matched for all waveforms.

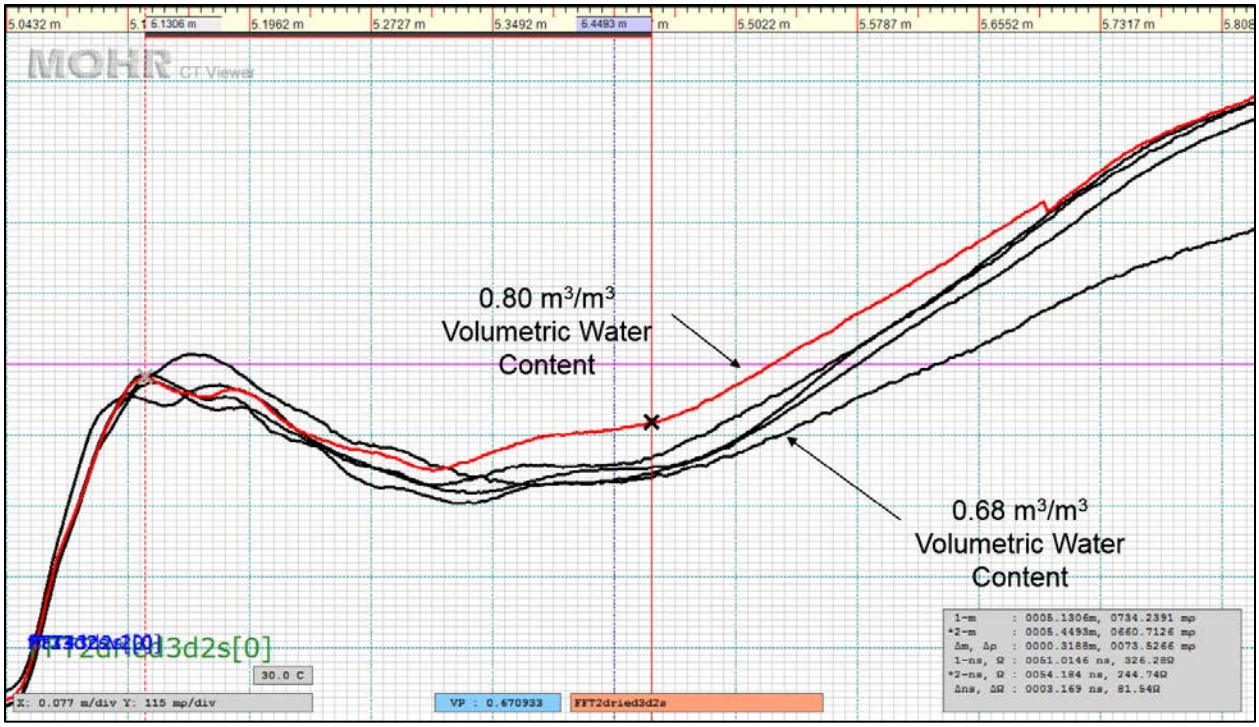

Figure 4.33 – Three-rod sheathed Delrin® D2 prototype probe aggregate waveform for FFT testing. Note multiple and moving peaks for the x_1 locations as well as multiple troughs for the x_2 locations. Locations for both x_1 and x_2 points of the 0.80 m^3/m^3 volumetric water content FFT indicated by cursors (red waveform). Labelling of all individual waveforms neglected for clarity. Vertical scales matched for all waveforms.

4.8.2 Interpreted Results from FFT Testing

The Topp equation is known to underestimate the volumetric water content in high water content soils (e.g. FFT) (Sorta et al. 2013). Sorta et al. (2013) fit an equation to tailings from the northeastern Alberta Albian Sands Energy Inc. Muskeg River oil sands mine that better expressed the relationship between dielectric constant and volumetric water content for their specific samples. Despite the fact that the Sorta equation was developed for tailings from a different oil sands mine, the equation was applied to these results from the Syncrude tailings since it was likely similar in composition.

Plots of the actual water contents compared with the measured values using both the Topp and Sorta equations are shown in Figure 4.34, Figure 4.35 and Figure 4.36. Water content results

from the FFT sub-samples themselves are provided in Appendix D. A summary of the trendline parameters are given in Table 4.9. Results from the two unsheathed Delrin® probe configurations were poor, largely due to the fact that the measured dielectric constants were very high, especially with the three-rod probe. This is indicative of the probes verging on shorting out. Applying either of the two equations to these data did not result in useful, relevant data, and as a result the data was not considered further.

In general, the sheathed three-rod Delrin® probes were marginally more sensitive and produced a relatively better fit than the two-rod configurations. Sensitivity was also slightly increased when the Sorta equation was applied to the data as opposed to the Topp equation. The conventional sheathed probe provided similar results, although the fit was somewhat better, and the increase in sensitivity was larger. Application of the Sorta equation to the conventional unsheathed probe, however, dramatically increased sensitivity relative to that of the Topp equation such that it plotted along the 1:1 line. This was the only instance where the probes did not underestimate the water contents. The fit of the conventional unsheathed probe data was good for both the Topp and Sorta equations; however, more variation in the water contents of the tested FFT could likely have further improved the fit.

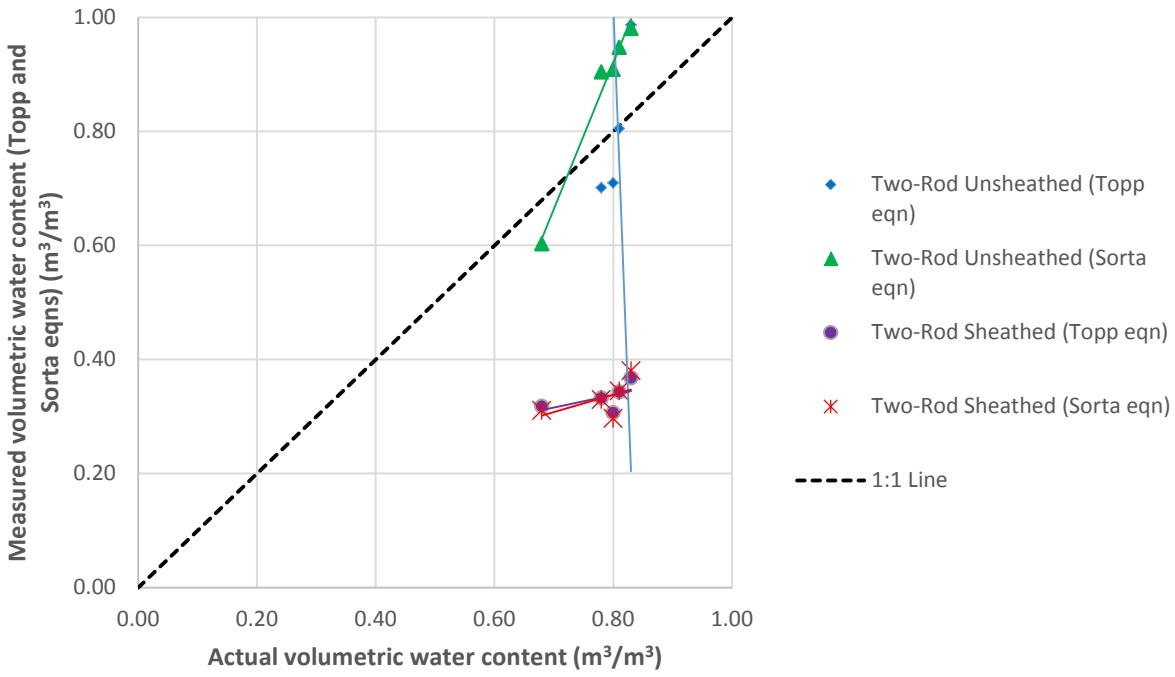

Figure 4.34 – Measured volumetric water contents (Topp and Sorta equations) from FFT testing at various water contents using two-rod Delrin® prototype probes.

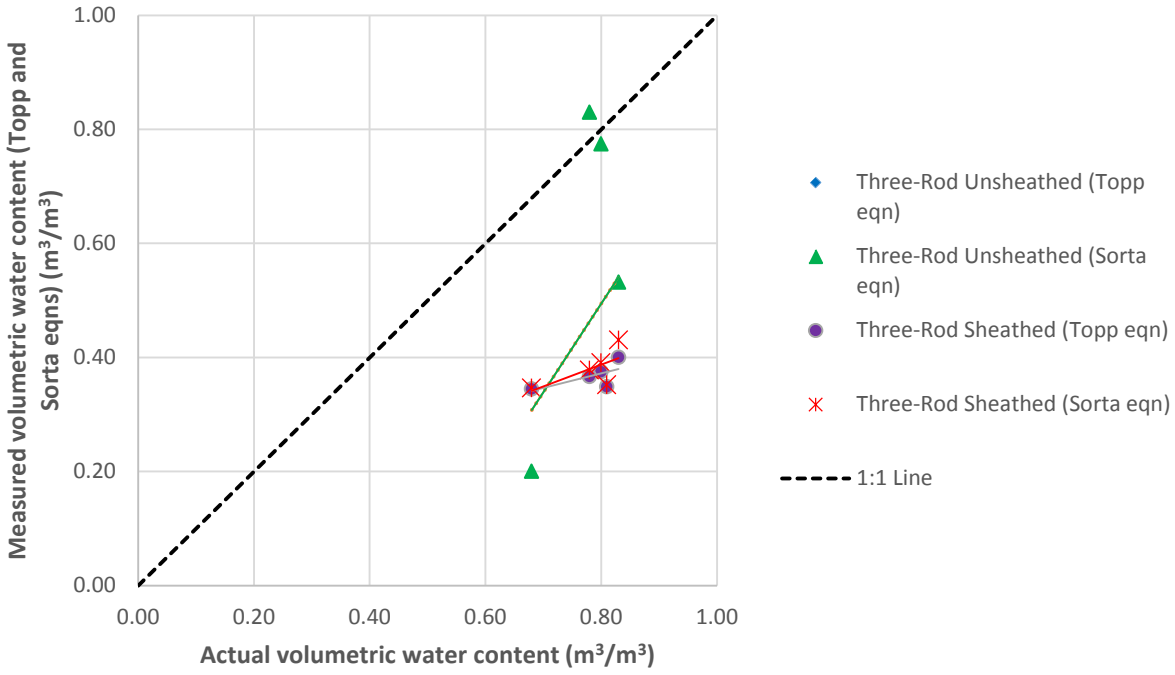

Figure 4.35 – Measured volumetric water contents (Topp and Sorta equations) from FFT testing at various water contents using testing results from three-rod Delrin® prototype probes. Note that the unsheathed rods' measured dielectric constant results were nonsensical. Some results from these unsheathed rods fall outside of the plot area.

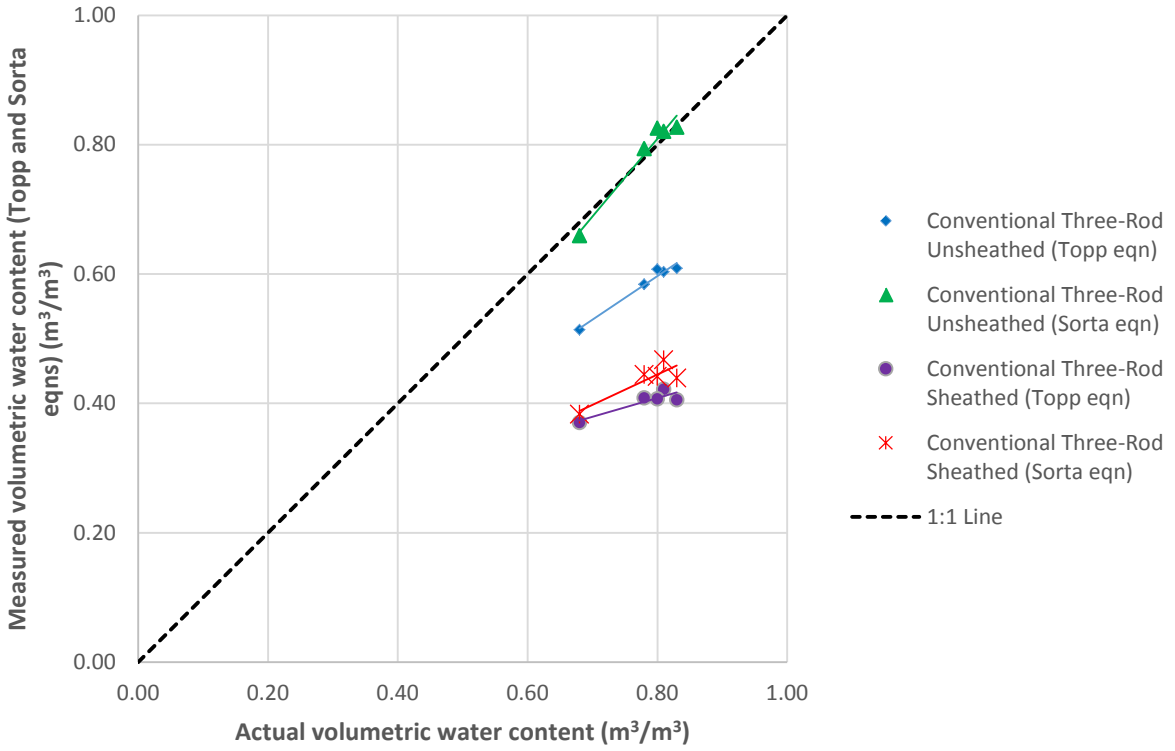

Figure 4.36 – Measured volumetric water contents (Topp and Sorta equations) from FFT testing at various water contents using conventional three-rod probes.

Table 4.9 – Summary of trendline parameters for prototype and conventional probe testing in FFT at various water contents.

Probe Configuration	Vol. W.C. Equation	Slope	Y-intercept	R^2
2-rod unsheathed Delrin® *	Topp	-27.295	22.859	0.866
	Sorta	2.563	-1.131	0.981
2-rod sheathed Delrin®	Topp	0.222	0.160	0.301
	Sorta	0.306	0.093	0.308
3-rod unsheathed Delrin® *	Topp	-10.814	14.010	0.061
	Sorta	1.553	-0.748	0.062
3-rod sheathed Delrin®	Topp	0.254	0.169	0.446
	Sorta	0.382	0.082	0.439
Conventional 3-rod unsheathed	Topp	0.675	0.057	0.971
	Sorta	1.199	0.150	0.965
Conventional 3-rod sheathed	Topp	0.291	0.175	0.798
	Sorta	0.469	0.070	0.783

* Dielectric constant measurements from the two-rod and three-rod unsheathed Delrin® probes were very high, resulting in data that was meaningless.

4.8.3 General Commentary on FFT Testing

The fact that the unsheathed Delrin® probes measured higher dielectric constants in the FFT samples than they did for de-ionized water suggests that the electrical conductivity of the FFT is close to the maximum for these probe configurations before they short out. It is interesting, however, that the three-rod prototype probe measured much higher dielectric constants than the two-rod probe since conventional unsheathed two-rod probes are more susceptible to salinity effects than three-rod ones (Zegelin et al. 1989). It is unknown why the unsheathed conventional three-rod probe testing showed realistic results when the unsheathed Delrin® probe configurations, with partially embedded rods, did not. This may suggest that the unsheathed probes' apparent range extension seen in the elevated salinity testing may be limited in some

conditions. This might be the case if the actual bulk conductivity of the FFT was higher than that of the tailings sand, since only the conductivity of the leachable salt solution, and not the soil as a whole, was measured for the tailings sand.

It is clear from the analysis that the Sorta equation improves the accuracy (i.e. increased sensitivity with less underestimation) of the measured volumetric water content for FFT, particularly for the conventional unsheathed probes. As a result, it is suggested that the Sorta equation be used for the sheathed Delrin® probe testing in FFT.

Despite the good results obtained for the conventional probe with the Sorta equation, the methodology for determining the actual volumetric water contents of the FFT was not as rigorous as that of the tailings sand testing. As a result, there may be some uncertainty in the data since applying this methodology to some of the rigorously calculated sand data resulted in overestimates of volumetric water content.

Overall, the three-rod sheathed Delrin® probe provided slightly better data than the two-rod one in terms of better fit and sensitivity, but not substantially so.

4.9 Push-Test

The final test in this phase of the research program was inserting the probe into a cylinder of sand which contained a series of layers constructed with different water contents. This final test was intended to be more representative of a field situation in which the connections to the probe are permanent and the probe is pushed into the soil using the push rig. Only the two-rod unsheathed D2 probe configuration was used in this testing.

4.9.1 Waveform Observations

The aggregate waveform for this testing was very encouraging in terms of its quality and interpretability. Common x_1 points were evident across all of the waveforms, with clearly progressing end of probe reflections for increasing water contents. The quality of the waveforms was very good, with negligible amounts of noise and bumps. Interpretability of the waveforms

was straight-forward with the only issue being an inconsistent slope following the reflection in the last, and wettest, waveform. An image of the aggregate waveform is shown in Figure 4.37.

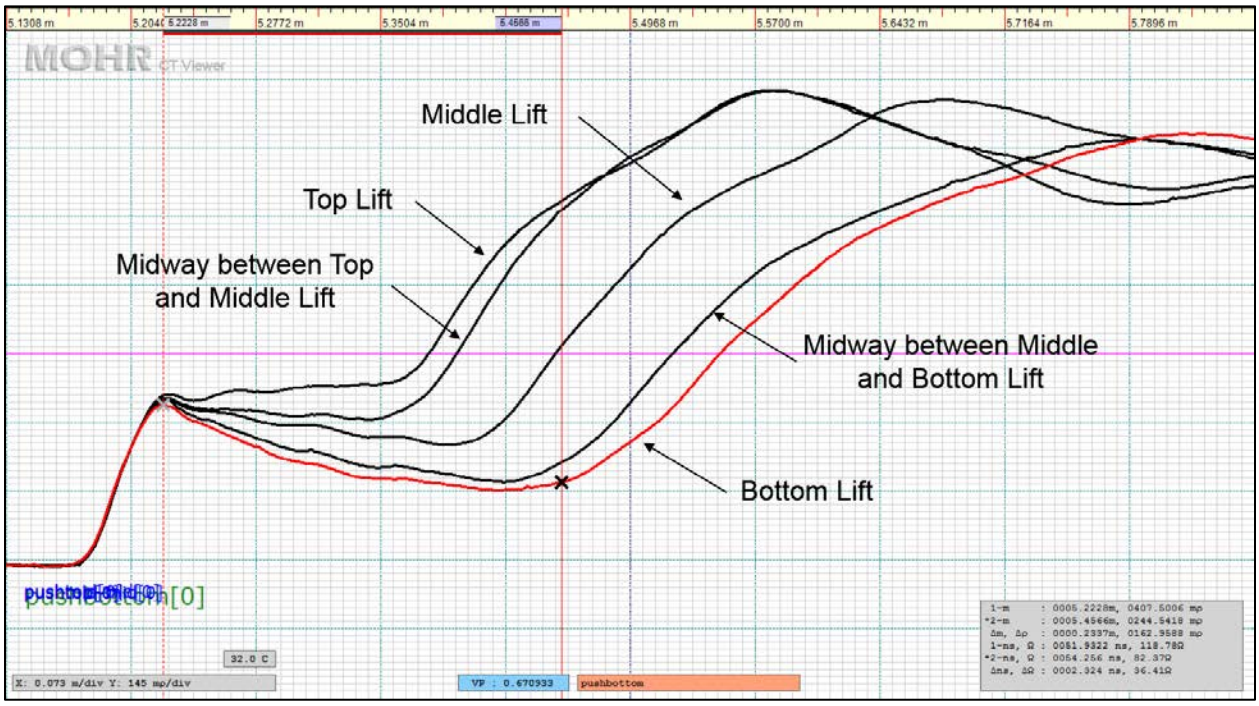

Figure 4.37 – Two-rod unsheathed Delrin® D2 prototype probe aggregate waveform for push-test in Beaver Creek sand. Locations for both x_1 and x_2 points of the bottom lift indicated by cursors (red waveform). Vertical scales matched for all waveforms.

4.9.2 Interpreted Results from Push-Test

Results from the interpreted waveforms are found in Appendix C, and volumetric water contents measured by various methods with depth are presented in Figure 4.38 and Figure 4.39. Water content results from the column itself are given in Appendix D. It should be noted that the methods for determining the actual volumetric water contents had a certain amount of uncertainty associated with them. As a consequence, these results are interpreted with a certain level of caution.

Figure 4.38 shows very similar trends to the two-rod unsheathed prototype probe results for the tailings sand shown in Figure 4.17, with the D2 probe continuing to overestimate the water

contents of the drier sand. The sensitivity of the probe is higher in this test, although this may be due to the fact that there is no air-dry sand to consider in this test. Fit for the data was good.

The volumetric water contents calculated from the prototype probe results show a general tracking of the water contents' increase with depth, as shown in Figure 4.39. In the top lift and its interface with the middle lift, the probe provides a relatively accurate measurement of the water content. This accuracy decreases, however, as the water content increases with depth and the associated degree of underestimation also increases.

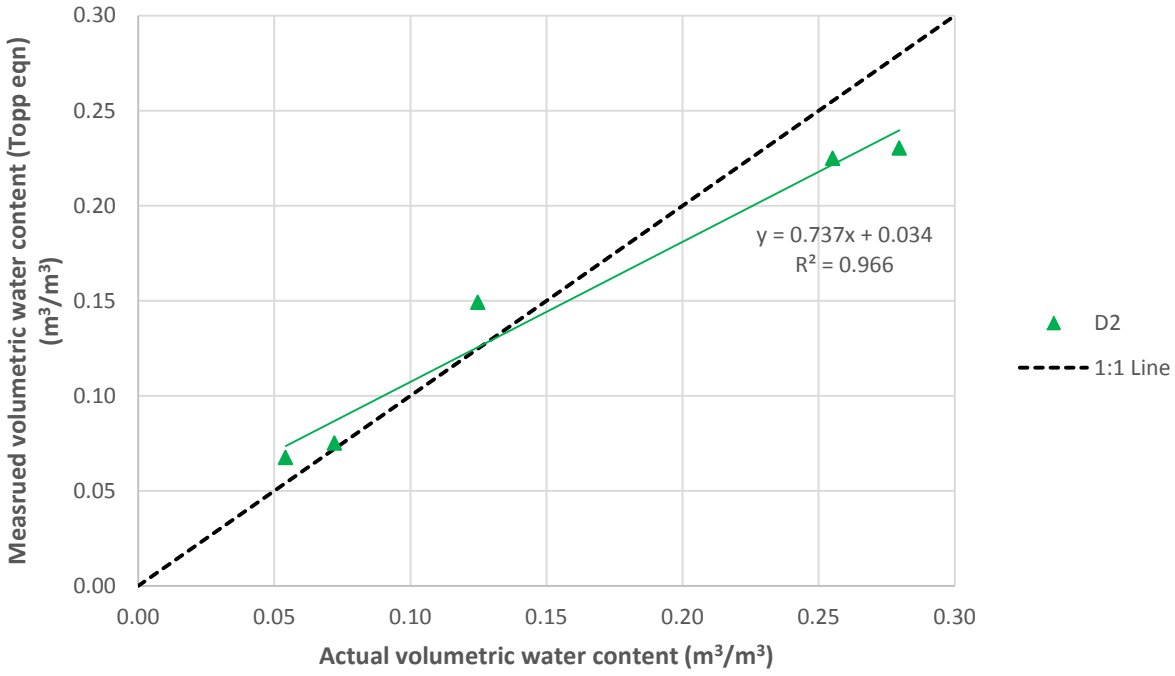

Figure 4.38 – Measured volumetric water content from push-test through column of sand at various water contents using two-rod unsheathed D2 Delrin® prototype. Actual volumetric water content approximated using short tube samples taken at similar depths to those of the TDR readings.

It is noted that the water content with depth at the time of testing was different than when it was packed. At the time of packing, the middle lift was lowest in water content while the top and bottom lifts were both equally higher. Following testing, however, an "S-curve" type of pattern

can be seen in the water content with depth. In this pattern the water content is relatively consistent with depth in both the top (driest), and the bottom (wettest) lifts, while there is quite a substantial change in water content in the middle lift from drier to wetter with depth.

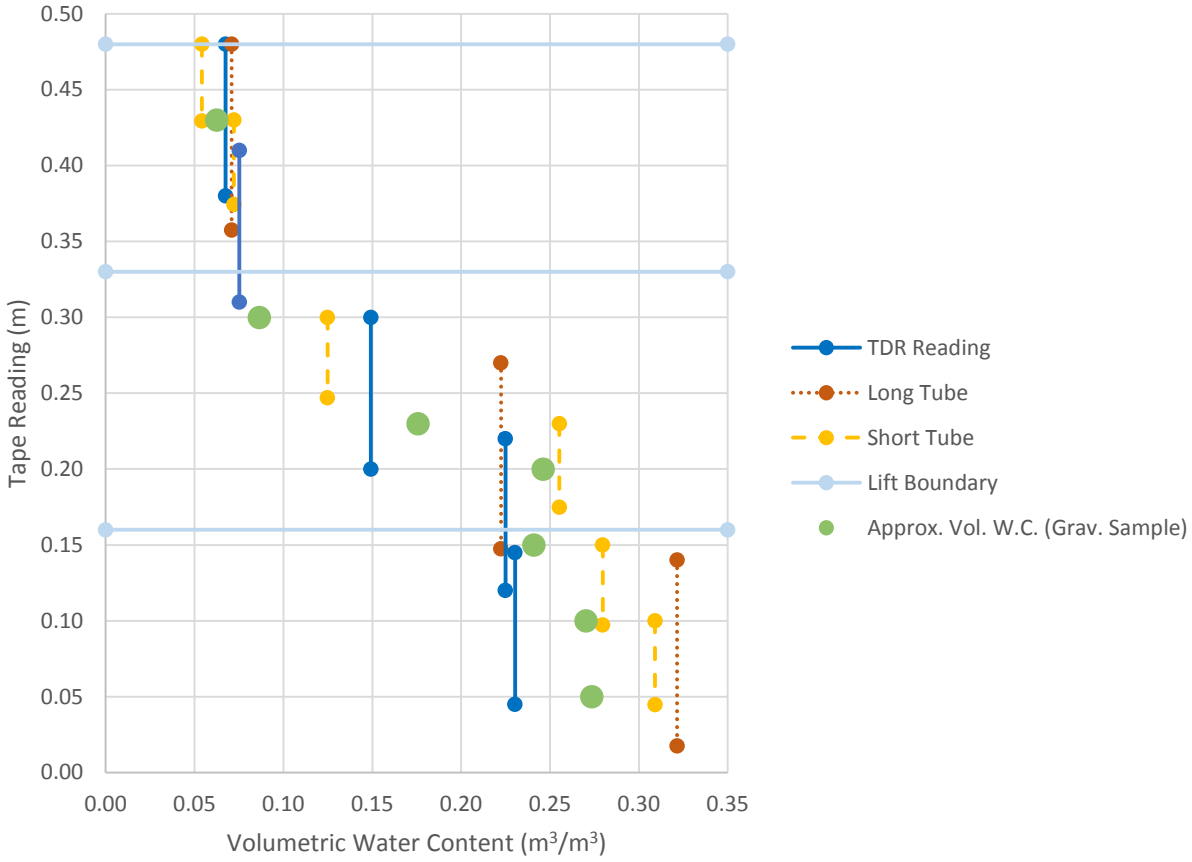

Figure 4.39 – Plot of various volumetric water content measurements with depth from push-test in Beaver Creek sand. Surface of top lift of sand was at a tape reading of 0.48 m.

4.9.3 General Commentary on Push-Test Results

Overall, these results are promising since they are quite similar to those of the controlled testing. This suggests that the probe shows consistency and is sensitive to changing water contents in field-like conditions. Furthermore, the consistency of the x_1 points and the high degree of quality and interpretability of the aggregate waveform indicate that a fixed connection is important for generating good results.

It was surprising that the water content of the three lifts changed as much as they did, since the top and middle lifts had been placed at much different water contents. The resulting water content profile was likely from drainage through the column along with evaporation which drew some of the water out of the top lift. Similar trends had been seen in the compacted tailings sand cylinder testing, as discussed, although not to the same degree.

While water content samples were taken as soon as possible after testing, it took some time to fully remove the sand from the garbage container. This led to some concern with the accuracy of water contents being measured with depth, as some additional water may have percolated down in the column during that time. However, a measurement with the probe just prior to deconstructing the bottom lift showed that the water content had essentially stayed constant, implying that the water content measurements were relatively accurate. This data is provided in Appendix D but neglected in Figure 4.39 to avoid confusion.

Loading on the probe was monitored on the hydraulic press during insertion in order to ensure the probe did not puncture the bottom of the garbage container. At the end of the insertion a load of 750 N was applied to the probe. No spike in the loading force was seen leading up to this point, so it was assumed the probe had not contacted the base of the container. This was confirmed visually after the test. No damage to the Delrin® in terms of excessive abrasion was noted after the test.

4.10 Correction Equations

As seen in many of the plots, the interpreted results from the prototype probes do not accurately provide the actual volumetric water content of the soil during testing. In order to improve these results, trendline correction equations for the four configurations of the D2 probe are provided below (two-rod unsheathed, two-rod sheathed, three-rod unsheathed, and three-rod sheathed, respectively),

$$\theta_{actual} = 2.50\,\theta_{calc} - 0.173 \quad [4\text{-}1]$$

$$\theta_{actual} = 9.55\,\theta_{calc} - 0.734 \quad [4\text{-}2]$$

$$\theta_{actual} = 1.74\,\theta_{calc} - 0.174 \quad [4\text{-}3]$$

$$\theta_{actual} = 6.07\,\theta_{calc} - 0.593 \quad [4\text{-}4]$$

where θ_{actual} is the actual volumetric water content, and θ_{calc} is the calculated (i.e. Topp equation) volumetric water content from interpretation of the prototype probe results. Statistics for these equations in terms of scatter and goodness of fit (R^2), and the estimation error (root mean squared error) are presented in Table 4.10. These equations were calculated from the non-elevated salinity tailings sand results, and should be applied accordingly. These equations would not apply to FFT data, or soils with elevated electrical conductivities. Data from the push-test was not used to develop these equations due to the uncertainty associated with it. Equations are only provided for the D2 probe configurations as it was seen as the most promising prototype to proceed forward with.

Considering the statistics of the correction equations, it would appear that for the unsheathed and sheathed probe options, the two-rod and three-rod configurations, respectively, are the most effective. In fact, in the case of the two-rod unsheathed probe configuration the corrected equation performs quite well.

Generally speaking, the acceptable error for a device depends on the user's goals. In terms of measuring groundwater recharge, which this device will ultimately play a part, a high error of estimation may not necessarily make the device unacceptable. Assuming both a constant estimation error for each soil type and a high water content over the depth of interest, a relatively high estimation error could still give a useful estimate of the volume of water with depth. For instance, with an estimation error of ±0.05 m^3/m^3, in a relatively dry soil with a water content of 0.10 m^3/m^3, the estimation would be within 50% of the actual. In a wetter soil, however, with a water content of 0.30 m^3/m^3, the same estimation error would put the measured value within 17% of the actual. This could be accurate enough to satisfy the user trying to quantify recharge.

Table 4.10 – Evaluation of scatter and goodness of fit, as well as estimation error of trendline correction equations.

Probe Configuration	Equation	R^2	RMSE (m^3/m^3)
Two-Rod Unsheathed	[4-1]	0.953	0.017
Two-Rod Sheathed	[4-2]	0.635	0.057
Three-Rod Unsheathed	[4-3]	0.795	0.038
Three-Rod Sheathed	[4-4]	0.777	0.040

4.11 Summary

The laboratory tests conducted for this experiment have provided a detailed investigation into the response of various prototypes to a number of different test media. These tests have helped to refine the design of the prototypes through this phase of testing and also to guide prototype development for the next phase of testing. As discussed throughout this chapter, the D2 probe configuration appeared overall to be the best design to proceed forward with. It provided a reasonable level of sensitivity and generally good results, but also had the ability to protect the integrity of the probe to some degree. No obvious advantage was seen for using either the two- or three-rod probes exclusively, however. It should be noted that while the results for the conventional probe testing were superior to the prototype probes, they were used only for

comparative purposes. Conventional probes are practical only for obtaining near-surface volumetric soil water contents.

Recommendations for the next stage of development based on the observations from this testing are summarized in the next chapter.

5 CONCLUSIONS AND RECOMMENDATIONS

Design is an iterative process, with an assessment of the lessons learned from one round of testing being used to further refine and improve the prototype for further testing. This chapter summarizes the lessons from this phase of the project, and provides recommendations for further development of the probe in the project's next phase.

5.1 Conclusions

Evaluating the performance of mine sites following their closure includes, among other things, measuring the volume of water stored in the landforms. This is an essential component in the larger task of tracking the movement of water through the site. Determining a method for efficiently measuring the water content with depth has been explored in this research project, specifically working towards the design of a TDR device that could be integrated onto a CPT probe. This phase of the research has involved assessing the response of various prototypes to a number of tests to better understand the behaviour of the prototypes and provide recommendations for further development.

Three objectives were identified to guide the research, and conclusions related to each of these objectives are summarized in this section.

The first objective of the project was to determine an appropriate configuration of the TDR probe through laboratory testing that could be adapted to a CPT shaft. Successful design elements from this testing will be used to guide the next phase of the project which will involve further design refinement and more rigorous laboratory and field trials.

A number of different prototype designs were initially investigated including a horizontal ring mounted on a section of steel pipe, horizontal rings mounted on Delrin® cylinders and vertical rods mounted on Delrin® cylinders. In the case of the Delrin® cylinder prototypes, one of the horizontal rings and one of the vertical rods were sheathed to mitigate the effect of highly electrically conductive testing media. All of these prototypes were tested in fluids of known dielectric constants or known salinities (i.e. reference solutions) to observe their general response to a broad range of basic testing conditions. From this testing it was determined that both the vertical rod and horizontal ring Delrin® cylinder prototypes showed potential for further development. However, given the conditions that would be encountered in field testing (i.e. general friction and rocks in the soil scraping against the insertion shaft) it was felt that a probe with vertical rods would be the most resilient design.

The next stage of the project involved refining the design of the vertical rod prototype for advanced testing. The refined prototype was the same diameter as the CPT cone tip, and it had a steel shaft in the centre of the Delrin® cylinder through which the insertion force of the CPT system could be transferred through the cylinder to the cone tip. Suggested criteria from the literature was considered in the design including Ferré and Topp's (2002b) recommendation of minimum rod length. The suggested ratio of rod spacing to rod diameter set out by Knight (1992) was also met for most of the prototype probe configurations.

Three variants of this design were produced, with each variant having a different depth of rod embedment within the Delrin® cylinder. These rod embedments ranged from being flush with the outside of the cylinder (D1 probe) to being attached directly to the exterior of the cylinder (D3 probe). Each of these variants had four rods: three that were unsheathed and one that was fully sheathed within the wall of the Delrin® cylinder. This allowed sheathed and unsheathed two- and three-rod probe combinations to be tested on each probe variant. The sensitivity of the measurements to rod embedment depth and sheathing were investigated in this testing.

Consistent responses of decreasing probe sensitivity with increasing rod embedment were observed in both the reference solution and in testing using compacted non-elevated salinity

tailings sand. A far greater reduction in probe sensitivity was found in the same testing done with the fully sheathed probe configurations.

Following testing of the three alternative designs, the probe with the partially embedded rods (D2) was chosen for further advanced testing. While the D3 probe displayed more sensitivity than the D2 probe, the non-embedded rods of the D3 probe would be far more susceptible to damage than the D2 probe. Testing of the D2 probe in compacted tailings sand with fixed water content but different levels of elevated salinity showed that, contrary to the literature, rod spacing of the two-rod configurations did not have a significant effect on results. This may have been due to the fact that the level of salinity was not high enough to generate a difference in response, but further testing to confirm this should be undertaken. It was also found that improved electrical connections enhanced the interpretability of the TDR waveforms, and may lead to an increase in accuracy. Evidence of better electrical connections producing improved waveform interpretability was also seen in earlier rounds of testing. An investigation into the effect of non-symmetrical cable lengths in three-rod testing was also completed, although these results were inconclusive. The D2 probe was also tested in FFT at different water contents. While no additional results of note with regards to probe configuration were found, the use of the Sorta equation (Sorta et al. 2013) was found to provide more accurate volumetric water content results than the Topp equation (Topp et al. 1980) at high water contents.

The final test of the project involved pushing the D2 probe into a column containing three layers of sand prepared at different initial water contents. This was intended to simulate a field testing situation. In order to prevent the cable connections from being removed from the rods during insertion, permanent connections to the rods were made. For reasons of simplicity, only the two-rod unsheathed configuration was tested. This testing provided further confirmation that improved electrical connections improve the response of the probes. The key finding from this test, however, was the fact that the probe was able to measure the variations in water content through the column. This was encouraging as it suggests that the probe could be successfully used in field testing conditions.

In general, there was no clear advantage for using either the two- or three-rod probes exclusively. There were instances where the three-rod data had more scatter than the two-rod configuration, something that was assumed to be the result of the poorer quality of the three-rod electrical connections. Cases also existed, however, where the three-rod data appeared to be slightly better than the two-rod. The three-rod configuration also measured higher dielectric constants in some instances, the opposite of what was found through confirmation testing done using conventional probes. The reason for this discrepancy is unknown. It should be emphasized that conventional probe testing was done solely for the purpose of comparing the results of the prototype testing. The superior performance of the conventional probes was expected, but given that conventional probes are used only for near-surface testing, they were never considered to be a viable design option for this project.

The second objective of the project was to identify a method of sheathing to mitigate the effect of electrically conductive soils. Considerations also had to be made for maintaining the integrity of the probe as it is pushed into the ground.

Initial testing of the preliminary sheathed Delrin® prototypes in the saline reference solutions found that the vertical rod probes performed much better than the probes with horizontal rings. In fact, the preliminary vertical rod probes did not show signs shorting out in any of the solutions, while the refined prototype probes completely shorted out before the most saline solution was tested. It is assumed that the reason for the good results in the preliminary rod prototypes was the shorter rod lengths that were used, although this was not confirmed through testing. Even though the refined sheathed prototypes shorted out prior to the 49 dS/m (30 g/L) saline solution being tested, they were still able to provide good measurements at lower salinities. This shows that the sheathed prototype probes were able to mitigate the effect of conductivity to some degree. All of the unsheathed probes shorted out in the saline solutions.

There was some evidence from the testing of the compacted tailings sand with elevated salinity to suggest that the range of the unsheathed prototype probe may be greater than that of conventional probes in moderately conductive soils. This implies that there is some benefit to be gained from partial sheathing while at the same time maintaining a greater level of sensitivity

than the fully sheathed probe configurations. A different trend was seen in the FFT testing, however, as the unsheathed prototype probe shorted out before the unsheathed conventional probe did. The reason for the discrepancy in the results is unknown. The sheathed prototype probe configurations did not short out in either test.

While specific tests were not done to evaluate the ability of the Delrin® to physically protect the probes, no obvious damage was observed following the insertion of the probe in the push-test. While this is good, it is not particularly surprising since Delrin® is used for its resiliency, and this test was not particularly trying in that regard. It is clear from the tests conducted within this program that Delrin® is effective for sheathing the probes to some degree.

The third objective of this project was to determine a suitable method for manually analyzing the TDR signal waveform. A methodology for this analysis was based generally on those described in the literature. However, a number of adaptations were required to deal with waveforms that did not follow the "textbook" waveform pattern. These atypical waveforms were especially prevalent in the compacted tailings sand testing, and were largely attributed to the presence of air gaps or poor electrical connections. While efforts were made to interpret the waveforms as consistently as possible, in some instances the waveforms were sufficiently unique for this not to be achievable. Interpretation was one of the most challenging parts of this project; any improvements that could be made to avoid these challenges would be extremely beneficial.

5.2 Recommendations

A number of recommendations have been suggested for consideration in the subsequent stages of development and testing to improve upon the prototypes used in this phase of testing. These recommendations include suggestions for improvements to probe design and data analysis, as well as additional laboratory testing.

5.2.1 Probe Design Improvements

The most important improvement that could be made to the probe design is improved electrical connections. Having connections that contact more of the rods' available connection surface

area will result in simpler waveform interpretation and potentially more accurate results. Improved connections will also allow for a more adequate evaluation of the differences between two- and three-rod probe configurations, and determining whether symmetrical cable lengths are necessary for three-rod configurations.

A number of other less important changes could be made to optimize performance, including the following:

- Evaluation of an optimal sheathing thickness or embedment should be done to ensure probe sensitivity while also providing protection for the TDR rods during insertion.
- An investigation of rod diameter with respect to sampling volume of the probe should be carried out. In particular, Robinson et al. (2003) suggests that increasing the diameter of the central or live rod relative to the ground rod(s), as opposed to equally increasing the diameter of all the rods, may increase the probe's sampling volume. Similar effects may be achieved by using different sized plates instead of rods, although this may lead to other problems with regards to sheathing and probe integrity, as well as susceptibility to conductive losses (Robinson et al. 2003).
- Assessing the response of shorter rod lengths on mitigating the effects of electrical conductivity should be completed given the success of the preliminary vertical rod prototypes over the refined one. Although this may prove useful for the effects of electrical conductivity, thought should also be given to issues with waveform interpretation and probe resolution associated with shorter rod lengths. Consideration might also be given to how longer probes such as those used successfully by Nichol et al. (2002) could be used on the probe.
- Further testing into closer rod spacing should also be performed, as it may be possible to extend a probe's range and generally improve results in highly electrically conductive soils by having closer spaced rods.

While these recommended improvements are important to investigate, making the prototypes to test them all may be prohibitively expensive and time-consuming. As a result, efforts to model

the effect of these different improvements on the field that is generated would likely be much more efficient in terms of optimizing the design of the probes. Furthermore, knowing the sampling volume for a particular prototype from a model could also be useful for establishing a dielectric mixing model for the particular prototype. The dielectic mixing model could then be used as another method for evaluating the performance of the probe, being used to compare the actual dielectric constant to that measured by the prototype.

Functionality of the probe could also be improved by considering changes to other design elements of the probe in more general terms. Improvements on waveform interpretation in general, and easier determination of x_1 and x_2 points in particular, could possibly be done by adding shorting diodes to the probe (Hook et al. 1992). Adding a balun to the TDR probe to match the probe's impedance with the cable could also improve waveform interpretability by limiting signal attenuation; however, its necessity is questionable (Spaans and Baker 1993, Kelly et al. 1995).

Another change that may improve the interpretability of waveforms is a probe with a slightly different design: a time domain transmissometry (TDT) probe. TDT is similar to TDR in that it measures the dielectric constant of the soil by determining a signal's travel time through a test medium (Topp et al. 2001). A TDT probe is different from a TDR probe, however, in that the transmission line is a loop rather than a combination of individual rods, with connections being necessary at both the beginning and end of the probe rather than just the one end (Sun and Young 2001, Will and Rolfes 2013). The main purported benefits of TDT are waveforms that are easier to interpret than those of TDR, and electronics that can be simpler than those required for TDR (Sun and Young 2001, Topp et al. 2001, Will et al. 2012, Will and Rolfes 2013). TDT may also have a greater tolerance for highly conductive testing media, as testing has been possible in saline solutions with an electrical conductivity of just under 200 dS/m (Zheng et al. 2011).

In addition to waveform interpretation, there are changes that could improve the probe's response to different testing conditions. Integrating a conductivity bridge with the probe by which to measure the bulk soil electrical conductivity might be considered if correcting for the losses associated with electrical conductivity is done in the future (Topp et al. 2000). A sensor

such as this could also be used to determine whether air gaps existed next to the probe during sampling, in which case suspect data could be discarded if necessary.

Having the capability to select different rod lengths and spacing, along with the number of rods being used would also allow for "customizing" the probe for the testing conditions. This could be achieved by having a number of rods in series along the length of the probe, and a number of these groups of rods around the probe's circumference. With the use of digital switches it would be possible to select the optimal length or spacing of the rods depending on the conductivity or composition of the soil. The number of rods being used (i.e. two-rod or three-rod) could also be selected in this way. This capability could be useful if rods were ripped off during insertion as well. Should this occur, another probe configuration could be chosen in order to continue with testing, despite the fact that it may not be optimal for the conditions.

Further improvements that could be made later in the process include having the ability to use this instrument on less conventional vehicles, such as ATVs, and developing a TDR unit for incorporation within the CPT probe itself. Using ATVs would be beneficial in terms of potentially allowing cheaper and more rapid testing of reclaimed mine sites, albeit to shallower depths. Having a down-hole TDR unit would eliminate issues with attenuation from long cable lengths, essentially removing the limitation of a maximum testing depth for the probe.

Should this device be adopted for field use, it is recommended that confirmations of data quality be conducted at specified intervals. For instance, if the probe was found to be reasonably robust and used for multiple holes, it may be advisable to confirm the data quality after each hole. If the probe was discarded after one hole, it would be recommended to evaluate the performance of the new probe before each hole. This could be done with a series of reference solutions. Should the probe be found to be outside the desired performance range, the probe could be either discarded or recalibrated, depending on the circumstance. It is also recommended that occasional confirmation tests be performed against soil samples obtained in a more conventional manner, such as Shelby tubes.

5.2.2 Data Interpretation Improvements

Improvements to the methodology of data interpretation could be achieved in a number of ways. One such method would be to use the smoothing function in CT Viewer to filter out noise in the waveforms. This has the potential to improve the certainty of waveform analysis; however, care must be taken to ensure that the filtered data is truly noise. Another improvement to consider would be the use of a fixed x_1 point for the analysis of waveforms from a given probe. Using a set point would simplify the analysis, and as long as the electrical connections and cable characteristics did not change any generated error should be minimal. This assumption would need to be tested, however, to confirm that the error was within acceptable limits. Of course, automating the waveform interpretation would be of great benefit, making the entire process of water content determination much more efficient.

Applying the Sorta equation instead of the Topp equation for measurements within high water content slurries such as FFT appeared to provide more accurate water content results. Determining whether this equation is truly suitable for FFT and slurries in general will require more testing. However, if the equation is appropriate, its application would be valuable given the prevalence of these types of soils at Syncrude's site and other mine sites in general.

5.2.3 Further Laboratory Testing

A number of additional laboratory tests would be useful for further understanding the response of the prototype probes. One important type of testing that should be carried out includes testing in shale or clay soils, both at non-elevated and elevated salinities. These soils are encountered at Syncrude's site, and the electrical properties of these solutions and soil particles may have an impact on the probe's response. It is important to have an understanding of this response and account for it accordingly during the prototype development. Testing on a broader range of salinities in general should also be done to determine how significant the effect of salinity is on the range of both sheathed and unsheathed probes. Specifically, mid-range salinity conditions should be tested as this was not done in this phase of the project. Testing with other salts and chemical constituents found in soils and tailings from other geographic areas would also be useful for the general development of the probe. While the effect of temperature on dielectric

constant measurement was not considered in this phase of testing, it should be considered in the next phase to understand changes in probe response to the more extreme temperatures that could be encountered during field testing.

Testing to evaluate the resilience of Delrin® to damage from both friction in the soil and shearing that could occur from sharp rocks being scratched along the surface of the probe should be considered as well. This testing could be extended to observe the robustness of the embedded rods under the same conditions. Observations of changes to probe response as the Delrin® sheathing was worn down would be useful both in terms of anticipating changes to the probe measurements as insertion wear was encountered and for determining an appropriate sheathing thickness for the probe.

REFERENCES

American Public Health Association, American Water Works Association, and Water Environment Federation. 2005. Standard methods for the examination of water and wastewater. 21st edition. American Public Health Association, American Water Works Association, and Water Environment Federation, Washington, D.C.

American Society for Testing and Materials. 2008. Standard test method for determination of water (moisture) content of soil by microwave oven heating. ASTM International, West Conshohocken, PA. doi: 10.1520/D4643-08.

Andrews, J.R. 1994. Time domain reflectometry. *In* Proceedings of Symposium and Workshop on Time Domain Reflectometry in Environmental, Infrastructure, and Mining Applications, Evanston, IL, 7-9 September 1994. U.S. Bureau of Mines, Minneapolis, pp. 4–13.

Baer, T.J. 2014. An evaluation of the use of natural stable isotopes of water to track water movement through oil sands mine closure landforms. M.Sc. thesis, Department of Civil and Geological Engineering, University of Saskatchewan, Saskatoon, SK.

Bittelli, M., Salvatorelli, F., and Pisa, P.R. 2008. Correction of TDR-based soil water content measurements in conductive soils. Geoderma, **143**(1-2): 133–142. doi: 10.1016/j.geoderma.2007.10.022.

Bower, C.A., and Wilcox, L. V. 1965. Soluble Salts. *In* Methods of Soil Analysis Part 2. *Edited by* C.A. Black, D.D. Evans, J.L. White, L.E. Ensminger, and F.E. Clark. American Society of Agronomy, Madison, WI. pp. 933–951.

Bruch, P.G. 1993. A laboratory study of evaporative fluxes in homogeneous and layered soils. M.Sc. thesis, Department of Civil Engineering, University of Saskatchewan, Saskatoon, SK.

Casanova, J.J., Evett, S.R., and Schwartz, R.C. 2012a. Design and field tests of an access-tube soil water sensor. Applied Engineering in Agriculture, **28**(4): 603–610.

Casanova, J.J., Evett, S.R., and Schwartz, R.C. 2012b. Design of access-tube TDR sensor for soil water content: Testing. IEEE Sensors Journal, **12**(6): 2064–2070. doi: 10.1109/JSEN.2012.2184282.

Cassel, D.K., Kachanoski, R.G., and Topp, G.C. 1994. Practical considerations for using a TDR cable tester. Soil Technology, **7**(2): 113–126.

Cataldo, A., Piuzzi, E., De Benedetto, E., and Cannazza, G. 2014. Experimental characterization and performance evaluation of flexible two-wire probes for TDR monitoring of liquid level. IEEE Transactions on Instrumentation and Measurement. In press. 10 pp.

Chen, Y., Wang, H., Chen, R., and Chen, Y. 2014. A newly designed TDR probe for soils with high electrical conductivities. Geotechnical Testing Journal, **37**(1): 36–45. doi: 10.1520/GTJ20120227.

Collier, R. 2013. Transmission lines. Cambridge University Press, Cambridge, UK.

Davis, J.L., and Chudobiak, W.J. 1975. In situ meter for measuring relative permittivity of soils. Geological Survey of Canada,(Paper 75-1, Part A): 75–79. Project 630049.

Dobson, M.C., Ulaby, F.T., Hallikainen, M.T., and El-rayes, M.A. 1985. Microwave dielectric behavior of wet soil-Part II: Dielectric mixing models. IEEE Transactions on Geoscience and Remote Sensing, **GE-23**(1): 35–46. doi: 10.1109/TGRS.1985.289498.

DuPont. (n.d.). Delrin design guide, Volume 3. Wilmington, DE. Available from http://plastics.dupont.com/plastics/pdflit/americas/delrin/230323c.pdf. [accessed 25 April 2014].

Evett, S.R. 2000a. Some aspects of time domain reflectometry (TDR), neutron scattering, and capacitance methods of soil water content measurement. *In* Comparison of soil water measurement using the neutron scattering, time domain reflectometry and capacitance methods. International Atomic Energy Agency, Vienna, Austria. pp. 5–49. IAEA–TECDOC–1137.

Evett, S.R. 2000b. The TACQ computer program for automatic time domain reflectometry measurements: II. Waveform interpretation methods. Transactions of ASAE, **43**(6): 1947–1956.

Fellner-Feldegg, H. 1969. The measurement of dielectrics in the time domain. The Journal of Physical Chemistry, **73**(3): 616–623.

Ferré, P.A., Knight, J.H., Rudolph, D.L., and Kachanoski, R.G. 1998. The sample area of conventional and alternative time domain relectometry probes. The sample areas of conventional and alternative time domain reflectometry probes, **34**(11): 2971–2979.

Ferré, P.A., Rudolph, D.L., and Kachanoski, R.G. 1996. Spatial averaging of water content by time domain reflectometry: Implications for twin rod probes with and without dielectric coatings. Water Resources Research, **32**(2): 271–279.

Ferré, P.A., and Topp, G.C. 2002a. Methods for measurement of soil water content. *In* Methods of Soil Analysis Part 4 Physical Methods, Number 5 in the Soil Science Society of America Book Series. *Edited by* G.S. Campbell, R. Horton, W.A. Jury, D.R. Nielsen, H.M. van Es, P.J. Wierenga, J.H. Dane, G.C. Topp, L. Al-Amoodi, and W.A. Dick. Soil Science Society of America, Inc., Madison, WI. pp. 422–423.

Ferré, P.A., and Topp, G.C. 2002b. Time domain reflectometry. *In* Methods of Soil Analysis Part 4 Physical Methods, Number 5 in the Soil Science Society of America Book Series. *Edited by* G.S. Campbell, R. Horton, W.A. Jury, D.R. Nielsen, H.M. van Es, P.J. Wierenga, J.H. Dane, G.C. Topp, L. Al-Amoodi, and W.A. Dick. Soil Science Society of America, Inc., Madison, WI. pp. 434–446.

Ferré, T. 1997. Design and analysis of time domain reflectometry probes for measuring water content and bulk electrical conductivity under steady and transient flow conditions. Ph.D. thesis, Department of Earth Sciences, University of Waterloo, Waterloo, ON.

Fujiyasu, Y., Pierce, C.E., Fan, L., and Wong, C.P. 2004. High dielectric insulation coating for time domain reflectometry soil moisture sensor. Water Resources Research, **40**(4): 1–7. doi: 10.1029/2003WR002460.

Gadani, D.H., Rana, V.A., Bhatnagar, S.P., Prajapati, A.N., and Vyas, A.D. 2012. Effect of salinity on the dielectric properties of water. Indian Journal of Pure and Applied Physics, **50**(6): 405–410.

Heimovaara, T.J. 1993. Design of triple-wire time domain reflectometry probes in practice and theory. Soil Science Society of America Journal, **57**(6): 1410–1417.

Heimovaara, T.J., Bouten, W., and Verstraten, J.M. 1994. Frequency domain analysis of time domain reflectometry waveforms 2. A four-component complex dielectric mixing model for soils. Water Resources Research, **30**(2): 201–209.

Herkelrath, W.N., Hamburg, S.P., and Murphy, F. 1991. Automatic, real-time monitoring of soil moisture in a remote field area with time domain reflectometry. Water Resources Research, **27**(5): 857–864.

Hignett, C., and Evett, S.R. 2008. Direct and surrogate measures of soil water content. *In* Field estimation of soil water content. International Atomic Energy Agency, Vienna, Austria. pp. 1–22.

Hilderman, J.N. 2011. Net percolation as a function of topographic variation in a reclamation cover over a saline-sodic overburden dump. M.Sc. thesis, Department of Civil and Geological Engineering, University of Saskatchewan, Saskatoon, SK.

Hilhorst, M.A., and Dirksen, C. 1994. Dielectric water content sensors: time domain versus frequency domain. *In* Proceedings of Symposium and Workshop on Time Domain Reflectometry in Environmental, Infrastructure, and Mining Applications, Evanston, IL, 7-9 September 1994. U.S. Bureau of Mines, Minneapolis, pp. 23–33.

Ho, Y.-K.A. 1985. The effects of brine contamination on the properties of soils. M.Sc. thesis, Department of Civil Engineering, University of Saskatchewan, Saskatoon, SK.

Hoekstra, P., and Delaney, A. 1974. Dielectric properties of soils at UHF and microwave frequencies. Journal of Geophysical Research, **79**(11): 1699–1708.

Hook, W.R., Livingston, N.J., Sun, Z.J., and Hook, P.B. 1992. Remote diode shorting improves measurement of soil water by time domain reflectometry. Soil Science Society of America Journal, **56**(5): 1384–1391.

Huang, M., Bruch, P.G., and Barbour, S.L. 2013. Evaporation and water redistribution in layered unsaturated soil profiles. Vadose Zone Journal, **12**(1): 14 pp. doi: 10.2136/vzj2012.0108.

Jackson, T.J., and O'Neill, P.E. 1987. Salinity effects on the microwave emission of soils. IEEE Transactions on Geoscience and Remote Sensing, **GE-25**(2): 214–220. doi: 10.1109/TGRS.1987.289820.

Jones, S.B., Wraith, J.M., and Or, D. 2002. Time domain reflectometry measurement principles and applications. Hydrological Processes, **16**(1): 141–153. doi: 10.1002/hyp.513.

Kelly, S.F., Selker, J.S., and Green, J.L. 1995. Using short soil moisure probes with high-bandwidth time domain reflectometry instruments. Soil Science Society of America Journal, **59**(1): 97–102.

Klein, L.A., and Swift, C.T. 1977. An improved model for the dielectric constant of sea water at microwave frequencies. IEEE Transactions of Antennas and Propogation, **25**(1): 104–111.

Knight, J.H. 1992. Sensitivity of time domain reflectometry measurements to lateral variations in soil water content. Water Resources Research, **28**(9): 2345–2352.

Knight, J.H., White, I., and Zegelin, S.J. 1994. Sampling volume of TDR probes used for water content monitoring. *In* Proceedings of Symposium and Workshop on Time Domain Reflectometry in Environmental, Infrastructure, and Mining Applications, Evanston, IL, 7-9 September 1994. U.S. Bureau of Mines, Minneapolis, pp. 93–104.

Kosugi, K., Yamakawa, Y., Masaoka, N., and Mizuyama, T. 2009. A combined penetrometer–moisture probe for surveying soil properties of natural hillslopes. Vadose Zone Journal, **8**(1): 52-63. doi: 10.2136/vzj2008.0033.

Ledieu, J., De Ridder, P., De Clerck, P., and Dautrebande, S. 1986. A method of measuring soil moisture by time-domain reflectometry. Journal of Hydrology, **88**(3-4): 319–328. doi: 10.1016/0022-1694(86)90097-1.

Lefebvre, M.E. 1997. The feasibility of coaxial time domain reflectometry as an insitu site characterization tool for determining the moisture content of mine tailings. M.Sc. thesis, Department of Civil and Environmental Engineering, University of Alberta, Edmonton, AB.

Li, M., Barbour, S.L., and Si, B.C. 2014. Measuring solid percentage of oil sands mature fine tailings using the dual probe heat pulse method. Journal of Environmental Quality. In press. doi: 10.2134/jeq2014.06.0262.

Lin, C.-P., Chung, C.-C., and Tang, S.-H. 2006. Geoelectrical measurements by TDR penetrometer. *In* Proceedings of TDR 2006: Third International Symposium and Workshop on Time Domain Reflectometry for Innovative Soils Applications, Purdue University, West Lafayette, IN, 17-20 September 2006. Purdue University, West Lafayette. 15 pp. Paper ID 19.

Maheshwarla, S. V., Venkatasubramanian, R., and Boehm, R.F. 1995. Comparison of time domain refiectometry performance factors for several dielectric geometries: Theory and experiments. Water Resources Research, **31**(8): 1927–1933.

McIsaac, G.R. 2010. Time domain reflectometry measurement of water content and electrical conductivity using a polyolefin coated TDR probe. M.Sc. thesis, Department of Geography, University of Waterloo, Waterloo, ON.

Miyamoto, H., and Chikushi, J. 2006. Calibration of column-attaching TDR probe based on dielectric mixing model. *In* Proceedings of TDR 2006: Third International Symposium and Workshop on Time Domain Reflectometry for Innovative Soils Applications, Purdue University, West Lafayette, IN, 17-20 September 2006. Purdue University, West Lafayette. 7 pp. Paper ID 23.

Mohr. 2012. MOHR CT100 Series high-resolution automated metallic TDR cable testers. Available from http://www.mohr-engineering.com/ct100-metallic-tdr-documents.php. [accessed 28 August 2014].

Mojid, M.A., Wyseure, G.C.L., and Rose, D.A. 1998. The use of insulated time-domain reflectometry sensors to measure water content in highly saline soils. Irrigation Science, **18**(2): 55–61. doi: 10.1007/s002710050044.

Mojid, M.A., Wyseure, G.C.L., and Rose, D.A. 2003. Electrical conductivity problems associated with time-domain reflectometry (TDR) measurement in geotechnical engineering. Geotechnical and Geological Engineering, **21**(3): 243–258. doi: 10.1023/A:1024910309208.

Moret, D., Arrúe, J.L., López, M.V., and Gracia, R. 2006. A new TDR waveform analysis approach for soil moisture profiling using a single probe. Journal of Hydrology, **321**(1-4): 163–172. doi: 10.1016/j.jhydrol.2005.07.041.

Moret-Fernández, D., Lera, F., Arrúe, J.L., and López, M. V. 2009. Measurement of soil bulk electrical conductivity using partially coated TDR probes. Vadose Zone Journal, **8**(3): 594–600. doi: 10.2136/vzj2008.0144.

Nichol, C., Beckie, R., and Smith, L. 2002. Evaluation of uncoated and coated time domain reflectometry probes for high electrical conductivity systems. Soil Science Society of America Journal, **66**(5): 1454–1465.

Nissen, H.H., Moldrup, P., and Henriksen, K. 1998. High-resolution time domain reflectometry coil probe for measuring soil water content. Soil Science Society of America Journal, **62**(5): 1203–1211.

Noborio, K. 2001. Measurement of soil water content and electrical conductivity by time domain reflectometry: a review. Computers and Electronics in Agriculture, **31**(3): 213–237.

O'Connor, K.M., and Dowding, C.H. 1999. Geomeasurements by pulsing TDR cables and probes. CRC Press, Boca Raton, FL.

Persson, M., and Dahlin, T. 2010. A profiling TDR probe for water content and electrical conductivity measurements of soils. European Journal of Soil Science, **61**(6): 1106–1112. doi: 10.1111/j.1365-2389.2010.01306.x.

Persson, M., and Wraith, J.M. 2002. Shaft-mounted time domain reflectometry probe for water content and electrical conductivity measurements. Vadose Zone Journal, **1**(2): 316–319.

Robinson, D.A., Jones, S.B., Wraith, J.M., Or, D., and Friedman, S.P. 2003. A review of advances in dielectric and electrical conductivity measurement in soils using time domain reflectometry. Vadose Zone Journal, **2**(4): 444–475.

Roth, K., Schulin, R., Fluhler, H., and Attinger, W. 1990. Calibratrion of time domain reflectometry for water content measurement using a composite dielectric approach. Water Resources Research, **26**(10): 2267–2273.

Schaap, M.G., de Lange, L., and Heimovaara, T.J. 1996. TDR calibration of organic forest floor media. Soil Technology, **11**(2): 205–217.

Schwartz, R.C., Evett, S.R., and Bell, J.M. 2009. Complex permittivity model for time domain reflectometry soil water content sensing: II. Calibration. Soil Science Society of America Journal, **73**(3): 898–909. doi: 10.2136/sssaj2008-0195.

Shinn, J.D., Timian, D.A., Morey, R.M., Mitchell, G., Antle, C.L., and Hull, R. 1998. Development of a CPT deployed probe for in situ measurement of volumetric soil moisture content and electrical resistivity. Field Analytical Chemistry and Technology, **2**(2): 103–109.

Sorta, A.R., Sego, D.C., and Wilson, G.W. 2013. Time domain reflectometry measurements of oil sands tailings water content: a study of influencing parameters. CIM Journal, **4**(2): 109–119.

Spaans, E.J.A., and Baker, J.M. 1993. Simple baluns in parallel probes for time domain reflectometry. Soil Science Society of America Journal, **57**(3): 668–673.

Sperazza, M., Moore, J.N., and Hendrix, M.S. 2004. High-resolution particle size analysis of naturally occurring very fine-grained sediment through laser diffractometry. Journal of Sedimentary Research, **74**(5): 736–743.

Stogryn, A. 1971. Equations for calculating the dielectric constant of saline water. IEEE Transactions on Microwave Theory and Techniques, **19**(8): 733–736.

Strangeways, I. 2003. Measuring the natural environment. Cambridge University Press, Cambridge, UK.

Sun, Z.J., and Young, G.D. 2001. A cost effective soil moisture instrument based on time-domain transmission measurement. *In* Proceedings of TDR 2001: Second International Symposium and Workshop on Time Domain Reflectometry for Innovative Geotechnical Applications, Northwestern University, Evanston, IL, 5-7 September 2001. Infrastructure Technology Institute, Evanston. pp. 109–115.

Syncrude Canada Ltd. 2012. Material safety data sheet for mature fine tails.

Topp, G.., and Davis, J.L. 1981. Detecting infiltration of water through soil cracks by time-domain reflectometry. Geoderma, **26**(1-2): 13–23.

Topp, G.C., Davis, J.L., and Annan, A.P. 1980. Electromagnetic determination of soil water content: measurements in coaxial transmission lines. Water Resources Research, **16**(3): 574–582.

Topp, G.C., Lapen, D.R., Cook, F.J., Morrison, M.J., and Pillai-McGarry, U. 2006. Facilitating soil- and plant-water research through the use of TDR. *In* Proceedings of TDR 2006: Third International Symposium and Workshop on Time Domain Reflectometry for Innovative Soils Applications, Purdue University, West Lafayette, IN, September 2006. Purdue University, West Lafayette. 22 pp. Paper ID 39.

Topp, G.C., Lapen, D.R., Edwards, M.J., and Young, G.D. 2003. Laboratory calibration, in-field validation and use of a soil penetrometer measuring cone resistance and water content. Vadose Zone Journal, **2**(4): 633–641.

Topp, G.C., Lapen, D.R., Young, G.D., and Edwards, M. 2001. Evaluation of shaft-mounted TDT readings in disturbed and undisturbed media. *In* Proceedings of TDR 2001: Second International Symposium and Workshop on Time Domain Reflectometry for Innovative Geotechnical Applications, Northwestern University, Evanston, IL, 5-7 September 2001. Infrastructure Technology Institute, Evanston. pp. 62–71.

Topp, G.C., Zegelin, S., and White, I. 2000. Impacts of the real and imaginary components of relative permittivity on time domain reflectometry measurements in soils. Soil Science Society of America Journal, **64**(4): 1244–1252.

Vaz, C.M.P. 2003. Use of a combined penetrometer-TDR moisture probe for soil compaction studies. *In* Proceedings of College on Soil Physics, Trieste, Italy, 3-21 March 2003. ICTP, Trieste, pp. 450–457. LNS0418036.

Vaz, C.M.P., and Hopmans, J.W. 2001. Simultaneous measurement of soil penetration resistance and water content with a combined penetrometer–TDR moisture probe. Soil Science Society of America Journal, **65**(1): 4–12.

Whalley, W.R. 1993. Considerations on the use of time-domain reflectometry (TDR) for measuring soil water content. Journal of Soil Science, **44**(1): 1–9.

Will, B., Gerding, M., Schulz, C., Baer, C., Musch, T., and Rolfes, I. 2012. A time domain transmission measurement system for dielectric characterizations. International Journal of Microwave and Wireless Technologies, **4**(3): 349–355. doi: 10.1017/S1759078712000347.

Will, B., and Rolfes, I. 2013. Comparative study of moisture measurements by time domain transmissometry. *In* Proceedings of 2013 IEEE Sensors, Baltimore, MD, 3-6 November 2013. IEEE, Baltimore, pp. 1–4. doi: 10.1109/ICSENS.2013.6688529.

Wilson, G.W. 1990. Soil evaporative fluxes for geotechnical engineering problems. Ph.D. thesis, Department of Civil Engineering, University of Saskatchewan, Saskatoon, SK.

Wilson, G.W., Fredlund, D.G., and Barbour, S.L. 1994. Coupled soil-atmosphere modelling for soil evaporation. Canadian Geotechnical Journal, **31**(2): 151–161.

Wohlfarth, C. 2013. Permittivity (dielectric constant) of liquids. *In* CRC Handbook of Chemistry and Physics (online edition), 94th Edition. *Edited by* W.M. Haynes. CRC Press. pp. 6–187 – 6–208.

Wraith, J.M., and Or, D. 1999. Temperature effects on soil bulk dielectric permittivity measured by time domain reflectometry: experimental evidence and hypothesis development. Water Resources Research, **35**(2): 361–369.

Yamakawa, Y., Kosugi, K., Masaoka, N., Tada, Y., and Mizuyama, T. 2010. Use of a combined penetrometer-moisture probe together with geophysical methods to survey hydrological properties of a natural slope. Vadose Zone Journal, **9**(3): 768–779. doi: 10.2136/vzj2010.0012.

Yoon, H.-K., Chun, O.-H., Park, M.-C., and Lee, J.-S. 2014. Slime thickness evaluation of bored piles by electrical resistivity probe. Journal of Applied Geophysics, **108**:167-175. doi: 10.1016/j.jappgeo.2014.07.004.

Zegelin, S.J., White, I., and Jenkins, D.R. 1989. Improved field probes for soil water content and electrical conductivity measurement using time domain reflectometry. Water Resources Research, **25**(11): 2367–2376.

Zheng, R., Li, Z., and Gong, Y. 2011. A coated helical transmission line time domain transmission sensor for measuring water content in saline soils. Soil Science Society of America Journal, **75**(2): 397–407. doi: 10.2136/sssaj2009.0371.

APPENDIX A:
COMPREHENSIVE DESCRIPTION OF LIFT COMPACTION PROCEDURE FOR TAILINGS SAND

Uniform bulk density of the various lifts was necessary for achieving the necessary level of control in testing, requiring a high level of precision in how the lifts were compacted. Furthermore, it was necessary to avoid damaging the cylinder with the hydraulic press. This section details the procedure for compacting the lifts while avoiding damage to the cylinder from excessive force.

Compaction of each lift began initially with all the sand for the lift being added to the cylinder at once; however, it was found that gaps were forming within the lift. As a result, the procedure was changed, and roughly half of the mass of the respective lift was added to the cylinder at a time. The compaction plate was lowered onto the sand after the first half was added to give a minimal level of compaction and to avoid the formation of gaps. Compaction of the sand to its target density was not completed or desired at this stage.

After this preliminary compaction was done, the entire surface of the sand was poked with the fork in order to break up any clumps in the sand and prevent the formation of gaps in the lift. Penetration of the fork tines was approximately 10 mm, although there was no control on this. In some cases the limited space inside the cylinder prevented the full depth of penetration. The rest of the sand for the lift was then added, and the levelling and fork penetration procedure repeated. To ensure the full mass of sand for the respective lift was added, the bowl was placed back on the balance to ensure it returned to a value of zero.

Final compaction of the lift was done following all the sand being added to the cylinder, and the sand's surface prepared. Compaction of the sand was achieved in two different ways. The first step of the compaction process was to bring the loading plate, and therefore the cylinder, up towards the compaction plate. This was the fastest mode of compaction, but also the coarsest in terms of control, so this was only used for preliminary compaction. A safety buffer in terms of a depth above the target depth was chosen to ensure the lift was not over-compacted. Following compaction to the safety buffer depth, the compaction plate was extracted from the cylinder. The fork was again used to poke the sand to continue to control the density of the lift.

After the lift was poked for the final time, the loading base was again brought up to compact the loosened portion of the lift. The safety buffer was maintained. Following this coarse re-compaction, the crosshead was brought down to compact the lift to the final target depth. This movement was much slower, but it also allowed substantially more control over the compaction process.

The process of compacting the lifts was slowest for the first few lifts in the cylinder, growing faster with subsequent lifts. With the exception of some upper lifts in the wettest sands, all lifts required some amount of vibration to re-align the sand particles and achieve the target lift thickness. In some cases loading and unloading of the cylinder together with vibration was also necessary. The cylinder was vibrated by striking the side of the cylinder with a rubber mallet.

Given that the hydraulic press was typically used for compression tests on concrete specimens, it would have been possible to exert a tremendous amount of force on the sand. However, the risk of the cylinder breaking from either the compression plate binding at higher loads, or too great of a horizontal force being generated from excessive loading was seen as too great. In order to protect the cylinder, a safety loading limit of 6000 N was set in the press' control software. This value was arrived at through conservative calculations and considering the effect of a number of unknowns. While the press' hydraulic system was set to shut down at 6000 N, it would typically spike to 10 000 N before the pump shut off and the force started to dissipate. As a result, vibration was relied on to achieve the necessary compaction.

In general, the process of moving the crosshead down was done iteratively while monitoring the load exerted by the press. Initially, vibration would be done after relatively small loads (e.g. 1000 to 2000 N) had built up in the system. However, as the compaction procedure progressed the load would be increased to around 4000 N before the vibration was done. This was because less and less reduction in the applied force would be seen as a result of the vibration. In a number of cases, the relief would be so minimal from the vibration that the cylinder would have to be unloaded, vibrated, and reloaded. Even with the process of unloading and reloading, it would often take approximately one hour to satisfactorily compact the lower lifts in the cylinder.

Progressing around the cylinder's perimeter with the mallet blows seemed to be the most effective way of vibrating the cylinder, as opposed to hitting it in only one place. Striking a ball-peen hammer on a piece of steel on the loading base was also investigated as an alternative vibration method, but it was ineffective.

APPENDIX B:
COMPREHENSIVE DESCRIPTION OF PROBE RE-INSERTION PROCEDURE FOR TAILINGS SAND

Removing and re-inserting prototype probes in wetted sand was seen to be an effective way of increasing the expediency of testing. Successfully completing this process without jeopardizing the test results or damaging the cylinder required a number of careful procedures to be followed. These procedures are outlined in this section.

After the initial packing of the cylinder, the compaction plate assembly and the probe-securing frame were removed to facilitate the removal of the probe with the press' crosshead. Using the hole in the crosshead which held the compaction plate assembly's threaded receiver, a drill chuck from a drill press was installed. The drill chuck was installed by wrapping its shaft in a few layers of electrical tape and knocking it into the hole with a hammer until it was snugly in place. Slight adjustments were made to the alignment of the chuck following installation to make it as plumb as possible.

After the drill chuck was in place, the compaction cylinder and the drill chuck were brought together by moving the crosshead and loading base of the hydraulic press. The smooth 12.7 mm diameter probe-stabilizing rod used to support the probe during compaction was re-inserted in the probe assembly to mate with the drill chuck. With the drill chuck jaws fully open, the probe-stabilizing rod was inserted sufficiently far into the drill chuck, and the chuck's jaws were closed and tightened. The probe was then extracted by moving the crosshead and loading base apart, and the next probe screwed on to the stabilizing rod to begin the re-insertion procedure.

As with probe extraction, movement of the crosshead and loading base were used to re-insert the probes. Re-inserting the probe was difficult to do, for the main reason that it was difficult to tell visually when it was fully inserted. One reason for this difficulty was an obstructed field of view of the sand surface due to disturbance of the sand from the probe extraction process. The other reason was that crosshead movement increments of fractions of a millimetre made it difficult to judge insertion progress. On a coarse scale, when the probe was visibly close to being fully inserted, the crosshead would be lowered in small increments. Since there was increased friction from the sand as the cone tip came closer to being fully seated at the base of the cylinder, the system's load would start to increase faster during loading as the probe approached full insertion. Dissipation of the system's load would also be progressively slower at this stage when active

loading was not taking place. In most cases, loading during re-insertion was limited to approximately 130 N in order to prevent damage to the cylinder. When there was minimal load dissipation from 130 N, the probe was assumed to be fully inserted.

It should be noted that the press' position data was tied only to movement in the crosshead; movements in the loading plate are not measured. As a result, simply returning to the same position as before the probe was extracted was not an option.

After the probe was inserted, the compaction plate assembly was re-attached to the crosshead to re-compact the disturbed sand. This worked well for cases where the D1 probe was used; however, for nearly all the D3 cases, and some of the D2 cases, this could not be successfully accomplished. Re-inserted probes were usually slightly off-plumb, and the small gap that originally existed between the probe's rods and the compaction plate hole was not large enough to prevent the compaction plate contacting the rods. As a result, a small amount of excess sand was lightly spread around the top of the probe. The sand was then compacted lightly with fingertips or a short length of a 25.4 mm diameter capped PVC pipe. This sand filled in the air gaps in the annulus at the top of the probe and packed down the disturbed sand. In most instances, there was very little side-to-side freedom of movement in the re-inserted probe, suggesting a general absence of air gaps in the sand. Increases in the density of the packed sand was assumed to be negligible from any of the re-compaction efforts.

Despite efforts to re-insert the probe as completely as possible, in some cases the top of the Delrin® probe would not be completely flush with the sand's surface. While observations were generally made on the amount of probe protrusion, specific measurements were overlooked in some of the earlier cases. Measurements were not taken on any of the 7% gravimetric water content sand packings, or on the D2 re-insertion of the 14% gravimetric water content sand; however, protrusion was typically 4 mm or less on the re-insertions that were measured. Measuring this protrusion accurately was difficult due to a lack of clear sightlines, especially as the cylinder became more scratched with testing. The best measurement technique seemed to be placing a straightedge on the top of the probe body, and measuring the distance above the original surface a distance away from the probe with a ruler perpendicular to the straightedge.

The ruler that was available had a 3 mm gap before the start of the graduation marks, so in cases with less than 3 mm of protrusion the distance was estimated. A number of measurements were typically taken to account for the probe being off-plumb.

APPENDIX C:
INTERPRETED WAVEFORM RESULTS

LIST OF TABLES

Table C.1 – Reference solution testing results from unsheathed two-rod D1 probe (testing done October 2, 2013).

Test Medium	File Name	x_2 (m)	x_1 (m)	V_p	L (m)	ε_b	$\varepsilon_{theoretical}$
Air	air2D1	5.2910	5.1427	0.670933	0.100	4.886	1.000
De-ionized Water	DI2D1	5.5182	5.1462	0.670933	0.100	30.742	81.000
0.2 Ethanol	02etoh2D1	5.4885	5.1525	0.670933	0.100	25.080	67.300
0.4 Ethanol	04etoh2d1	5.4727	5.1466	0.670933	0.100	23.623	56.300
0.6 Ethanol	06etoh2d1	5.4441	5.1426	0.670933	0.100	20.194	41.600
0.8 Ethanol	08etoh2d1	5.4121	5.1450	0.670933	0.100	15.849	29.600
1.0 Ethanol	1etoh2d1	5.3969	5.1396	0.670933	0.100	14.707	19.000

Table C.2 – Reference solution testing results from unsheathed two-rod D2 probe (testing done October 2, 2013).

Test Medium	File Name	x_2 (m)	x_1 (m)	V_p	L (m)	ε_b	$\varepsilon_{theoretical}$
Air	air2d2	5.2841	5.1546	0.670933	0.100	3.725	1.000
De-ionized Water	di2d2	5.5825	5.1485	0.670933	0.100	41.843	81.000
0.2 Ethanol	02etoh2d2	5.5471	5.1485	0.670933	0.100	35.295	67.300
0.4 Ethanol	04etoh2d2	5.5231	5.1505	0.670933	0.100	30.841	56.300
0.6 Ethanol	06etoh2d2	5.4738	5.1478	0.670933	0.100	23.609	41.600
0.8 Ethanol	08etoh2d2	5.4385	5.1478	0.670933	0.100	18.773	29.600
1.0 Ethanol	1etoh2d2	5.4205	5.1498	0.670933	0.100	16.279	19.000

Table C.3 – Reference solution testing results from unsheathed two-rod D3 probe (testing done October 2, 2013).

Test Medium	File Name	x_2 (m)	x_1 (m)	V_p	L (m)	ε_b	$\varepsilon_{theoretical}$
Air	air2d3	5.2747	5.1499	0.670933	0.100	3.460	1.000
De-ionized Water	di2d3	5.6287	5.1494	0.670933	0.100	51.034	81.000
0.2 Ethanol	02etoh2d3	5.5829	5.1509	0.670933	0.100	41.458	67.300
0.4 Ethanol	04etoh2d3	5.5522	5.1502	0.670933	0.100	35.900	56.300
0.6 Ethanol	06etoh2d3	5.5019	5.1509	0.670933	0.100	27.369	41.600
0.8 Ethanol	08etoh2d3	5.4652	5.1502	0.670933	0.100	22.043	29.600
1.0 Ethanol	1etoh2d3	5.4292	5.1479	0.670933	0.100	17.578	19.000

Table C.4 – Reference solution testing results from unsheathed two-rod conventional probe (testing done September 25, 2013).

Test Medium	File Name	x_2 (m)	x_1 (m)	V_p	L (m)	ε_b	$\varepsilon_{theoretical}$
Air	Air2	5.2709	5.1755	0.670933	0.101	1.982	1.000
De-ionized Water	Water2	5.8010	5.1608	0.670933	0.101	89.255	81.000
0.2 Ethanol	02E2	5.7416	5.1579	0.670933	0.101	74.196	67.300
0.4 Ethanol	04E2	5.7052	5.1637	0.670933	0.101	63.855	56.300
0.6 Ethanol	06E2	5.6266	5.1637	0.670933	0.101	46.663	41.600
0.8 Ethanol	08E2	5.5633	5.1656	0.670933	0.101	34.444	29.600
1.0 Ethanol	1E2	5.5058	5.1589	0.670933	0.101	26.206	19.000

Table C.5 – Reference solution testing results from sheathed two-rod D1 probe (testing done October 2, 2013).

Test Medium	File Name	x_2 (m)	x_1 (m)	V_p	L (m)	ε_b	$\varepsilon_{theoretical}$
Air	air2d1s	5.2915	5.1435	0.670933	0.100	4.866	1.000
De-ionized Water	di2d1s	5.4725	5.1420	0.670933	0.100	24.265	81.000
0.2 Ethanol	02etohd1s	5.4690	5.1403	0.670933	0.100	24.002	67.300
0.4 Ethanol	04etoh2d1s	5.4510	5.1400	0.670933	0.100	21.486	56.300
0.6 Ethanol	06etoh2d1s	5.4280	5.1430	0.670933	0.100	18.044	41.600
0.8 Ethanol	08etoh2d1s	5.4050	5.1475	0.670933	0.100	14.730	29.600
1.0 Ethanol	1etoh2d1s	5.3869	5.1487	0.670933	0.100	12.604	19.000

Table C.6 – Reference solution testing results from sheathed two-rod D2 probe (testing done October 2, 2013).

Test Medium	File Name	x_2 (m)	x_1 (m)	V_p	L (m)	ε_b	$\varepsilon_{theoretical}$
Air	air2d2s	5.2885	5.1502	0.670933	0.100	4.249	1.000
De-ionized Water	di2d2s	5.4983	5.1502	0.670933	0.100	26.918	81.000
0.2 Ethanol	02etoh2d2s	5.4811	5.1509	0.670933	0.100	24.221	67.300
0.4 Ethanol	04etoh2d2s	5.4638	5.1496	0.670933	0.100	21.931	56.300
0.6 Ethanol	06etoh2d2s	5.4403	5.1489	0.670933	0.100	18.863	41.600
0.8 Ethanol	08etoh2d2s	5.4211	5.1489	0.670933	0.100	16.460	29.600
1.0 Ethanol	1etoh2d2s	5.4001	5.1476	0.670933	0.100	14.163	19.000

Table C.7 – Reference solution testing results from sheathed two-rod D3 probe (testing done October 2, 2013).

Test Medium	File Name	x_2 (m)	x_1 (m)	V_p	L (m)	ε_b	$\varepsilon_{theoretical}$
Air	air2d3s	5.2797	5.1517	0.670933	0.100	3.640	1.000
De-ionized Water	di2d3s	5.5118	5.1489	0.670933	0.100	29.256	81.000
0.2 Ethanol	02etoh2d3s	5.4984	5.1510	0.670933	0.100	26.810	67.300
0.4 Ethanol	04etoh2d3s	5.4821	5.1489	0.670933	0.100	24.663	56.300
0.6 Ethanol	06etoh2d3s	5.4559	5.1481	0.670933	0.100	21.046	41.600
0.8 Ethanol	08etoh2d3s	5.4304	5.1489	0.670933	0.100	17.603	29.600
1.0 Ethanol	1etoh2d3s	5.4092	5.1489	0.670933	0.100	15.052	19.000

Table C.8 – Reference solution testing results from conventional sheathed two-rod probe (testing done September 25, 2013).

Test Medium	File Name	x_2 (m)	x_1 (m)	V_p	L (m)	ε_b	$\varepsilon_{theoretical}$
Air	Air2S	5.2675	5.1704	0.670933	0.100	2.094	1.000
De-ionized Water	Water2S	5.5038	5.1617	0.670933	0.100	25.998	81.000
0.2 Ethanol	02E2S	5.4998	5.1637	0.670933	0.100	25.095	67.300
0.4 Ethanol	04E2S	5.4959	5.1629	0.670933	0.100	24.634	56.300
0.6 Ethanol	06E2S	5.4856	5.1645	0.670933	0.100	22.905	41.600
0.8 Ethanol	08E2S	5.4658	5.1645	0.670933	0.100	20.167	29.600
1.0 Ethanol	1E2S	5.4255	5.1653	0.670933	0.100	15.040	19.000

Table C.9 – Reference solution testing results from unsheathed three-rod D1 probe (testing done October 2, 2013).

Test Medium	File Name	x_2 (m)	x_1 (m)	V_p	L (m)	ε_b	$\varepsilon_{theoretical}$
Air	air3d1	5.3064	5.1510	0.670933	0.100	5.365	1.000
De-ionized Water	di3d1	5.5649	5.1503	0.670933	0.100	38.186	81.000
0.2 Ethanol	02etoh3d1	5.5656	5.1533	0.670933	0.100	37.763	67.300
0.4 Ethanol	04etoh3d1	5.5264	5.1503	0.670933	0.100	31.423	56.300
0.6 Ethanol	06etoh3d1	5.4887	5.1533	0.670933	0.100	24.990	41.600
0.8 Ethanol	08etoh3d1	5.4356	5.1526	0.670933	0.100	17.792	29.600
1.0 Ethanol	1etoh3d1	----	----	0.670933	0.100	----	19.000

---- Data not analyzed

Table C.10 – Reference solution testing results from unsheathed three-rod D3 probe (testing done October 2, 2013).

Test Medium	File Name	x_2 (m)	x_1 (m)	V_p	L (m)	ε_b	$\varepsilon_{theoretical}$
Air	air3d2	5.2804	5.1539	0.670933	0.100	3.555	1.000
De-ionized Water	di3d2	5.6416	5.1555	0.670933	0.100	52.492	81.000
0.2 Ethanol	02etoh3d2	5.6039	5.1570	0.670933	0.100	44.367	67.300
0.4 Ethanol	04etoh3d2	5.5593	5.1532	0.670933	0.100	36.636	56.300
0.6 Ethanol	06etoh3d2	5.5239	5.1539	0.670933	0.100	30.412	41.600
0.8 Ethanol	08etoh3d2	5.4678	5.1539	0.670933	0.100	21.889	29.600
1.0 Ethanol	1etoh3d2	5.4439	5.1578	0.670933	0.100	18.183	19.000

Table C.11 – Reference solution testing results from unsheathed three-rod D3 probe (testing done October 3, 2013).

Test Medium	File Name	x_2 (m)	x_1 (m)	V_p	L (m)	ε_b	$\varepsilon_{theoretical}$
Air	air3d3	5.2887	5.1419	0.670933	0.100	4.787	1.000
De-ionized Water	di3d3	5.6756	5.1410	0.670933	0.100	63.489	81.000
0.2 Ethanol	02etoh3d3	5.6303	5.1434	0.670933	0.100	52.665	67.300
0.4 Ethanol	04etoh3d3	5.6223	5.1434	0.670933	0.100	50.948	56.300
0.6 Ethanol	06etoh3d3	5.5449	5.1441	0.670933	0.100	35.686	41.600
0.8 Ethanol	08etoh3d3	5.5084	5.1412	0.670933	0.100	29.953	29.600
1.0 Ethanol	1etoh3d3	5.4719	5.1449	0.670933	0.100	23.754	19.000

Table C.12 – Reference solution testing results from conventional unsheathed three-rod probe (testing done September 23, 2013).

Test Medium	File Name	x_2 (m)	x_1 (m)	V_p	L (m)	ε_b	$\varepsilon_{theoretical}$
Air	airz	1.0682	0.9897	0.670933	0.102	1.316	1.000
De-ionized Water	waterz	1.6072	0.9879	0.670933	0.102	81.892	81.000
0.2 Ethanol	02ez	1.5545	0.9879	0.670933	0.102	68.548	67.300
0.4 Ethanol	04ez	1.5012	0.9885	0.670933	0.102	56.127	56.300
0.6 Ethanol	06ez	1.4332	0.9885	0.670933	0.102	42.226	41.600
0.8 Ethanol	08ez	1.3699	0.9885	0.670933	0.102	31.060	29.600
1.0 Ethanol	1ez	1.3065	0.9892	0.670933	0.102	21.497	19.000

Table C.13 – Reference solution testing results from sheathed three-rod D1 probe (testing done October 2, 2013).

Test Medium	File Name	x_2 (m)	x_1 (m)	V_p	L (m)	ε_b	$\varepsilon_{theoretical}$
Air	air3d1s	5.3090	5.1498	0.670933	0.100	5.630	1.000
De-ionized Water	di3d1s	5.5015	5.1511	0.670933	0.100	27.275	81.000
0.2 Ethanol	02etoh3d1s	5.4817	5.1511	0.670933	0.100	24.280	67.300
0.4 Ethanol	04etoh3d1s	5.4628	5.1496	0.670933	0.100	21.791	56.300
0.6 Ethanol	06etoh3d1s	5.4438	5.1496	0.670933	0.100	19.228	41.600
0.8 Ethanol	08etoh3d1s	5.4321	5.1481	0.670933	0.100	17.918	29.600
1.0 Ethanol	1etoh3d1s	5.4175	5.1489	0.670933	0.100	16.027	19.000

Table C.14 – Reference solution testing results from sheathed three-rod D2 probe (testing done October 2, 2013).

Test Medium	File Name	x_2 (m)	x_1 (m)	V_p	L (m)	ε_b	$\varepsilon_{theoretical}$
Air	air3d2s	5.3090	5.1567	0.670933	0.100	5.153	1.000
De-ionized Water	di3d2s	5.5174	5.1529	0.670933	0.100	29.515	81.000
0.2 Ethanol	02etoh3d2s	5.3815	5.1574	0.670933	0.100	11.156	67.300
0.4 Ethanol	04etoh3d2s	5.3699	5.1546	0.670933	0.100	10.297	56.300
0.6 Ethanol	06etoh3d2s	5.3692	5.1576	0.670933	0.100	9.947	41.600
0.8 Ethanol	08etoh3d2s	5.3592	5.1561	0.670933	0.100	9.164	29.600
1.0 Ethanol	1etoh3d2s	5.3467	5.1563	0.670933	0.100	8.053	19.000

Table C.15 – Reference solution testing results from sheathed three-rod D3 probe (testing done October 3, 2013).

Test Medium	File Name	x_2 (m)	x_1 (m)	V_p	L (m)	ε_b	$\varepsilon_{theoretical}$
Air	air3d3s	5.3127	5.1443	0.670933	0.100	6.300	1.000
De-ionized Water	di3d3s	5.4965	5.1432	0.670933	0.100	27.729	81.000
0.2 Ethanol	02etoh3d3s	5.4527	5.1527	0.670933	0.100	19.993	67.300
0.4 Ethanol	04etoh3d3s	5.3604	5.1535	0.670933	0.100	9.510	56.300
0.6 Ethanol	06etoh3d3s	5.3550	5.1520	0.670933	0.100	9.154	41.600
0.8 Ethanol	08etoh3d3s	5.3520	5.1535	0.670933	0.100	8.753	29.600
1.0 Ethanol	1etoh3d3s	5.3335	5.1507	0.670933	0.100	7.423	19.000

Table C.16 – Reference solution testing results from conventional sheathed three-rod probe (testing done September 25, 2013).

Test Medium	File Name	x_2 (m)	x_1 (m)	V_p	L (m)	ε_b	$\varepsilon_{theoretical}$
Air	AirZS	1.0678	0.9890	0.670933	0.103	1.300	1.000
De-ionized Water	WaterZS	1.3729	0.9885	0.670933	0.103	30.941	81.000
0.2 Ethanol	02EZS	1.3606	0.9885	0.670933	0.103	28.993	67.300
0.4 Ethanol	04ESZ	1.3460	0.9885	0.670933	0.103	26.762	56.300
0.6 Ethanol	06EZS	1.3239	0.9885	0.670933	0.103	23.556	41.600
0.8 Ethanol	08EZS	1.2959	0.9879	0.670933	0.103	19.864	29.600
1.0 Ethanol	1EZS	1.2512	0.9885	0.670933	0.103	14.451	19.000

Table C.17 – Reference solution testing results from conventional unsheathed two-rod probe (testing done September 25, 2013).

Test Medium	File Name	x_2 (m)	x_1 (m)	V_p	L (m)	ε_b	$\varepsilon_{theoretical}$
Air	Air2	5.2709	5.1755	0.670933	0.101	1.982	1.000
De-ionized Water	Water2	5.8010	5.1608	0.670933	0.101	89.255	81.000
0.2 Ethanol	02E2	5.7416	5.1579	0.670933	0.101	74.196	67.300
0.4 Ethanol	04E2	5.7052	5.1637	0.670933	0.101	63.855	56.300
0.6 Ethanol	06E2	5.6266	5.1637	0.670933	0.101	46.663	41.600
0.8 Ethanol	08E2	5.5633	5.1656	0.670933	0.101	34.444	29.600
1.0 Ethanol	1E2	5.5058	5.1589	0.670933	0.101	26.206	19.000

Table C.18 – Reference solution testing results from re-tested unsheathed three-rod D2 probe (testing done February 20, 2014).

Test Medium	File Name	x_2 (m)	x_1 (m)	V_p	L (m)	ε_b	$\varepsilon_{theoretical}$
De-ionized Water	DI3D2	5.6211	5.1374	0.670933	0.100	51.975	81.000
0.2 Ethanol	02etoh3d2	5.6013	5.1393	0.670933	0.100	47.416	67.300
0.4 Ethanol	04eohd2	5.5635	5.1345	0.670933	0.100	40.884	56.300
0.6 Ethanol	06rtohd2	5.5155	5.1336	0.670933	0.100	32.400	41.600
0.8 Ethanol	08etohd2	5.4834	5.1364	0.670933	0.100	26.749	29.600
1.0 Ethanol	10etohd2	5.4589	5.1336	0.670933	0.100	23.508	19.000

Table C.19 – Reference solution testing results from unsheathed three-rod D2 probe with secondary jumper cable (testing done February 20 and 26, 2014).

Test Medium	File Name	x_2 (m)	x_1 (m)	V_p	L (m)	ε_b	$\varepsilon_{theoretical}$
De-ionized Water	DI3D2J	5.6871	5.2055	0.670933	0.100	51.525	81.000
0.2 Ethanol	02etoh3d2jv2	5.6414	5.2084	0.670933	0.100	41.650	67.300
0.4 Ethanol	04etoh3d2jv2	5.5704	5.2130	0.670933	0.100	28.376	56.300
0.6 Ethanol	06etoh3d2jv2	5.5348	5.2118	0.670933	0.100	23.176	41.600
0.8 Ethanol	08etoh3d2jv2	5.5291	5.2210	0.670933	0.100	21.087	29.600
1.0 Ethanol	1etoh3d2jv2	5.4730	5.2130	0.670933	0.100	15.017	19.000

Table C.20 – Reference solution testing results from re-tested sheathed three-rod D2 probe (testing done February 20, 2014).

Test Medium	File Name	x_2 (m)	x_1 (m)	V_p	L (m)	ε_b	$\varepsilon_{theoretical}$
De-ionized Water	DI3d2s	5.4901	5.1952	0.670933	0.100	19.319	81.000
0.2 Ethanol	02etoh3d2s	5.4745	5.1853	0.670933	0.100	18.580	67.300
0.4 Ethanol	04etoh3d2s	5.4679	5.1829	0.670933	0.100	18.044	56.300
0.6 Ethanol	06etoh3d2s	5.4482	5.1878	0.670933	0.100	15.063	41.600
0.8 Ethanol	08etoh3d2s	5.4350	5.1845	0.670933	0.100	13.940	29.600
1.0 Ethanol	10etoh3d2s	5.4194	5.1853	0.670933	0.100	12.174	19.000

Table C.21 – Reference solution testing results from sheathed three-rod D2 probe with secondary jumper cable (testing done February 20, 2014).

Test Medium	File Name	x_2 (m)	x_1 (m)	V_p	L (m)	ε_b	$\varepsilon_{theoretical}$
De-ionized Water	DI3d2js	5.4359	5.2154	0.670933	0.100	10.801	81.000
0.2 Ethanol	02etoh3d2js	5.4314	5.2082	0.670933	0.100	11.067	67.300
0.4 Ethanol	04etoh3d2js	5.4458	5.2163	0.670933	0.100	11.701	56.300
0.6 Ethanol	06etoh3d2js	5.4647	5.2100	0.670933	0.100	14.411	41.600
0.8 Ethanol	08etoh3d2js	5.4494	5.2109	0.670933	0.100	12.636	29.600
1.0 Ethanol	10etoh3d2js	5.4026	5.2100	0.670933	0.100	8.241	19.000

Table C.22 – Reference solution testing results from re-tested conventional unsheathed three-rod Zegelin-type probe (testing done February 20, 2014).

Test Medium	File Name	x_2 (m)	x_1 (m)	V_p	L (m)	ε_b	$\varepsilon_{theoretical}$
De-ionized Water	DI3d2s	5.4901	5.1952	0.670933	0.100	19.319	81.000
0.2 Ethanol	02etoh3d2s	5.4745	5.1853	0.670933	0.100	18.580	67.300
0.4 Ethanol	04etoh3d2s	5.4679	5.1829	0.670933	0.100	18.044	56.300
0.6 Ethanol	06etoh3d2s	5.4482	5.1878	0.670933	0.100	15.063	41.600
0.8 Ethanol	08etoh3d2s	5.4350	5.1845	0.670933	0.100	13.940	29.600
1.0 Ethanol	10etoh3d2s	5.4194	5.1853	0.670933	0.100	12.174	19.000

Table C.23 – Saline solution testing results from sheathed two-rod D1 probe (testing done October 3, 2013).

Test Medium	File Name	x_2 (m)	x_1 (m)	V_p	L (m)	ε_b
De-ionized Water	di2d1s	5.4725	5.1420	0.670933	0.100	24.265
5 g/L NaCl	5nacl2d1s	5.5004	5.1551	0.670933	0.100	26.487
10 g/L NaCl	10nacl2d1s	5.7305	5.1521	0.670933	0.100	74.319
15 g/L NaCl	15nacl2d1s	5.9011	5.1534	0.670933	0.100	124.193

Table C.24 – Saline solution testing results from sheathed two-rod D2 probe (testing done October 3, 2013).

Test Medium	File Name	x_2 (m)	x_1 (m)	V_p	L (m)	ε_b
De-ionized Water	di2d2s	5.4983	5.1502	0.670933	0.100	26.918
5 g/L NaCl	5nacl2d2s	5.4877	5.1528	0.670933	0.100	24.916
10 g/L NaCl	10nacl2d2s	5.5222	5.1522	0.670933	0.100	30.412
15 g/L NaCl	15nacl2d2s	5.8139	5.1542	0.670933	0.100	96.680
20 g/L NaCl	20nacl2d2s	5.9112	5.1542	0.670933	0.100	127.301

Table C.25 – Saline solution testing results from sheathed two-rod D3 probe (testing done October 3, 2013).

Test Medium	File Name	x_2 (m)	x_1 (m)	V_p	L (m)	ε_b
De-ionized Water	di2d3s	5.5118	5.1489	0.670933	0.100	29.256
5 g/L NaCl	5nacl2d3s	5.4936	5.1526	0.670933	0.100	25.832
10 g/L NaCl	10nacl2d3s	5.7536	5.1436	0.670933	0.100	82.661
15 g/L NaCl	15nacl2d3s	5.9244	5.1484	0.670933	0.100	133.772

Table C.26 – Saline solution testing results from sheathed two-rod D3 probe (testing done October 3, 2013).

Test Medium	File Name	x_2 (m)	x_1 (m)	V_p	L (m)	ε_b
De-ionized Water	di2d3s	5.5118	5.1489	0.670933	0.100	29.256
5 g/L NaCl	5nacl2d3s	5.4936	5.1526	0.670933	0.100	25.832
10 g/L NaCl	10nacl2d3s	5.7536	5.1436	0.670933	0.100	82.661
15 g/L NaCl	15nacl2d3s	5.9244	5.1484	0.670933	0.100	133.772

Table C.27 – Saline solution testing results from conventional sheathed two-rod probe (testing done October 3, 2013).

Test Medium	File Name	x_2 (m)	x_1 (m)	V_p	L (m)	ε_b
De-ionized Water	Water2S	5.5038	5.1617	0.670933	0.100	25.998
5 g/L NaCl	5nacl	5.5380	5.1443	0.670933	0.101	33.754
10 g/L NaCl	10nacl	5.7563	5.1428	0.670933	0.101	81.965
15 g/L NaCl	15nacl	5.7789	5.1466	0.670933	0.101	87.065
20 g/L NaCl	20nacl	5.8190	5.1491	0.670933	0.101	97.728
25 g/L NaCl	25nacl	5.9244	5.1541	0.670933	0.101	129.217
30 g/L NaCl	30nacl	6.0611	5.1579	0.670933	0.101	177.651

Table C.28 – Saline solution testing results from sheathed three-rod D1 probe (testing done October 3, 2013).

Test Medium	File Name	x_2 (m)	x_1 (m)	V_p	L (m)	ε_b
De-ionized Water	di3d1s	5.5015	5.1511	0.670933	0.100	27.275
5 g/L NaCl	5nacl3d1s	5.4787	5.1423	0.670933	0.100	25.139
10 g/L NaCl	10nacl3d1s	5.5665	5.1452	0.670933	0.100	39.430
15 g/L NaCl	15nacl3d1s	5.8851	5.1502	0.670933	0.100	119.977

Table C.29 – Saline solution testing results from sheathed three-rod D2 probe (testing done October 3, 2013).

Test Medium	File Name	x_2 (m)	x_1 (m)	V_p	L (m)	ε_b
De-ionized Water	di3d2s	5.5174	5.1529	0.670933	0.100	29.515
5 g/L NaCl	5nacl3d2s	5.5359	5.1521	0.670933	0.100	32.723
10 g/L NaCl	10nacl3d2s	5.5874	5.1521	0.670933	0.100	42.094
15 g/L NaCl	15nacl3d2s	5.9116	5.1533	0.670933	0.100	127.739

Table C.30 – Saline solution testing results from sheathed three-rod D3 probe (testing done October 3, 2013).

Test Medium	File Name	x_2 (m)	x_1 (m)	V_p	L (m)	ε_b
De-ionized Water	di3d3s	5.4965	5.1432	0.670933	0.100	27.729
5 g/L NaCl	5nacl3d3s	5.5536	5.1538	0.670933	0.100	35.508
10 g/L NaCl	10nacl3d3s	5.6044	5.1527	0.670933	0.100	45.325

Table C.31 – Saline solution testing results from conventional sheathed three-rod probe (testing done October 3, 2013).

Test Medium	File Name	x_2 (m)	x_1 (m)	V_p	L (m)	ε_b
De-ionized Water	WaterZS	1.3729	0.9885	0.670933	0.103	30.941
5 g/L NaCl	5naclz	1.3594	0.9891	0.670933	0.101	29.861
10 g/L NaCl	10naclz	1.3635	0.9888	0.670933	0.101	30.575
15 g/L NaCl	15naclz	1.4118	0.9896	0.670933	0.101	38.818

Table C.32 – Compacted non-elevated salinity tailings sand testing results from unsheathed two-rod D1 probe (testing done December 2013).

Test Medium (Target Grav. W.C.)	File Name	x_2 (m)	x_1 (m)	V_p	L (m)	ε_b	Calc'd Vol. W.C. (m^3/m^3) (Topp method)
Air-dry Sand	0sand2d1	5.3165	5.1735	0.670933	0.100	4.543	0.069
7% Sand	7sand2d1	5.3123	5.1507	0.670933	0.100	5.801	0.099
7% Sand (1st re-insertion)	7sand2d1r	5.3223	5.1781	0.670933	0.100	4.619	0.071
7% Sand (2nd re-insertion)	7sand2d1rr	5.3094	5.1698	0.670933	0.100	4.329	0.063
14% Sand	14sand2d1	5.3152	5.1556	0.670933	0.096	6.140	0.107
14% Sand (re-insertion)	14sand2d1r	5.319	5.164	0.670933	0.096	5.791	0.098
19% Sand	19sand2d1	5.3294	5.1527	0.670933	0.100	6.936	0.125
19% Sand (re-insertion)	19sand2d1r	5.3385	5.1752	0.670933	0.100	5.924	0.102

Table C.33 – Compacted non-elevated salinity tailings sand testing results from unsheathed two-rod D2 probe (testing done December 2013).

Test Medium (Target Grav. W.C.)	File Name	x_2 (m)	x_1 (m)	V_p	L (m)	ε_b	Calc'd Vol. W.C. (m^3/m^3) (Topp method)
Air-dry Sand	0sand2d2	5.3199	5.1741	0.670933	0.100	4.722	0.073
7% Sand	7sand2d2	5.3142	5.148	0.670933	0.100	6.136	0.106
7% Sand (re-insertion)	7sand2d2r	5.3151	5.1523	0.670933	0.100	5.888	0.101
14% Sand (re-insertion)	14sand2d2	5.3381	5.1609	0.670933	0.099	7.117	0.129
19% Sand (re-insertion)	19sand2d2	5.3548	5.1576	0.670933	0.099	8.814	0.165

Table C.34 – Compacted non-elevated salinity tailings sand testing results from unsheathed two-rod D3 probe (testing done December 2013).

Test Medium (Target Grav. W.C.)	File Name	x_2 (m)	x_1 (m)	V_p	L (m)	ε_b	Calc'd Vol. W.C. (m^3/m^3) (Topp method)
Air-dry Sand	0sand2d3	5.2995	5.1572	0.670933	0.100	4.498	0.073
7% Sand	7sand2d3	5.3201	5.1515	0.670933	0.100	6.315	0.111
7% Sand (re-insertion)	7sand2d3r	5.3067	5.1501	0.670933	0.099	5.558	0.093
14% Sand (re-insertion)	14sand2d3	5.3435	5.1556	0.670933	0.096	8.510	0.158
19% Sand (re-insertion)	19sand2d3	5.369	5.1562	0.670933	0.099	10.368	0.195

Table C.35 – Compacted non-elevated salinity tailings sand testing results from conventional unsheathed two-rod probe (testing done December 2013).

Test Medium (Target Grav. W.C.)	File Name	x_2 (m)	x_1 (m)	V_p	L (m)	ε_b	Calc'd Vol. W.C. (m^3/m^3) (Topp method)
Air-dry Sand	0sand2cp	5.3099	5.166	0.670933	0.100	4.600	0.070
7% Sand	7sand2cp	5.3343	5.159	0.670933	0.100	6.827	0.122
14% Sand	14sand2cp	5.3891	5.1658	0.670933	0.100	11.077	0.209
19% Sand	19sandcp	5.4232	5.1557	0.670933	0.100	15.896	0.289

Table C.36 – Compacted non-elevated salinity tailings sand testing results from sheathed two-rod D1 probe (testing done December 2013).

Test Medium (Target Grav. W.C.)	File Name	x_2 (m)	x_1 (m)	V_p	L (m)	ε_b	Calc'd Vol. W.C. (m^3/m^3) (Topp method)
Air-dry Sand	0sand2d1s	5.3206	5.1679	0.670933	0.100	5.180	0.084
7% Sand	7sand2d1s	5.3103	5.1780	0.670933	0.100	3.888	0.052
7% Sand (1^{st} re-insertion)	7sand2d1sr	5.3141	5.1675	0.670933	0.100	4.774	0.074
7% Sand (2^{nd} re-insertion)	7sand2d1srr	5.3136	5.1737	0.670933	0.100	4.348	0.064
14% Sand	14sand2d1s	5.3284	5.1627	0.670933	0.096	6.618	0.117
14% Sand (re-insertion)	14sand2d1sr	5.3069	5.1522	0.670933	0.096	5.769	0.098
19% Sand	19sand2d1s	5.3140	5.1534	0.670933	0.100	5.730	0.097
19% Sand (re-insertion)	19sand2d1sr	5.3156	5.1397	0.670933	0.100	6.873	0.123

Table C.37 – Compacted non-elevated salinity tailings sand testing results from sheathed two-rod D2 probe (testing done December 2013).

Test Medium (Target Grav. W.C.)	File Name	x_2 (m)	x_1 (m)	V_p	L (m)	ε_b	Calc'd Vol. W.C. (m^3/m^3) (Topp method)
Air-dry Sand	0sand2d2s	5.3016	5.1490	0.670933	0.100	5.173	0.084
7% Sand	7sand2d2s	5.3139	5.1664	0.670933	0.100	4.833	0.076
7% Sand (re-insertion)	7sand2d2sr	5.3112	5.1586	0.670933	0.100	5.173	0.084
14% Sand (re-insertion)	14sand2d2s	5.318	5.1586	0.670933	0.099	5.759	0.098
19% Sand (re-insertion)	19sand2d2s	5.3121	5.1500	0.670933	0.099	5.956	0.102

Table C.38 – Compacted non-elevated salinity tailings sand testing results from sheathed two-rod D3 probe (testing done December 2013).

Test Medium (Target Grav. W.C.)	File Name	x_2 (m)	x_1 (m)	V_p	L (m)	ε_b	Calc'd Vol. W.C. (m^3/m^3) (Topp method)
Air-dry Sand	0sand2d3s	5.3024	5.1534	0.670933	0.100	4.932	0.078
7% Sand	7sand2d3s	5.3108	5.1556	0.670933	0.100	5.351	0.088
7% Sand (re-insertion)	7sand2d3sr	5.3125	5.1739	0.670933	0.099	4.354	0.064
14% Sand (re-insertion)	14sand2d3s	5.3143	5.1554	0.670933	0.096	6.086	0.105
19% Sand (re-insertion)	19sand2d3s	5.3275	5.1627	0.670933	0.099	6.156	0.107

Table C.39 – Compacted non-elevated salinity tailings sand testing results from conventional sheathed two-rod probe (testing done December 2013).

Test Medium (Target Grav. W.C.)	File Name	x_2 (m)	x_1 (m)	V_p	L (m)	ε_b	Calc'd Vol. W.C. (m^3/m^3) (Topp method)
Air-dry Sand	0sand2cps	5.3038	5.1599	0.670933	0.100	4.600	0.070
7% Sand	7sand2cps	5.326	5.156	0.670933	0.100	6.420	0.113
14% Sand	14sand2cps	5.3804	5.1679	0.670933	0.100	10.031	0.189
19% Sand	19sand2cps	5.3995	5.1622	0.670933	0.100	12.509	0.235

Table C.40 – Compacted non-elevated salinity tailings sand testing results from unsheathed three-rod D1 probe (testing done December 2013).

Test Medium (Target Grav. W.C.)	File Name	x_2 (m)	x_1 (m)	V_p	L (m)	ε_b	Calc'd Vol. W.C. (m^3/m^3) (Topp method)
Air-dry Sand	0sand3d1	5.3183	5.1252	0.670933	0.100	8.283	0.154
7% Sand	7sand3d1	5.3200	5.1351	0.670933	0.100	7.595	0.139
7% Sand (1^{st} re-insertion)	7sand3d1r	5.3142	5.1340	0.670933	0.100	7.214	0.131
7% Sand (2^{nd} re-insertion)	7sand3d1rr	5.3183	5.1439	0.670933	0.100	6.757	0.121
14% Sand	14sand3d1	5.3317	5.1415	0.670933	0.096	8.720	0.163
14% Sand (re-insertion)	14sand3d1r	5.3375	5.1375	0.670933	0.096	9.642	0.181
19% Sand	19sand3d1	5.3457	5.1240	0.670933	0.100	10.919	0.206
19% Sand (re-insertion)	19sand3d1r	5.3288	5.1281	0.670933	0.100	8.948	0.167

Table C.41 – Compacted non-elevated salinity tailings sand testing results from unsheathed three-rod D2 probe (testing done December 2013).

Test Medium (Target Grav. W.C.)	File Name	x_2 (m)	x_1 (m)	V_p	L (m)	ε_b	Calc'd Vol. W.C. (m^3/m^3) (Topp method)
Air-dry Sand	0sand3d2	5.3071	5.1381	0.670933	0.100	6.345	0.111
7% Sand	7sand3d2	5.3276	5.1295	0.670933	0.100	8.718	0.163
7% Sand (re-insertion)	7sand3d2r	5.3257	5.1452	0.670933	0.100	7.238	0.131
14% Sand (re-insertion)	14sand3d2	5.3539	5.1548	0.670933	0.099	8.985	0.168
19% Sand (re-insertion)	19sand3d2	5.3749	5.1309	0.670933	0.099	13.494	0.251

Table C.42 – Compacted non-elevated salinity tailings sand testing results from unsheathed three-rod D3 probe (testing done December 2013).

Test Medium (Target Grav. W.C.)	File Name	x_2 (m)	x_1 (m)	V_p	L (m)	ε_b	Calc'd Vol. W.C. (m^3/m^3) (Topp method)
Air-dry Sand	0sand3d3	5.3034	5.1349	0.670933	0.100	6.307	0.110
7% Sand	7sand3d3	5.3261	5.1317	0.670933	0.100	8.395	0.156
7% Sand (re-insertion)	7sand3d3r	5.3287	5.1449	0.670933	0.099	7.657	0.140
14% Sand (re-insertion)	14sand3d3	5.3498	5.1365	0.670933	0.096	10.967	0.207
19% Sand (re-insertion)	19sand3d3	5.3945	5.1249	0.670933	0.099	16.474	0.298

Table C.43 – Compacted non-elevated salinity tailings sand testing results from conventional unsheathed three-rod probe (testing done December 2013).

Test Medium (Target Grav. W.C.)	File Name	x_2 (m)	x_1 (m)	V_p	L (m)	ε_b	Calc'd Vol. W.C. (m^3/m^3) (Topp method)
Air-dry Sand	0sand3z	1.1067	0.9898	0.670933	0.104	2.807	0.025
7% Sand	7sand3z	1.1417	0.9891	0.670933	0.104	4.783	0.075
14% Sand	14sand3z	1.1955	0.9894	0.670933	0.104	8.724	0.163
19% Sand	19sand3z	1.2374	0.9883	0.670933	0.104	12.744	0.239

Table C.44 – Compacted non-elevated salinity tailings sand testing results from sheathed three-rod D1 probe (testing done December 2013).

Test Medium (Target Grav. W.C.)	File Name	x_2 (m)	x_1 (m)	V_p	L (m)	ε_b	Calc'd Vol. W.C. (m^3/m^3) (Topp method)
Air-dry Sand	0sand3d1s	5.3222	5.1631	0.670933	0.100	5.623	0.095
7% Sand	7sand3d1s	5.3080	5.1380	0.670933	0.100	6.420	0.113
7% Sand (1st re-insertion)	7sand3d1sr	5.3283	5.1803	0.670933	0.100	6.420	0.113
7% Sand (2nd re-insertion)	7sand3d1srr	5.3216	5.162	0.670933	0.100	5.659	0.095
14% Sand	14sand3d1s	5.3283	5.1592	0.670933	0.096	6.893	0.124
14% Sand (re-insertion)	14sand3d1sr	5.3216	5.1598	0.670933	0.096	6.310	0.110
19% Sand	19sand3d1s	5.3427	5.1382	0.670933	0.100	9.290	0.174
19% Sand (re-insertion)	19sand3d1sr	5.3266	5.1304	0.670933	0.100	8.551	0.159

Table C.45 – Compacted non-elevated salinity tailings sand testing results from sheathed three-rod D2 probe (testing done December 2013).

Test Medium (Target Grav. W.C.)	File Name	x_2 (m)	x_1 (m)	V_p	L (m)	ε_b	Calc'd Vol. W.C. (m^3/m^3) (Topp method)
Air-dry Sand	0sand3d2s	5.3222	5.1583	0.670933	0.100	5.968	0.103
7% Sand	7sand3d2s	5.3270	5.1600	0.670933	0.100	6.195	0.108
7% Sand (re-insertion)	7sand3d2sr	5.3130	5.1413	0.670933	0.100	6.549	0.116
14% Sand (re-insertion)	14sand3d2s	5.3283	5.1600	0.670933	0.099	6.420	0.113
19% Sand (re-insertion)	19sand3d2s	5.3274	5.1422	0.670933	0.099	7.774	0.143

Table C.46 – Compacted non-elevated salinity tailings sand testing results from sheathed three-rod D3 probe (testing done December 2013).

Test Medium (Target Grav. W.C.)	File Name	x_2 (m)	x_1 (m)	V_p	L (m)	ε_b	Calc'd Vol. W.C. (m^3/m^3) (Topp method)
Air-dry Sand	0sand3d3s	5.3237	5.1254	0.670933	0.100	8.735	0.163
7% Sand	7sand3d3s	5.3231	5.1265	0.670933	0.100	8.586	0.160
7% Sand (re-insertion)	7sand3d3sr	5.3406	5.1644	0.670933	0.099	7.037	0.127
14% Sand (re-insertion)	14sand3d3s	5.3342	5.1254	0.670933	0.096	10.509	0.198
19% Sand (re-insertion)	19sand3d3s	5.3337	5.1482	0.670933	0.099	7.799	0.143

Table C.47 – Compacted non-elevated salinity tailings sand testing results from conventional sheathed three-rod probe (testing done December 2013).

Test Medium (Target Grav. W.C.)	File Name	x_2 (m)	x_1 (m)	V_p	L (m)	ε_b	Calc'd Vol. W.C. (m^3/m^3) (Topp method)
Air-dry Sand	0sand3zs	1.0402	1.0039	0.670933	0.104	0.271	-0.045
7% Sand	7sand3zs	1.1407	0.9889	0.670933	0.104	4.733	0.073
14% Sand	14sand3zs	1.1811	0.9889	0.670933	0.104	7.587	0.139
19% Sand	19sandzs	1.2101	0.9885	0.670933	0.104	10.086	0.190

Table C.48 – Legend for test configurations of the elevated salinity tailings sand testing.

Abbreviation	Meaning
2	Two-rod conventional probe
3	Three-rod conventional probe
L	long spacing
C	close spacing
S	sheathed
V	vertically oriented connection
H	horizontally oriented connection
R	first re-insertion
RR	second re-insertion

Table C.49 – Compacted 19% target gravimetric water content 2.5 g/L salinity tailings sand testing results from unsheathed two-rod D2 probe (testing done January 14, 2014).

Test Configuration	File Name	x_2 (m)	x_1 (m)	V_p	L (m)	ε_b	Calc'd Vol. W.C. (m^3/m^3) (Topp method)
L / V	19sand2-5tds2d2L	5.3501	5.1595	0.670933	0.100	8.070	0.149
C / V	19sand2-5tds2d2c	5.3538	5.1569	0.670933	0.100	8.613	0.160
L / V / R	19sand2-5tds2d2Lr	5.3512	5.1579	0.670933	0.100	8.301	0.154
C / V / R	19sand2-5tds2d2cr	5.3544	5.1532	0.670933	0.100	8.993	0.168
L / V / RR	19sand2-5tds2d2Lrr	5.3486	5.1453	0.670933	0.100	9.182	0.172
C / V / RR	19sand2-5tds2d2crr	5.3607	5.1621	0.670933	0.100	8.762	0.164

Table C.50 – Compacted 19% target gravimetric water content 2.5 g/L salinity tailings sand testing results from sheathed two-rod D2 probe (testing done January 14, 2014).

Test Configuration	File Name	x_2 (m)	x_1 (m)	V_p	L (m)	ε_b	Calc'd Vol. W.C. (m^3/m^3) (Topp method)
L / S / V	19sand2-5tds2d2Ls	5.3217	5.1328	0.670933	0.100	7.927	0.146
C / S / V	19sand2-5tds2d2cs	5.3223	5.1305	0.670933	0.100	8.172	0.151
L / S / V / R	19sand2-5tds2d2Lsr	5.3223	5.1305	0.670933	0.100	8.172	0.151
C / S / V / R	19sand2-5tds2d2csr	5.3195	5.1377	0.670933	0.100	7.342	0.133
L / S / V / RR	19sand2-5tds2d2Lsrr	5.3289	5.1594	0.670933	0.100	6.382	0.112
C / S / V / RR	19sand2-5tds2d2csrr	5.3245	5.1688	0.670933	0.100	5.385	0.089

Table C.51 – Compacted 19% target gravimetric water content 2.5 g/L salinity tailings sand testing results from unsheathed three-rod D2 probe (testing done January 14, 2014).

Test Configuration	File Name	x_2 (m)	x_1 (m)	V_p	L (m)	ε_b	Calc'd Vol. W.C. (m^3/m^3) (Topp method)
V	19sand2-5tds3d2	5.3754	5.1221	0.670933	0.100	14.253	0.264
V / R	19sand2-5tds3d2r	5.3748	5.1277	0.670933	0.100	13.564	0.253
V / RR	19sand2-5tds3d2rr	5.3532	5.1327	0.670933	0.100	10.801	0.204

Table C.52 – Compacted 19% target gravimetric water content 2.5 g/L salinity tailings sand testing results from sheathed three-rod D2 probe (testing done January 14, 2014).

Test Configuration	File Name	x_2 (m)	x_1 (m)	V_p	L (m)	ε_b	Calc'd Vol. W.C. (m^3/m^3) (Topp method)
S / V	19sand2-5tds3d2s	5.3344	5.1635	0.670933	0.100	6.488	0.114
S / V / R	19sand2-5tds3d2sr	5.3280	5.1265	0.670933	0.100	9.020	0.169
S / V / RR	19sand2-5tds3d2srr	5.3325	5.1246	0.670933	0.100	9.602	0.180

Table C.53 – Compacted 19% target gravimetric water content 2.5 g/L salinity tailings sand testing results from conventional probes (testing done January 15, 2014).

Test Configuration	File Name	x_2 (m)	x_1 (m)	V_p	L (m)	ε_b	Calc'd Vol. W.C. (m^3/m^3) (Topp method)
2 / V	19sand2-5tdscp	5.4061	5.1494	0.670933	0.100	14.638	0.270
2 / S / V	19sand2-5tdscps	5.3787	5.1502	0.670933	0.100	11.599	0.218
3	19sand2-5tds3z	1.2318	0.9891	0.670933	0.103	12.334	0.232
3 / S	19sand2-5tds3zs	1.2058	0.9884	0.670933	0.103	9.897	0.186

Table C.54 – Compacted 19% target gravimetric water content 5 g/L salinity tailings sand testing results from unsheathed two-rod D2 probe (testing done January 20, 2014).

Test Configuration	File Name	x_2 (m)	x_1 (m)	V_p	L (m)	ε_b	Calc'd Vol. W.C. (m^3/m^3) (Topp method)
L / V	19sand5tds2d2Lv	5.3559	5.1589	0.670933	0.100	8.621	0.161
L / H	19sand5tds2d2Lh	5.3520	5.1474	0.670933	0.100	9.299	0.174
C / V	19sand5tds2d2cv	5.3630	5.1605	0.670933	0.100	9.109	0.171
C / H	19sand5tds2d2ch	5.3612	5.1483	0.670933	0.100	10.069	0.190
L / V / R	19sand5tds2d2Lvr	5.3533	5.1621	0.670933	0.098	8.456	0.157
L / H / R	19sand5tds2d2Lhr	5.3559	5.1531	0.670933	0.098	9.513	0.179
C / V / R	19sand5tds2d2cvr	5.3490	5.1569	0.670933	0.098	8.536	0.159
C / H / R	19sand5tds2d2chr	5.3429	5.1453	0.670933	0.098	9.032	0.169
L / V / RR	19sand5tds2d2Lvrr	5.3508	5.1582	0.670933	0.099	8.408	0.156
L / H / RR	19sand5tds2d2Lhrr	5.3463	5.1455	0.670933	0.099	9.139	0.171
C / V / RR	19sand5tds2d2cvrr	5.3685	5.1685	0.670933	0.099	9.066	0.170
C / H / RR	19sand5tds2d2chrr	5.3533	5.1410	0.670933	0.099	10.216	0.192

Table C.55 – Compacted 19% target gravimetric water content 5 g/L salinity tailings sand testing results from sheathed two-rod D2 probe (testing done January 20, 2014).

Test Configuration	File Name	x_2 (m)	x_1 (m)	V_p	L (m)	ε_b	Calc'd Vol. W.C. (m^3/m^3) (Topp method)
L / S / V	19sand5tds2d2Lsv	5.3307	5.1710	0.670933	0.100	5.666	0.096
L / S / H	19sand5tds2d2Lsh	5.3213	5.1597	0.670933	0.100	5.801	0.099
C / S / V	19sand5tds2d2csv	5.3273	5.1673	0.670933	0.100	5.687	0.096
C / S / H	19sand5tds2d2csh	5.3081	5.1448	0.670933	0.100	5.924	0.102
L / S / V / R	19sand5tds2d2Lsvr	5.3210	5.1710	0.670933	0.098	5.204	0.085
L / S / H / R	19sand5tds2d2Lshr	5.3341	5.1609	0.670933	0.098	6.939	0.125
C / S / V / R	19sand5tds2d2csvr	5.3216	5.1692	0.670933	0.098	5.372	0.089
C / S / H / R	19sand5tds2d2cshr	5.3239	5.1585	0.670933	0.098	6.328	0.111
L / S / V / RR	19sand5tds2d2Lsvrr	5.3189	5.1627	0.670933	0.099	5.530	0.092
L / S / H / RR	19sand5tds2d2Lshrr	5.3201	5.1627	0.670933	0.099	5.615	0.094
C / S / V / RR	19sand5tds2d2csvrr	5.3159	5.1680	0.670933	0.099	4.958	0.079
C / S / H / RR	19sand5tds2d2cshrr	5.3239	5.1611	0.670933	0.099	6.007	0.103

Table C.56 – Compacted 19% target gravimetric water content 5 g/L salinity tailings sand testing results from sheathed three-rod D2 probe (testing done January 20, 2014).

Test Configuration	File Name	x_2 (m)	x_1 (m)	V_p	L (m)	ε_b	Calc'd Vol. W.C. (m^3/m^3) (Topp method)
V	19sand5tds3d2v	5.3786	5.1280	0.670933	0.100	13.951	0.259
H	19sand5tds3d2h	5.3866	5.1640	0.670933	0.100	11.008	0.208
V / R	19sand5tds3d2vr	5.3693	5.1220	0.670933	0.098	14.146	0.262
H / R	19sand5tds3d2hr	5.3493	5.1420	0.670933	0.098	9.940	0.187
V / RR	19sand3d2vrr	5.3802	5.1282	0.670933	0.099	14.394	0.266
H / RR	19sand5tds3d2hrr	5.3680	5.1353	0.670933	0.099	12.273	0.230

Table C.57 – Compacted 19% target gravimetric water content 5 g/L salinity tailings sand testing results from sheathed three-rod D2 probe (testing done January 20, 2014).

Test Configuration	File Name	x_2 (m)	x_1 (m)	V_p	L (m)	ε_b	Calc'd Vol. W.C. (m^3/m^3) (Topp method)
S / V	19sand5tds3d2sv	5.3319	5.1604	0.670933	0.100	6.534	0.116
S / H	19sand5tds3d2sh	5.3228	5.1459	0.670933	0.100	6.952	0.125
S / V / R	19sand5tds3d2svr	5.3167	5.1276	0.670933	0.098	8.271	0.153
S / H / R	19sand5tds3d2shr	5.3142	5.1430	0.670933	0.098	6.779	0.121
S / V / RR	19sand5tds3d2svrr	5.3197	5.1288	0.670933	0.099	8.260	0.153
S / H / RR	19sand5tds3d2shrr	5.3137	5.1457	0.670933	0.099	6.397	0.112

Table C.58 – Compacted 19% target gravimetric water content 5 g/L salinity tailings sand testing results from conventional probes (testing done January 22, 2014).

Test Configuration	File Name	x_2 (m)	x_1 (m)	V_p	L (m)	ε_b	Calc'd Vol. W.C. (m^3/m^3) (Topp method)
2 / V	19sand5tdscpv	5.4294	5.1676	0.670933	0.100	15.379	0.282
2 / H	19sand5tdscph	5.4103	5.1443	0.670933	0.100	15.877	0.289
2 / S / V	19sand5tdscpsv	5.3940	5.1652	0.670933	0.100	11.746	0.221
2 / S / H	19sand5tdscpsh	5.3870	5.1524	0.670933	0.100	12.350	0.232
3	19sand5tds3z	1.2362	0.9891	0.670933	0.103	12.785	0.239
3 / S	19sand5tds3zs	1.2044	0.9884	0.670933	0.103	9.770	0.184

Table C.59 – Compacted 19% target gravimetric water content 10 g/L salinity tailings sand testing results from unsheathed two-rod D2 probe (testing done January 27, 2014).

Test Configuration	File Name	x_2 (m)	x_1 (m)	V_p	L (m)	ε_b	Calc'd Vol. W.C. (m^3/m^3) (Topp method)
L / V	19sand10tds2d2Lv	5.3586	5.1464	0.670933	0.100	10.003	0.188
L / H	19sand10tds2d2Lh	5.3580	5.1534	0.670933	0.100	9.299	0.174
C / V	19sand10tds2d2cv	5.3577	5.1584	0.670933	0.100	8.824	0.165
C / H	19sand10tds2d2ch	5.3537	5.1550	0.670933	0.100	8.771	0.164
L / V / R	19sand10tds2d2Lvr	5.3810	5.1604	0.670933	0.099	11.030	0.208
L / H / R	19sand10tds2d2Lhr	5.3669	5.1464	0.670933	0.099	11.020	0.208
C / V / R	19sand10tds2d2cvr	5.3597	5.1584	0.670933	0.099	9.185	0.172
C / H / R	19sand10tds2d2chr	5.3584	5.1430	0.670933	0.099	10.516	0.198
L / V / RR	19sand10tds2d2Lvrr	5.3561	5.1546	0.670933	0.098	9.392	0.176
L / H / RR	19sand10tds2d2Lhrr2	5.3587	5.1494	0.670933	0.098	10.133	0.191
C / V / RR	19sand10tds2d2cvrr	5.3590	5.1617	0.670933	0.098	9.004	0.168
C / H / RR	19sand10tds2d2chrr	5.3497	5.1457	0.670933	0.098	9.626	0.181

Table C.60 – Compacted 19% target gravimetric water content 10 g/L salinity tailings sand testing results from sheathed two-rod D2 probe (testing done January 27, 2014).

Test Configuration	File Name	x_2 (m)	x_1 (m)	V_p	L (m)	ε_b	Calc'd Vol. W.C. (m^3/m^3) (Topp method)
L / S / V	19sand10tds2d2Lsv	5.3267	5.1558	0.670933	0.100	6.488	0.114
L / S / H	19sand10tds2d2Lsh	5.3228	5.1559	0.670933	0.100	6.188	0.108
C / S / V	19sand10tds2d2csv	5.3245	5.1582	0.670933	0.100	6.144	0.107
C / S / H	19sand10tds2d2csh	5.3237	5.1531	0.670933	0.100	6.465	0.114
L / S / V / R	19sand10tds2d2Lsvr	5.3261	5.1731	0.670933	0.099	5.306	0.087
L / S / H / R	19sand10tds2d2Lshr	5.6552	5.1512	0.670933	0.099	57.575	0.626
C / S / V / R	19sand10tds2d2csvr	5.3286	5.1349	0.670933	0.099	8.504	0.158
C / S / H / R	19sand10tds2d2cshr	5.3232	5.1366	0.670933	0.099	7.892	0.145
L / S / V / RR	19sand10tds2d2Lvsrr	5.3212	5.1580	0.670933	0.098	6.161	0.107
L / S / H / RR	19sand10tds2d2Lhsrr	5.3186	5.1532	0.670933	0.098	6.328	0.111
C / S / V / RR	19sand10tds2d2cvsrr	5.3210	5.1635	0.670933	0.098	5.738	0.097
C / S / H / RR	19sand10tds2d2chsrr	5.3208	5.1484	0.670933	0.098	6.875	0.123

Table C.61 – Compacted 19% target gravimetric water content 10 g/L salinity tailings sand testing results from unsheathed three-rod D2 probe (testing done January 27, 2014).

Test Configuration	File Name	x_2 (m)	x_1 (m)	V_p	L (m)	ε_b	Calc'd Vol. W.C. (m^3/m^3) (Topp method)
V	19sand10tds3d2	5.3911	5.1577	0.670933	0.100	12.102	0.227
H	19sand10tds3d2h	5.5745	5.1535	0.670933	0.100	39.374	0.507
V / R	19sand10tds3d2vr	5.4064	5.1576	0.670933	0.099	14.030	0.260
H / R	19sand10tds3d2hr	5.5731	5.1576	0.670933	0.099	39.130	0.505
V / RR	19sand10tds3d2vrr	5.3623	5.1501	0.670933	0.098	10.416	0.196
H / RR	19sand10tds3d2hrr	5.3786	5.1495	0.670933	0.098	12.141	0.228

Table C.62 – Compacted 19% target gravimetric water content 10 g/L salinity tailings sand testing results from sheathed three-rod D2 probe (testing done January 27, 2014).

Test Configuration	File Name	x_2 (m)	x_1 (m)	V_p	L (m)	ε_b	Calc'd Vol. W.C. (m^3/m^3) (Topp method)
S / V	19sand10tds3d2sv	5.3251	5.1595	0.670933	0.100	6.092	0.105
S / H	19sand10tds3d2sh	5.3265	5.1529	0.670933	0.100	6.695	0.119
S / V / R	19sand10tds3d2svr	5.3239	5.1545	0.670933	0.099	6.504	0.115
S / H / R	19sand10tds3d2shr	5.3385	5.1550	0.670933	0.099	7.632	0.140
S / V / RR	19sand10tds3d2vsrr	5.3401	5.1273	0.670933	0.098	10.474	0.197
S / H / RR	19sand10tds3d2hsrr	5.3411	5.1566	0.670933	0.098	7.874	0.145

Table C.63 – Compacted 19% target gravimetric water content 10 g/L salinity tailings sand testing results from conventional probes (testing done January 28, 2014).

Test Configuration	File Name	x_2 (m)	x_1 (m)	V_p	L (m)	ε_b	Calc'd Vol. W.C. (m^3/m^3) (Topp method)
2 / V	19sand10tdscpv	5.8217	5.1600	0.670933	0.100	97.267	1.541
2 / H	19sand10tdscph	5.7824	5.1468	0.670933	0.100	89.745	1.246
2 / S / V	19sand10tdscpsv	5.3934	5.1581	0.670933	0.100	12.299	0.231
2 / S / H	19sand10tdscpsh	5.3927	5.1588	0.670933	0.100	12.154	0.228
3	19sand10tds3z	1.2466	0.9894	0.670933	0.103	13.852	0.257
3 / S	19sand10tds3zs	1.2085	0.9893	0.670933	0.102	10.259	0.193

Table C.64 – FFT testing results from unsheathed two-rod D2 probe (testing done February and March 2014).

FFT Test Medium (m^3/m^3 Vol. W.C.)	File Name	x_2 (m)	x_1 (m)	V_p	L (m)	ε_b	Calc'd Vol. W.C. (m^3/m^3) (Topp method)	Calc'd Vol. W.C. (m^3/m^3) (Sorta method)
0.83 FFT	fft12d2v2	5.7682	5.1647	0.670933	0.100	80.909	0.987	0.981
0.81 FFT	fft22d2v2	5.7205	5.1508	0.670933	0.100	72.100	0.805	0.948
0.80 FFT	FFT2dried2d2	5.6861	5.1428	0.670933	0.100	65.572	0.709	0.909
0.78 FFT	fft32d2v2	5.6900	5.1494	0.670933	0.100	64.922	0.701	0.904
0.68 FFT	FFT42d2	5.9365	5.1521	0.670933	0.100	136.684	4.643	0.603

Table C.65 – FFT testing results from sheathed two-rod D2 probe (testing done February and March 2014).

FFT Test Medium (m^3/m^3 Vol. W.C.)	File Name	x_2 (m)	x_1 (m)	V_p	L (m)	ε_b	Calc'd Vol. W.C. (m^3/m^3) (Topp method)	Calc'd Vol. W.C. (m^3/m^3) (Sorta method)
0.83 FFT	fft12d2sv2	5.4765	5.1625	0.670933	0.100	21.903	0.368	0.380
0.81 FFT	fft2d2sv2	5.4719	5.1732	0.670933	0.100	19.820	0.343	0.344
0.80 FFT	FFT2dried2d2s	5.4229	5.1458	0.670933	0.100	17.057	0.306	0.296
0.78 FFT	fft32d2sv2	5.4415	5.1493	0.670933	0.100	18.967	0.332	0.330
0.68 FFT	FFT42d2s	5.4509	5.1674	0.670933	0.100	17.855	0.317	0.310

Table C.66 – FFT testing results from unsheathed three-rod D2 probe (testing done February and March 2014).

FFT Test Medium (m^3/m^3 Vol. W.C.)	File Name	x_2 (m)	x_1 (m)	V_p	L (m)	ε_b	Calc'd Vol. W.C. (m^3/m^3) (Topp method)	Calc'd Vol. W.C. (m^3/m^3) (Sorta method)
0.83 FFT	fft13d2v2	5.9791	5.1834	0.670933	0.100	140.650	5.138	0.532
0.81 FFT	fft23d2v2	6.0047	5.1451	0.670933	0.100	164.148	8.939	-0.022
0.80 FFT	FFT2dried3d2	5.9007	5.1506	0.670933	0.100	124.991	3.401	0.774
0.78 FFT	fft3d2dv2	5.9207	5.1853	0.670933	0.100	120.140	2.973	0.830
0.68 FFT	FFT43d2	6.0193	5.1816	0.670933	0.100	155.890	7.423	0.200

Table C.67 – FFT testing results from sheathed three-rod D2 probe (testing done February and March 2014).

FFT Test Medium (m^3/m^3 Vol. W.C.)	File Name	x_2 (m)	x_1 (m)	V_p	L (m)	ε_b	Calc'd Vol. W.C. (m^3/m^3) (Topp method)	Calc'd Vol. W.C. (m^3/m^3) (Sorta method)
0.83 FFT	fft13d2sv2	5.4716	5.1363	0.670933	0.100	24.975	0.400	0.431
0.81 FFT	fft23d2sv2	5.4786	5.1765	0.670933	0.100	20.274	0.349	0.352
0.80 FFT	FFT2dried3d2s	5.4493	5.1306	0.670933	0.100	22.563	0.375	0.391
0.78 FFT	fft33d2sv2	5.4448	5.1318	0.670933	0.100	21.764	0.366	0.378
0.68 FFT	FFT43d2s	5.4601	5.1605	0.670933	0.100	19.940	0.345	0.347

Table C.68 – FFT testing results from conventional unsheathed three-rod probe (testing done February and March 2014).

FFT Test Medium (m^3/m^3 Vol. W.C.)	File Name	x_2 (m)	x_1 (m)	V_p	L (m)	ε_b	Calc'd Vol. W.C. (m^3/m^3) (Topp method)	Calc'd Vol. W.C. (m^3/m^3) (Sorta method)
0.83 FFT	FFT1z	1.5036	0.9888	0.670933	0.103	55.494	0.609	0.827
0.81 FFT	FFT2z	1.5005	0.9888	0.670933	0.103	54.827	0.603	0.820
0.80 FFT	FFT2dried3z	1.5021	0.988	0.670933	0.103	55.343	0.607	0.825
0.78 FFT	FFT3z	1.4870	0.988	0.670933	0.103	52.140	0.584	0.794
0.68 FFT	FFT4z	1.4333	0.9888	0.670933	0.104	40.581	0.514	0.659

Table C.69 – FFT testing results from conventional sheathed three-rod probe (testing done February and March 2014).

FFT Test Medium (m^3/m^3 Vol. W.C.)	File Name	x_2 (m)	x_1 (m)	V_p	L (m)	ε_b	Calc'd Vol. W.C. (m^3/m^3) (Topp method)	Calc'd Vol. W.C. (m^3/m^3) (Sorta method)
0.83 FFT	FFT1zs	1.3403	0.988	0.670933	0.104	25.492	0.405	0.439
0.81 FFT	FFT2zs	1.3535	0.9891	0.670933	0.104	27.273	0.422	0.467
0.80 FFT	FFT2dried3zs	1.3425	0.9891	0.670933	0.104	25.651	0.407	0.442
0.78 FFT	FFT3zs	1.3409	0.9896	0.670933	0.103	25.842	0.408	0.445
0.68 FFT	FFT4zs	1.3172	0.9891	0.670933	0.104	22.110	0.370	0.383

Table C.70 – Push-test results from two-rod unsheathed Delrin® D2 probe (testing done April 24, 2014).

Lift Description	File Name	x_2 (m)	x_1 (m)	V_p	L (m)	ε_b	Calc'd Vol. W.C. (m^3/m^3) (Topp method)
Top Lift	pushtop	5.3680	5.2265	0.670933	0.100	4.493	0.067
Between Top/Mid	pushtop-mid	5.3713	5.2249	0.670933	0.100	4.809	0.075
Middle Lift	pushmid	5.4139	5.2242	0.670933	0.100	8.075	0.149
Between Mid/Bottom	pushmid-mid	5.4569	5.2260	0.670933	0.100	11.963	0.225
Bottom Lift	push bottom	5.4566	5.2228	0.670933	0.100	12.265	0.230
Bottom Lift before removal	pushbottomlast	5.4628	5.2286	0.670933	0.100	12.307	0.231

APPENDIX D:
WATER CONTENT DATA

LIST OF TABLES

Table D.1 – Compacted air-dried tailings sand water content data from D1 probe testing (testing done December 4, 2013).

Pre-compaction gravimetric water content: 0 (assumed to be completely dry)

Target dry density for packed lifts (g/mL): 1.60

Bulk density of packed lifts (g/mL): 1.60

Post-test gravimetric water content data:

Mass of Bulk Soil Mixture (g)	Mass of Water (g)	Mass of Soil (g)	Gravimetric W.C.	Sample Location (Position in Lift)
83.07	0.06	83.01	0.001	Lift 6 (top)
81.99	0.06	81.93	0.001	Lift 4 (mid)
80.07	0.07	80.00	0.001	Lift 2 (mid)

Average post-test gravimetric water content: 0.001

Actual post-test dry density of sand (g/mL): 1.60

Actual post-test volumetric water content of sand (m^3/m^3): 0.001

Table D.2 – Compacted air-dried tailings sand water content data from D2 probe testing (testing done December 5, 2013).

Pre-compaction gravimetric water content: 0 (assumed to be completely dry)

Target dry density for packed lifts (g/mL): 1.60

Bulk density of packed lifts (g/mL): 1.60

Post-test gravimetric water content data:

Mass of Bulk Soil Mixture (g)	Mass of Water (g)	Mass of Soil (g)	Gravimetric W.C.	Sample Location (Position in Lift)
80.49	0.06	80.43	0.001	Lift 6 (top)
80.00	0.08	79.92	0.001	Lift 4 (mid)
79.95	0.06	79.89	0.001	Lift 2 (mid)

Average post-test gravimetric water content: 0.001

Actual post-test dry density of sand (g/mL): 1.60

Actual post-test volumetric water content of sand (m^3/m^3): 0.001

Table D.3 – Compacted air-dried tailings sand water content data from D3 probe testing (testing done December 6, 2013).

Pre-compaction gravimetric water content: 0 (assumed to be completely dry)

Target dry density for packed lifts (g/mL): 1.60

Bulk density of packed lifts (g/mL): 1.60

Post-test gravimetric water content data:

Mass of Bulk Soil Mixture (g)	Mass of Water (g)	Mass of Soil (g)	Gravimetric W.C.	Sample Location (Position in Lift)
82.49	0.05	82.44	0.001	Lift 7 (top)
78.87	0.05	78.82	0.001	Lift 5 (mid)
80.65	0.07	80.58	0.001	Lift 3 (top)

Average post-test gravimetric water content: 0.001

Actual post-test dry density of sand (g/mL): 1.60

Actual post-test volumetric water content of sand (m^3/m^3): 0.001

Table D.4 – Compacted air-dried tailings sand water content data from conventional probe testing (testing done December 6, 2013).

Pre-compaction gravimetric water content: 0 (assumed to be completely dry)

Target dry density for packed lifts (g/mL): 1.60

Bulk density of packed lifts (g/mL): 1.60

Post-test gravimetric water content data:

Mass of Bulk Soil Mixture (g)	Mass of Water (g)	Mass of Soil (g)	Gravimetric W.C.	Sample Location (Position in Lift)
83.05	0.05	83.00	0.001	Lift 6 (top)
76.47	0.05	76.42	0.001	Lift 4 (mid)
84.56	0.04	84.52	0.000	Lift 2 (mid)

Average post-test gravimetric water content: 0.001

Actual post-test dry density of sand (g/mL): 1.60

Actual post-test volumetric water content of sand (m^3/m^3): 0.001

Table D.5 – Compacted 7% target gravimetric water content tailings sand water content data from D1 (and re-inserted D2 and D3) probe testing (testing done December 10, 2013).

Pre-compaction gravimetric water content: 0.067

Target dry density for packed lifts (g/mL): 1.41

Bulk density of packed lifts (g/mL): 1.50

Post-test gravimetric water content data:

Mass of Bulk Soil Mixture (g)	Mass of Water (g)	Mass of Soil (g)	Gravimetric W.C.	Sample Location (Position in Lift)
84.93	7.59	77.34	0.098	Lift 6 (mid)
76.92	4.28	72.64	0.059	Lift 4 (mid)
80.49	1.19	79.30	0.015	Lift 2 (top)

Average post-test gravimetric water content: 0.079

Actual post-test dry density of sand (g/mL): 1.39

Actual post-test volumetric water content of sand (m^3/m^3): 0.109

Table D.6 – Compacted 7% target gravimetric water content tailings sand water content data from D2 (initial packing) probe testing (testing done December 11, 2013).

Pre-compaction gravimetric water content: 0.067

Target dry density for packed lifts (g/mL): 1.41

Bulk density of packed lifts (g/mL): 1.50

Post-test gravimetric water content data:

Mass of Bulk Soil Mixture (g)	Mass of Water (g)	Mass of Soil (g)	Gravimetric W.C.	Sample Location (Position in Lift)
78.49	4.18	74.31	0.056	Lift 6 (top)
83.49	4.58	78.91	0.058	Lift 4 (mid)
84.46	4.65	79.81	0.058	Lift 2 (mid)

Average post-test gravimetric water content: 0.057

Actual post-test dry density of sand (g/mL): 1.42

Actual post-test volumetric water content of sand (m^3/m^3): 0.081

Table D.7 – Compacted 7% target gravimetric water content tailings sand water content data from D3 (initial packing) probe testing (testing done December 14, 2013).

Pre-compaction gravimetric water content: 0.067

Target dry density for packed lifts (g/mL): 1.41

Bulk density of packed lifts (g/mL): 1.50

Post-test gravimetric water content data:

Mass of Bulk Soil Mixture (g)	Mass of Water (g)	Mass of Soil (g)	Gravimetric W.C.	Sample Location (Position in Lift)
86.03	4.00	82.03	0.049	Lift 6 (mid)
84.07	3.96	80.11	0.049	Lift 4 (bottom)
82.77	3.86	78.91	0.049	Lift 2 (top)

Average post-test gravimetric water content: 0.049

Actual post-test dry density of sand (g/mL): 1.43

Actual post-test volumetric water content of sand (m^3/m^3): 0.070

Table D.8 – Compacted 7% target gravimetric water content tailings sand water content data from conventional probe testing (testing done December 14, 2013).

Pre-compaction gravimetric water content: 0.067

Target dry density for packed lifts (g/mL): 1.41

Bulk density of packed lifts (g/mL): 1.50

Post-test gravimetric water content data:

Mass of Bulk Soil Mixture (g)	Mass of Water (g)	Mass of Soil (g)	Gravimetric W.C.	Sample Location (Position in Lift)
78.08	3.62	74.46	0.049	Lift 6 (mid)
82.12	4.06	78.06	0.052	Lift 4 (mid)
83.34	4.34	79.00	0.055	Lift 2 (top)

Average post-test gravimetric water content: 0.050

Actual post-test dry density of sand (g/mL): 1.43

Actual post-test volumetric water content of sand (m^3/m^3): 0.072

Table D.9 – Compacted 14% target water content tailings sand water content data from D1 (and re-inserted D2 and D3) probe testing (testing done December 17, 2013).

Pre-compaction gravimetric water content: 0.118

Target dry density for packed lifts (g/mL): 1.40

Bulk density of packed lifts (g/mL): 1.57

Post-test gravimetric water content data:

Mass of Bulk Soil Mixture (g)	Mass of Water (g)	Mass of Soil (g)	Gravimetric W.C.	Sample Location (Position in Lift)
81.45	8.05	73.40	0.110	Lift 6 (mid)
83.92	8.23	75.69	0.109	Lift 5 (mid)
83.96	8.86	75.10	0.118	Lift 4 (mid)
83.11	9.10	74.01	0.123	Lift 3 (mid)
84.79	9.88	74.91	0.132	Lift 2 (mid)

Average post-test gravimetric water content: 0.112

Actual post-test dry density of sand (g/mL): 1.41

Actual post-test volumetric water content of sand (m^3/m^3): 0.158

Table D.10 – Compacted 14% target water content tailings sand water content data from conventional probe testing (testing done December 18, 2013).

Pre-compaction gravimetric water content: 0.118

Target dry density for packed lifts (g/mL): 1.40

Bulk density of packed lifts (g/mL): 1.57

Post-test gravimetric water content data:

Mass of Bulk Soil Mixture (g)	Mass of Water (g)	Mass of Soil (g)	Gravimetric W.C.	Sample Location (Position in Lift)
84.08	8.12	75.96	0.107	Lift 6 (mid)
84.21	8.79	75.42	0.117	Lift 5 (mid)
78.11	8.68	69.43	0.125	Lift 4 (mid)
80.63	9.51	71.12	0.134	Lift 3 (mid)
84.74	10.54	74.20	0.142	Lift 2 (mid)

Average post-test gravimetric water content: 0.116

Actual post-test dry density of sand (g/mL): 1.41

Actual post-test volumetric water content of sand (m^3/m^3): 0.163

Table D.11 – Compacted 19% target water content tailings sand water content data from D1 (and re-inserted D2 and D3) probe testing (testing done December 19, 2013).

Pre-compaction gravimetric water content: 0.184

Target dry density for packed lifts (g/mL): 1.40

Bulk density of packed lifts (g/mL): 1.66

Post-test gravimetric water content data:

Mass of Bulk Soil Mixture (g)	Mass of Water (g)	Mass of Soil (g)	Gravimetric W.C.	Sample Location (Position in Lift)
87.30	11.29	76.01	0.149	Lift 6 (bottom)
82.15	11.04	71.11	0.155	Lift 5 (bottom)
85.14	11.86	73.28	0.162	Lift 4 (mid)
79.28	11.73	67.55	0.174	Lift 3 (mid)
85.20	13.39	71.81	0.186	Lift 2 (mid)

Average post-test gravimetric water content: 0.155

Actual post-test dry density of sand (g/mL): 1.44

Actual post-test volumetric water content of sand (m^3/m^3): 0.223

Table D.12 – Compacted 19% target water content tailings sand water content data from conventional probe testing (testing done December 20, 2013).

Pre-compaction gravimetric water content: 0.184

Target dry density for packed lifts (g/mL): 1.40

Bulk density of packed lifts (g/mL): 1.66

Post-test gravimetric water content data:

Mass of Bulk Soil Mixture (g)	Mass of Water (g)	Mass of Soil (g)	Gravimetric W.C.	Sample Location (Position in Lift)
80.58	10.86	69.72	0.156	Lift 6 (bottom)
76.47	10.82	65.65	0.165	Lift 5 (bottom)
80.86	11.79	69.07	0.171	Lift 4 (mid)
86.18	13.26	72.92	0.182	Lift 3 (mid)
77.61	12.44	65.17	0.191	Lift 2 (mid)

Average post-test gravimetric water content: 0.168

Actual post-test dry density of sand (g/mL): 1.42

Actual post-test volumetric water content of sand (m^3/m^3): 0.239

Table D.13 – Compacted 19% target gravimetric water content 2.5 g/L salinity tailings sand water content data from D2 probe testing (testing done January 14, 2014).

Pre-compaction gravimetric water content: 0.163

Target dry density for packed lifts (g/mL): 1.40

Bulk density of packed lifts (g/mL): 1.63

Post-test gravimetric water content data:

Mass of Bulk Soil Mixture (g)	Mass of Water (g)	Mass of Soil (g)	Gravimetric W.C.	Sample Location (Position in Lift)
82.58	10.52	72.06	0.146	Lift 6 (mid)
93.77	12.56	81.21	0.155	Lift 5 (mid)
84.51	12.28	72.23	0.170	Lift 4 (mid)
88.78	13.49	75.29	0.179	Lift 3 (mid)
89.31	13.70	75.61	0.181	Lift 2 (top)

Average post-test gravimetric water content: 0.157

Actual post-test dry density of sand (g/mL): 1.41

Actual post-test volumetric water content of sand (m^3/m^3): 0.221

Table D.14 – Compacted 19% target gravimetric water content 2.5 g/L salinity tailings sand water content data from conventional probe testing (testing done January 15, 2014).

Pre-compaction gravimetric water content: 0.163

Target dry density for packed lifts (g/mL): 1.40

Bulk density of packed lifts (g/mL): 1.63

Post-test gravimetric water content data:

Mass of Bulk Soil Mixture (g)	Mass of Water (g)	Mass of Soil (g)	Gravimetric W.C.	Sample Location (Position in Lift)
96.35	12.13	84.22	0.144	Lift 6 (mid)
102.66	13.85	88.81	0.156	Lift 5 (mid)
96.52	13.95	82.57	0.169	Lift 4 (mid)
102.65	15.64	87.01	0.180	Lift 3 (mid)
96.87	15.60	81.27	0.192	Lift 2 (top)

Average post-test gravimetric water content: 0.162

Actual post-test dry density of sand (g/mL): 1.40

Actual post-test volumetric water content of sand (m^3/m^3): 0.227

Table D.15 – Compacted 19% target gravimetric water content 5.0 g/L salinity tailings sand water content data from D2 probe testing (testing done January 20, 2014).

Pre-compaction gravimetric water content: 0.183

Target dry density for packed lifts (g/mL): 1.40

Bulk density of packed lifts (g/mL): 1.66

Post-test gravimetric water content data:

Mass of Bulk Soil Mixture (g)	Mass of Water (g)	Mass of Soil (g)	Gravimetric W.C.	Sample Location (Position in Lift)
95.82	11.77	84.05	0.140	Lift 6 (mid)
103.3	13.21	90.09	0.147	Lift 5 (mid)
112.71	15.53	97.18	0.160	Lift 4 (mid)
110.06	15.88	94.18	0.169	Lift 3 (mid)
103.75	16.05	87.7	0.183	Lift 2 (top)

Average post-test gravimetric water content: 0.149

Actual post-test dry density of sand (g/mL): 1.45

Actual post-test volumetric water content of sand (m^3/m^3): 0.215

Table D.16 – Compacted 19% target gravimetric water content 5.0 g/L salinity tailings sand water content data from conventional probe testing (testing done January 22, 2014).

Pre-compaction gravimetric water content: 0.183

Target dry density for packed lifts (g/mL): 1.40

Bulk density of packed lifts (g/mL): 1.66

Post-test gravimetric water content data:

Mass of Bulk Soil Mixture (g)	Mass of Water (g)	Mass of Soil (g)	Gravimetric W.C.	Sample Location (Position in Lift)
100.57	13.08	87.49	0.150	Lift 6 (mid)
102.22	13.96	88.26	0.158	Lift 5 (mid)
108.58	15.73	92.85	0.169	Lift 4 (mid)
107.27	16.28	90.99	0.179	Lift 3 (mid)
106.27	16.45	89.82	0.183	Lift 2 (top)

Average post-test gravimetric water content: 0.164

Actual post-test dry density of sand (g/mL): 1.43

Actual post-test volumetric water content of sand (m^3/m^3): 0.233

Table D.17 – Compacted 19% target gravimetric water content 10.0 g/L salinity tailings sand water content data from D2 probe testing (testing done January 27, 2014).

Pre-compaction gravimetric water content: 0.173

Target dry density for packed lifts (g/mL): 1.40

Bulk density of packed lifts (g/mL): 1.64

Post-test gravimetric water content data:

Mass of Bulk Soil Mixture (g)	Mass of Water (g)	Mass of Soil (g)	Gravimetric W.C.	Sample Location (Position in Lift)
108.39	13.24	95.15	0.139	Lift 6 (mid)
98.80	12.89	85.91	0.150	Lift 5 (mid)
105.43	14.63	90.80	0.161	Lift 4 (mid)
99.58	14.53	85.05	0.171	Lift 3 (mid)
102.46	15.52	86.94	0.179	Lift 2 (top)

Average post-test gravimetric water content: 0.150

Actual post-test dry density of sand (g/mL): 1.43

Actual post-test volumetric water content of sand (m^3/m^3): 0.214

Table D.18 – Compacted 19% target gravimetric water content 10.0 g/L salinity tailings sand water content data from conventional probe testing (testing done January 28, 2014).

Pre-compaction gravimetric water content: 0.173

Target dry density for packed lifts (g/mL): 1.40

Bulk density of packed lifts (g/mL): 1.64

Post-test gravimetric water content data:

Mass of Bulk Soil Mixture (g)	Mass of Water (g)	Mass of Soil (g)	Gravimetric W.C.	Sample Location (Position in Lift)
106.08	13.58	92.50	0.147	Lift 6 (top)
106.70	14.90	91.80	0.162	Lift 5 (mid)
111.43	16.46	94.97	0.173	Lift 4 (mid)
111.28	17.03	94.25	0.181	Lift 3 (mid)
116.47	18.14	98.33	0.184	Lift 2 (top)

Average post-test gravimetric water content: 0.166

Actual post-test dry density of sand (g/mL): 1.41

Actual post-test volumetric water content of sand (m^3/m^3): 0.234

Table D.19 – Water content data from FFT testing (testing done February and March 2014).

Sample	Mass of Bulk Mixture (g)	Mass of Water (g)	Mass of Solids (g)	Volumetric W.C. (m^3/m^3)
FFT 1	157.29	102.96	54.33	0.834
FFT 2	191.21	116.56	74.65	0.805
FFT 2 (dried)	98.25	59.31	38.94	0.801
FFT 3	163.28	92.95	70.33	0.778
FFT 4	129.38	58.06	71.32	0.683

Note that a density of water of 1.00 g/cm^3, and a density of solids of 2.65 g/cm^3 were assumed in these calculations.

Table D.20 – Volumetric sampling tube water content data from push-test (testing done April 24, 2014).

Volume of Sampling Tube (mL)	Mass of Water (g)	Mass of Soil (g)	Gravimetric W.C.	Volumetric W.C. (m^3/m^3)	Sample Location (Tape Reading)
139.8	9.92	201.75	0.049	0.071	From surface
8.3	0.45	10.40	0.043	0.054	From surface
9.1	0.66	12.84	0.051	0.072	From ~43 cm
8.7	1.09	12.37	0.088	0.125	From ~30 cm
139.8	31.09	201.92	0.154	0.222	From ~27 cm
9.1	2.31	13.12	0.176	0.255	From ~23 cm
139.8	44.95	213.93	0.210	0.322	From ~14 cm
8.7	2.42	12.82	0.189	0.280	From ~15 cm
9.1	2.80	13.53	0.207	0.309	From ~10 cm

Table D.21 – Gravimetric water content sampling data from push-test (testing done April 24, 2014).

Mass of Bulk Soil Mixture (g)	Mass of Water (g)	Mass of Soil (g)	Gravimetric W.C.	Approx. Volumetric W.C. (m^3/m^3)	Sample Location (Tape Reading)
115.93	5.00	110.93	0.045	0.063	From ~43 cm
148.14	9.47	138.67	0.068	0.086	From ~30 cm
160.16	19.52	140.64	0.139	0.176	From ~23 cm
235.82	38.39	197.43	0.194	0.246	From ~20 cm
151.04	23.25	127.79	0.182	0.241	From ~15 cm
168.97	28.64	140.33	0.204	0.270	From ~10 cm
219.14	37.51	181.63	0.207	0.274	From ~5 cm

Note that volumetric water content was calculated based on an approximated dry density of each lift: Bottom Lift of 1.32 g/mL, Middle Lift of 1.27 g/mL, and Top Lift of 1.39 g/mL.

APPENDIX E:
SPSS OUTPUT SUMMARY

LIST OF TABLES

Table E.1 – Mean volumetric water contents (m^3/m^3; using Topp equation) measured by Delrin® D2 probe configurations in response to various levels of elevated salinity in compacted tailings sand. Means in the same row with the same superscript letters are not significantly different at α=0.05. No comparison done between rows. First set of brackets indicates standard deviation, second indicates population size.

	Salinity (g/L)		
	2.5	5.0	10.0
2-Rod Probe	0.1459^a (0.0241) (n=12)	0.1341^b (0.0392) (n=24)	0.1507^a (0.0386) (n=23)
3-Rod Probe	0.1973^a (0.0557) (n=6)	0.1827^a (0.0606) (n=12)	0.1734^a (0.0553) (n=10)

Table E.2 – Mean volumetric water contents (m^3/m^3; using Topp equation) measured by two-rod Delrin® D2 probe using rods with long and close spacing in compacted elevated salinity tailings sand. Means with the same superscript letters are not significantly different at α=0.05. First set of brackets indicates standard deviation, second indicates population size.

Long	Close
0.1430^a (0.0383) (n=29)	0.1429^a (0.0356) (n=30)

Table E.3 – Mean volumetric water contents (m^3/m^3; using Topp equation) measured by Delrin® D2 probe configurations with vertical and horizontal electrical connection orientations in compacted elevated salinity tailings sand. Means in the same row with the same superscript letters are not significantly different at α=0.05. No comparison done between rows. First set of brackets indicates standard deviation, second indicates population size.

	Vertical	Horizontal
2-Rod Probe	0.1391^a (0.0355) (n=36)	0.1490^b (0.0384) (n=23)
3-Rod Probe	0.1942^a (0.0588) (n=18)	0.1615^a (0.0470) (n=10)

Table E.4 – Mean volumetric water contents (m^3/m^3; using Topp equation) measured by non-sheathed and sheathed Delrin® D2 probe configurations in compacted elevated salinity tailings sand. Means in the same row with the same superscript letters are not significantly different at α=0.05. No comparison done between rows. First set of brackets indicates standard deviation, second indicates population size.

	Non-Sheathed	Sheathed
2-Rod Probe	0.1737^a (0.0152) (n=30)	0.1112^b (0.0221) (n=29)
3-Rod Probe	0.2342^a (0.0285) (n=13)	0.1377^b (0.0279) (n=15)

Table E.5 – Mean volumetric water contents (m^3/m^3; using Topp equation) measured by Delrin® D2 and conventional probes in compacted elevated salinity tailings sand. Means with the same superscript letters are not significantly different at α=0.05. First set of brackets indicates standard deviation, second indicates population size.

Delrin® Probe	Conventional Probe
0.1505^a (0.0473) (n=29)	0.2323^b (0.0317) (n=14)

Table E.6 – Mean volumetric water contents (m^3/m^3; using Topp equation) measured by two- and three-rod Delrin® D2 and conventional probes in compacted elevated salinity tailings sand. Means in the same row with the same superscript letters are not significantly different at α=0.05. No comparison done between rows. First set of brackets indicates standard deviation, second indicates population size.

	2-Rod	3-Rod
Delrin® Probe	0.1430^a (0.0366) (n=59)	0.1825^b (0.0563) (n=28)
Both Delrin® and Conventional Probes	0.1710^a (0.0569) (n=28)	0.1886^a (0.0588) (n=15)

Table E.7 – Mean volumetric water contents (m^3/m^3; using Topp equation) measured by Delrin® D2 probe configurations over three consecutive insertions (one initial insertion and two subsequent re-insertions) in compacted elevated salinity tailings sand. Means in the same row with the same superscript letters are not significantly different at α=0.05. No comparison done between rows. First set of brackets indicates standard deviation, second indicates population size.

	Insertion Number		
	1	2	3
2-Rod Probe	0.1414^{ab} (0.0332) (n=20)	0.1503^{a} (0.0378) (n=19)	0.1375^{b} (0.0395) (n=20)
3-Rod Probe	0.1708^{a} (0.0674) (n=9)	0.1844^{a} (0.0597) (n=9)	0.1913^{a} (0.0455) (n=10)
Both 2- and 3-Rod Probes	0.1505^{a} (0.0473) (n=29)	0.1613^{a} (0.0477) (n=28)	0.1554^{a} (0.0483) (n=30)